BERGISCHE
UNIVERSITÄT
WUPPERTAL

Metamodel for complex scenarios in fire risk analysis of road tunnels

Dissertation
zur Erlangung des
Doktorgrades Dr.-Ing.

an der Fakultät für
Architektur und Bauingenieurwesen
der
Bergischen Universität Wuppertal

von

Florian Berchtold
aus Buchloe

Wuppertal 2019

The PhD thesis can be quoted as follows:

urn:nbn:de:hbz:468-20200114-101029-6
[http://nbn-resolving.de/urn/resolver.pl?urn=urn%3Anbn%3Ade%3Ahbz%3A468-20200114-101029-6]

DOI: 10.25926/evq8-h241
[https://doi.org/10.25926/evq8-h241]

Diese Dissertation wurde begutachtet durch:

Prof. Dr.
Armin Seyfried

Erstgutachter
Bergische Universität Wuppertal
Fakultät für
Architektur und Bauingenieurwesen

Associate Professor Dr.
Sebastian Thöns

Zweitgutachter
Technical University of Denmark
Department of Civil Engineering

Datum der Disputation:
28.10.2019

Abstract

The risk analysis of road tunnels faces a growing complexity in fire scenarios, e.g. caused by new energy carriers. Essentially, such complex scenarios involve many interactions between the tunnel users, the fire source and the safety measures. One example is the alarm of tunnel users either initiated by the perception of smoke or by the fire alarm system. To consider these interactions for the quantification of consequences, e.g. fatalities, risk analysis requires a complex model. However, the complex model can compute in practice only few discrete scenarios due to its high computational cost, whereas risk analysis generally needs the consequences of a high number of random scenarios. Metamodels can solve this contradiction. They are able to approximate the consequences of many random scenarios with low computational cost based on the consequences of few discrete scenarios computed with the complex model. The efficiency of metamodels depends on the required number of these discrete scenarios. In this sense, this dissertation proposes an efficient metamodel within an innovative methodology for risk analysis of road tunnels to allow to consider an increased complexity of scenarios.

This metamodel applies the following methods or models: the projection array-based design method specifies the experimental design for the discrete scenarios; the combination of the fire model FDS and the microscopic evacuation model FDS+Evac constitutes the complex model; and moving least squares produces the response surface model. The response surface model approximates the consequences of the random scenarios and therewith introduces an uncertainty, called metamodel uncertainty, which is quantified with the prediction interval method. Additionally, stochastic individual characteristics of tunnel users in discrete scenarios computed with FDS+Evac attribute evacuation uncertainties to the consequences. An original development in this dissertation, the 'direct approach', directly transfers the evacuation uncertainties of the discrete scenarios to any random scenario.

The evaluation of the metamodel in this dissertation shows following results. Firstly, the response surface model sufficiently represents the consequences of the complex model. Secondly, the metamodel uncertainty is also essential for this representation, but the prediction interval method reveals a drawback in the risk analysis. Potential approaches to deal with this drawback are discussed. Finally, the direct approach reproduces the evacuation uncertainty of the complex model which then clearly affects the consequences of random scenarios. Therefore, the consideration of the evacuation uncertainty plays an important role for the risk analysis. Furthermore, the projection array-based design method was adapted in this dissertation with two approaches, namely the combination of the experimental designs for FDS and FDS+Evac as well as their sequential refinement. Both approaches contribute to the efficiency of the metamodel.

These results lead to following conclusions. Firstly, the metamodel efficiently integrates the consequences of discrete scenarios into risk analysis and thus allows to consider an increased complexity. Secondly, the metamodel is an advancement for risk analysis not only for road tunnels but also more general in fire safety engineering. For these two reasons, the metamodel might be interesting for other methodologies for risk analysis. In addition, the metamodel is generic and is therefore widely applicable on other issues beside from risk analysis, e.g. to assess the safety of structures related to time-consuming experiments depending on multiple variables.

Kurzfassung

Risikoanalysen für Straßentunnel müssen eine immer größere Komplexität in Brandszenarien berücksichtigen, beispielsweise verursacht durch neue Energieträger. Dabei hängt die Komplexität von Szenarien mit einer Vielzahl von Interaktionen zwischen den Tunnelnutzern, der Brandquelle und den Sicherheitsmaßnahmen zusammen. Zum Beispiel werden Tunnelnutzer entweder direkt durch Rauch oder durch die Brandmeldeanlage alarmiert. Um die Interaktionen bei der Berechnung der Konsequenzen, wie z.B. getötete Personen, zu berücksichtigen, benötigen Risikoanalysen komplexe Modelle. Allerdings können komplexe Modelle wegen ihres hohen Zeitaufwandes nur wenige diskrete Szenarien simulieren, wohingegen Risikoanalysen auf Konsequenzen einer Vielzahl von Zufallsszenarien basieren. Als Lösung dieses Widerspruchs kommen Metamodelle in Betracht. Sie können die Konsequenzen von vielen Zufallsszenarien innerhalb kurzer Zeit näherungsweise berechnen und verwenden dafür die Konsequenzen von wenigen mit dem komplexen Modell simulierten diskreten Szenarien. Die Effizienz von Metamodellen hängt dabei mit der nötigen Anzahl von diskreten Szenarien zusammen. Demnach wird in dieser Dissertation ein effizientes Metamodell in eine selbst erstellte Methodik zur Risikoanalyse für Straßentunnel integriert, um damit eine höhere Komplexität der Szenarien einbeziehen zu können.

Das Metamodell setzt sich aus folgenden Methoden und Modellen zusammen: die 'projection array-based design'-Methode definiert den Simulationsplan für die diskreten Szenarien; eine Kombination aus dem Brandmodell FDS und dem mikroskopischen Evakuierungsmodell FDS+Evac bildet das komplexe Modell; und 'moving least squares' dient zur Erstellung des Antwortflächenmodells. Das Antwortflächenmodell berechnet näherungsweise die Konsequenzen der Zufallsszenarien und erzeugt dadurch eine Unsicherheit, die Metamodellunsicherheit. Sie wird mit der 'prediction interval'-Methode bestimmt. Zusätzlich verursachen individuelle Eigenschaften der Tunnelnutzer in den mit FDS+Evac simulierten diskreten Szenarien Evakuierungsunsicherheiten in den Konsequenzen. Ein in der Dissertation neu entwickelter Ansatz, der 'direkte Ansatz', überträgt die Evakuierungsunsicherheit der diskreten Szenarien unmittelbar auf die Zufallsszenarien.

Die Untersuchung des Metamodels in der Dissertation führte zu folgenden Ergebnissen. Erstens, das Antwortflächenmodell bildet die Konsequenzen der diskreten Szenarien ausreichend genau ab. Zweitens, dazu trägt die Metamodellunsicherheit wesentlich bei. Allerdings zeigt die 'prediction-interval'-Methode einen Nachteil für die Risikoanalyse. Zur Lösung dieses Nachteils werden potentielle Ansätze diskutiert. Und drittens, der direkte Ansatz gibt die Evakuierungsunsicherheiten des komplexen Modells wieder, welche dann die Konsequenzen der Zufallsszenarien deutlich beeinflussen. Aus diesem Grund ist die Evakuierungsunsicherheit für die Risikoanalyse wichtig. Zusätzlich wurde die 'projection array-based design'-Methode in dieser Dissertation mit zwei Ansätzen angepasst: der Verknüpfung beider Simulationspläne für FDS und FDS+Evac sowie deren schrittweisen Verfeinerung. Die Effizienz des Metamodels wird durch beide Ansätze erhöht.

Diese Ergebnisse führen zu folgenden Schlussfolgerungen: erstens, das Metamodell integriert die Konsequenzen der diskreten Szenarien auf eine effiziente Weise in die Risikoanalyse und ermöglicht dadurch die Berücksichtigung einer höheren Komplexität; und zweitens, das Metamodell stellt einen Fortschritt für Risikoanalysen nicht nur für Straßentunnel sondern auch allgemein im Brandingenieurwesen dar. Aus diesen beiden Gründen kann das Metamodell für andere Methodiken zur Risikoanalyse interessant sein. Zudem ist das Metamodel flexibel auf andere Problemstellungen außerhalb der Risikoanalyse anwendbar, wie z.B. der Bewertung der Bauwerkssicherheit, welche von zeitaufwändigen Untersuchung und mehreren Variablen abhängt.

Danksagung / Acknowledgements

Diese Dissertation fasst meine Forschung in mehreren wissenschaftlichen Feldern während der letzten sechseinhalb Jahre zusammen. Das Ergebnis wäre natürlich nicht ohne die Unterstützung zahlreicher Personen möglich geworden, bei denen ich mich besonders bedanken möchte.

Zuerst bei meinen Betreuern und Gutachtern Lukas Arnold, Armin Seyfried und Sebastian Thöns von der Bergischen Universität Wuppertal bzw. dem Forschungszentrum Jülich und der Dänischen Technischen Universität. Die Diskussionen mit ihnen und ihre konstruktive Kritik hat mich viel gelehrt und nicht nur in meiner Arbeit weitergebracht. Ganz besonders möchte ich ihnen aber auch für ihr Vertrauen in mich danken.

Bei Christian Knaust und Andreas Rogge von der Bundesanstalt für Materialforschung und –prüfung (BAM). Dank gilt ihnen vor allem dafür, dass sie mir die Zeit und Freiheit gelassen haben, um meinen Weg zu finden, aber natürlich auch für die problemlose und selbst motivierte Verlängerung meiner Verträge. Sie haben großen Anteil daran, dass ich positiv an die Zeit während der Doktorarbeit zurück denke und nach wie vor viel Freude an der Forschung finde.

Auch bei Pablo Cuéllar von der BAM, zuerst für seine gute Laune und positive Grundhaltung, aber natürlich auch für seine Freude am Korrekturlesen meiner Arbeit. Danke für das kritische Hinterfragen und die spitzfindigen Anmerkungen.

Weiterhin will ich vielen anderen danken, die mich oft ohne genaues Wissen über meine Arbeit unterstützt haben. Insbesondere der IT und den Sekretärinnen der BAM, vor allem Monika Jooß-Köstler, Kerstin Bonitz und Margrit Kayser, sowie meinen Mensa-Kollegen. Nicht zu vergessen seien zudem Hanna Luderer und Wolfgang Schwabe ohne deren Hilfe und Unterstützung ich die Arbeit nie beendet hätte.

Danken möchte ich natürlich auch meinen Freunden für ihr Verständnis für die lange Abwesenheit und ihre immer offenen Arme. Ein ganz besonderer Dank geht dabei an Paul Geoerg, Freund und steten Begleiter, weil wir immer Probleme in und außerhalb der Arbeit offen diskutieren konnten. Außerdem für seine Ermutigungen zum Loslassen und für seine Ermahnungen zur Objektivität und Flexibilität.

Nicht zuletzt will ich meiner gesamten Familie danken, besonders meinen Eltern Karin und Wolfgang, sowie Andi, Leonie, Fritz und Berndi. Ihre Unterstützung fing natürlich schon lange vor der Doktorarbeit an. In den letzten Jahren waren für mich aber ihre Ratschläge und offenen Meinungen wichtig. Außerdem will ich mich für ihr Verständnis für die endlosen Telefonate bedanken.

Danke!

Für alle die noch nicht so genau wissen, um was meine Arbeit geht: dank Lukas Arnold habe ich die letzten Tagen vor der Abgabe an einer Zusammenfassung gefeilt, die allgemein verständlich sein soll. Ihr findet sie auf der nächsten Seite. Ich hoffe, die Zeit hat sich gelohnt.

‘Drawing lines between points’ - Three questions to the title.

What is a metamodel?

Fire safety engineers often want to know the maximum temperature in a room fire and for this, they apply complex models. Complex models are able to compute the temperature everywhere in the room at every time in detail. Hence, they cause high computational costs and therewith limit the number of simulations. For this reason, fire safety engineers can compute the maximum temperature in only few discrete scenarios, e.g. with a small and a large fire size, like of a radio and a couch. But if they want to know the maximum temperature for many different fire sizes, e.g. because many different things in the room can burn, complex models can no longer be used.

In this case, a metamodel can help. The metamodel needs the maximum temperatures of only few discrete scenarios computed with the complex model, for example with the small and the large fire size. These discrete scenarios, with its maximum temperature and its fire size, can be imagined as points shown in the figure below. With these points, the metamodel can predict the maximum temperature for different fire sizes with only small computational costs. In other words, the metamodel can quickly draw a line between the points. The line represents unknown points, which could not be computed with the complex model.

Of course, the metamodel cannot predict the maximum temperature precisely. As a consequence, there will be a difference between the maximum temperature determined with the metamodel and the unknown maximum temperature, which (was not, but) would be computed with the complex model. This difference is called metamodel uncertainty and can be illustrated by the thickness of the line.

Where is the problem with complex scenarios in risk analysis of road tunnels?

An important aim of risk analysis is to evaluate the effects of safety measures on the safety of tunnel users. Hence, there are many interactions between the fire, the tunnel users and the safety measures. These interactions make the fire scenario complex. For instance, the fire alarm system detects the smoke and alerts the tunnel users. To cover all these interactions, risk analysis requires complex models. But the complex model allows to compute only few discrete scenarios, whereas the risk analysis needs many different scenarios. This contradiction limits the complexity of scenarios to be considered in the risk analysis.

How does the metamodel of this dissertation help for the risk analysis?

A metamodel can solve this contradiction as illustrated in the figure. For this, the discrete scenario depends not only on the fire size but also on the fire growth, the number of tunnel users and their individual reaction time. And its outcome are fatalities instead of the

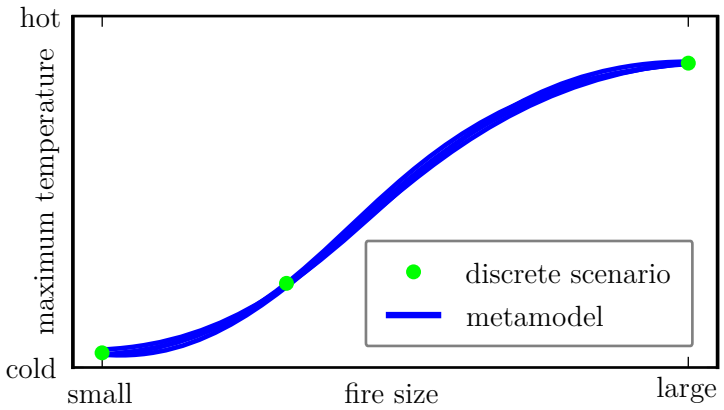

maximum temperature. To compute the fatalities, the complex model additionally includes the evacuation. The evacuation involves e.g. the random individual walking speed. As a consequence, repeated simulations of the same discrete scenario will lead to variations in the fatalities, called evacuation uncertainty.

The metamodel comprises several approaches to reduce the required number of discrete scenarios. For instance, it allows their stepwise simulation until the metamodel uncertainty is low enough. Hence, these approaches reduce the computational costs and increase the efficiency of the metamodel.

As a result, the efficient metamodel allows to consider an increased complexity of scenarios in the risk analysis. This is especially true in comparison to the direct use of discrete scenarios, common in other risk analyses. Moreover, the metamodel includes the metamodel uncertainty and the evacuation uncertainty into risk analysis. The evacuation uncertainty is realised with an original approach. Both uncertainties are important for the results of risk analysis but were ignored in most other risk analyses. To conclude, this metamodel is an advancement for risk analysis and might therefore be interesting. Furthermore, everyone can employ it to simply draw lines between points whatever the points shall mean.

Nomenclature

The page numbers refer to the first introduction of the abbreviations and symbols.

Abbreviations

App.	appendix	p. 7
CFD	computational fluid dynamics	p. 2
ED	experimental design	p. 4
FA	failure of tunnel alarm	p. 1
FDS	Fire Dynamics Simulator	p. 2
FF	fraction of fatalities; fractions of fatalities (FFs)	p. 14
FFD	full factorial design	p. 31
FoM	first order method	p. 41
HGV	heavy good vehicle	p. 17
HRR	heat release rate	p. 2
LHD	Latin hypercube design	p. 31
LIl	linear local interpolation	p. 40
LIn	nearest local interpolation	p. 40
MLS	moving least squares	p. 38
ORS	observed random sample	p. 23
PA	projection array	p. 32
PAD	projection array-based design	p. 31
RSM	response surface model	p. 4
sc	scenario	p. 14
SoM	second order method	p. 41
Subs.	subsection	p. 7
TA	tunnel alarm	p. 1

Risk factors and intermediate nodes

χ_{HGV}	ratio of HGV	p. 19
fa	failure of tunnel alarm (node)	p. 19
f_{sc}	frequency of scenario in $\frac{1}{year}$	p. 14
HRR_{max}	maximum heat release rate	p. 18
$\dot{N}_{adtv}$	average daily traffic volume	p. 19
N_{tu}	number of tunnel users	p. 14
t_{max}	time to maximum heat release rate	p. 19
t_{pre}	maximum pre-evacuation time	p. 19
l_{tunnel}	tunnel length	p. 19

FF ξ and results y where $y \equiv \xi$ and $Y \equiv \boldsymbol{\xi}$

ξ	fraction of fatalities	p. 14
ξ^c	FF (complex model) of a single replication	p. 23
$\bar{\boldsymbol{\xi}}^c$	data base for the mean FF of all scenarios in an ED	p. 24
$\bar{\xi}^c$	mean FF (complex model)	p. 23
$\bar{\xi}^c_{lim}$	limit for data points in the evacuation uncertainty	p. 49
$\widetilde{\boldsymbol{\xi}}^c$	data base for the FF of all replications of each scenario in an ED	p. 24
$\widetilde{\xi}^c$	FF (complex model) with all replications, ORS	p. 23
$\widehat{\boldsymbol{\xi}}^c$,$\widehat{\xi}^c$	relative ORS (complex model)	p. 47
$\bar{\boldsymbol{\xi}}$,$\bar{\xi}$	FF (RSM) for multiple or one random scenarios	p. 25
$\widetilde{\boldsymbol{\xi}}$,$\widetilde{\xi}$	FF (metamodel) with metamodel uncertainty and evacuation uncertainty	p. 25
$\widetilde{\boldsymbol{\xi}}^{\boldsymbol{\epsilon}}$,$\widetilde{\xi}^{\epsilon}$	FF (metamodel) integrating the evacuation uncertainty	p. 43
$\widetilde{\boldsymbol{\xi}}^{\boldsymbol{m}}$,$\widetilde{\xi}^{m}$	FF (metamodel) integrating the metamodel uncertainty	p. 41
$\bar{\boldsymbol{\xi}}^{\mathrm{FoM}}$	FF (FoM model)	p. 41
$\bar{\boldsymbol{\xi}}^{\mathrm{LIl}}$	FF (LIl model)	p. 40
$\bar{\boldsymbol{\xi}}^{\mathrm{LIn}}$	FF (LIn model)	p. 40
$\bar{\boldsymbol{\xi}}^{\mathrm{MLS}}$	FF (MLS model)	p. 41
$\bar{\boldsymbol{\xi}}^{\mathrm{SoM}}$	FF (SoM model)	p. 41
$\boldsymbol{\Delta}\bar{\boldsymbol{\xi}}^{m}$,$\Delta\bar{\xi}^{m}$	prediction interval	p. 42
$\boldsymbol{\delta}\widetilde{\boldsymbol{\xi}}^{m}$,$\delta\widetilde{\xi}^{m}$	metamodel uncertainty	p. 41
$\mathrm{D}\widetilde{\xi}^c_q$	largest absolute difference	p. 27

Ξ^*	unclipped FF in the system model without specifications	p. 50
$\widetilde{\Xi}$	FF in the system model	p. 20
$\bar{\Xi}$	FF in the system model based on $\bar{\boldsymbol{\xi}}$	p. 50
$\widetilde{\Xi}^{\epsilon}$	FF in the system model based on $\widetilde{\boldsymbol{\xi}}^{\boldsymbol{\epsilon}}$	p. 50
$\widetilde{\Xi}^{m}$	FF in the system model based on $\widetilde{\boldsymbol{\xi}}^{\boldsymbol{m}}$	p. 50

Greek letters

α	confidence level	p. 27
α^*	empirical confidence level	p. 43
$\boldsymbol{\beta}$	regression coefficients	p. 38
$\widetilde{\boldsymbol{\epsilon}}$,$\widetilde{\epsilon}$	relative evacuation uncertainty	p. 43
η^{ind}	relative effect of a risk factor on individual risk	p. 28
η^{soc}	relative effect of a risk factor on societal risk	p. 28
μ	arithmetic mean	p. 23
ρ^{sp}	Spearman's rank correlation coefficient	p. 28
σ^2_X	variance estimator using the complete data base	p. 40
σ^2_{-i}	variance estimator using the leave-one-out approach	p. 40
ω	weighting parameter for MLS	p. 44

Latin letters (lower case)

b	MLS estimators	p. 41
b_{ls}	least squares estimators of $\boldsymbol{\beta}$	p. 39
d	euclidean distance between two data points	p. 33
erd	euclidean relative difference between two RSMs at evaluation points	p. 51
erd_q	erd between quantiles of two frequency distributions	p. 51
i,j,n	integer for iteration	p. 15
p	probability	p. 18
$\widetilde{\wp}$	polynomial terms of an arbitrary point	p. 39
$p_{stretch}$	stretching parameter	p. 35
$\boldsymbol{s}^2$,s^2	prediction variance	p. 42
$\boldsymbol{s}^2_{q90}$	90%-quantile of the prediction variances $\boldsymbol{s}^2$ at multiple arbitrary points	p. 45
var	variance	p. 38
w	weighting function	p. 41

x	risk factor	p. 14
$\vec{x}$	set of risk factors	p. 14
$\vec{x}^{\text{evac}}$	evacuation scenario	p. 22
$\vec{x}^{\text{fire}}$	fire scenario	p. 22
$\vec{x}_i$	discrete scenario, data point	p. 22
$\widetilde{x}$	random scenario	p. 14

Latin letters (upper case)

$\mathcal{D}$	discrete distribution	p. 15
N_{dps}	number of data points or scenarios in an ED	p. 23
N_{fat}	number of fatalities	p. 14
N_{mami}	number of EDs used for the maximin optimisation	p. 33
N_{mima}	number of EDs used for the minimax optimisation	p. 33
N_{nb}	number of neighbours	p. 44
N_{rep}	number of replications	p. 23
N_{rf}	number of risk factors	p. 14
N_{terms}	number of terms	p. 38
$\boldsymbol{P}$	polynomial terms of the ED X	p. 38
$\mathcal{R}$	risk analysis	p. 27
$\mathcal{R}^{ind}$	individual risk	p. 11
$\mathcal{R}^{soc}$	societal risk curve	p. 11
$\mathcal{S}$	system model simulation	p. 27
$\mathcal{T}$	Student distribution	p. 42
$\mathcal{U}$	uniform distribution	p. 18
$\boldsymbol{W}$	weighting matrix	p. 41
X	experimental design	p. 23
X^{evac}	experimental design for evacuation scenarios	p. 23
X^{fire}	experimental design for fire scenarios	p. 23
X^{FFD}	full factorial design	p. 31
X^{PAD}	projection array-based design	p. 32
$\widetilde{X}$	random scenarios in a Monte-Carlo simulation	p. 14

Contents

A Introduction

App. G.1 defines and explains some '*terms*' highlighted in the text.

A.1 Motivation and objectives

Complexity of real fire scenarios in road tunnels

'As new energy carriers find their way into tunnels, they will, likewise, require further study. Naturally, the primary foci of such future research should be on the fires behaviours and on risks for tunnel users and firefighters' [1, p. 1446]. The need of research on risks of tunnel users becomes even more pressing with view on future huge tunnel projects such as in Sydney [2] or very large fire scenarios in road tunnels in combination with spilled liquids as in a Norwegian road tunnel in 2015 [3].

In real fire scenarios like the one in the Norwegian road tunnel, many '*events*' and interactions take place between the tunnel users, the fire source and the safety measures. For example, the individual alarm of the tunnel users by the perception of smoke depends on the smoke spreading in the tunnel as well as on the individual position of the tunnel user. In case of a tunnel alarm (TA) the fire alarm system detects smoke and alerts all tunnel users simultaneously. In this case, there can be also a failure of the tunnel alarm (FA). A further interaction between the fire source and the safety measures can be illustrated by the emergency ventilation: the ventilation system forces longitudinal ventilation with fans aiming to influence the smoke spread.

These interactions show that real fire scenarios are complex. In general, complex systems can consist of a 'myriad [of] subsystems; each of which can be characterised by a hierarchy of shared or interacting components' [4, p. 85]. In other words complexity 'is linked to the difficulty of predicting system behaviour based on the system's constituents parts' and 'is an acknowledgement of limitations in the understanding of [...]' systems [5, p. 169]. In this sense, the description of future trends in research on tunnel fires emphasises the complexity by acknowledging 'huge gaps in knowledge on fire characteristics inside tunnels' [6, p. 42]. It also highlights the growing 'Interest in use of water-based fire suppression systems in tunnels' as well as that 'Nowadays, the use of alternative fuel vehicles such as electric battery vehicles has been widely spread worldwide.' Thus, the complexity of real fire scenarios might increase in the coming years especially when alternative fuel vehicles 'are running in urban underground tunnels with heavy traffics' [6, p. 42].

Introduction to risk analysis

A '*risk analysis*' provides information to evaluate the effect of safety measures in complex scenarios with the aim of limiting the risks for the tunnel users [7, p. 58]. Risk analysis in this dissertation is understood as the quantification of risks with risk measures. '*Risk*' means the combination of frequencies and '*consequences*' of scenarios where the consequences are expressed in terms of fatalities among tunnel users.

Risk analysis quantifies the frequency and consequences in a high number of random scenarios, i.e. scenarios with random values of risk factors. '*Risk factors*', also named as '*risk indicators*'

in Berchtold 2016 [8] and Berchtold 2018 [9], are factors which have effects on risks of tunnel users, e.g. the maximum heat release rate (HRR). For the quantification of risks, risk analysis uses simplified system models of real fire scenarios. The structure of the system model comprises multiple risk factors. Furthermore, risk analysis directs at random scenarios on the entire domain of risk factors which is named as '*global objective*' [10, p. 17], e.g. fire scenarios with maximum HRRs from five to 200 MW. To be more clear, '*local objective*' in contrast would focus on a single scenario, e.g. for the optimisation of the ventilation system for a maximum HRR of 30 MW.

Complex models can be applied to determine the consequences within the system model. In general, a complex model causes high computational cost. Examples are models based on computational fluid dynamics (CFD) methods like the Fire Dynamics Simulator (FDS) [11], which are named in the following as CFD models. In this dissertation the complex model is a combination of

- a fire model based on a CFD method, which computes the fire scenarios, i.e. the spread of heat and smoke, and considers fire risk factors related to the fire source;
- an evacuation model for the evacuation of tunnel users, which computes the evacuation scenarios obtaining the smoke spread from the fire model and considers evacuation risk factors related to the evacuation of tunnel users as well as fire risk factors to consider the smoke spread;
- and an incapacitation model to determine the occurrence of fatalities.

The uncertainties in a fire model are mostly specified in the risk factors whereas the evacuation model further considers individual characteristics of tunnel users and their variations. These variations cause uncertainties called evacuation uncertainties.

Due to the high computational cost, complex models can only be used to determine the consequences of a limited number of scenarios with discrete values of risk factors, briefly called '*discrete scenarios*'. However, the limited number of discrete scenarios should cover the global objective of risk analysis.

Current state of methodologies for risk analysis of road tunnels

Different methodologies for risk analysis or '*risk assessment*' for road tunnels exist to evaluate the risks of tunnel users and the effects of safety measures. This dissertation exemplifies the current state of the art with some methodologies and in particular focuses on their approaches used to determine the consequences. A more comprehensive overview was published by the World Road Association [12, p. 64ff].

A direct comparison of the following methodologies with the innovative methodology developed in this dissertation was not possible, since these methodologies provide more a framework describing risk factors and boundary conditions rather than detailed calculation methods. Thus, the engineering offices conducting risk analyses often use their own proprietary approaches. Nevertheless, these approaches could adopt parts of this innovative methodology.

The methodologies of Germany [13] and in Austria [14] employ CFD models, both suggesting FDS, to determine the smoke spread in discrete fire scenarios with the maximum HRRs shown in Tab. A.1. The methodology of Austria furthermore combines the CFD model with a one-dimensional tunnel model which provides the initial ventilation conditions influenced by traffic conditions. With regard to the evacuation scenario, the methodology of Germany applies a one-dimensional evacuation model which considers the effects of smoke and temperature on the deterministic walking speed of tunnel users. The methodology of Austria also applies a one-dimensional evacuation model which considers the effect of smoke on the

Table A.1: Overview on fire scenarios with discrete maximum HRRs in different methodologies for risk analysis of road tunnels.

methodology	fire model	maximum HRR
Germany [13]	CFD model (e.g. FDS)	5, 30, 50, 100 MW
Austria (TuRisMo) [14]	CFD model (e.g. FDS) in combination with one-dimensional tunnel model	5, 30, 100 MW
Schubert 2011 [15]	expert judgement	5, 30, 100 MW
The Netherlands [16]	–	5, 10, 25, 50, 100, 200 MW

walking speed as well as variations of individual characteristics of tunnel users. Accordingly, both methodologies employ a combination of a CFD model and a one-dimensional evacuation model to determine the consequences in discrete scenarios.

Furthermore, the methodology of Austria [14] applies the 'mapping approach' to determine the consequences in random scenarios. For this, the methodology uses few fire scenarios analysed with simulations of the CFD model and many simulations of random evacuation scenarios. The evacuation scenarios obtain the smoke spread of the fire scenarios. If a random evacuation scenario requires a fire scenario between two available simulations with the CFD models e.g. with a maximum HRR of 75 MW, then the probabilities of consequences of both neighbouring simulations with the CFD models, i.e. 30 MW and 100 MW, are weighted linearly according to the maximum HRR. In conclusion, the mapping approach is similar to a local linear interpolation of consequences.

The methodology for risk analysis of road tunnels of Schubert 2011 in cooperation with the Federal Roads Office in Switzerland and the Norwegian Public Roads Administration [15] was developed for its application in Switzerland and Norway. This methodology determines the consequences in fire and evacuation scenarios based on expert judgement. The system model comprises 21 risk factors in total, i.e. fire risk factors, evacuation risk factors as well as risk factors for the frequency of the scenario. The structure of the system model consists of a Bayesian network whereas the other methodologies use event trees.

The methodology of the Netherlands [16] considers next to the hazard fire additionally other hazards from dangerous goods. The documentation on the methodology is only available in Dutch language. Thus, the overview here is also based on further documents or publications like in Nelisse 2016 [17]. The methodology uses tabular data and considers the spread of smoke and temperatures in discrete fire scenarios shown in Tab. A.1. It serves as basis for other methodologies in European countries.

Moreover, Berchtold 2014 [18] has shown that methodologies for risk analysis of road tunnels differ in many parts. Examples provided in this dissertation are the different number of risk factors in the system model, e.g. the methodology of Germany with regard to the event tree for the fire scenarios [13, p. 27f] in comparison to the Bayesian network with 21 risk factors in Schubert 2011 [15, p. 18]. The methodologies also determine the consequences with different fire models, either with CFD models, based on expert judgement [15] or with the mapping approach using results of simulations of complex models for random scenarios as in the methodology of Austria [14].

Introduction to the metamodel

The mapping approach constitutes an example for the application of a metamodel in a

methodology for risk analysis of road tunnels. The methodology of Austria applies it to get the consequences of a high number of random scenarios required for risk analysis. Namely, it derives the consequences by local linear interpolation. In more detail, a metamodel is 'A model which is intended to give an all-inclusive picture of a process, system, etc., especially by abstracting from more detailed individual models contained within it' [19]. Or in other words, it is a 'model of the system being modelled by the computer simulation' [20, p. 481] which in brief means that a metamodel is a model of the complex model.

The metamodel uses results, i.e. consequences, of few discrete scenarios computed with the complex model and determines the consequences of many random scenarios with low computational cost. As a result, it represents the unknown consequences of the complex model for random scenarios which are then adopted in the risk analysis. Principally, the metamodel consists of three parts e.g. summarised in Queipo 2005 [21, p. 3]: first, the experimental design (ED); second, the data base for results of scenarios computed with the complex model; and third the response surface model (RSM).

Since the metamodel simplifies the complex model and given that simplifications cause 'model uncertainties' which are the 'inability of [...] models to accurately represent the true physical behaviour of the system' [22, p. 9], metamodels cause 'metamodel uncertainties'. The metamodel uncertainty depends on the number of scenarios in the data base. Thus, an efficient metamodel reduces the number of simulations of scenarios with the complex model which are required to get an adequate RSM, namely shown by '*verification*' and '*validation*'.

Motivation and objectives of this dissertation

Looking at the differences in methodologies for risk analysis of road tunnels and on the increasing complexity of real fire scenarios, this dissertation bases on *assumption 1 (complex scenarios): the analysis of consequences in complex scenarios requires complex models as well as multiple risk factors*. In more detail, the complex model is able to reproduce interactions in complex scenarios, e.g. the smoke spread in the tunnel, the individual alarm of tunnel users by the perception of smoke or interactions between the ventilation system and the smoke spread. Multiple risk factors are required e.g. for the HRR of the fire including the fire growth, the evacuation of tunnel users as well as the failure of safety measures.

Since risk analysis directs at complex scenarios with the global objective, assumption 1 can arise to a challenge: complex models with their high computational cost and the global objective limit the number of risk factors and the number of scenarios computed with the complex model. But both limitations impose therefore constraints to the complexity of scenarios which can be considered in risk analysis. Concerning the limitation of risk factors, for instance, experiments show large variations in the time to the maximum HRR, i.e. the risk factor which describes the fire growth [23, p. 3]. But the methodology of Austria explicitly avoids a variation of the time to the maximum HRR in order to reduce the number of simulations with the CFD model [14, p. 21]. Consequently, possible effects of the time to the maximum HRR on consequences, e.g. in relation to the time of tunnel users required for evacuation or the time to full emergency ventilation, are not taken into account. Concerning the limitation of the number of scenarios, the consequences are determined only for discrete scenarios with maximum HRRs of e.g. 30 MW and 100 MW. But there might be unknown interactions between the maximum HRR and the consequences, for instance, the smoke layer might affect the tunnel users only above a specific maximum HRR. Then, there will be a strong change in the consequences of scenarios around this specific maximum HRR. Only two discrete scenarios can obviously not replicate this strong change. These different consequences might be important for risk analysis which for this reason directs at a high number of different scenarios. Another conclusion of the challenge might be to avoid complex models, e.g. as in

the methodology for Switzerland and Norway of Schubert 2011 [15]. But without complex models difficulties in modelling of interactions and thus of their effect on consequences may arise, e.g the individual alarm of tunnel users or the TA which depends on the spread and the detection of smoke. Concluding, the application of complex models to increase the complexity of scenarios can actually reduce the complexity of scenarios by neglecting possible interactions.

The motivation of this dissertation is to overcome this challenge and to allow to consider an increased complexity of scenarios in risk analysis of road tunnels to take into account the growing complexity of real fire scenarios. For this reason, this dissertation develops an innovative methodology for risk analysis of road tunnels which aims at two objectives.

- *Objective 1 (metamodel)* is to introduce *a metamodel to integrate complex scenarios, in more detail complex models and multiple risk factors, into the risk analysis.* For this: *a) the RSM should represent the unknown results of the complex model with focus on the global objective*; *b) the metamodel should reproduce the evacuation uncertainty of the complex model*; and *c) the methodology for risk analysis should lead to reproducible results.* Objective 1a and objective 1c seem to be obvious. But objective 1a directs in particular on the global objective which is essential for risk analysis and objective 1c is important because the results of risk analysis should be independent from the specific metamodel.
- *Objective 2 (efficiency) is the efficiency of the metamodel to allow to focus on the complexity in scenarios.* The efficiency is not quantified in comparison to other metamodels since the results are specific to the data base. But it is realised by the metamodel itself as well as by the specification of particular approaches within the metamodel.

To sum up, this dissertation focuses on the metamodel within the methodology for risk analysis of road tunnels. Thus, the methodology for risk analysis bases on the hypothesis that a metamodel is able to solve the challenge. To be noted, the combinations of fire, evacuation and incapacitation models to a complex model is readily available and for this reason is not examined in detail in this dissertation.

Finally, there is ongoing work on the 'validation' of and to increase the 'trust in risk management' [24, p. 123] because for risk analyses in safety science the 'quality control mechanisms for assessing the credibility [...] and the validity of their results are not equally well developed' compared to other scientific disciplines. To follow this work, this dissertation attempts to validate the results of the methodology for risk analysis by questioning their plausibility. With the focus of this dissertation on the metamodel and the knowledge on the metamodel uncertainty and the evacuation uncertainty, this dissertation states *assumption 2 (plausibility): the metamodel uncertainty and the evacuation uncertainty are required to increase the plausibility of results of risk analysis.*

Expected impact

The methodology for risk analysis together with the metamodel of this dissertation can have an impact in three different parts. First, since the methodology for risk analysis aims at objective 1 and objective 2, it allows an increased complexity of scenarios. Bearing the growing complexity of real fire scenarios in mind, an influence on other methodologies for risk analyses of road tunnels can be expected. Second, due to the efficiency of the metamodel, the methodology can be also interesting for risk analysis of other complex systems with focus fire safety engineering. For this reason, the flexibility of methods is one argument for their selection, esp. for the system model and the complex model. Third, as a consequence of the general applicability of the metamodel and due to objective 1 and objective 2, the metamodel can also support in various issues with similar challenges, i.e. related to complex models but

also complex experiments with multiple '*variables*' and global objective, like the assessment of the safety of structures.

A.2 Outline

According to its objectives, this dissertation proposes and evaluates an innovative methodology for risk analysis of road tunnels. For this, it parts into the five following chapters. Chapter B, Chapter C and Chapter D describe the methodology developed in this dissertation. They split up into two parts: the first section introduces the theory in general whereas the following sections detail the methods and models applied in the methodology of this dissertation. Subsequently, the fifth chapter evaluates the methodology and queries the assumptions and objectives. Finally, the last chapter summarises the results and concludes with regard to the expected impact.

Chapter B illustrates the entire methodology and introduces the basic terms. It begins with the approach to quantify risks and proceeds with the fire and evacuation scenario in the system model. Yet, its focus lies on the model to determine the consequences, namely the consequence model, and therewith also on the complex model, its CFD model and microscopic evacuation model, as well as the metamodel.

Next, Chapter C details the first part of the metamodel. The ED is subjected to the projection array-based design method of Leoppky 2012 [25] which in particular provides the basis for objective 2 (efficiency). And, since this method extends the Latin hypercube design [26], it also suffices objective 1 (metamodel). So, after its reasoned selection, the algorithms in the projection array-based design method are explained, esp. with respect to the assumptions and objectives.

After the complex model and the ED which together result in the second part of the metamodel, the data base, Chapter D completes the metamodel describing the RSM, the metamodel uncertainty and the evacuation uncertainty. In detail, the RSM derives from the response surface method moving least squares [27]. Moving least squares was selected in order to meet assumption 1 (complex scenarios) and to provide the basis for objective 1 (metamodel). Correspondingly, the metamodel uncertainty is based on the prediction interval method by Kim 2008 [28]. And last but not least, the 'direct approach' was originally developed in this dissertation to reproduce the evacuation uncertainty of the complex model according to objective 1 (metamodel). The idea for the direct approach stems from the averaged variance in Salemi 2016 [29]. Therefore, next to the description of these three methods, the chapter also outlines approaches for their verification, '*calibration*' and validation.

The evaluation in Chapter E concentrates on the assumptions and objectives in this dissertation as condensed in Tab. A.2. Section E.1 covers all data bases used in the system model and therewith establishes the first and the second part of the metamodel. Consecutively, Section E.2 directs at the RSM subjected to moving least squares but it also studies the prediction interval method, i.e. the metamodel uncertainty arising from the RSM. The aims of this section are to specify the default RSM used for subsequent evaluations as well as to validate both methods. To complete the evaluation of the metamodel, the evacuation uncertainty within the complex model is first assessed in Section E.3 and second, the direct approach is calibrated and validated. Afterwards, Section E.4 is dedicated to the results of risk analysis. In particular, it questions: the effects of the metamodel uncertainty and of the evacuation uncertainty; the reproducibility of the results; as well as the effects of risk factors. And to conclude, it scrutinises these results as an attempt for the validation of the entire methodology for risk analysis.

Table A.2: Assumptions (A) and objectives (O) investigated in the sections of Chapter E; the highlighted sections reason their final evaluation.

A1	O1a	O1b	O1c	O2	A2
E.4.3	E.2.1	E.2.1	E.2.1	*E.2.2*	E.4.1
	E.2.2	E.3.1	*E.4.2*		*E.4.4*
	E.2.3	*E.3.2*	E.4.4		
	E.2.4				
	E.2.5				

At the end of this dissertation, the assumptions and objectives are revisited in Chapter F and summarised with their confirmation or refutation. Additionally, it is argued why this dissertation can advance risk analyses not only for road tunnels but also for fire safety engineering in general. Then, the chapter focuses on the expected impact, in particular, that the metamodel can be not only applied on complex models but also on time consuming experiments. Lastly, the it stresses the contribution of the direct approach to the expected impact.

A.3 Current state of research

The current state of research of this dissertation splits up into the different parts of the methodology for risk analysis. In more detail, it is described at the beginning of each chapter from Chapter A to Chapter D, namely in:

- Subs. 'Current state of methodologies for risk analysis of road tunnels' (p. 2) in Chapter A;
- Subs. 'Current research on methodologies for risk analysis in fire safety engineering' (p. 9) as well as Subs. 'Current research on the theory of risk analysis' (p. 13) in Chapter B;
- Subs. 'Current methods for EDs' (p. 31) in Chapter C;
- and finally, an overview on response surface methods in Section D.1.2.

The latter two chapters describe the current state of research which derives from a structured literature overview and respectively leads to the choice of the projection array-based design method and of moving least squares. Summing up, the first section of each chapter sketches the theoretical framework whereas the following sections detail the methods and models applied within the methodology.

The literature referenced in this dissertation comes from a literature study which was not limited to but considered in particular publications with regard to methodologies for risk analysis, the system model of the road tunnel and the application of metamodels. It was performed over the entire period of this dissertation and based mainly on: the structured literature overviews on ED methods and response surface methods; commonly known relevant books, further references of publications as well as different sources in the internet; and a monthly review of journals. This monthly review comprised the following six journals published by Elsevier, Springer or Wiley: Fire Safety Journal, Fire Technology, Reliability Engineering and System Safety, Risk Analysis, Safety Science, and Tunnelling and Underground Space Technology. Thus, these peer reviewed journals were central to the literature study and cover the research fields fire, risk and tunnels.

In total, the literature study comprises approximately 350 review or research articles, 100 chapters or contributions of about 75 books or proceedings, and 60 standards or other reports.

These publications were studied with a different level of detail, i.e. from an overview to a comprehensive understanding of their content. Finally, the study resulted in about 1700 personal notes structured and tagged with an open source software for reference management and knowledge organisation.

B Innovative methodology for risk analysis

This dissertation concentrates on the development of a metamodel used for risk analysis of road tunnels. But first, all parts of the methodology for risk analysis are introduced. Section B.1 explains the decisions for the methods, models and approaches in these parts and finally sets them in relation to current research on the theory of risk analysis. Then, Section B.2 outlines the approach for risk analysis using the Monte-Carlo method and Section B.3 illustrates the system model emphasising the graph as well as the fire and evacuation scenario. Next, Section B.4 describes the consequence model with focus on the metamodel. And finally, Section B.5 closes with methods used to evaluate the methodology for risk analysis.

B.1 Overview on literature

Next to the different methodologies for risk analysis outlined in Section A.1, also a variety of methodologies in fire safety engineering with other focus than road tunnels exist. These methodologies are subjected to a higher variety of methods and models for they are less specialised on their application in practice than the methodologies for risk analysis of road tunnels. Subs. 'Current research on methodologies for risk analysis in fire safety engineering' (p. 9) sketches the current state with some examples. This overview helps to identify several methods, models or approaches applied in the methodology for risk analysis of this dissertation which then contribute to its innovation. Hence, the subsequent subsections outline: the system model used for risk analysis; the consequence model; the metamodel uncertainty and the evacuation uncertainty; as well as the current state of research on the theory of risk analysis.

Current research on methodologies for risk analysis in fire safety engineering

Some publications were selected from the literature study conducted during this dissertation to give a short overview on the current state of research on risk analysis in fire safety engineering. These publications do not necessarily describe comprehensive methodologies for risk analysis but may also concentrate on specific parts. Additional criteria for the selection were the recency as well as the use of fire models, e.g. based on CFD methods. The publications are condensed in this subsection with regard to the system model, the consequence model and, if available, the metamodel.

To begin, Albrecht 2014 [30] expresses the life safety in a multi-purpose community assembly building with the probability for safe evacuation. The probability for safe evacuation derives from a comparison of the required safe egress times with the available safe egress times of random scenarios. On the one side, a 'simple evacuation' [31, p. 1060] model determines the required safe egress time in evacuation scenarios with one evacuation risk factor and three '*environmental variables*'. And on the other side, the fire model FDS analyses the available safe egress time in fire scenarios depending on five fire risk factors. More precisely, the available safe egress times of the random scenarios stem from a metamodel with a central composite design as ED and moving least squares as response surface method [31]. The metamodel is set up in sequential refinement steps to reduce the metamodel uncertainty as

well as the number of risk factors. The sequential refinement of the metamodel directs at the local objective, namely where the available safe egress time equals the required safe egress times.

Next, the methodology published by de Sanctis 2016 [32] aims at the risk-based optimisation of the door width in a retail building in case of fire. For this, it compares available safe egress times with the required safe egress times in random scenarios and finally obtains the life quality index. The required safe egress time depends on three evacuation risk factors and five environmental variables and is quantified with a one-dimensional evacuation model. The fire model computes the available safe egress time in fire scenarios with four risk factors. Describing the selection of the fire model, the publication reasons that CFD models are more appropriate in case of emergency ventilation with fans whereas zone models are suitable for compartment fires without emergency ventilation. Accordingly, the zone model OZone determines the smoke layer thickness. Then, the height of the smoke-free layer is assumed to be uncertain. At last, a metamodel with polynomial chaos expansion and 10^4 'quasi-random' data points with the uncertain results from OZone lead to the probability density function of the required safe egress time.

Weyenberge 2017 [33] describes a risk analysis for life safety in a multi-purpose community assembly compartment. It refers to Weyenberge 2016 [34] which only sketches a methodology for risk analysis but details the bow-tie structure used as the structure of the system model in a rail tunnel. The risk analysis of Weyenberge 2017 [33] consists of successive parts: the fire model FDS; the metamodel for the fire model; the evacuation model; the metamodel for the evacuation model; the incapacitation model; and finally the reliability analysis. The main focus lies on the comparison of two metamodels for the fire model, both with Latin hypercube designs as EDs but with the different response surface methods moving least squares and polynomial chaos expansion. For the comparison, the metamodels are validated with an additional validation set. Then, they quantify the CO concentration in fire scenarios with three risk factors plus two spatial and one temporal variables. At the end, the publication gives an outlook to include uncertainties in the metamodel for the evacuation model with variables describing the group of occupants, i.e. risk factors, and environmental variables for individual characteristics of occupants.

Most recently, Anderson 2018 [35] conducted a risk-based analysis of the community-averaged extent of fire damage in residential buildings of the United States. In particular, the study comprises representative single family homes based on statistical data. It investigates the consequence 'floor area of a home damaged by a fire' in more than 5000 random scenarios applying the zone model CFAST. Arguments for the decision for CFAST were 'familiarity to the authors, speed of computation, and its history of verification and validation' and 'other potential options' for the fire model would have been the 'Fire Dynamics Simulator (FDS) or New Zealand's BRANZFIRE' in Anderson 2018 [35, p. 6].

Risk analysis and the system model

Beside from event trees, methodologies for risk analysis also apply different structures for their system models like the bow-tie structure in Weyenberge 2016 [34] or Bayesian networks in Schubert 2011 [15]. The bow-tie structure splits the scenario in a fault tree which specifies the 'critical event' e.g. the fire in the road tunnel, and the event tree leading to the consequences. In contrast, Bayesian networks combine the description of the scenario and the determination of consequences in a single directed acyclic graph. This graph is 'efficient in regard to the graphical representation of complex systems' [15, p. 14]. In other words, its clear structure supports the flexibility for adaptions in the system model and also for

other complex systems than road tunnels. Because of this flexibility, a directed acyclic graph establishes the structure of the system model in this dissertation.

The system model serves to analyse the frequency and consequences in random scenarios. To generate the random scenarios, the methodologies for risk analysis commonly carry out Monte-Carlo simulations. For risk analysis, it is essential to cover scenarios with rare events because of their potentially high consequences, for instance the large fire with spilled liquids mentioned in Section A.1. In the understanding of this dissertation, a rare event is linked to the FA in combination with a maximum HRR of 100 MW. The latter value derives from the methodologies for risk analysis of road tunnels esp. from Germany, shown in Tab. A.1 (p. 3). Since scenarios with rare events have small frequencies in a Monte-Carlo simulation, risk analysis requires a high number of random scenarios to consider their consequences appropriately. For example, importance sampling in the Monte-Carlo method [36, p. 296] reduces the required number of random scenarios by adapting the frequency of rare events with the aim to increase the frequency of random scenarios with rare events.

After the Monte-Carlo simulation, risk analysis ends with the quantification of risks with risk measures. Common risk measures in risk analysis of road tunnels are the individual risk and the societal risk [12, p. 21, 28]. Other risk measures are for example: first, the probability of safe evacuation in Albrecht 2014 [30]; second, measures which do not consider the safety of occupants like the floor area in Anderson 2018 [35]; or third, based on financial aspects to value the life of an occupant in Schubert 2011 [15] or de Sanctis 2016 [32]. But the first and second of the other measures are not in the meaning of 'risk' used in this dissertation and the third of these measures demands additional variables. Concluding, with the focus of this dissertation on the metamodel, the risks are quantified with the common risk measures individual risk and societal risk.

In general, the individual risk $\mathcal{R}^{ind}$ is defined as the 'Measure of fire risk limited to consequences experienced by an individual and based on the individual's pattern of life' [37, p. 3] and the societal risk $\mathcal{R}^{soc}$ is the 'Measure of fire risk combining consequences experienced by every affected individual' [37, p. 4]. Applied on road tunnels, the individual risk is '*the probability that an average unprotected person, permanently present at a certain location, is killed due to an accident resulting from a hazardous activity*' [38, p. 383] and the societal risk '*reflects the relationship between frequency and the number of people suffering from a specified level of harm in a given population from the realization of specified hazards*' [38, p. 383].

Consequence model

Both risk measures take into account the frequency and the consequences of random scenarios. The frequency of fires in road tunnels can be quantified as exemplified in Nelisse 2016 [17], even for fires with rare events and small statistical basis. With regard to the consequences, the quantification on basis of statistical data is e.g. possible for single family houses in case of small fires [39]. But the frequency of real fire scenarios in road tunnels is very small [15, p. 65f; 38, p. 385] and the frequency of fire scenarios with consequences in terms of fatalities is evidently lower. This fact explains the lack of empirical models for consequences in road tunnels and the few models based on expert judgement, e.g. in Schubert 2011 [15, p. 65f]. Therefore, the term 'consequences model' in this dissertation means the model used to determine the consequences on the basis of a complex model, namely a '*deterministic fire model*', a '*stochastic evacuation model*' and an incapacitation model.

The consequence models of methodologies for risk analysis in fire safety engineering usually apply CFD models for the fire model but also zone models where appropriate. Then, they mostly combine the fire model with a one-dimensional evacuation model. Looking at the incapacitation model, the methodologies often refer to threshold values e.g. for the optical

density in Albrecht 2011 [31], the height of the smoke-free layer in de Sanctis 2016 [32] or the carbon monoxide concentration in Weyenberge 2017 [33]. An alternative is the cumulative fractional effective dose during the evacuation of occupants, e.g. in the methodology of Albrecht 2011 [31] or is discussed in Weyenberge 2017 [33]. Moreover, the consequence model can also comprise a metamodel, for example the mapping approach in the methodology of Austria [14] for risk analysis of road tunnels. Other methodologies use metamodels for deterministic results of the CFD models in Albrecht 2011 [31], in Weyenberge 2017 [33] or for results of a deterministic zone model also subjected to uncertainties in case of de Sanctis 2016 [32].

This summary provides the background for conclusions on the consequence model in this dissertation. First, a CFD model is used as fire model to account the interactions in complex scenarios. Second, the evacuation of tunnel users is computed with a microscopic evacuation model despite the common use of one-dimensional evacuation models in other methodologies for risk analysis. This choice has two reasons: to evaluate whether microscopic evacuation models are required with respect to complex scenarios; and to increase the flexibility of the methodology for other complex systems. Third, the fractional effective dose by Purser [40] models the incapacitation because of the cumulative effect of smoke on tunnel users. Furthermore, the fire model as well as the evacuation model were also chosen in order to question assumption 1 (complex scenarios). For the same reason, the fire scenario considers two fire risk factors for the HRR and the evacuation scenario depends on three evacuation risk factors to describe the tunnel users as well as the failure of tunnel alarm. And last but not least, the metamodel is also a part of the consequence model as stated in objective 1 (metamodel) to integrate complex scenarios into risk analysis with its global objective. With respect to objective 2 (efficiency), sequential refinement, as in Albrecht 2014 [30], could improve the efficiency of the metamodel but with the global objective and not with the local objective. To sum up, the decision for a CFD model, a microscopic evacuation model, the number of risk factors, as well as the metamodel comply with the objectives and assumptions in Section A.1 and contribute to the innovation of the methodology of this dissertation.

Metamodel uncertainty and evacuation uncertainty

In general, Der Kiureghian 2009 [41, p. 105ff] distinguishes uncertainties in two types. On the one hand, epistemic uncertainties are 'caused by the lack of knowledge' to which 'the modeller sees a possibility to reduce them by gathering more data or by refining models'. On the other hand, aleatory uncertainty originate from an 'intrinsic randomness of a phenomenon' and the 'modeller does not foresee the possibility of reducing them'. And additionally, 'it is the job of the model builder to make the distinction'. These definitions allow to categorise the metamodel uncertainty as well as the evacuation uncertainty introduced in Section A.1 into these two types and to generalise their application. Since the 'inaccuracy of the metamodels can be interpreted as the metamodel uncertainty where the true response is unknown except at the sample points' [28, p. 1] and the 'inaccuracy' of the metamodel could be reduced by sequential refinement, the metamodel uncertainty is an epistemic uncertainty. The methodology by de Sanctis 2016 [32] describes model uncertainties in the 'smoke layer thickness' which is an example for another epistemic uncertainty. Next, the evacuation of tunnel users is subjected to 'intrinsic' randomness [42, p. 178; 43, p. 1; 44, p. 166] due to environmental variables like individual characteristics of tunnel users. Accordingly, the evacuation uncertainty is considered to be an aleatory uncertainty.

The methodologies for risk analysis in fire safety engineering account the metamodel uncertainty and the evacuation uncertainty in different ways. The metamodel uncertainty is either used for: refinement of the metamodel with the aim of reducing metamodel uncertainty in

Albrecht 2014 [30]; and the validation of the metamodel in Weyenberge 2016 [34]. But both methodologies do not transfer the metamodel uncertainty to the results of risk analysis. The evacuation uncertainty arises from variations in individual characteristics of occupants in the methodologies of Austria [14], of Albrecht 2014 [30] or of de Sanctis 2016 [32]. And also the methodology published in Weyenberge 2017 [33] provides an outlook to include evacuation uncertainties into the metamodel. To conclude, this dissertation innovatively integrates the metamodel uncertainty and evacuation uncertainty into the metamodel and in the results of risk analysis, esp. with regard to assumption 2 (plausibility).

Current research on the theory of risk analysis

Subs. 'Risk analysis and the system model' (p. 10) shows that the approach used for risk analysis in this dissertation is also common in other methodologies for risk analysis in fire safety engineering. This approach refers to the definition of risk provided in Subs. 'Terms related to risk analysis' (p. G-1) of App. G.1 and applies Monte-Carlo simulations for its calculation. But there is lots of research on the theory of risk analysis itself. Thus, this subsection briefly sketches few publications to show the current state of research and then closes with their relation to this dissertation.

To begin, Goerlandt 2017 [24] summarises and discusses the current research on the theory to risk. For instance, Goerlandt 2017 refers to critical reviews like Pasman 2017 [45]. This publication reveals weaknesses in methods used for the quantification of consequences in risk analysis of the oil and gas industry.

Aven provides the theoretical background for several publication in Goerlandt 2017 [24]. In detail, Aven 2012 [46] comprehensively describes the theory to risk analysis. Aven 2012 begins with the historical development of risk analyses and then introduces the classical approach using Monte-Carlo simulation to model probabilities. Afterwards, this classical approach is criticised because the 'Risk is a constructed quantity that puts focus in the wrong place, on measuring fictional quantities' [46, p. 36]. Accordingly, Aven 2012 [46, p. 47ff] proposes another concept of risk. In this concept, risk is understood as consequences of events and their associated uncertainties. In particular, it includes further background knowledge on the uncertainties. Together with several other publications, Aven 2014 [47] puts this concept into a conceptual risk framework, e.g. to avoid simplifications in models with the aim to increase the knowledge on uncertainties.

Next, Berner 2016 [48] contributes to the proposed concept of risk by Aven 2012 [46] and therefore describes an approach to decide which assumptions within a risk analysis have to be strengthened by further knowledge. This approach consists of six settings. The last setting refers to assumptions having high effect on the risk measure but they base only on poor knowledge and there is a high belief that this assumption might not be true. Berner 2016 further discusses this case and for instance suggests to apply 'imprecise probabilities' to these assumptions.

Coming back to the issue of complexity introduced in Section A.1, Jensen 2018 defines 'an activity is considered complex if we have poor knowledge about the consequences of the activity' [5, p. 171]. After profound discussion from different perspectives, Jensen 2018 concludes that the 'concept of risk makes sense in conjunction with complex systems' but the 'lack of knowledge regarding causal chains [...] make the [...] the assessment of risk difficult' [5, p. 173]. The first conclusion also yields for the concept of risk applied in this dissertation in particular and also in general for fire safety engineering.

Additional to Jensen 2018 [5], Haimes 2018 [4, p. 95f] develops ten guiding principles for risk analysis of complex 'systems of systems'. These principles for instance are: the 'metamodeling and subsystems integration', which 'must derive from the intrinsic states of the

system of system'; the consideration of 'epistemic and aleatory uncertainty'; and to 'account for risks of low probability with extreme consequences'.

Last but not least, Hansson 2014 [49] asks in the title: 'Is risk analysis scientific'? To answer this question, Hansson 2014 discusses important elements of science and therewith mentions aspects like: the aim of science to find the 'most reliable knowledge'; its 'capability of self-improvement'; 'hypothesis testing' as well as the 'acceptance of different types of explanations'. Hansson 2014 also remarks that 'the representation of epistemic uncertainty is a major challenge for risk analysis' [49, p. 1180] and finally, comes to the conclusion that: 'risk analysis is scientific, when understood as consisting of [...] knowledge about risk-related phenomena, [and of] [...] approaches [...] to [...] assess [...] risk' [49, p. 1181]. Thus, this conclusion is also true for the risk analysis in this dissertation.

To sum up, the current research on the theory of risk analysis address several issues which are also related to this dissertation. First, the challenge stated in Section A.1 copes with the complexity within the calculation of consequences and the use of complex models also emphasised in Haimes 2018 [4], Jensen 2018 [5], Pasman 2017 [45] and Aven 2014 [47]. Second, the concerns with epistemic uncertainties in Haimes 2018 and Hansson 2014 [49] which matter not only within the metamodel but also in the complex model of this dissertation. Third, the consideration of rare events with large consequences described in Haimes 2018 and Berner 2016 [48] is also discussed in Subs. 'Risk factors' (p. G-5) of App. G.2. Concluding, several developments can be made within the methodology for risk analysis developed in this dissertation but up to now, the focus is on the metamodel.

B.2 Risk analysis

The results of a risk analysis derive from random scenarios of a Monte-Carlo simulation. For this, the system model specifies a random scenario with specific random values of all risk factors and calculates its frequency f_{sc} in $\frac{1}{year}$ where the subscript means 'scenario' and its fraction of fatalities (FF) ξ. The FF results from Eq. B.1 with the number of fatalities N_{fat} and the number of tunnel users N_{tu}. Additionally, Tab. B.1 introduces the notation for risk factors and random scenarios.

Table B.1: Notation used to denote risk factors and scenarios.

notation	description
x	risk factor
$\vec{x} = [x_1, \ldots]$	set of risk factors
$\widetilde{x}$	random scenario with random values of the risk factors $\vec{x}$
N_{rf}	number of risk factors, $N_{\mathrm{rf}} \equiv \|\vec{x}\|$
$\widetilde{X}$	random scenarios of a Monte-Carlo simulation, i.e. $\widetilde{x} \in \widetilde{X}$
N_{mcs}	number of random scenarios in a Monte-Carlo simulation $N_{\mathrm{mcs}} \equiv \left\|\widetilde{X}\right\|$

$$\xi = \frac{N_{fat}}{N_{tu}} \tag{B.1}$$

A rare event in a random scenario of a Monte-Carlo simulation is caused by a specific value x_i of at least one risk factor with a low probability in its original discrete probability distribution, namely $\mathcal{D}_{or}(x_i) = \varepsilon$ with $\varepsilon \approx 0$. In order to increase the frequency of a random scenario with this rare event, importance sampling adapts the original probability distribution to $\mathcal{D}_{is}$ with

$\mathcal{D}_{is}(x_i) > 0$. Consequently, this adaption needs adjustments in the frequency of the random scenario, i.e. the frequency is weighted with the weighting factor shown in Eq. B.2.

$$\omega_{is,i} = \frac{\mathcal{D}_{or}\left(x_i\right)}{\mathcal{D}_{is}\left(x_i\right)} \tag{B.2}$$

Both risk measures, the individual risk and the societal risk, consider importance sampling. Eq. B.3 defines the individual risk $\mathcal{R}^{ind}$ with the index i denoting the different random scenarios of the Monte-Carlo simulation. Societal risks are usually expressed in societal risk curves $\mathcal{R}^{soc}$ given in Eq. B.4 and first exemplified in Fig. E.18b (p. 80). In more detail, the frequency of all random scenarios with a specific number of fatalities N_{fat} of the societal risk curve is given in Eq. B.5. The part of the societal risk curve with small numbers of fatalities is called the 'lower part' in contrast to the 'upper part' for high numbers of fatalities up to the upper limit $N_{fat,max}$. To concentrate on reproducible results, societal risk curves in this dissertation are reduced to numbers of fatalities that exceed a frequency of $\mathcal{R}^{soc}\left(N_{fat}\right) > 10^{-8}\frac{1}{year}$.

$$\mathcal{R}^{ind} = \frac{1}{N_{\text{mcs}}} \sum_{i=1}^{N_{\text{mcs}}} \omega_{is,i} \cdot f_{sc,i} \cdot \xi_i \tag{B.3}$$

$$\mathcal{R}^{soc} = \left[\mathcal{R}^{soc}\left(N_{fat}=0\right), \mathcal{R}^{soc}\left(N_{fat}=1\right), \ldots, \mathcal{R}^{soc}\left(N_{fat}=N_{fat,max}\right)\right] \tag{B.4}$$

$$\mathcal{R}^{soc}\left(N_{fat}\right) = \frac{1}{N_{\text{mcs}}} \sum_{i=1}^{N_{\text{mcs}}} \omega_{is,i} \cdot f_{sc,i} \cdot \delta_K \quad \text{with} \quad \delta_K = \begin{cases} 1 \text{ for } N_{fat,i} \geq N_{fat} \\ \text{else } 0 \end{cases} \tag{B.5}$$

B.3 System model

The system model simplifies real fire scenarios for risk analysis. To explain the system model: first, the structure of the system model is outlined; second, the scenario is illustrated qualitatively; and finally, the risk factors and the entire structure of the system model are detailed more precisely.

Graph structure of the system model

A review illustrated in Berchtold 2014 [18] first provided the basis for the graph of the system model. Here, Fig. B.1 depicts the directed acyclic graph used as structure of the system model and App. G.3 briefly outlines its implementation. The directed edges of the graph connect the parent nodes to their subsequent nodes. And the nodes of the graph are split up into risk factors and intermediate nodes. The former ones describe the random scenario and the latter ones help to structure the graph clearly.

According to Berchtold 2016 [8], the system model can be divided into the three subsystems frequency, fire and evacuation connected to the frequency model, the fire model and the evacuation model respectively. But the system model in Berchtold 2016 [8] comprises twelve risk factors whereas the system model in this dissertation distinguishes between eight risk factors and six intermediate nodes. This discrepancy derives from Berchtold 2016 [8] which first, includes the failure of tunnel alarm in the risk factor 'time of tunnel alarm', second, does not consider the nodes 'frequency of scenario' and 'fraction of fatalities', but third, considers the specific frequency of fire to be a risk factor. Now, the system model amalgamates the specific frequency of fire and the intermediate node frequency of scenarios as detailed in

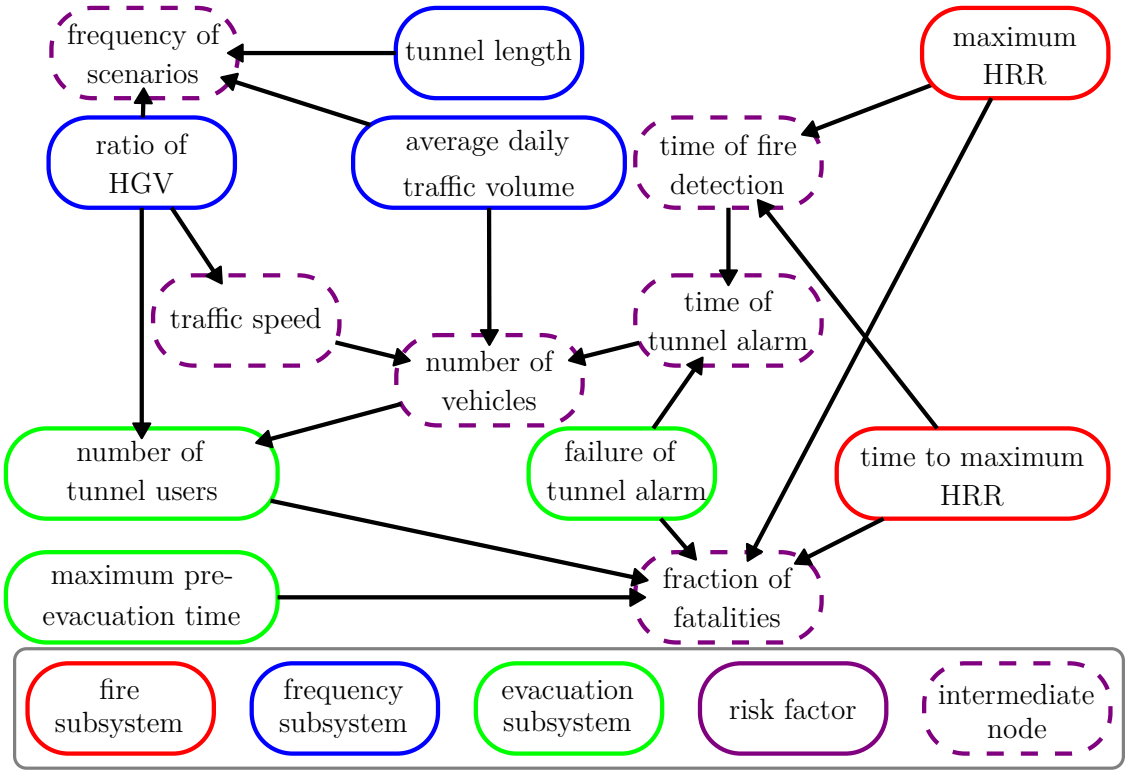

Figure B.1: Graph structure of risk factors and intermediate nodes highlighting the subsystems for: frequency, fire and evacuation and frequency which are connected to the frequency model, fire model and evacuation model.

App. G.2.3. These differences yield the two additional nodes in the system model of this dissertation. Hence, both system models are equal, but the illustration and notation changed.

Tab. B.2 shows the brief notation for the risk factors. For the sake of brevity and without loss of information in the text, the brief notation serves for both, to name the node and to symbolise its results. Only the node 'fraction of fatalities' is briefly denoted with 'node FF' to clearly differentiate between the node and its results.

Table B.2: Probability distributions of risk factors: default models (above); and additional uniform distributions $\mathcal{U}$ for HRR_{max} and N_{tu} (below).

risk factor	notation	model
maximum HRR (default)	HRR_{max}/MW	$\mathcal{D}(\{5, 30, 50, 100\}) = \{0.9, 0.09, 0.009, 0.001\}$
time to maximum HRR	t_{max}/s	$\mathcal{U}(600, 1200)$
maximum pre-evacuation time	t_{pre}/s	$\mathcal{U}(100, 300)$
number of tunnel users (default)	N_{tu}	analytical model
failure of tunnel alarm	fa	$\mathcal{D}(\{\mathrm{TA}, \mathrm{FA}\}) = \{0.99, 0.01\}$
ratio of HGV	χ_{HGV}	$\mathcal{U}(0.05, 0.45)$
average daily traffic volume	$\dot{N}_{adtv}$/(veh. / day)	$\mathcal{U}(5000, 40000)$
tunnel length	l_{tunnel}/km	$\mathcal{U}(1, 3)$
maximum HRR (uniform)	HRR_{max}/MW	$\mathcal{U}(25, 200)$
number of tunnel users (uniform)	N_{tu}	$\mathcal{U}(30, 180)$

To sum up, the risk factors and intermediate nodes in the graph specify each fire and evacuation scenario.

Fire and evacuation scenario

Fig. B.2 depicts the bi-directional road tunnel with two lanes, a width of 9.5 m, a height of 4.5 m and a slope of 1%. The tunnel length varies within the system model according to its risk factor but the domain of the complex model is fixed to 650 m. App. G.2.1 provides further information on this geometry, the layout and the equipment which in summary represents a common road tunnel in Germany and is conform to German legislation [50].

The fire scenario begins with the ignition of a vehicle after an accident or a technical defect. Its frequency f_{sc} is affected by the risk factors average daily traffic volume $\dot{N}_{adtv}$ and tunnel length l_{tunnel}. The ignition initiates a tailback of vehicles but still more vehicles enter the tunnel. Then, the HRR of the fire grows depending on the risk factors maximum HRR HRR_{max} and time to maximum HRR t_{max}. As soon as the HRR reaches five MW, the fire detection system recognises the fire. At the same time, the longitudinal emergency ventilation system starts and produces a gas flow in downhill direction to maintain a thermally-driven uphill gas speed of less than 1.5 $\frac{\text{m}}{\text{s}}$. It takes 30 seconds to full emergency ventilation and the fans are switched off again before disturbing the smoke layer. Also immediately with the fire detection, the TA, if not failed because of the risk factor fa, triggers the tunnel closing which prevents further vehicles from entering the tunnel.

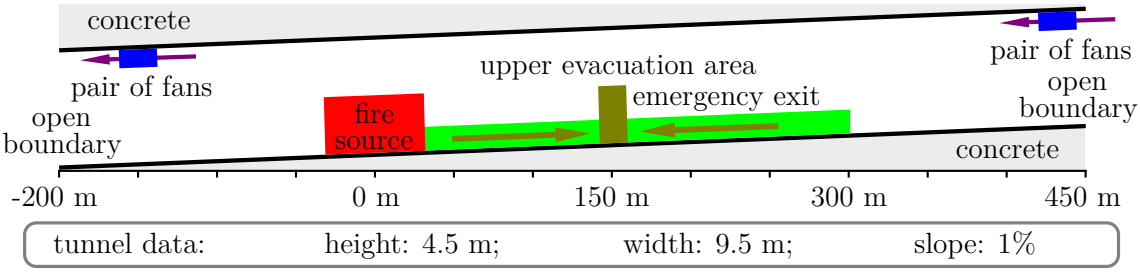

Figure B.2: Geometry and layout of the road tunnel in the system model; figure is not in scale.

The evacuation scenario focuses on the upper evacuation area next to the fire source and takes into account the smoke spread of the fire scenario. The number of tunnel users N_{tu} in the evacuation area depends on the numbers of cars, heavy good vehicles (HGVs) and buses. Each tunnel user is either alerted individually by smoke or simultaneously with the other tunnel users by the TA. Subsequently to the alarm, the tunnel users start to evacuate to the emergency exit after their individual pre-evacuation times. The individual pre-evacuation times are drawn from a uniform distribution between zero and the risk factor maximum pre-evacuation time t_{pre} denoted with $\mathcal{U}(0, t_{pre})$. The individual walking speed can be impeded by two factors: jams at the emergency exit, i.e. a bottleneck [51]; and the smoke spreading in the road tunnel. Furthermore, the smoke can incapacitate the tunnel users. The evacuation scenario ends when all tunnel users either reached the emergency exit or were incapacitated. At last, the FF derives from the number of fatalities and the number of tunnel users in the upper evacuation area.

In accordance with the focus on the upper evacuation area, the definitions of risk measures [38, p. 383] require adaptions. The individual risk is now defined with '*the annual frequency that an unprotected tunnel user being permanently present in the upper evacuation area next to the fire source will die*'. And the societal risk is '*the annual frequency that a specified*

minimum number of tunnel user will die in the upper evacuation area next to the fire source'. Both risk measures are not specific to the tunnel length and thus depend on this risk factor.

Next to the jam of tunnel users at the emergency exit, the TA constitutes a discrete event in the evacuation scenario. In case of a scenario with TA, the TA alerts multiple tunnel users simultaneously. But the distribution of the individual pre-evacuation times blurs the peak of tunnel users starting to walk. In case of a scenario with FA, the individual pre-evacuation times of the tunnel users are not affected by the discrete event TA. Hence, the scenarios with TA are more complex than scenarios with FA.

In line with Section A.1, the complexity of the system model and of the fire and evacuation scenario are defined: by a system which comprises many subsystems; and, by the difficulty of predicting the effects of risk factors on the FF because of interactions in the fire and evacuation scenario. First, as Fig. B.1 highlights, the system model can be split into different subsystems for frequency, fire and evacuation. Moreover, e.g. the subsystem fire contains further subsystems like the fire source or the ventilation system. Second, the fire source, the tunnel users and the safety measures interact in many ways in the fire and evacuation scenario. Examples are: the individual alarm of tunnel users in combination with the smoke, the TA of all tunnel users, or the emergency ventilation interacting with the smoke spread. Because of these interactions, each risk factor in the system model has an unknown effect on the FF. In conclusion, the system model but also the fire and evacuation scenario in the complex model are complex.

At last, the fire scenario and the evacuation scenario originate from the fire model and from the evacuation model respectively. But the terms 'fire scenario' and 'evacuation scenario' are only applied in this dissertation to emphasise their origins. For brevity, the term 'scenario' means the evacuation scenario based on the fire scenario. And again for brevity, specific scenarios are shortly named for instance with sc(100 MW, 1000 s, 120 s, 105, $fa = 0$) for the scenario with $\mathrm{HRR}_{max} = 100\,\mathrm{MW}$, $t_{max} = 1000\,\mathrm{s}$, $t_{pre} = 120\,\mathrm{s}$, $N_{tu} = 105$ and $fa = \mathrm{TA}$.

Risk factors

After the qualitative illustration of the scenario in the system model, this subsection now outlines the risk factors. Tab. B.2 summarises their models and App. G.2.2 details the background and provides the original references.

Tab. B.2 also shows the default model and the uniform distribution of the risk factor maximum HRR HRR_{max}. The default model is subjected to a discrete distribution, in generally denoted for any risk factor x with $\mathcal{D}(\{x_1, \ldots\}) = \{p_1, \ldots\}$, the value on the domain x_i and the corresponding probability p_i. It considers fully developed fires with more than five MW either caused by accidents or by technical defects and does not distinguish between vehicle types. Because of the small probability for large fires, importance sampling adapts the original discrete probability distribution as given in Tab. B.3. Additionally, the uniform distribution serves for evaluations within the consequence model.

Nota bene, also the probabilities in the probability distribution of the risk factor maximum HRR, and not only its results, clearly influence the risk measures. For instance, random scenarios with high maximum HRRs and small probabilities occur rarely during a Monte-Carlo simulation and their increased FFs are averaged in Eq. B.3 and Eq. B.5 of the risk measures. As a result, these random scenarios contribute less to the risk measures than other random scenarios. Importance sampling clarifies this effect by reducing the product of frequency and FF with the weighting factor of Eq. B.2. A similar effect can be observed in the risk factor failure of tunnel alarm.

Table B.3: Probabilities for the original discrete distribution $\mathcal{D}_{or}$ and the adapted discrete distribution $\mathcal{D}_{is}$ of the importance sampling for the risk factors HRR_{max} and fa.

HRR_{max} /MW	5	30	50	100
$\mathcal{D}_{or}$	0.9	0.099	0.0009	0.0001
$\mathcal{D}_{is}$	0.1	0.3	0.3	0.3
fa	TA	FA		
$\mathcal{D}_{or}$	0.99	0.01		
$\mathcal{D}_{is}$	0.5	0.5		

The model for the failure of tunnel alarm fa describes an original probability of FA per demand of 1%. This probability is increased with the model for importance sampling in Tab. B.3.

The time to maximum HRR t_{max} and the maximum pre-evacuation time t_{pre} are based on uniform distributions with their minimum and maximum values taken from experiments or studies. The maximum pre-evacuation time includes the reaction time and time to leave the vehicle. But this model neglects tunnel users deciding to stay in their vehicles.

The number of tunnel users N_{tu} results from the number and the type of vehicles in the upper evacuation area, namely cars, HGVs and buses. Thus, the analytical model relates to the parent nodes number of vehicles and ratio of HGV. Disregarding these relations, this node is a risk factor and not an intermediate node because of its clear visualisation of the evacuation scenario. Next to the analytical model, the risk factor also comprises the uniform distribution in Tab. B.2 because of its direct link to the evacuation model. The uniform distribution is merely based on assumptions and is used for evaluations within the consequence model.

Finally, the parent nodes of the frequency of scenario f_{sc}, namely the ratio of HGV χ_{HGV}, the average daily traffic volume $\dot{N}_{adtv}$ and the tunnel length l_{tunnel} all apply general models. A general model means a large domain for the independent variables of the probabilistic model. In contrast, tunnel specific models have specific domains of one particular tunnel. Thus, the uniform distributions of the risk factors stem from statistics of many German road tunnels. The risk factor ratio of HGV not only determines results for HGV but also for cars and buses. And, results of the node tunnel length are valid in the system model but not in the consequence model.

Intermediate nodes

As for the risk factors, App. G.2.3 provides the background and the references for the intermediate nodes.

The analytical model for the frequency of scenario f_{sc} depends on the parent nodes average daily traffic volume and tunnel length. It is valid for road tunnels with bi-directional traffic on two lanes without additional access roads. Also, it produces results for the frequency of fully developed fires with a maximum HRR of more than five MW as consequence of accidents or technical defects. In the latter case, burning vehicles can sometimes leave the tunnel which reduces the frequency of a fire.

The intermediate nodes time of fire detection and time of tunnel alarm are closely connected. The time of fire detection is equal to the time when the HRR reaches five MW. Failures of the fire detection system are not assumed. Then, the result of the node time of tunnel alarm is also identical with the time of fire detection as long as no FA occurs. Thus, it additionally depends on the node failure of tunnel alarm.

The number of vehicles has the parent nodes average daily traffic volume, time of tunnel alarm and traffic speed. The node traffic speed is the weighted average of the allowed traffic speeds of cars and HGVs in road tunnels and therefore requires the risk factor ratio of HGV. All vehicles in the the upper evacuation area next to the fire source count to the number of vehicles under the assumption of free-flowing traffic. The counting splits up between two phases: first, before the time of tunnel alarm where the vehicles stop at the end of the tailback; and second, after the time of tunnel alarm where all vehicles stop immediately with the TA.

Finally, the parent nodes maximum HRR and time to maximum HRR, maximum pre-evacuation time, number of tunnel users and failure of tunnel alarm amalgamate in the intermediate node FF. This node directly connects to the consequence model and hence also to the metamodel. But the metamodel can lead to a FF below zero and above one which contradicts the 'fraction' of fatalities in the system model. For this reason, the results of the metamodel have to be clipped to comply with the system model. To distinguish both FFs, the unclipped FF within the metamodel is denoted with ξ, and the clipped FF in the system model is denoted with $0 \leq \widetilde{\Xi} \leq 1$.

B.4 Consequence model with the metamodel

The consequence model within the node FF consists of the complex model as well as of the metamodel. This section first details the discrete scenario computed within the complex model and reasons the choice of the CFD model and the microscopic evacuation model. Then, it introduces the complex model from the perspective of the system model as well as the metamodel. Since the evacuation model of the complex model causes evacuation uncertainties, the section finally outlines some approaches to examine the results of discrete scenarios subjected to uncertainties. The notation mostly concentrates on the FF as results of the consequence model. But the notation does not narrow the general applicability of the metamodel on various other issues. Accordingly, Subs. 'Remarks on the mathematical notation' (p. G-3) of App. G.1 defines the more general notation.

Discrete scenario in FDS and FDS+Evac

The description of the scenario is now completed with its realisation in the CFD model and the microscopic evacuation model. For this purpose, the next paragraphs first outline publications with regard to the application of FDS and the microscopic evacuation model FDS with Evacuation (FDS+Evac) [52], then sketch the fire and evacuation scenarios and provide a short discussion of epistemic uncertainties in the FF of the complex model.

FDS and FDS+Evac are common fire and evacuation models in fire safety engineering and thus contribute to the current state of research in this field. For instance, the methodologies for risk analysis by Albrecht 2014 [30] and Weyenberge 2017 [33] apply FDS and Anderson 2018 [35] at least discusses its use. Even in more complex geometries, like metro stations, FDS serves to determine the available safe egress time [53]. In the context of road tunnels, e.g. the methodologies for risk analysis of Germany [13] and Austria [14] suggest FDS as fire model. Truchot 2018 [54] examines the consequences determined with the fractional effective dose in FDS with regard to a real fire scenario in a road tunnel. To end this line, there are several other examples for the application and validations of FDS for road tunnels briefly summarised in Seike 2017 [55]. Seike 2017 [55] additionally gives an overview on microscopic evacuation models used for road tunnels, among them FDS+Evac. Next, Ronchi 2013 [56] evaluates FDS+Evac and other microscopic evacuation models simulating

the effects of fires on the evacuation of tunnel users in a road tunnel. And also interesting for the evacuation through emergency exits, FDS+Evac was successfully validated for the flow of persons through bottlenecks but at the same time it revealed discrepancies in other measures like the walking speed [57]. Concluding, both, FDS and FDS+Evac are commonly used and evaluated with regard to road tunnels and thus, both models are also suitable for their application within the methodology of this dissertation.

The fire scenario is realised in FDS with the tunnel geometry and the layout depicted in Fig. B.2 (p. 17). For this, the domain consists of a single mesh with a cell size of 0.25 m and ends with two open boundaries. Its length of 650 m is independent to the corresponding risk factor in the system model. Because of the length of the domain, the pressure solver in FDS led to numerical instabilities during the setup of the fire scenario. This issue could be solved with four leaks, i.e. small open boundaries without real analogies, distributed over the entire tunnel length close to the ceiling. A later discussion with a developer of FDS corroborated that this approach might be the only way to attain stable solutions. The arrangement of the leaks resulted from a screening and led to the least effect on the gas flow in the road tunnel. The screening further comprised for instance the length of the domain, the mesh design together with the cell size, as well as parameters related to the longitudinal emergency ventilation system and the fire source. The ventilation system comprises two pairs of fans which interact with the gas and smoke spread. Namely, the fans automatically adapt their mass flow to the gas velocity in the road tunnel and detect smoke to switch off the ventilation. Beside the fans, the three-dimensional fire source representing a HGV, is the only additional obstacle like cars. The HRR of the fire source depends on the risk factors maximum HRR and time to maximum HRR. It follows an exponential function describing the growth and the decay period [58, p. 260] as detailed in Subs. 'Exponential HRR curve of the fire source' (p. G-11) of App. G.4. In the same section, Subs. 'FDS input file' (p. G-12) complements the description of the entire model of the road tunnel.

There are different ways to adopt the smoke spread of FDS in the evacuation scenario. e.g. Weyenberge 2017 [33] in Subs. 'Current research on methodologies for risk analysis in fire safety engineering' (p. 9) applies a metamodel to indirectly connect FDS with a one-dimensional evacuation model. But in case of FDS+Evac, its developers intend to directly link evacuation scenarios to fire scenarios of FDS. Therefore, the complex model in this dissertation corresponds to this intention.

The evacuation scenario defined in Subs. 'FDS+Evac input file' (p. G-15) of App. G.4 is focused on the upper evacuation area next to the fire source. During its initialisation, N_{tu} tunnel users are uniformly distributed over the entire length of the evacuation area. But, they only occupy both evacuation paths with a width of two metres on each side of the road. Their individual characteristics, i.e. environmental variables like the walking speed or the body size, are attributed to default parameters of FDS+Evac. After the initialisation, the evacuation scenario begins at the same time as the ignition of the fire source in the fire scenario. The tunnel users are either alerted by TA at a HRR of five MW or individually by smoke. The individual alarm depends on the position of each tunnel user as well as on a threshold value for the local smoke density, i.e. the visibility. This threshold value was determined during a screening. After the alarm of tunnel users, their individual pre-evacuation time passes. It derives from the risk factor maximum pre-evacuation time. Subsequently, the tunnel users move alongside the road to the emergency exit in the centre of the evacuation area. They can overtake each other but are only allowed to cross the road in the vicinity of the emergency exit. Their individual walking speed can be impeded by smoke according to an experimental correlation [52, p. 23]. The correlation depends on the minimum walking speed which was specified for road tunnels according to publications [59, p. E.1; 60, p. 550; 61, p. 31]. The smoke also affects their incapacitation calculated with the fractional effective

dose method by Purser [40]. To sum up, the evacuation scenario was specified with default parameters of FDS+Evac as well as with parameters and assumptions identified during a screening or derived from other publications. Moreover, its plausibility was reasoned during the setup. e.g. without effects of smoke, the movement of tunnel users seems to be plausible because of the simple geometry of the road tunnel and the virtually unimpeded walking speed due to the small number of tunnel users.

However, the FF as result of fire and evacuation scenarios is subjected to high epistemic uncertainties. e.g. particular epistemic uncertainties lie in the calculation of gas concentrations with FDS [52, p. 15]. And with regard to the evacuation scenario, few examples are: the different correlations between the visibility and walking speed as discussed in Ronchi 2013 [56]; 'the general lack of theoretical understanding on human performance [walking speed] in smoke [which] makes it difficult to provide a definite interpretation of the available data-sets [correlations]' [62, p. 419]; as well as uncertainties in the fractional effective dose concept 'because the endpoints [e.g. for incapacitation] cannot be fully quantified within narrow limits without performing experimental human exposures to a variety of complex and dangerous toxic effluent mixtures' [40, p. 2/90]. But there are some hints not to falsify the results in the fire and evacuation scenarios: 'FDS+Evac has been the model that best represented the impact of smoke on agent walking speeds' [56, p. 152]; Truchot 2018 [54] found no inconsistencies between the fractional effective dose of simulations with FDS in comparison to a real tunnel fire incident; and, Berchtold 2016 [8] compared three real tunnel fires to FDS and FDS+Evac simulations and did not reveal obvious contradiction in the number of fatalities.

This short discussion of epistemic uncertainties in the complex model shall suffice, because this dissertation focuses on the metamodel. Hence, the epistemic uncertainties in the complex model are not quantified and not considered in the methodology for risk analysis. Though, epistemic uncertainties are considered to be crucial for risk analysis as discussed in Subs. 'Current research on the theory of risk analysis' (p. 13) and hence, an approach to include these epistemic uncertainties would be similar to the metamodel uncertainty and is exemplified in de Sanctis 2016 [32]. Concluding, the complex model with FDS and FDS+Evac is used in this dissertation to quantify the FF acknowledging the epistemic uncertainties.

Complex model within the system model

Within the complex model, the fire model FDS provides the smoke spread of a fire scenario for the evacuation model FDS+Evac. For this, the discrete fire scenario $\vec{x}_i^{\text{fire}} = [\text{HRR}_{max,i}, t_{max,i}]$ depends on the fire risk factors maximum HRR and time to maximum HRR. Subsequently, the evacuation model computes the discrete evacuation scenario with the evacuation risk factors maximum pre-evacuation time, number of tunnel uses and failure of tunnel alarm. Since the evacuation scenario also takes the smoke spread into account, it additionally adopts the values of the fire risk factors in the fire scenario $\vec{x}_j^{\text{evac}} = \Big[\text{HRR}_{max,i}, t_{max,i}, t_{pre,j}, N_{tu,j}, fa_j\Big]$. During the simulation of the evacuation scenario, the incapacitation model of FDS+Evac determines the number of fatalities and afterwards Eq. B.1 yields the FF. Accordingly, the result of the complex model, i.e. the FF, comes from simulations of the discrete fire and evacuation scenarios. To describe the discrete scenarios in the complex model, the notation follows Tab. B.4.

But FFs of evacuation scenarios are subjected to evacuation uncertainties. To quantify the evacuation uncertainties, an evacuation scenario consists of N_{rep} replications. A replication is a repeated simulation of a stochastic model with equal values of the '*control variables*' but with by their nature varying values of the environmental variables. E.g. replications are used in Salemi 2016 [29] to quantify aleatory uncertainties in general or in Ronchi 2014 [43] to analyse evacuation uncertainties. In this dissertation, the replications of one discrete scenario

Table B.4: Notation used for the complex model.

notation	description
$\vec{x}_i$	discrete scenario, data point
$\vec{x}^{\text{fire}}$	fire scenario
$\vec{x}^{\text{evac}}$	evacuation scenario
N_{rep}	number of replications of a discrete scenario
ξ^c	FF of a single replication
$\widetilde{\xi}_i^c = \left[\xi_{i,1}^c, \xi_{i,2}^c, \ldots, \xi_{i,N_{\text{rep}}}^c\right]$	FF of a discrete scenario with all replications (ORS)
$\bar{\xi}_i^c$	mean FF of $\widetilde{\xi}_i^c$

with equal values in the risk factors produce the result $\widetilde{\xi}_i^c \equiv \widetilde{\xi}^c(\vec{x}_i) = \left[\xi_{i,1}^c, \xi_{i,2}^c, \ldots, \xi_{i,N_{\text{rep}}}^c\right]$. Another term for this result is observed random sample (ORS). This term signalises the results of a discrete scenario and emphasises its frequency distribution. Despite the evacuation uncertainty, the arithmetic mean $\bar{\xi}_i^c = \mu(\widetilde{\xi}_i^c)$ and the variance of the FF are considered to be deterministic in case of a sufficient number of replications, esp. with regard to the effects caused by risk factors.

The mean FF on the entire domain of the fire and evacuation risk factors establishes the response surface of the complex model. But the exact '*shape of the response surface*' is unknown because the complex model computes only some discrete scenarios. In this dissertation the shape of the response surface is continuous between the theoretical limits zero and one. Even discrete events in the scenario like the TA do not cause discontinuities since the occurrence of discrete events changes continuously together with the values of the risk factors. But discrete events might contribute to the complexity of the response surface. The complexity of the response surface concerns with its shape on the entire domain. A complex response surface has a shape with large second derivatives and might reveal inflection points. To sum up, the shape of the response surface for the FF is continuous, should be differentiable, and is expected to be more complex than a quadratic polynomial because of its lower and upper limits.

Metamodel

The metamodel aims to reproduce the response surface of the complex model, or shortly to build a RSM. For this, the metamodel comprises three integral parts: the ED, the data base and the RSM. Beside these integral parts, the metamodel uncertainty arises from the simplifications in the RSM, and the evacuation uncertainty comes from the evacuation model. Thus, the metamodel uncertainty and the evacuation uncertainty take also part to integrate the results of the complex model into the system model. The integration consists of two steps: first, the results of the RSM, the metamodel uncertainty and the evacuation uncertainty join to the results of the metamodel; then, the node FF integrates the FF of the system model. Fig. B.3 depicts the integral parts as well as the integration into the system model and App. G.3 sketches its implementation. The following paragraphs detail the integral parts of the metamodel and finally outline possible approaches to achieve higher efficiency. Also Tab. B.5 summarises the notation for the metamodel and therefore supplements Tab. B.1 and Tab. B.4.

An ED serves for the 'specification of points [discrete scenarios] in the experimental region [domain] at which we wish to compute the response [result].' according to Santner 2003 [10, p. 121]. Hence, the ED $X = \left[\vec{x}_1, \vec{x}_2, \ldots, \vec{x}_{N_{\text{dps}}}\right]^T$ specifies N_{dps} '*data points*', i.e. discrete

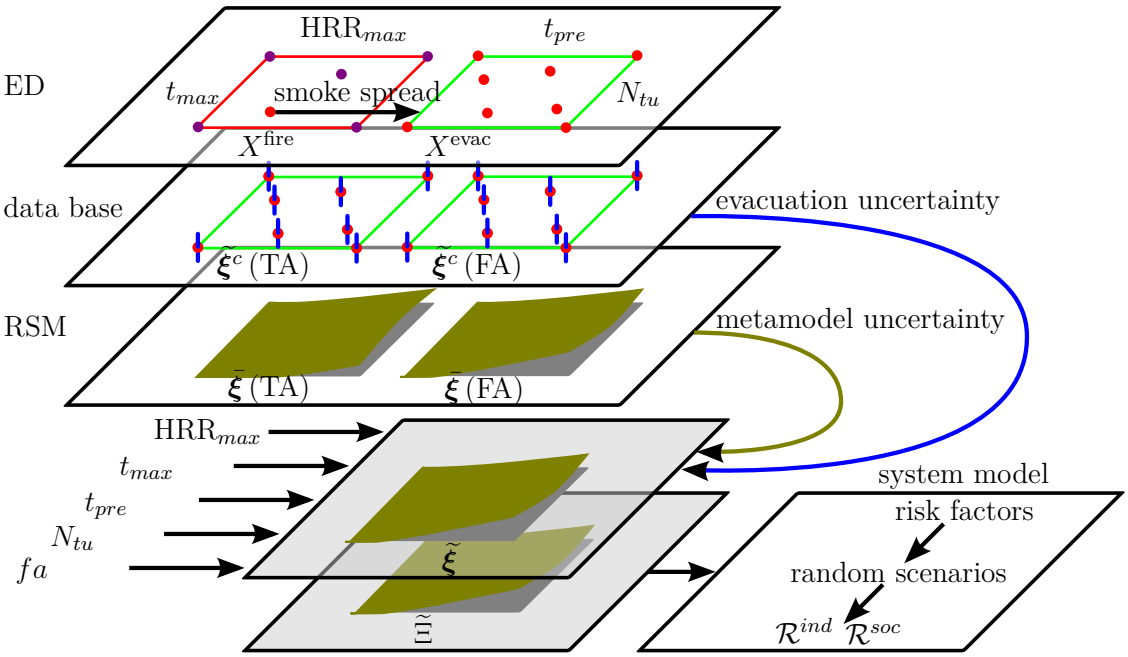

Figure B.3: Three integral parts of the metamodel (white layers): in the EDs, the evacuation scenarios X^{evac} adopt the smoke spread of the fire scenario $\vec{x}^{\text{fire}} \in X^{\text{fire}}$ (red point), the other evacuation scenarios are not shown; the data base contains the results of all replications which lead to the evacuation uncertainty (sketched blue); the RSM approximates the results at random scenarios and causes the metamodel uncertainty. Next, the node FF (grey layers) integrates the results of random scenarios in the metamodel into the system model.

scenarios, for the data base. The number of data points in some specific EDs is also denoted with $\|X\|$.

The complex model with its fire model and evacuation model demands two different EDs. On the one hand, the ED X^{fire} defines fire scenarios with the fire risk factors $\vec{x}^{\text{fire}} = \left[\text{HRR}_{max,i}, t_{max,i}\right]$. And on the other hand, the ED X^{evac} describes the evacuation scenarios $\vec{x}^{\text{evac}} = \left[\text{HRR}_{max,i}, t_{max,i}, t_{pre,i}, N_{tu,i}\right]$. For brevity, the ED X^{evac} is commonly denoted with X, but the symbols X^{evac} and X^{fire} highlight the different scenarios if required.

The domains for fire risk factors and evacuation risk factors in the EDs are equal to the domains of the uniform distributions in Tab. B.2 (p. 16). Therefore, the two risk factors maximum HRR and number of tunnel user deviate from their default models. The deviating domain of the risk factor maximum HRR is based on the assumption that fire scenarios with $\text{HRR}_{max} < 25\,\text{MW}$ do not lead to fatalities, and the domain for the number of tunnel users is reasoned in App. G.2.2.

After simulating the scenarios of the EDs with the complex model, the results are saved in the corresponding data base of the metamodel used in the consequence model of the system model, or shortly data base for the system model. Thus, the data base for the system model contains the data points together with the results of the simulations. Basically, the ORS, i.e. all replications of the scenario, constitute the results. Accordingly, the data base is '*boldly denoted*' with $\widetilde{\boldsymbol{\xi}}^c \equiv \widetilde{\boldsymbol{\xi}}^c_X = \left[\widetilde{\xi}^c_1, \widetilde{\xi}^c_2, \ldots, \widetilde{\xi}^c_{N_{\text{dps}}}\right]^T$ with the ED X. But to emphasise the deterministic results, namely the mean FF, the data base is symbolised with $\bar{\boldsymbol{\xi}}^c \equiv \bar{\boldsymbol{\xi}}^c_X = \left[\bar{\xi}^c_1, \bar{\xi}^c_2, \ldots, \bar{\xi}^c_{N_{\text{dps}}}\right]^T$.

Table B.5: Notation used for the metamodel.

notation	description
X	ED
N_{dps}	number of data points in the ED $N_{\text{dps}} \equiv \|X\|$
X^{fire}	ED for fire scenarios
X^{evac}	ED for evacuation scenarios, also briefly denoted with X
$\widetilde{\boldsymbol{\xi}}^c$	data base for the FFs of all replications of all scenarios in an ED
$\bar{\boldsymbol{\xi}}^c$	data base for the mean FF of all scenarios in an ED
$\widetilde{\xi}$	FF of the metamodel with the combined integration of the metamodel uncertainty and evacuation uncertainty for one random scenario
$\bar{\xi}$	FF of the RSM or of the metamodel without metamodel uncertainty or evacuation uncertainty for one random scenario
$\widetilde{\boldsymbol{\xi}}$, $\bar{\boldsymbol{\xi}}$	corresponding results for multiple random scenarios

Next, the response surface method applies a data base to set up the model of the response surface, literally the response surface model. In this dissertation, the response surface methods generally use deterministic results of the complex model and their RSMs produce deterministic results. This approach has two reasons: first, it is common in case of evacuation models to compute multiple replications and draw separate conclusions from the means of their results and their variances, e.g. as outlined in Ronchi 2014 [43]; and second, to separate the evacuation uncertainty from the RSM in order to question assumption 2 (plausibility). The deterministic result of a RSM for a random scenario $\widetilde{x}$, or in other words '*arbitrary point*', and the data base $\bar{\boldsymbol{\xi}}^c_X$ is denoted with $\bar{\xi}_X$. It approximates the unknown deterministic result of the complex model $\bar{\xi}^c(\widetilde{x})$ for this random scenario.

Tab. B.5 extends the notation for results of the metamodel. For the sake of brevity, the symbols for multiple results are also used to directly name the RSM or metamodel without referring to the results. Vice versa, the terms 'RSM' or 'metamodel' sometimes, and in particular in tables, have the meaning of 'results of the RSM' or 'results of the metamodel'.

To be noted, the ED for simulations with the evacuation model neglects the evacuation risk factor failure of tunnel alarm because of its two discrete results TA and FA. In order to include this risk factor, two different data bases comprise either scenarios with TA or scenarios with FA but stem from the same ED as illustrated in Fig. B.3. Consequently, both corresponding RSMs also use the same ED. This dissertation usually describes both data bases or RSMs independent from TA or FA but if required distinguishes the RSMs of the ED X_i with $\bar{\boldsymbol{\xi}}_{X_{i,0}}$ or $\bar{\boldsymbol{\xi}}_{X_i}$ (TA) for scenarios with TA and $\bar{\boldsymbol{\xi}}_{X_{i,1}}$ or $\bar{\boldsymbol{\xi}}_{X_i}$ (FA) for scenarios with FA.

With respect to the efficiency of the metamodel in objective 2 (efficiency), it is crucial to reduce the required number of simulations with the fire model, i.e. CFD model. In contrast, the number of simulations with the evacuation model is less important because CFD models cause substantially higher computational cost. Hence, the metamodel pursues two approaches to increase the efficiency: the combination of EDs and the sequential refinement. The combination of the ED for fire scenarios and the ED for evacuation scenarios allows that multiple evacuation scenarios obtain the smoke spread of a single fire scenario as exemplified in Fig. B.3. Thus, the number of data points in the ED for fire scenarios is smaller than for evacuation scenarios, namely $\left\|X^{\text{fire}}\right\| < \|X^{\text{evac}}\|$ and with $\left\|\vec{x}^{\text{fire}}\right\| < \|\vec{x}^{\text{evac}}\|$. Next, the sequential refinement of the metamodel comprises different refinement steps with focus on high metamodel uncertainties. Fig. B.4 sketches the four successive steps within one refine-

ment step. The successive steps are: first, to set up the initial ED with a small number of data points; second, to perform the simulations with the complex model at the data points and to add their results to the data base; third, to set up the RSM; fourth, to evaluate the metamodel, e.g. for its use in the risk analysis; and finally before revisiting step two again, to add new data points to the ED with focus on regions of the domain with high metamodel uncertainty. Summing up, the sequential refinement targets at two capabilities: to focus on regions with high metamodel uncertainties, briefly named as 'focused sequential refinement'; and to avoid conservative estimates of the number of data points in the initial ED. The latter capability differs to a batch design, i.e. an ED with a single batch of data points without sequential refinement.

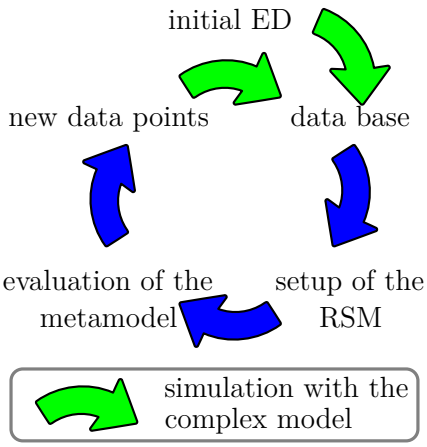

Figure B.4: Successive steps within one refinement step in the sequential refinement of the metamodel.

Evaluation of ORSs

The evaluation of the frequency distribution of ORSs provides an important basis for the reproduction of the evacuation uncertainty of the complex model. For this, this subsection describes three approaches. The main focus lies on an approach to determine the required number of replications in the ORSs. Then, the last two paragraphs deal with approaches to compare the frequency distributions of ORSs and to test their distribution type.

First, the bootstrap approach [63] is suitable to assess the entire frequency distribution of ORSs in contrast to Ronchi 2014 [43]. In general, the approach is used to determine standard errors for statistics of an empirical frequency distribution of an ORS. For this, it draws random samples from the empirical frequency distribution and determines the statistic for each random sample to get the standard error. The random samples are called bootstrap samples in this dissertation. In detail, a bootstrap sample results from a random experiment with replacement with the ORS as data base and has the same number of replications.

Accordingly, the bootstrap approach serves to determine the required number of replications in this dissertation. The number of replications is sufficient if the ORS reproduces the 'unknown probability distribution'. The term 'unknown probability distribution' describes the real probability distribution of the results of the stochastic complex model behind the ORS and thus is equal to the term 'evacuation uncertainty'. But it applies for available ORS of discrete scenarios whereas 'evacuation uncertainty' is used for results of random scenarios disregarding specific ORSs. Since the ORS is the single available information on the unknown probability distribution of a discrete scenario, the reproducibility of the ORS itself implies that it also reproduces the unknown probability distribution. So, if the frequency

distributions of bootstrap samples are different to the ORS, a reproduction of the unknown probability distribution seems unlikely and more replications are required. On the other hand, if the frequency distributions of the bootstrap samples are similar to the ORS, the ORS is reproducible. At the same time, it is likely that the ORS reproduces the unknown probability distribution.

Second, the bootstrap approach bases on the comparison of frequency distributions. Qualitatively, one option is to visually juxtapose the frequency distributions of the ORS with a randomly chosen bootstrap sample. Quantitatively, the quantiles q_j of the FFs in the bootstrap samples are compared. More precisely, the mean of all bootstrap samples for each quantile, i.e. the mean bootstrap quantiles $\widetilde{\xi}^{*}_{q_j}$ are compared to the quantiles of the FF in the ORS $\widetilde{\xi}^{c}_{q_j}$. Then, Eq. B.6 quantifies the largest absolute difference. If it is smaller than a threshold value, the bootstrap samples and the ORS are similar. The threshold value is derived from a visual analysis of the results.

$$\mathrm{D}\widetilde{\xi}^{c}_{q} = \max\left\{\left|\widetilde{\xi}^{c}_{q_j} - \widetilde{\xi}^{*}_{q_j}\right|, \ldots | \forall q_j\right\} \tag{B.6}$$

Third, the test of the distribution type of ORSs follows the one-sample Kolmogorov-Smirnoff test [64, p. 352f]. In this test, the null hypothesis states that the ORS is subjected to e.g. a normal distribution and the test statistic is $d_{KS,crit} = \sqrt{\frac{-0.5\ln(\alpha/2)}{N_{\mathrm{rep}}}}$ with N_{rep} as sample size and the two-sided confidence level α. The test returns $d_{KS,max}$ and the p-value p_{KS} of the test. The null hypothesis is to reject if $d_{KS,max} > d_{KS,crit}$ or if $p_{KS} < \alpha$.

B.5 Approaches for the evaluation of risk analysis

The consequence model provides the FF of the system model for Monte-Carlo simulations. The Monte-Carlo simulations have two different foci and are named with 'system model simulation' and 'risk analysis'. The system model simulation $\mathcal{S}$ serves for the evaluation of single nodes in the system model, esp. of the metamodel in the node FF. For this, the risk factors maximum HRR and number of tunnel users use their uniform distributions shown Tab. B.2 on p. 16. Hence, all risk factors generate uniformly distributed results which favours an even spread of random scenarios on the entire domain. Contrary, risk analyses $\mathcal{R}$ using the default models of all risk factors aim at random scenarios with frequencies corresponding to real tunnel fires. However, their assessment does not necessarily look at their risk measures but can also concentrate on the node FF.

The differences in the methodologies for risk analysis of road tunnels outlined in Section A.1 motivate the evaluation of risk analyses $\mathcal{R}$ with regard to: the effect of risk factors on their results; and the plausibility of their risk measures. But first, risk analyses must lead to converging results during Monte-Carlo simulations. Thus, the evaluation bases on the following approaches.

Convergence in the Monte-Carlo simulation

The convergence measure υ_{conv} in Eq. B.7 serves to quantify the convergence of a scalar measure $\boldsymbol{\Upsilon}$ in a Monte-Carlo simulation, e.g. the FF or the individual risk. It applies the arithmetic mean of the scalar measure with $\mu\left(\boldsymbol{\Upsilon}\right)_n = \frac{1}{n}\sum_{i=1}^{n}\Upsilon_i$ for different numbers of random scenarios $n \leq N_{\mathrm{mcs}}$ and with $\Upsilon_i \in \boldsymbol{\Upsilon}$ for one random scenario. Additionally, the successive arithmetic means $\vec{\mu} = [\mu_1, \ldots, \mu_{N_{\mathrm{mcs}}}]$ illustrate the convergence. So, the convergence measure, similar to Ronchi 2014 [43], can be used to determine the required number of random scenarios until its convergence in a Monte-Carlo simulations.

$$v_{conv} = \frac{\mu_{N_{\mathrm{mcs}}} - \mu_{0.9 \cdot N_{\mathrm{mcs}}}}{\mu_{N_{\mathrm{mcs}}}} \tag{B.7}$$

Effect of risk factors on risk measures

The Spearman's rank correlation coefficient ρ^{sp} [64, p. 372] is a measure for monotonic correlations, e.g. between a risk factor and the FF. This measure does not directly inform on quantitative effects. But a clear the monotonic correlation of one risk factor implies smaller influences of other risk factors as long as the monotonic correlation is reasonable. Thus, a high correlation coefficient of one risk factor qualitatively indicates smaller effects of other risk factors and vice versa for low correlation coefficients.

Complementing these qualitative results, the relative effect of risk factors on risk measures quantifies the effects directly. The relative effect was already published by Berchtold 2016 [8] but was later adapted to be more clear.

The relative effect of a risk factor x on individual risk in Eq. B.8 is defined with the 'relative difference between the maximum and minimum individual risks proportional to the mean individual risk' and is depicted in Fig. B.5a. For this definition, the maximum and minimum individual risks consider random scenarios of different regions in the domain of the risk factor. Namely, $\mathcal{R}^{ind}_{\substack{\min \\ \max}} = \overset{\min}{\max}\left\{\mathcal{R}^{ind}_1, \ldots, \mathcal{R}^{ind}_n\right\}$ where the individual risk with random scenarios of each region of the risk factor is $\mathcal{R}^{ind}_i \equiv \mathcal{R}^{ind}(x_i)$. And, the mean individual risk takes into account all random scenarios the entire domain of the risk factor.

$$\eta^{ind} = \frac{\mathcal{R}^{ind}_{max} - \mathcal{R}^{ind}_{min}}{\mathcal{R}^{ind}(x)} \tag{B.8}$$

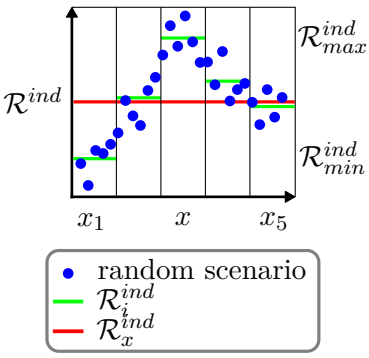

(a) relative effect η^{ind} of the risk factor x on individual risk $\mathcal{R}^{ind}$

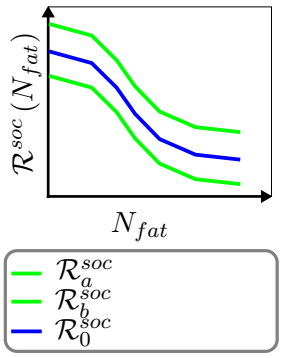

(b) relative effect η^{soc} on the societal risk curve $\mathcal{R}^{soc}$

Figure B.5: Terms used to determine the relative effect of risk factors.

Similarly, the relative effect on societal risk in Eq. B.9 and Fig. B.5b is the 'mean over all number of fatalities of the absolute difference between the lower and the upper societal risk curve proportional to the common societal risk curve' with the absolute difference in Eq. B.10. The lower and the upper societal risk curve are denoted with $\mathcal{R}^{soc}_a \equiv \mathcal{R}^{soc}(x_a)$ as well as $\mathcal{R}^{soc}_b \equiv \mathcal{R}^{soc}(x_b)$. They consider random scenarios with intervals between the 10%- and 50%-quantiles of the domain of the risk factor $x_{q_{10}} < x_a < x_{q_{50}}$ as well as $x_{q_{50}} < x_b < x_{q_{90}}$ respectively. In contrast, the common societal risk curve $\mathcal{R}^{soc}_0 = \mathcal{R}^{soc}(x)$ is subjected to random scenarios on the entire domain. To increase the reproducibility of this relative effect,

different steps have been introduced, e.g. the limitation of the maximum number of fatalities. These steps reduce dispersions in the upper part of the societal risk curve.

$$\eta^{soc} = \frac{1}{N_{fat}} \sum_{N_{fat,i}=1}^{N_{fat}} \frac{\Delta\mathcal{R}^{soc}\left(N_{fat,i}\right)}{\mathcal{R}_0^{soc}\left(N_{fat,i}\right)} \tag{B.9}$$

$$\Delta\mathcal{R}^{soc}\left(N_{fat,i}\right) = \left|\mathcal{R}_a^{soc}\left(N_{fat,i}\right) - \mathcal{R}_b^{soc}\left(N_{fat,i}\right)\right| \tag{B.10}$$

Plausibility of risk measures

The discussion of the plausibility of results of risk analyses bases on the concept of falsification. For this, Popper's falsifiability criterion tells that 'statements or systems of statements, in order to be ranked as scientific, must be capable of conflicting with possible or conceivable observations' as discussed in Hansson 2014 [49, p. 1175]. Accordingly, if 'statements', i.e. risk measures, contradict 'observations', the results of risk analyses are falsified and seem not to be plausible.

The first observation relates to accepted risk measures. The accepted individual risk in the Netherlands depends on 'the degree to which the activity is voluntary', e.g. $\mathcal{R}_{accepted}^{ind} = 10^{-4}\frac{1}{year}$ for 'employees' to $\mathcal{R}_{accepted}^{ind} = 10^{-6}\frac{1}{year}$ for 'persons living near the [road] tunnel' [65, p. 218f]. Also, Vrijling 1998 [66, p. 143] describes a difference by an order of magnitude of two for activities with 'direct benefit'. Looking at the accepted societal risk curve, it varies in the same order [65, p. 218f; 66, p. 143; 67, Fig. 2] where Wahlström 2018 [67, Fig. 2] depicts accepted societal risk curves of seven European countries as shown in Fig. B.6. Additionally, the limiting and the accepted societal risk curves in Bedford 2001 [68, p. 8f] differ with an equal range. The former one is $\mathcal{R}_{limit}^{soc}\left(N_{fat}\right) = 10^{-3-2N_{fat}}\frac{1}{year}$ which is not to be exceeded, and the latter one is $\mathcal{R}_{accepted}^{soc}\left(N_{fat}\right) = 10^{-5-2N_{fat}}\frac{1}{year}$.

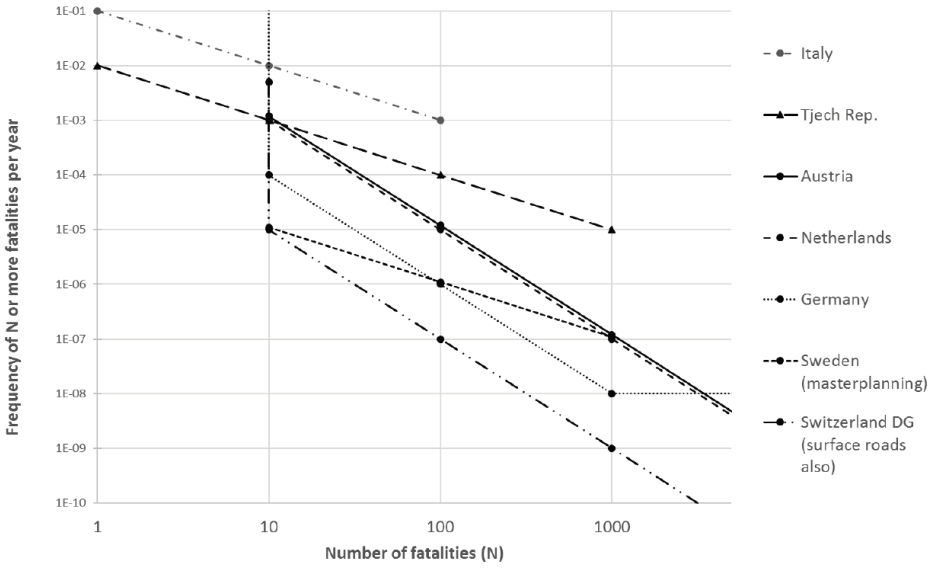

Figure B.6: Accepted societal risk curves of European countries; the figure was adopted from Wahlström 2018 [67, Fig. 2].

Next, observation two stems from an overview on societal risk curves in 'several hypothetical and comparable real [road] tunnels' of Wahlström 2018 [67, Fig. 6] depicted in Fig. B.7. In particular, these societal risk curves comprise scenarios with more than 100 fatalities.

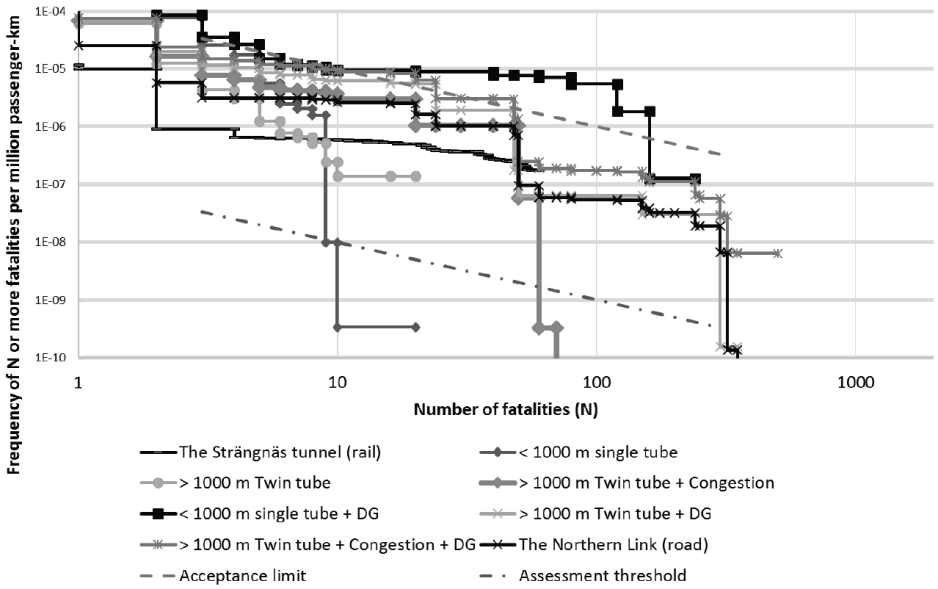

Figure B.7: Risk curves from risk analyses of 'hypothetical and comparable real [road] tunnels'; the figure was adopted from Wahlström 2018 [67, Fig. 6].

Concluding, the evaluation of the plausibility of risk measures derives from falsification with two observations: first, the accepted risk measures with the individual risk between $10^{-6}\frac{1}{year} \leq \mathcal{R}^{ind} \leq 10^{-4}\frac{1}{year}$ and the societal risk curve between the accepted and the limiting societal risk curves; and second, the societal risk curve should resemble the results of other risk analyses in [67, Fig. 6], esp. with respect to the number of fatalities. Beside, the risk measures of risk analyses should not be subjected to larger variations than an order of magnitude of two.

But the focus on the upper evacuation area in the system model requires some discussion as already detailed in Berchtold 2016 [8]. With regard to the individual risk, the FF in the upper evacuation area is expected to be higher than in other parts of the road tunnel. Hence, the individual risk considering the entire tunnel is elevated in this methodology for risk analysis. On the other hand, the number of fatalities is only counted in the upper evacuation area. This focus underestimates the number of fatalities in the entire road tunnel, particularly in case of scenarios with rare events and also affects the frequency of scenarios in the upper part of the societal risk curve.

To be noted, both observations derive from theory or other risk analyses and not from real fire scenarios. Thus, the comparison will only be used to question the results of the methodology for risk analysis in this dissertation and not to calibrate or improve the risk analysis itself.

C Experimental design

The ED constitutes the first integral part of the metamodel and specifies the discrete scenarios for the simulations with the complex model. Section C.1 introduces different methods used for the setup of an ED. Then, Section C.2 describes the projection array-based design (PAD) as it is used in this dissertation and details some differences to the original publication of the PAD method in Leoppky 2012 [25]. Section C.3 briefly summarises the entire setup of an ED and sketches the selection process. The selection process finally results in an ED which serves for the data base, the second integral part, of the metamodel.

C.1 Overview on literature

In Subs. 'Metamodel' (p. 23) it is shortly reasoned why the RSMs in this dissertation are subjected to deterministic results of the complex model. Also, Santner 2003 [10, p. 124] assumes that deterministic models are generally applied for 'computer experiments' and hence 'A single observation at a given set of inputs [data point] gives us perfect information about the response [result of the complex model] at that set of inputs, so replication is unnecessary'. With this assumption, the publication then derives two principles for EDs: first, 'Designs should not take more than one observation [deterministic result] at any set of inputs [data point]'; and second, EDs '[...] should allow one to fit a variety of models and should provide information about all portions of the experimental region [entire domain]', in other words, the EDs should direct at the global objective. Hence, Santner 2003 recommends to 'use [experimental] designs that spread the points at which we observe the response evenly throughout the region' which is named as 'space-filling'. Equally, Myers 2002 [20, p. 482] describes the same principles for deterministic 'computer models'.

Current methods for EDs

Full factorial designs (FFD) [10, p. 126], denoted with X^{FFD}, are basic EDs which achieve both principles. In particular, a FFD with two levels having only data points at the outer vertices of the domain, is called two-level FFD.

Also, Latin hypercube designs (LHD), originally published in [26], meet both principles according to the publications [10, p. 125; 20, p. 482]. For instance, the risk analysis in fire safety engineering of Weyenberge 2017 [33] applies LHDs. Thus, the LHD method is suitable for objective 1 (metamodel). The setup of LHDs was already detailed in various ways, e.g. [10, p. 127; 69], which necessitates only to emphasise two characteristics: the LHD method is subjected to a structure which can lead to issues in the sequential refinement of a LHD; and LHDs can lack of space-filling due the randomness in their setup.

Accordingly, the aim of a structured literature overview on EDs for computer experiments was to choose a method for EDs on the basis of the current state of research with: the capability for focused sequential refinement on regions of the domain; and an improved space-filling compared to the LHD method. As a result, the PAD method of Leoppky 2012 [25] serves for the ED in this dissertation. Therewith, the ED can improve the efficiency of the metamodel

and directs at the global objective. Hence, the PAD method provides the basis for objective 2 (efficiency) and objective 1 (metamodel) respectively.

In detail, the PAD method extends the structure of LHDs as depicted in Fig. C.1. The structure of LHDs consists of 'disjoint subsets [...] of equal probability' [69, p. 312] named as substrata. Thus, the LHD-condition is to yield exactly one data point in each substratum of the ED. Accordingly, the number of data points equals the number of substrata. Moreover, a PAD X^{PAD} is subjected to a structure of projection arrays (PA) formed by strata. The number of strata is $N_{strata} = \left\lceil N_{\mathrm{dps}}^{\frac{1}{N_{\mathrm{rf}}}} \right\rceil$ with $\lceil\,\rceil$ as the ceiling function, and the number of projection arrays is $N_{strata}^{N_{\mathrm{rf}}}$ [25]. The additional PA-condition is to have at maximum one data point in each PA of the ED. Concluding, the PA-condition supports the LHD-condition and enhances the even spread of data points on the entire domain. In other words, the PAD method improves the space-filling of the LHD method.

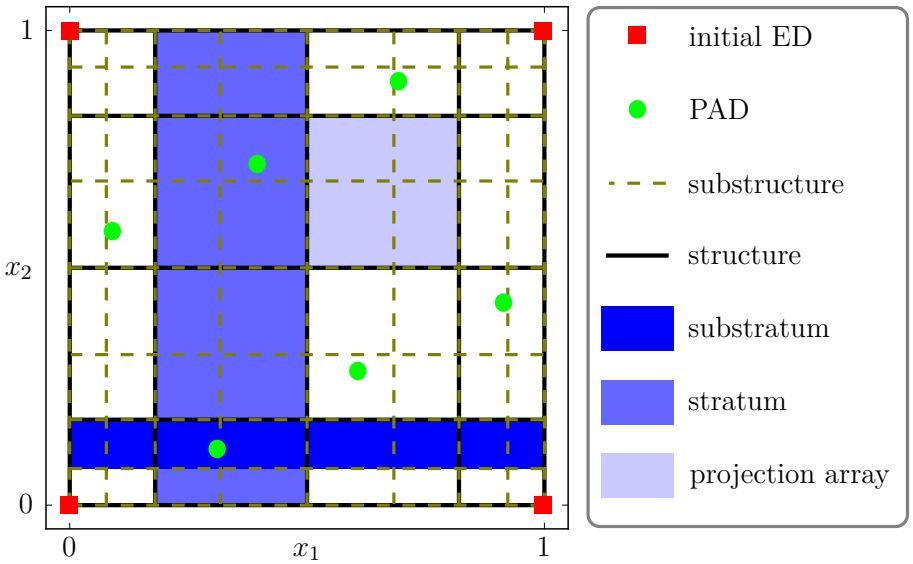

Figure C.1: Composed ED with focus on the outer vertices of the domain with the risk factors x_1 and x_2; the initial ED is located at the outer vertices.

Focused sequential refinement and improvement of space-filling

Originally, the PAD method allows to focus on single strata or projection arrays during the sequential refinement as illustrated in Leoppky 2012 [25, Fig. 4]. This approach can cause large differences in the number of data points between neighbouring projection arrays or strata. In contrast, the approach applied in the metamodel of this dissertation accounts for a steady increase of the number of data points to the region of the domain in focus.

Leoppky 2012 [25, p. 1495f] illustrates and recommends near orthogonal arrays to improve space-filling, similar to orthogonal array-based LHDs [21]. However, this approach subjects data points to random positions within a PA which requires further improvement of space-filling, e.g. with the optimisation of distance measures as in publications [10, p. 138] and [69, p. 311]. Therefore, the PAD method in this dissertation neglects the orthogonality of arrays but merely optimises distance measures resulting in good space-filling of the EDs.

Optimisations of distance measures, i.e. the maximin or minimax distances, are useful in case of randomness in the setup of EDs, e.g. with the LHD or the PAD method. The maximin optimisation specifies the maximin distance $d_{maximin}$ of an ED. In other words,

it maximises the minimum euclidean distance between all data points in N_{mami} random EDs according to Eq. C.1 with Eq. C.2. Next, the minimisation of the maximum euclidean distance from any arbitrary point $\widetilde{x} \in \widetilde{X}$ in the domain to its closest data point is called the minimax optimisation. It results in the minimax distance $d_{minimax}$ with Eq. C.3 and Eq. C.4 after evaluating N_{mima} random EDs. Beside the maximin and minimax optimisation, this dissertation also minimises the coefficient of variation of euclidean distances between all data points d_{cov}. As a result, the distance measures $d_{maximin}$, $d_{minimax}$ and d_{cov} can be used to evaluate space-filling of EDs.

$$d_{maximin} = \max\left\{d_{min}\left(X_1\right), \ldots, d_{min}\left(X_{N_{mami}}\right)\right\} \tag{C.1}$$

$$d_{min}\left(X\right) = \min\left\{d\left(\vec{x}_i, \vec{x}_k\right), \ldots \middle| \forall \vec{x}_i \in X \wedge \vec{x}_i \neq \vec{x}_k \in X\right\} \tag{C.2}$$

$$d_{minimax} = \min\left\{d_{max}\left(X_1\right), \ldots, d_{max}\left(X_{N_{mima}}\right)\right\} \tag{C.3}$$

$$d_{max}\left(X\right) = \max\left\{d\left(\widetilde{x}, \vec{x}_i\right), \ldots \middle| \forall \vec{x}_i \in X, \widetilde{x} \in \widetilde{X}\right\} \tag{C.4}$$

C.2 Projection array-based design applied in the metamodel

Subs. 'Metamodel' (p. 23) provides the background on the ED with regard to the efficiency of the metamodel, in particular it introduces the focused sequential refinement on regions of the domain as well as the combination of EDs. Now, the entire algorithm to setup an ED in this dissertation is described with, firstly, some preliminary assumptions, details to the PAD algorithm espacially with regard to the focus, the sequential refinement and last the space-filling of the ED. Finally, the combination of EDs for fire and evacuation scenarios is explained. This algorithm completely uses a unit hypercube with the domain $[0, \ldots, 1]$ for each risk factor.

Preliminary assumptions

The ED in this dissertation is composed of a two-level FFD $X_0 = X^{\mathrm{FF2}}$ as initial ED and a PAD X_1^{PAD} in the first refinement step: $X_1 = \left[X^{\mathrm{FF2}^T}, X_1^{\mathrm{PAD}^T}\right]^T$. This composition prevents extrapolation of RSMs. Because the two-level FFD has multiple data points at the outer vertices of the domain, the number of substrata has to be adapted in the setup of the PAD. In detail, $2 \cdot 2^{\|\vec{x}\|-1} = \|X^{\mathrm{FF2}}\|$ data points of the two-level FFD are in the outer substrata of all risk factors as it is obvious in Fig. C.1. Two options for adaptions are apparent. First, to keep the number of substrata equal to the number of data points in the composed ED. But this option would lead to two substrata empty on each risk factor. And second, to not consider the data points of the two-level FFD at all causing three data points at the outer substrata. Another option is to consider multiple data points of an outer substratum as only one data point on each risk factor. Hence, the number of substrata in the composed ED is by two higher than the number of data points in the mere PAD, namely $\|X^{\mathrm{PAD}}\| + 2$. The latter option seems to favour the evenly distributed data points and is for this reason used in this dissertation.

Commonly, the width of substrata of LHDs depends on the probability distribution of the risk factors, e.g. as for the improved sampling in Monte-Carlo simulations [69]. But the metamodel in this dissertation aims to reduce the metamodel uncertainty efficiently. Additionally, system

model simulations outlined in Section B.5 only use uniform distributions in all risk factors. As a consequence, the widths of substrata does not depend on the probability distributions in the risk factors but are adapted to focus on regions with high metamodel uncertainty.

PAD algorithm

The PAD algorithm for a batch of data points differs to the description in Leoppky 2012 [25] in order to flexibly compose EDs of different methods. It mainly differs in successively adding single data points to the existing ED instead of adding a batch of data points in a whole. But before adding all the data points of the entire batch, the levels of strata and substrata are specified to correspond to the final number of data points of the entire ED. Fig. C.2 shows the three steps to add one data point. First, a PA is randomly chosen among all PAs without a data point. Second, the substrata of this PA are prioritised with three priority levels for each risk factor. The priority of a substratum depends: on existing data points, i.e. free or full; and on whether the substratum is either completely in the PA or overlaps with the stratum limits, referred to as complete or overlapping. The priority levels are: three, for free and complete substrata; two, for free and overlapping substrata; and one, for full substrata. A data point added to a full substratum with the priority level one fails the LHD-condition. Therefore, the substrata with the priority level one are only considered in the PAD algorithm if necessary to complete the entire batch of data points. Third, the data point is added to the existing data points of the ED. For this, a substratum is randomly chosen among all substrata with the highest priority level and with a width-weighted probability. Then, the data point is uniformly distributed within the limits of the chosen PA and substrata. Finally, the PAD algorithm stops if the required number of data points of the batch is reached.

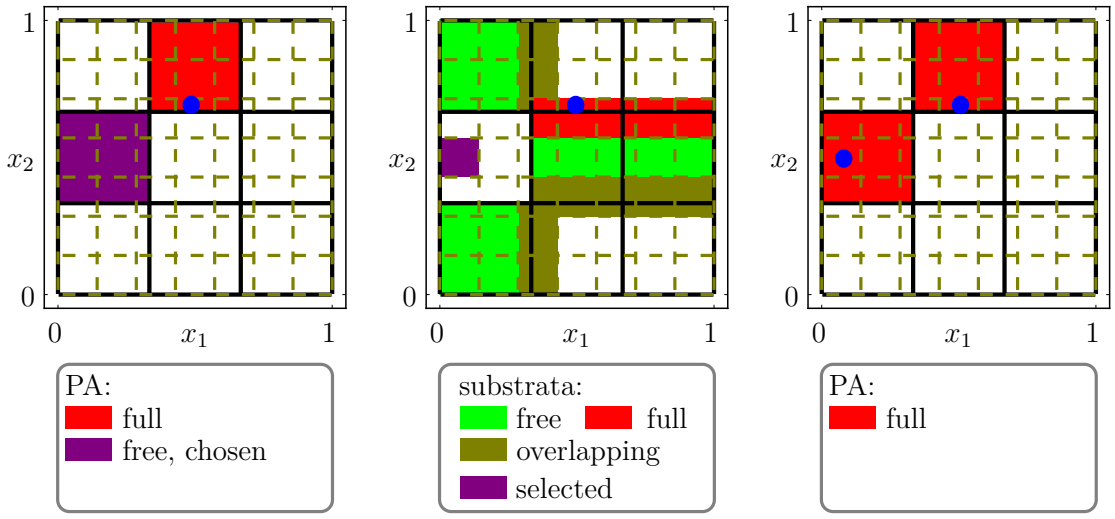

Figure C.2: Three steps of the PAD algorithm to add a new data point: first, to randomly choose a free PA without existing data point (left); second, to set the priority levels of the substrata within the PA for each risk factor and select the substratum with the highest priority level (centre); third, to add a new data point to the selected substrata (right).

The even spread of data points in the domain depends on the LHD-conditions of data points in the PAD. If data points are subjected to substrata with the priority level one and fail the LHD-condition, another substratum remains empty. The empty substratum leads to the preference of substrata completely lying in a stratum which means an uneven spread of data points in the domain of the risk factor. In case of complete LHD-condition, that is all data

points achieve the LHD-condition, the PAD algorithm guarantees an even spread of data points despite the prioritisation of substrata. The reasons are: the random choice of a PA without existing data point; the filling of all substrata with one data point according to the LHD-condition; and the width-weighted choice of a substratum. As a consequence, there is neither a preference of a PA nor of both parts of an overlapping substratum.

Focus on regions of the domain

The approach to focus on a region of the domain aims at the steady increase of the number of data points to this region. Basically, it stretches the level widths w_{level} of strata or substrata with Eq. C.5. The term 'level' specifies a particular stratum or substratum. Hence, the number of levels N_{levels} is equal to the number of strata or substrata. The stretching further depends on the level centre x_{level} of the risk factor $x \in [0, \ldots, 1]$ in the unit hypercube and is axially symmetric to the domain centre $x = 0.5$. After the stretching of all levels, the sum of all level widths is again normalised to the domain of the unit hypercube.

$$w_{level} = \frac{\exp\left(|x_{level} - 0.5| \cdot \log\left(p_{stretch}\right)\right)}{\sum_{level=1}^{N_{levels}} w_{level}} \tag{C.5}$$

The stretching parameter $p_{stretch}$ controls the focus on regions. $p_{stretch} = 1$ maintains equal level widths without focus on a particular region. With $p_{stretch} > 1$ the focus lies on the centre of the domain and with $p_{stretch} < 1$ the level widths shrink to the outer vertices as exemplified in Fig. C.1. Up to now, the same stretching parameter is valid for all risk factors leading to an identical focus.

Sequential refinement

Fig. B.4 on p. 26 depicts the successive steps within one sequential refinement step. Eq. C.6 summarises the first step of these successive steps, i.e. adding new data points X_{new}^{PAD} with the PAD algorithm, to get from the ED X_{i-1} to the ED X_i. The PAD algorithm begins with the setting of new strata and substrata for the ED X_i with respect to its number of data points and its stretching parameter. The new strata and substrata naturally differ to the previous ED X_{i-1} and as a consequence existing data points in the ED X_{i-1} can fail the PA- or LHD-conditions. In this case, Leoppky 2012 [25, p. 1501] accepts fails with the remark 'In general it is possible to have repeated combinations [more than one data point] in an induced PA structure [a projection array] from a PA-based design.'

$$X_i = \left[{X_{i-1}}^T, {X_{new}^{\mathrm{PAD}}}^T\right]^T \tag{C.6}$$

However, the PAD method in this dissertation applies an approach to prevent fails of PA- and LHD-conditions during the setup of the ED X_i. This approach bases on the assumption of the number of data points and the stretching parameter of a future ED X_{i+1}. Afterwards, it checks the PA- and LHD-conditions for the data points of the ED X_i with regard to the assumed strata and substrata of the future ED X_{i+1}. So, there is an option to discard the ED X_i during selection of the ED as a consequence of this additional check.

Improvement of space-filling

The automatic improvement of space-filling uses the maximin and minimax optimisations which both employ the randomness in the PAD algorithm. The maximin optimisation is nested in the minimax optimisation and also integrates the improvement of PA- and LHD-conditions.

For the setup of the ED X_i, the maximin optimisation generates N_{mami} EDs $\{X_{i,1}, \ldots, X_{i,N_{\text{mami}}}\}$ according to the PAD algorithm. It determines the distance measure d_{min} between new data points $X_{new,j}^{\text{PAD}}$ to all data points in $X_{i,j}$ for each ED $X_{i,j}$ with Eq. C.2. Also, the integrated improvement of PA- and LHD-conditions discards an ED $X_{i,j}$ if its data points fail more often in the PA- or LHD conditions than an automatically set threshold value. In this case, the ED $X_{i,j}$ does not count to the total number N_{mami}. A fail can be either caused in the PAD algorithm by the choice of a substrata with the priority level one, the adapted strata and substrata in the sequential refinement or by the combination of fire and evacuation scenarios. Finally, the maximin optimisation chooses the ED $X_i^{\text{mami}} \equiv X_{i,j}^{\text{mami}}$ with $d_{maximin}$ according to Eq. C.1.

The minimax optimisation first defines a FFD representing the arbitrary points $X^{\text{FFD}} \equiv \tilde{X}$ in Eq. C.4. The FFD has either 50 levels in the ED for fire scenarios X^{fire} with two risk factors or ten levels in the ED for evacuation scenarios with four risk factors. Next, the minimax optimisation produces N_{mima} EDs $\left\{X_{i,1}^{\text{mami}}, \ldots, X_{i,N_{\text{mima}}}^{\text{mami}}\right\}$ all subjected to the maximin optimisation and picks the ED $X_i^{\text{mima}} \equiv X_{i,j}^{\text{mima}}$ with $d_{minimax}$ in accordance with Eq. C.4 and Eq. C.3. To sum up, the ED X_i^{mima} was subjected to the maximin and minimax optimisations and finally serves for the selection of the ED X_i.

Combination of EDs

The discrete fire and evacuation scenarios for the complex model are based on two different EDs X^{fire} and X^{evac}. Usually, the values of fire risk factors of an evacuation scenario do not correspond to the values of fire risk factors of an fire scenario, namely $\vec{x}_i^{\text{fire}} \in X^{\text{evac}} \neq \vec{x}_j^{\text{fire}} \in X^{\text{fire}} \forall i, j$. Thus, the ED for evacuation scenarios has to be adapted in order to combine the evacuation scenarios with the fire scenarios, i.e. to consider the smoke spread. More precisely, the fire risk factors of the evacuation scenario $\vec{x}_i^{\text{evac}} \in X^{\text{evac}}$ adopt the values of the fire risk factors of a fire scenario $\vec{x}_j^{\text{fire}} \in X^{\text{fire}}$ leading to $\vec{x}_i^{\text{fire}} \in X^{\text{evac}} = \vec{x}_j^{\text{fire}} \in X^{\text{fire}}$. For this adaption, there are two basic modes to choose the fire scenario $\vec{x}_j^{\text{fire}} \in X^{\text{fire}}$ for the evacuation scenario $\vec{x}_i^{\text{evac}} \in X^{\text{evac}}$.

The mode 'projection array' compares the projection arrays with strata of the ED X^{fire} of an evacuation scenario $\text{PA}\left(\vec{x}_i^{\text{fire}} \in X^{\text{evac}}\right)$ with the projection arrays of all fire scenarios $\text{PA}\left(\vec{x}_j^{\text{fire}} \in X^{\text{fire}}\right) \forall j$. Then, the fire risk factors of the evacuation scenario $\vec{x}_i^{\text{evac}} \in X^{\text{evac}}$ adopt the values of the fire risk factors of the fire scenario $\vec{x}_j^{\text{fire}} \in X^{\text{fire}}$ with equal projection arrays $\text{PA}\left(\vec{x}_i^{\text{fire}} \in X^{\text{evac}}\right) = \text{PA}\left(\vec{x}_j^{\text{fire}} \in X^{\text{fire}}\right)$. But the ED X^{fire} does not necessarily occupy all PAs. Hence, there might be no fire scenario which matches the PA of the evacuation scenario: $\text{PA}\left(\vec{x}_i^{\text{fire}} \in X^{\text{evac}}\right) \neq \text{PA}\left(\vec{x}_j^{\text{fire}} \in X^{\text{fire}}\right) \forall j$. As a result, the combination of this evacuation scenario with a fire scenario is not successful. Therefore, the evacuation scenario has to be discarded leading to an empty substratum and a fail in the LHD-condition.

In the mode 'closest', the fire risk factors of the evacuation scenario $\vec{x}_i^{\text{evac}} \in X^{\text{evac}}$ adopt the values of the fire risk factors of the fire scenario $\vec{x}_j^{\text{fire}} \in X^{\text{fire}}$ with the smallest euclidean distance, $d\left(\vec{x}_i^{\text{fire}}, \vec{x}_j^{\text{fire}}\right) = \min\left\{d\left(\vec{x}_i^{\text{fire}} \in X^{\text{evac}}, \vec{x}_j^{\text{fire}} \in X^{\text{fire}}\right) \forall j\right\}$, between both scenarios. But the projection arrays of both scenarios may differ, i.e. $\text{PA}\left(\vec{x}_i^{\text{fire}} \in X^{\text{evac}}\right) \neq \text{PA}\left(\vec{x}_j^{\text{fire}} \in X^{\text{fire}}\right)$. Thus, the PAs of the fire risk factors in the evacuation scenario change which can result in the fail of the PA-condition.

Concluding, the combination of both basic modes brings advantages. In detail, if the mode 'projection array' does not lead to a successful combination of an evacuation scenario with a fire scenario and this evacuation scenario is required to reach the number of data points to

complete the entire batch in the ED X^{evac}, the mode 'closest' is used. The mode 'closest' definitely combines the evacuation scenario with a fire scenario. This combination leads to good space-filling due to the PA-condition with only some fails in PA- and LHD-conditions.

Finally, the number of fire scenarios is lower than the number of evacuation scenarios to increase the efficiency of the metamodel. Hence, multiple evacuation scenarios aggregate in the region of the same fire scenario as highlighted in Fig. E.2 on p. 54. In other words, these evacuation scenarios have equal values in their fire risk factors and consequently fail the LHD-condition. For this reason, the fire risk factors of evacuation scenarios are excluded for the evaluation of the LHD-condition.

C.3 Setup and selection of the experimental design

Fig. C.3 sketches the setup and selection of the final ED X_i in a refinement step of the ED X_{i-1}. The selection process begins with the definition of the new strata and substrata for the ED X_i and continues with the setup of multiple EDs $\{X_1^{mima}, \dots\}$. The setup is detailed in Section C.2, esp. with regard to Subs. 'PAD algorithm' (p. 34), Subs. 'Focus on regions of the domain' (p. 35) and Subs. 'Improvement of space-filling' (p. 35). Obviously, the setup of an ED for evacuation scenarios X_i^{evac} requires the corresponding ED for fire scenarios X_i^{fire} as explained in Subs. 'Combination of EDs' (p. 36). The selection process continues with the analysis of the distance measures $d_{minimax}$, $d_{maximin}$ and d_{cov}, as well as of the LHD- and PA-conditions. It is divided into successive steps each with focus on different measures. Hence, there are options to discard EDs, e.g. subjected to possible fails in PA- or LHD-conditions in future EDs discussed in Subs. 'Sequential refinement' (p. 35). And at the end, it remains one ED X_i which finally specifies the discrete scenarios for the data base used in the metamodel.

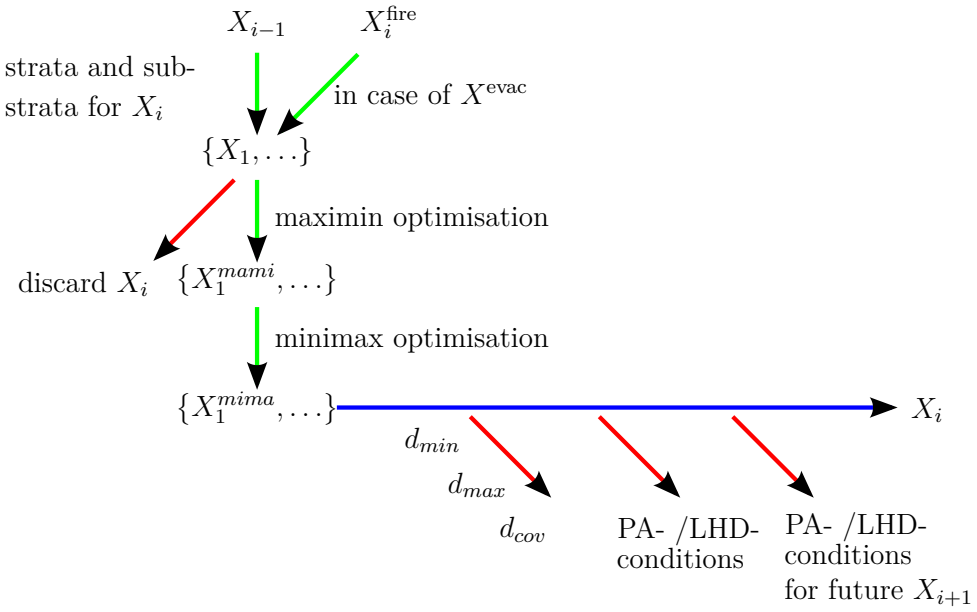

Figure C.3: Process to setup and select an ED X_i: the setup of one ED X_i^{mima} (green arrows) bases on $N_{\text{mami}} \cdot N_{\text{mima}}$ EDs subjected to maximin and minimax optimisations with the option to discard EDs failing the PA- or LHD-conditions (red arrow); and the selection process (blue arrow) bases on multiple X_i^{mima} and evaluates each ED with the distance measures $d_{minimax}$, $d_{maximin}$ and d_{cov} and with regard to the PA- and LHD-conditions (red arrows).

D Response surface method and metamodel

After the ED and the data base, the RSM is the third integral part of the metamodel. First, Section D.1 presents different response surface methods and provides the background to the metamodel uncertainty and the evacuation uncertainty. Then, Section D.2 describes specific approaches used for the RSM and the metamodel uncertainty in this dissertation. And Section D.3 concentrates on the direct approach originally developed for the evacuation uncertainty in this dissertation. Finally, Section D.4 outlines the integration and evaluation of the metamodel in the system model. To sum up, moving least squares (MLS) is established to be used in the system model. For this purpose, the subsections use the general notation outlined in Subs. 'Remarks on the mathematical notation' (p. G-3) of App. G.1 to emphasise the generality of the metamodel.

D.1 Overview on literature

In Subs. 'Metamodel' (p. 23) of Section B.4 the use of deterministic RSMs in this dissertation is explained. With this background and the background in Section D.1.1, Section D.1.2 gives an overview on different response surface methods used for risk analysis and provides the reasons for the selection of MLS in this dissertation. Afterwards, Section D.1.3 describes MLS in detail. And finally, the metamodel uncertainty as well as the evacuation uncertainty for the metamodel are established in Section D.1.4 and Section D.1.5.

D.1.1 Response surface methods and model adequacy checking

This section first introduces the general formulation of RSMs on the basis of the global least squares regression method. Then, it directs at methods for the validation of RSMs, or in other words for the model adequacy checking.

Global least squares regression method

Myers 2002 [20, p. 18ff] describes the background for the linear least squares regression method. For this method, Eq. D.1 defines a multiple linear regression model. It considers the deterministic results of the complex model at N_{dps} data points $\vec{x}_i \in X$ in the data base $\bar{\boldsymbol{Y}}^c$. Their corresponding approximation errors $\boldsymbol{\delta y}$ are supposed to be normally distributed with the mean $\mu(\boldsymbol{\delta y}) = 0$ and the variance $\mathrm{var}(\boldsymbol{\delta y})$. The underlying polynomial to the regression model consists of polynomial terms with the regression coefficients $\boldsymbol{\beta}$. The number of polynomial terms is denoted with $N_{\mathrm{terms}} \equiv \|\boldsymbol{\beta}\|$. Eq. D.2 and Eq. D.3 exemplify a linear and a quadratic polynomial for two control variables at the data point $\vec{x}_i = [x_{i,1}, x_{i,2}]$ [20, p. 56]. Accordingly, the polynomial terms $\boldsymbol{P}$ represent the ED X in a $N_{\mathrm{dps}} \times N_{\mathrm{terms}}$ matrix.

$$\bar{\boldsymbol{Y}}^c = \boldsymbol{P}\boldsymbol{\beta} + \boldsymbol{\delta y} \tag{D.1}$$

$$\bar{y}_i^c = \beta_0 + \beta_1 x_{i,1} + \beta_2 x_{i,2} \tag{D.2}$$

$$\bar{y}_i^c = \beta_0 + \beta_1 x_{i,1} + \beta_2 x_{i,2} + \beta_{11} x_{i,1}^2 + \beta_{22} x_{i,2}^2 + \beta_{12} x_{i,1} x_{i,2} \tag{D.3}$$

The linear regression in Eq. D.4 minimises the variance of the approximation errors var $(\boldsymbol{\delta y})$ and results in the least squares estimators b_{ls} of the regression coefficients $\boldsymbol{\beta}$. Next, the least squares estimators in the dot product of Eq. D.5 lead to the result of the RSM $\bar{y}_0 = \bar{y}\left(\widetilde{x}_0\right)$ at an arbitrary point with the polynomial terms $\widetilde{\varphi}_0$. Since the least squares estimators yield for the entire domain, Eq. D.4 and Eq. D.5 constitute a global RSM without '*spatial sensitivity*'.

$$b_{ls} = \left(\boldsymbol{P}^T \boldsymbol{P}\right)^{-1} \cdot \boldsymbol{P}^T \bar{\boldsymbol{Y}}^c \tag{D.4}$$

$$\bar{y}_0 = \widetilde{\wp}_0^T \cdot b_{ls} \tag{D.5}$$

In general, the RSM approximates the results of the complex model and does not interpolate them. The difference between approximation and interpolation lies in the residuals, i.e. the difference between the result of the RSM and the result of the complex model at a data point $\bar{y}^c\left(\vec{x}_i\right) - \bar{y}\left(\vec{x}_i\right)$. Approximation leads to residuals different to zero whereas the residuals are zero in case of interpolation. Furthermore, the term 'near interpolation' means an approximation with residuals close to zero.

Model adequacy checking

The validation of a RSM consists of two parts in which the residuals 'play an important role in judging model adequacy' according to Myers 2002 [20, p. 43]. The first part questions the assumption in the least squares regression on the normally distributed approximation errors in Eq. D.4. For this purpose, normal probability plots are used. The second part concerns with the accuracy of the RSM with regard to the results of the complex model and applies the generalisation error. Summing up, both parts of the model adequacy checking evaluate whether the metamodel fits adequately and therewith provides the basis for objective 1 (metamodel).

A normal probability plot illustrates the residuals of a RSM [20, p. 43]. For this, it shows the residuals of all data points normalised to the domain $[0, 1]$ on the vertical axis. The residuals are plotted in relation to the corresponding quantiles of a standard normal distribution on the horizontal axis. The first normal probability plot in this dissertation is exemplified in Fig. E.5 on p. 58.

Next, the generalisation error gmse in Eq. D.6 is based on the 'leave-one-out cross-validation' [21, p. 10]. 'Leave-one-out' means that the result $\bar{y}_{-i} \equiv \bar{y}_{X_{-i}}\left(\vec{x}_i\right)$ at the data point $\vec{x}_i$ stems from a RSM subjected to the data base of the ED excluding this data point $X_{-i} \equiv X_i \setminus \vec{x}_i$. The generalisation error is similar to the prediction error sum of squares in Myers 2002 [20, p. 46]. There, it was introduced for model adequacy checking, esp. to ensure that the RSM represents the response surface.

$$\text{gmse} = \frac{1}{N_{\text{dps}}} \sum_{i=1}^{N_{\text{dps}}} \left(\bar{y}_{-i} - \bar{y}_i^c\right)^2 \tag{D.6}$$

Close to Eq. D.6, the variance estimator of the RSM derives from Eq. D.7 where the degree of freedom is $N_{\text{dps}} - N_{\text{terms}}$ with $N_{\text{terms}} = \|\boldsymbol{\beta}\|$ [28, p. 3]. The residuals in Eq. D.7 are analysed

by two different ways in this dissertation. First, in the variance estimator σ_X^2, the result of the RSM $\bar{y}_i \equiv \bar{y}_X(\vec{x}_i)$ is subjected to the data base of the complete ED X. And second, the variance estimator σ_{-i}^2 uses the leave-one-out approach for the result of the RSM $\bar{y}_{-i}$ instead of $\bar{y}_i$ in Eq. D.7. Thus, it is similar to the generalisation error.

$$\sigma^2 = \frac{1}{N_{\text{dps}} - N_{\text{terms}}} \sum_{i=1}^{N_{\text{dps}}} (\bar{y}_i - \bar{y}_i^c)^2 \tag{D.7}$$

The generalisation error further provides information on the bias and variance of a RSM [20, p. 442]. Looking at the bias error, Santner 2003 [10, p. 124] continues the description of the ED cited in Section C.1 with: 'Uncertainty arises in computer experiments because we do not know the exact functional form of the relationship between the inputs [arbitrary point] and the response, although the response can be computed at any given input [data point]. Any functional models [response surface models] that we use to describe the relationship are only approximations [simplifications]. The discrepancy between the actual response produced by the computer code [result of the complex model at a data point] and the response we predict from the model we fit [response surface model] is our error. [...] we referred to such error as model bias.' Or briefly, the bias error is the difference between the result of the RSM and the result of the complex model. Therefore, it can be quantified with the residuals at all data points [21, p. 5]. The variance error 'measures the extent to which the surrogate model [RSM][...] is sensitive to a particular data set D [ED]. Each data set D corresponds to a random sample [data points] of the function of interest [response surface]' [21, p. 5]. In other words, it expresses qualitatively the sensitivity of the RSM to variations in the ED. And coming back to the generalisation error, there is always a 'trade-off between bias error and variance error' [21, p. 5] in the fitting of a RSM depending on its spatial sensitivity.

D.1.2 Current response surface methods

Apart from the global least squares regression method, a structured literature overview on the current research on response surface methods revealed the common use of neural networks as well as of MLS for risk analysis. Beside this common use, MLS was chosen for the methodologies for risk analysis in fire safety engineering by Albrecht 2014 [30] and Weyenberge 2017 [33] as revealed in Section B.1. Consequently, and because of its global objective, MLS serves as response surface method in this dissertation. But next to MLS, the global least squares regression method as well as two local interpolation methods used for risk analysis of road tunnels according to Section A.1 are evaluated.

The two local interpolation methods for nearest (LIn) as well as for linear (LIl) local interpolation are similar to the use of discrete scenarios in the methodology of Germany [13] and to the mapping approach in the methodology of Austria [14] respectively. Both methods are realised with a method for unstructured data points. On the one hand, a LIn model $\bar{\boldsymbol{Y}}^{\text{LIn}}$ directly adopts for the result at an arbitrary point the result of the data point with the smallest euclidean distance between both. Accordingly, LIn models are highly spatially sensitive and lead to a '*discontinuous*' shape. On the other hand, the result of the LIl model $\bar{\boldsymbol{Y}}^{\text{LIl}}$ at an arbitrary point derives from the linear interpolation between the '*neighbours*' disregarding other data points and thus, it neglects non-linearities. Hence, the shape of the LIl model is continuous but not differentiable at data points. Additionally, the LIl model adopts results of LIn in case of extrapolation, for instance occurring during the leave-one-out approach.

Section D.1.1 already introduced the global least squares regression method. In more detail, the first order method (FoM) and the second order method (SoM) base on polynomials

like Eq. D.2 and Eq. D.3 respectively. With these polynomials, Eq. D.5 leads to global RSMs, namely the FoM and SoM models, which are not spatially sensitive. Their results are denoted with $\bar{\boldsymbol{Y}}^{\mathrm{FoM}}$ and $\bar{\boldsymbol{Y}}^{\mathrm{SoM}}$.

D.1.3 Moving least squares method

MLS was first proposed by Lancaster 1981 [27] and e.g. more recently outlined by Most 2008 [70]. Basically, it applies a locally weighted least squares regression of a linear or quadratic polynomial according to Eq. D.2 or Eq. D.3 at an arbitrary point $\widetilde{x}_0$. For this, Eq. D.8 extends Eq. D.4 with the weighting matrix $\boldsymbol{W}_0 \equiv \boldsymbol{W}(\widetilde{x}_0)$. The weighting matrix is a diagonal matrix which maps the weighting function $w(\widetilde{x}_0, \vec{x}_i)$ to the data points $\vec{x}_i \in X$. More precisely, the weighting depends on the euclidean distance between the arbitrary point to each data point. Therewith, the MLS estimators $b_0 \equiv b(\widetilde{x}_0)$ are only valid for the arbitrary point. And as a consequence, Eq. D.9 leads to a local result of the MLS model $\bar{y}_0 \equiv \bar{y}(\widetilde{x}_0)$ in contrast to Eq. D.5. In general, the results of a MLS model are denoted with $\bar{\boldsymbol{Y}}$, the symbol $\bar{\boldsymbol{Y}}^{\mathrm{MLS}}$ is only used to clearly differentiate among other response surface methods.

$$\left(\boldsymbol{P}^T \boldsymbol{W}_0 \boldsymbol{P}\right) \cdot b_0 = \boldsymbol{P}^T \boldsymbol{W}_0 \bar{\boldsymbol{Y}}^c \tag{D.8}$$

$$\bar{y}_0 = \widetilde{\wp}_0^T \cdot b_0 \tag{D.9}$$

Usually, MLS is used for deterministic complex models but in Salemi 2016 [29] MLS is subjected to aleatory results of stochastic complex models. Furthermore, the MLS model in Salemi 2016 [29] depends on a large number of control variables. Hence, this example demonstrates that MLS is suitable for the evacuation uncertainty as well as that MLS suffices assumption 1 (complex scenarios) with regard to multiple risk factors. Moreover, the global objective of MLS is the basis for objective 1 (metamodel).

D.1.4 Metamodel uncertainty and the prediction interval method

Section B.1 introduces the metamodel uncertainty with the 'inaccuracy of the metamodel' [28, p. 1]. More precisely, the metamodel uncertainty $\delta\widetilde{y}_0^m$ is the difference between the result of the RSM and the unknown result of the complex model $\delta\widetilde{y}_0^m = \bar{y}_0 - \bar{y}_0^c$ at an arbitrary point $\widetilde{x}_0$. It is subjected to a normal distribution with the mean $\mu(\delta\widetilde{y}^m) = 0$ and the variance $\mathrm{var}(\delta\widetilde{y}^m)$. Eq. D.10 integrates the metamodel uncertainty into the metamodel, namely a non-relative integration equal to Nannapaneni 2016 [22, Eq. 7] or Kim 2008 [28, Eq. 25]. The result of the metamodel integrating the metamodel uncertainty at an arbitrary point is denoted with $\widetilde{y}_0^m$ and explicitly does not consider the evacuation uncertainty. Thus, this result represents the unknown result of the deterministic complex model $\bar{y}_0^c$ at an arbitrary point.

$$\widetilde{y}_0^m = \bar{y}_0 + \delta\widetilde{y}_0^m \tag{D.10}$$

After this background, a method to describe the metamodel uncertainty of MLS as well as methods for its evaluation are presented in Subs. 'Prediction interval method' (p. 42) and Subs. 'Validation of the prediction interval method' (p. 42). For this, Tab. D.1 repeats the notation introduced together with the response surface methods and extends the notation for the metamodel uncertainty. And in addition to the following precis, G.5 details the mathematical background of the prediction interval.

Table D.1: Notation related to response surface methods, the metamodel uncertainty and the evacuation uncertainty.

notation	description
$\boldsymbol{P}$	polynomial terms of the ED X
$\widetilde{\wp}$	polynomial terms of an arbitrary point
b_{ls}	least squares estimators
σ^2_{-i}	variance estimator using the leave-one-out approach
σ^2_X	variance estimator using the complete data base
$\boldsymbol{W}$	weighting matrix
w	weighting function
b	MLS estimators
$\delta\widetilde{y}^m$	metamodel uncertainty
$\widetilde{y}^m$	result of the metamodel integrating the metamodel uncertainty
$\Delta\bar{y}^m$	prediction interval
s^2	prediction variance
$\widetilde{\epsilon}$	relative evacuation uncertainty
$\widetilde{y}^\epsilon$	result of the metamodel integrating the evacuation uncertainty

Prediction interval method

The 'prediction interval is for predicting the interval of the "value of a single future observation" at a point. Therefore, the prediction interval of the response surface is used for the design optimization [...]' [28, p. 4]. Therewith, Kim 2008 [28] introduces a method for the metamodel uncertainty of MLS which is named as prediction interval method in this dissertation. Following this citation, the method serves for the calibration of the RSM and also to quantify the metamodel uncertainty.

Eq. D.11 [28, Eq. 25] defines the prediction interval $\Delta\bar{y}^m_0$ at an arbitrary point $\widetilde{x}_0$. The prediction interval is subjected to the Student distribution $\mathcal{T}$ with its statistic $t_{\alpha/2,N_{\text{dps}}-N_{\text{terms}}}$ for a two-sided confidence level α and the degree of freedom $N_{\text{dps}} - N_{\text{terms}}$. It further applies the 'variance of the prediction error' $s^2 \equiv s^2\left(\bar{y}_0 - \bar{y}^c_0\right)$, or shortly prediction variance, for the variance of the metamodel uncertainty $\text{var}\left(\delta\widetilde{y}^m\right)$. Eq. D.12 [28, Eq. 21] specifies the prediction variance with the variance estimator σ^2 according to Eq. D.7.

$$\Delta\bar{y}^m_0 = \left| t_{\alpha/2,N_{\text{dps}}-N_{\text{terms}}} \cdot \sqrt{s^2_0} \right| \tag{D.11}$$

$$s^2_0 = \sigma^2 \cdot \left(1 + \left(\widetilde{\wp}_0\right)^T \cdot \left(\boldsymbol{P}^T\boldsymbol{W}_0\boldsymbol{P}\right)^{-1} \cdot \boldsymbol{P}^T\boldsymbol{W}_0\boldsymbol{W}_0\boldsymbol{P} \cdot \left(\boldsymbol{P}^T\boldsymbol{W}_0\boldsymbol{P}\right)^{-1} \cdot \widetilde{\wp}_0\right) \tag{D.12}$$

Validation of the prediction interval method

The validation of the prediction interval method has two foci: its spatial sensitivity; as well as its predictive capability. The latter focus follows in particular the citation at the beginning of Subs. 'Prediction interval method' (p. 42).

Since MLS is subjected to linear or quadratic polynomials, local high second derivatives in the response surface should lead to locally increased residuals. Also, there should be a local correlation between residuals and metamodel uncertainties. Accordingly, the prediction interval method should be spatially sensitive to the shape of the response surface. Hence motivated by this rationale, the validation of the spatial sensitivity directs at the visual assessment of the correlation between prediction variances and residuals at data points.

Next, the predictive capability is validated with regard to the confidence level α of the prediction interval in Eq. D.11 of the RSM $\bar{\boldsymbol{Y}}_{X_{eval}}$. In this validation, the confidence level α is juxtaposed to an empirical confidence level α^*. The latter one is the probability p that other real data points lie within the prediction interval $\boldsymbol{\Delta}\bar{\boldsymbol{y}}^m_{X_{eval}}(\alpha)$ of the RSM $\bar{\boldsymbol{Y}}_{X_{eval}}$ as shown in Eq. D.13. This equation basically compares the results of two models: the RSM $\bar{\boldsymbol{Y}}_{X_{eval}}$ and the real model $\bar{\boldsymbol{Y}}^*$ providing the real data points. The real data points derive either from the results of another RSM $\bar{\boldsymbol{Y}}_{X_{real}}$ or directly of the results of the data base $\bar{\boldsymbol{Y}}^c_{X_{real}}$. In both cases, the real model $\bar{\boldsymbol{Y}}^*$ is based on the ED X_{real} which is a disjoint set to X_{eval}, i.e. $X_{real} \cap X_{eval} = \{\}$. In other words, the RSM $\bar{\boldsymbol{Y}}_{X_{eval}}$ is independent to the real model $\bar{\boldsymbol{Y}}^*$. Concluding, Eq. D.13 allows to validate the predictive capability in two approaches: the split-sample validation and the complete-sample validation.

$$\alpha^* = p\left(\bar{\boldsymbol{Y}}_{X_{eval}} - \boldsymbol{\Delta}\bar{\boldsymbol{y}}^m_{X_{eval}}(\alpha) < \bar{\boldsymbol{Y}}^* < \bar{\boldsymbol{Y}}_{X_{eval}} + \boldsymbol{\Delta}\bar{\boldsymbol{y}}^m_{X_{eval}}(\alpha)\right) \tag{D.13}$$

The split-sample validation is based on Queipo 2005 [21, p. 10]. It splits the data base of the ED X into the two disjoint equally sized random subsets X_{eval} and X_{real}. Then, $\bar{\boldsymbol{Y}}_{X_{eval}}$ is the RSM based on the ED X_{eval}. And $\bar{\boldsymbol{Y}}^* = \bar{\boldsymbol{Y}}^c_{X_{real}}$ directly represents the real data points $\vec{x}_i \in X_{real}$ of the complex model. Due to the randomness in the choice of the EDs X_{eval} and X_{real}, the empirical confidence level α^*_{mean} is the mean of n repetitions of the split-sample with Eq. D.13.

The complete-sample validation [28, p. 5] evaluates the prediction interval with results of another real model. The real model is either an analytical function as a substitute of the complex model or a second RSM. In contrast to the split-sample validation, the RSM $\bar{\boldsymbol{Y}}_{X_{eval}}$ applies the complete data base of the ED X_{eval}. Also, the results of the real model are: $\bar{\boldsymbol{Y}}^* = \bar{\boldsymbol{Y}}^c_{X_{real}}$ in case of an analytical function; or $\bar{\boldsymbol{Y}}^* = \bar{\boldsymbol{Y}}_{X_{real}}$ in case of another RSM based on the data base of the ED X_{real}. In both cases, the real model $\bar{\boldsymbol{Y}}^*$ provides the real data points at arbitrary points $\widetilde{X}$.

At last, the prediction interval method has predictive capabilities if both confidence levels $\alpha^* \approx \alpha$ are approximately the same. If the empirical confidence level is clearly increased $\alpha^* > \alpha$, the prediction interval is conservative. In other words, more real points of the real model $\bar{\boldsymbol{Y}}^*$ lie within the prediction interval as expected by the confidence level α.

D.1.5 Evacuation uncertainty and the averaged variance

Evacuation uncertainties, or aleatory uncertainties in general, originate from various environmental variables in the complex model according to Section B.1. As outlined in Subs. 'Complex model within the system model' (p. 22), the complex model produces ORSs with replications to describe the evacuation uncertainty at data points. The evacuation uncertainty at an arbitrary point $\widetilde{x}_0$ derives from these ORSs and is integrated into the metamodel with Eq. D.14 with the symbols in Tab. D.1. As a consequence, the evacuation uncertainty should be sufficiently spatially sensitive to reproduce differences in the ORSs.

The relative integration in Eq. D.14 requires the relative evacuation uncertainty $\widetilde{\epsilon}_0 \equiv \widetilde{\epsilon}(\widetilde{x}_0)$. And it leads to the result of the metamodel integrating the evacuation uncertainty $\widetilde{y}^\epsilon_0 \equiv \widetilde{y}^\epsilon(\widetilde{x}_0)$ but neglects the metamodel uncertainty. Concluding, the result of Eq. D.14 represents the unknown result of the stochastic complex model at the arbitrary point $\widetilde{x}_0$.

$$\widetilde{y}^\epsilon_0 = \bar{y}_0 \cdot \widetilde{\epsilon}_0 \tag{D.14}$$

Salemi 2016 [29] presents an approach to derive the aleatory uncertainty at an arbitrary point from the ORSs. This approach is integrated in a metamodel using MLS. It is sketched with: 'Run the simulation model [complex model] at design points [data points][...]. Compute the sample averages across replications [mean result] and estimate the variance of a replication at each of the design points' [29, p. 8]; and 'use the variance estimate at neighbors [...] to estimate' [29, p. 13] the averaged variance at an arbitrary point. Then, the averaged variance is used to determine the '*prediction window*' for MLS.

In more detail, the averaged variance at an arbitrary point $\widetilde{x}$ results in three steps: first, to define a subset of ORSs $\widetilde{Y}^c_{nb} = \{\widetilde{y}^c_0, \ldots, \widetilde{y}^c_{nb}\}$ of $N_{\mathrm{nb}} \equiv \|X_{nb}\|$ neighbours $X_{nb} \in X$ to the arbitrary point; second, to calculate the variances $\boldsymbol{\sigma^2}\left(\widetilde{Y}^c_{N_{\mathrm{nb}}}\right) = \{\sigma^2(\widetilde{y}^c_0), \ldots, \sigma^2(\widetilde{y}^c_{nb})\}$ of each ORS in the subset; and finally, to determine the mean of the variances of $\boldsymbol{\sigma^2}\left(\widetilde{Y}^c_{N_{\mathrm{nb}}}\right)$ with Eq. D.15 to yield the averaged variance at the arbitrary point.

$$\overline{\sigma}^2\left(\widetilde{Y}^c_{N_{\mathrm{nb}}}\right) = \frac{1}{N_{\mathrm{nb}}} \sum_{i=1}^{N_{\mathrm{nb}}} \sigma^2(\widetilde{y}^c_i) \quad \text{with} \quad \sigma^2(\widetilde{y}^c_i) \in \boldsymbol{\sigma^2}\left(\widetilde{Y}^c_{N_{\mathrm{nb}}}\right) \tag{D.15}$$

Salemi 2016 [29, p. 12] suggests the number of neighbours $N_{\mathrm{nb}} = 5 \cdot N_{\mathrm{rf}}$ which depends on the number of control variables. Additionally, it remarks that the choice of the number of neighbours is not critical but it should be high enough to reduce the uncertainties in the variance estimates at the data points. However, the definition of the 'prediction window' implies that the number of neighbours is a key parameter for the spatial sensitivity of the evacuation uncertainty.

D.2 Approaches applied in the metamodel

After the introduction of MLS and the metamodel uncertainty in Section D.1.1 to Section D.1.4 now follows the description of different specific approaches for the metamodel used in this dissertation. The description first directs at MLS, then comes to the prediction interval method and beside also sketches some approaches for other response surface methods. But in general, all methods and approaches in the metamodel base on the unit hypercube as domain of the control variables.

Weighting functions

The least squares regression of MLS in Eq. D.8 considers the local weighting of data points with a weighting function w in the weighting matrix. However, 'There are various types of weighting functions [...]' [28, p. 3], or shortly called 'weighting types' for MLS. The most common weighting types base either on polynomials or on Gaussian functions but also other weighting types have been developed, e.g. in Most 2008 [70].

MLS applies three different weighting types in this dissertation: the Gaussian function w_g [70, Eq. 12]; the polynomial function w_p [28, Eq. 4a]; and a function based on a quadratic fraction w_q [70, Eq. 16] shown in Eq. D.16, Eq. D.17 and Eq. D.18 respectively. They all depend on the euclidean distance $d_i \equiv d(\widetilde{x}, \vec{x}_i)$ between a data point $\vec{x}_i \in X$ and the arbitrary point $\widetilde{x}$ as well as on the weighting parameter $\omega > 0$. The weighting parameter is a global parameter which yields on the entire domain. In case of very small weighting parameters, the RSM is highly spatially sensitive whereas a very large weighting parameter results in a global RSM without spatial sensitivity.

$$w_{g,i} = \exp\left(-\frac{d_i^2}{\omega^2}\right) \tag{D.16}$$

$$w_{p,i} = \begin{cases} 1 - 6 \cdot \left(\frac{d_i}{\omega}\right)^2 + 8 \cdot \left(\frac{d_i}{\omega}\right)^3 - 3 \cdot \left(\frac{d_i}{\omega}\right)^4 & \text{for } \frac{d_i}{\omega} \leq 1 \\ 0 \quad \text{for } \frac{d_i}{\omega} > 1 \end{cases} \tag{D.17}$$

$$w_{q,i} = \frac{\omega^2}{(d_i + \omega)^2} \tag{D.18}$$

Calibration algorithm

The calibration algorithm aims to reduce the metamodel uncertainty of a MLS model according to its data base. As stated in Subs. 'Prediction interval method' (p. 42), the metamodel uncertainty depends on the prediction variance $\boldsymbol{s}^2$ in Eq. D.12 and thus also on the variance estimator. The variance estimator σ^2_{-i} is similar to the generalisation error according to Subs. 'Model adequacy checking' (p. 39). So, since the generalisation error is used for model adequacy checking, the prediction variance $\boldsymbol{s}^2$ is also suitable as measure for the model calibration of MLS, e.g. as in Kim 2008 [28]. Consequently, the calibration algorithm minimises the 90%-quantile $\boldsymbol{s}^2_{q90}$ of the prediction variance at $\|X^{\mathrm{FFD}}\| \geq 10^3$ arbitrary points evenly distributed on the entire domain.

For this minimisation, the calibration algorithm determines following MLS attributes: the polynomial degree, the weighting type and the weighting parameter. The polynomial degree is either one for a linear or two for a quadratic polynomial in the local weighted least squares regression of Eq. D.8. Commonly, the quadratic polynomial serves as default for Monte-Carlo simulations in the system model. But if the data base comprises less than three data points per control variable, i.e. $N_{\mathrm{dps}} < 3^{N_{\mathrm{rf}}}$, the calibration algorithm employs the linear polynomial. Next, the weighting functions is based on one of the weighting types in Eq. D.16, Eq. D.17 or Eq. D.18. And finally, the weighting parameter adapts to a wide range of values.

FoM and SoM models in the metamodel

For the sake of simplicity, the global least squares regression methods are also realised with the calibration algorithm of MLS. Hence, FoM and SoM models originate in Eq. D.8 with linear or quadratic polynomials and with the weighting matrix as an identity matrix. As a result, the global least squares regression is similar to Eq. D.4 without the weighting of data points. This simplification also entails that a SoM model equals a FoM model $\bar{\boldsymbol{\xi}}^{\mathrm{SoM}} \equiv \bar{\boldsymbol{\xi}}^{\mathrm{FoM}}$ if the data base contains less than three data points per control variable.

Integration of MLS models into the system model

The direct calculation of results with a MLS model at arbitrary points, called the direct mode, causes increased run times in comparison to other response surface methods, esp. local interpolation methods. For this reason, the system model applies the direct mode only in few Monte-Carlo simulations. Instead, it applies the 'indirect mode over fixed points' depicted in Fig. G.1 (p. G-9). This mode requires a precalculation of the results for each MLS model at $\|X^{\mathrm{FFD}}\| \geq 10^5$ evenly distributed fixed points on the entire domain. In other words, the fixed points constitute the data base for a second RSM, a LIl model. The LIl model stems from a method using structured data points and reproduces the results of MLS at arbitrary points. Summing up, the indirect mode over fixed points aims to achieve quick results in Monte-Carlo simulations with only negligible additional uncertainties in comparison to the direct mode.

Integration of the metamodel uncertainty

As outlined in Section D.1.4, the metamodel uncertainty derives from the prediction interval method and is integrated into the metamodel with Eq. D.10 on p. 41. In detail, the variance in the metamodel uncertainty at an arbitrary point $\widetilde{x}_0$ is subjected to the prediction variance $\operatorname{var}\left(\delta\widetilde{y}_0^m\right) = s^2\left(\widetilde{x}_0\right)$ of Eq. D.12. Hence, it is either based on the variance estimator σ_X^2 or σ_{-i}^2 in Eq. D.7 (p. 40). As a result, the metamodel uncertainty $\delta\widetilde{y}_0^m \equiv \delta\widetilde{y}^m\left(\widetilde{x}_0\right)$ is given by Eq. D.19 where $\widetilde{t}_{N_{\mathrm{dps}}-N_{\mathrm{terms}}} \sim \mathcal{T}$ is a random value drawn from the Student distribution $\mathcal{T}$ with the degree of freedom $N_{\mathrm{dps}} - N_{\mathrm{terms}}$. Concluding, the probability p that the metamodel uncertainty lies within the prediction interval of Eq. D.11 is equal to the confidence level α, namely $p\left(\delta\widetilde{y}_0^m \leq \Delta\overline{y}_0^m\left(\alpha\right)\right) = \alpha$.

$$\delta\widetilde{y}_0^m = s^2\left(\widetilde{x}_0\right) \cdot \widetilde{t}_{N_{\mathrm{dps}}-N_{\mathrm{terms}}} \tag{D.19}$$

Metamodel uncertainty for LIn and LIl models

The metamodel uncertainty for local interpolation methods is also integrated with Eq. D.10. But Eq. D.19 has to be adapted: first, the variance in the metamodel uncertainty bases on the variance estimator $\operatorname{var}\left(\delta\widetilde{y}_0^m\right) = \sigma_{-i}^2\left(\widetilde{x}_0\right)$ instead of the prediction variance s^2; and second, the degree of freedom of the Student distribution $N_{\mathrm{dps}} - N_{\mathrm{rf}}$ depends on the number of control variables. Additionally, it has to be noted, that a LIl model adopts results of LIn in case of extrapolation according to Section D.1.2. Consequently, the variance estimator in a LIl model is identical with the variance estimator in a LIn model, i.e. $\sigma_{-i}^2\left(\bar{\boldsymbol{\xi}}^{\mathrm{LIl}}\right) \equiv \sigma_{-i}^2\left(\bar{\boldsymbol{\xi}}^{\mathrm{LIn}}\right)$ if the leave-one-out approach is applied together with a small number of data points in the data base.

D.3 Original direct approach for the evacuation uncertainty

Inspired by Salemi 2016 [29], the original direct approach was developed to integrate the evacuation uncertainty at arbitrary points into the metamodel. It realises the relative evacuation uncertainty introduced in Section D.1.5 without the assumption of a distribution type, like the Student distribution in Subs. 'Integration of the metamodel uncertainty' (p. 46). Namely, it directly uses the ORSs and therewith takes into account that the assumption of a single distribution type might not be valid with regard to potential differences in the frequency distributions of ORSs. To describe the direct approach, the first subsection introduces the basis and Tab. D.2 summarises the notation. Then, the subsequent subsections provide a detailed description how to derive the evacuation uncertainty, discuss the direct approach and finally outline its calibration and validation. In contrast to the previous sections, this section applies the notation for the FF to comply with the discussion of the results in the system model. But it still uses the general wording which emphasises that the direct approach is broadly applicable for ORSs of different stochastic models.

Table D.2: Notation in the direct approach.

notation	description
$\widehat{\xi}^c$	relative ORS
$\widehat{\boldsymbol{\xi}}^c_{N_{\mathrm{nb}}}$	combined relative sample

Introduction

The evacuation uncertainty at an arbitrary point in the direct approach fundamentally bases on the ORSs of N_{nb} neighbours $X_{N_{\mathrm{nb}}}$ and is from this point of view similar to the averaged variance. The number of neighbours governs the spatial sensitivity of the evacuation uncertainty. For instance a small number of neighbours leads to high spatial sensitivity and vice versa.

More precisely, the direct approach comprises three principal steps. To begin, it determines the relative ORS $\widehat{\xi}_i^c \equiv \widehat{\xi}^c\left(\vec{x}_i\right) = \left\{\frac{\widetilde{\xi}_{i,0}^c}{\widehat{\xi}_i^c}, \ldots, \frac{\widetilde{\xi}_{i,N_{\mathrm{rep}}}^c}{\widehat{\xi}_i^c}\right\}$ for each data point $\vec{x}_i \in X$ in the data base. In other words, the results of all N_{rep} replications of an ORS are divided by its mean result and are then attributed to the discrete uniform distribution $\mathcal{U}_d\left(\left\{\widehat{\xi}_{i,j}^c, \ldots | \forall \widehat{\xi}_{i,j}^c \in \widehat{\xi}_i^c\right\}\right) = \left\{\frac{1}{\left\|\widehat{\xi}_i^c\right\|}, \ldots\right\}$. Next, the direct approach combines the relative ORSs of all N_{nb} neighbours of an arbitrary point $\widetilde{x} \in \widetilde{X}$ leading to the combined relative sample $\widehat{\boldsymbol{\xi}}_{N_{\mathrm{nb}}}^c = \left\{\widehat{\xi}_1^c, \ldots, \widehat{\xi}_{N_{\mathrm{nb}}}^c\right\}$. Thus, the combined relative sample contains $N_{\mathrm{rep}} \cdot N_{\mathrm{nb}}$ replications which are subjected to the specific discrete distribution $\mathcal{D}\left(\widehat{\boldsymbol{\xi}}_{N_{\mathrm{nb}}}^c\right)$. At last, Eq. D.20 directly draws a result of one replication from this discrete distribution. This result becomes the relative evacuation uncertainty $\widetilde{\epsilon}_0 \equiv \widetilde{\epsilon}\left(\widetilde{x}\right)$ which is finally integrated into the metamodel with Eq. D.14.

$$\widetilde{\epsilon}_0 \sim \mathcal{D}\left(\widehat{\boldsymbol{\xi}}_{N_{\mathrm{nb}}}^c\right) \tag{D.20}$$

Combination of the relative ORSs

Eq. D.21 details the general approach to combine the frequency distributions of the relative ORSs of all neighbours for an arbitrary point $\widetilde{x}$. In this combination, the sample weighting factor $\omega_{s,i}$ weights each relative ORS individually. Therefore, the probability to draw the result of a replication $\widehat{\xi}_{i,j}^c$ from the combined relative sample $\mathcal{D}\left(\widehat{\boldsymbol{\xi}}_{N_{\mathrm{nb}}}^c\right)$ is $p\left(\widehat{\xi}_{i,j}^c\right) = \frac{\omega_{s,i}}{\left\|\widehat{\xi}_i^c\right\|}$.

$$\mathcal{D}\left(\widehat{\boldsymbol{\xi}}_{N_{\mathrm{nb}}}^c\right) = \mathcal{D}\left(\omega_{s,i} \cdot \mathcal{D}\left(\widehat{\xi}_i^c\right), \ldots\right) = \left\{\left\{\frac{\omega_{s,i}}{\left\|\widehat{\xi}_i^c\right\|}, \ldots\right\}, \ldots\right\} \tag{D.21}$$

In contrast to this general approach, the direct approach realises the combination in three successive steps for each arbitrary point $\widetilde{x}$ as depicted in Fig. D.1:

1. to choose a relative ORS $\widehat{\xi}_i^c$ of a data point $\vec{x}_i \in X_{nb}$ with the probability $p\left(\vec{x}_i\right)$ of the discrete distribution $\mathcal{D}\left(\left\{\widehat{\xi}_i^c, \ldots | \forall \widehat{\xi}_i^c \in \widehat{\boldsymbol{\xi}}_{N_{\mathrm{nb}}}^c\right\}\right) = \left\{p\left(\vec{x}_i\right), \ldots\right\}$;
2. to draw a random result of a replication $\widehat{\xi}_{i,j}^c \in \widehat{\xi}_i^c$ from this ORS with the discrete uniform distribution $\mathcal{U}_d\left(\left\{\widehat{\xi}_{i,j}^c, \ldots | \forall \widehat{\xi}_{i,j}^c \in \widehat{\xi}_i^c\right\}\right) = \left\{\frac{1}{\left\|\widehat{\xi}_i^c\right\|}, \ldots\right\}$;
3. to integrate the relative evacuation uncertainty $\widetilde{\epsilon} = \widehat{\xi}_{i,j}^c$ into the metamodel model.

Concluding, the probability to draw the relative evacuation uncertainty $\widetilde{\epsilon} = \widehat{\xi}_{i,j}^c$ is $p\left(\widehat{\xi}_{i,j}^c\right) = p\left(\vec{x}_i\right) \cdot \frac{1}{\left\|\widehat{\xi}_i^c\right\|}$. Hence, this probability agrees with the general approach in Eq. D.21 if the probability to choose a relative ORS is identical with the sample weighting factor $p\left(\vec{x}_i\right) = \omega_{s,i}$. The combined relative sample should correspond to the unknown true evacuation uncertainty at the arbitrary point. However, there are no definite clues to the exact spatial relation between the frequency distributions of the ORSs that leads to the evacuation uncertainty. Moreover, this spatial relation is supposed to be different for each arbitrary point. Accordingly, the appropriate combination of relative ORSs in Eq. D.21 is unknown.

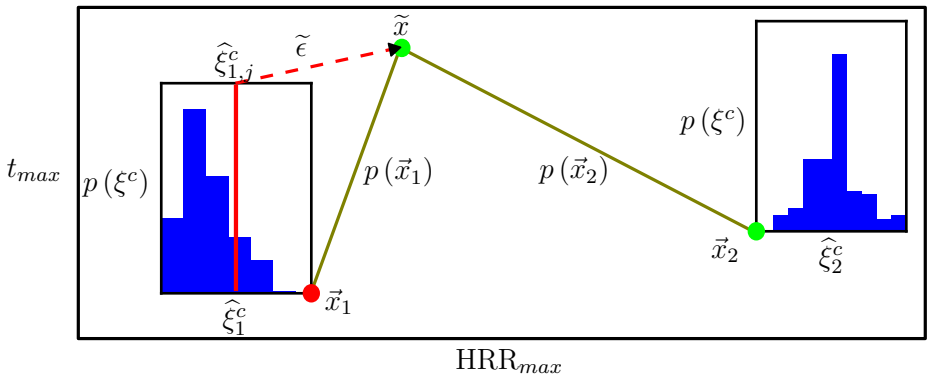

Figure D.1: Three steps (highlighted red) for the combination of ORSs for the arbitrary point $\widetilde{x}$ in the direct approach: first, random choice of the data point $\vec{x}_1$ with the probability $p(\vec{x}_1)$; second, random choice of a result of the relative ORS $\widehat{\xi}^c_{1,j} \in \widehat{\xi}^c_1$; third, integration of the relative evacuation uncertainty $\widetilde{\epsilon}$ into the metamodel.

As a consequence, the combination of relative ORSs bases on three combination modes, namely 'closest', 'uniform', and 'linear'. These combination modes specify the probability $p(\vec{x}_i)$ to choose a relative ORS $\widehat{\xi}^c_i$ on different basic ways. First, the combination mode closest chooses the closest data point $\vec{x}_i$ to the arbitrary point with the probability $p(\vec{x}_i) = 1$. In other words, the number of neighbours is $N_{\mathrm{nb}} = 1$ which leads to a spatially discontinuous relative evacuation uncertainty. Second, the combination mode uniform assigns equal probabilities $p(\vec{x}_i) = \frac{1}{N_{\mathrm{nb}}}$ to all neighbours. Accordingly, it averages the results of all neighbours similar to the averaged variance. And third, the combination mode linear linearly weights the neighbours with probabilities $p(\vec{x}_i)$ depending on their euclidean distance $d(\widetilde{x}, \vec{x}_i)$ to the arbitrary point.

The basic linear equation in the combination mode linear is $p(\vec{x}_i) = 1 - \frac{d(\widetilde{x},\vec{x}_i)}{d_{crit}}$ with the parameter critical distance $d_{crit} > 0$. With this equation, an arbitrary point at a data point $\widetilde{x} = \vec{x}_i \in X$ is assigned to the probability $p(d(\widetilde{x}, \vec{x}_i) = 0) = 1$ which matches the unknown evacuation uncertainty. Furthermore, it yields: $p(\vec{x}_i) \stackrel{!}{=} 0$ if $d(\widetilde{x}, \vec{x}_i) > d_{crit}$; and $\sum_{i=1}^{N_{\mathrm{nb}}} p(\vec{x}_i) \stackrel{!}{=} 1$ with $\vec{x}_i \in X_{nb}$. These conditions lead to the critical distance $d_{crit} = \frac{\sum_{i=1}^{N_{\mathrm{nb}}} d(\widetilde{x},\vec{x}_i)}{N_{\mathrm{nb}}-1}$ for $N_{\mathrm{nb}} > 1$. It requires an adaptive number of neighbours, e.g. because of the first condition with regard to $\widetilde{x} = \vec{x}_i \in X$. Consequently, different arbitrary points $\widetilde{x} \in \widetilde{X}$ consider different number of neighbours denoted in the set $\boldsymbol{N}_{\mathrm{nb}} = \{N_{\mathrm{nb}1}, \ldots\}$. And finally, the linear equation is $p(\vec{x}_i) = 1 - \frac{(N_{\mathrm{nb}}-1)\cdot d(\widetilde{x},\vec{x}_i)}{\sum_{i=1}^{N_{\mathrm{nb}}} d(\widetilde{x},\vec{x}_i)}$.

Discussion of the relative integration

The evacuation uncertainty at an arbitrary point derives from the ORSs of its neighbours. Therewith, the direct approach is similar to the averaged variance in Section D.1.5. But a non-relative combination of the ORSs like in Eq. D.15 can lead to following issue within the metamodel.

The issue might occur at an arbitrary point $\widetilde{x}$ which is close to a data point $\vec{x}_i \in X_{N_{\mathrm{nb}}}$ with a small mean result $\bar{\xi}^c_i \approx 0$ and also a small variance $\sigma^2\left(\widetilde{\xi}^c_i\right) \approx 0$. The RSM at the arbitrary point approximates the small mean result of the complex model and yields also $\bar{\xi}(\widetilde{x}) \approx 0$. Yet, another neighbour $\vec{x}_j \in X_{N_{\mathrm{nb}}}$ to the arbitrary point might be subjected to an elevated

mean result $\bar{\xi}_j^c > 0$. Obviously, its variance is increased in comparison to the variance of the other data point $\sigma^2\left(\widetilde{\xi}_j^c\right) > \sigma^2\left(\widetilde{\xi}_i^c\right)$. Consequently, the non-relative combination also leads to an increased variance $\overline{\sigma}^2\left(\widetilde{\boldsymbol{\xi}}_{N_{\mathrm{nb}}}^c\right) > 0$ at the arbitrary point which then results in an increased evacuation uncertainty and finally in an increased result of the metamodel $\widetilde{\xi}^{\epsilon}(\widetilde{x}) > 0$. Furthermore, a non-relative integration according to Eq. D.10 (p. 41) can still raise this result or in contrast contribute to a result below zero $\widetilde{\xi}^{\epsilon}(\widetilde{x}) < 0$. Summing up, the outcome of the metamodel at the arbitrary point based on the non-relative combination and integration can contradict the expected result, i.e. close to zero $\widetilde{\xi}^{\epsilon}(\widetilde{x}) \approx \bar{\xi}(\widetilde{x}) \approx 0$.

For this reason, the direct approach establishes the relative combination in Eq. D.21 and produces the relative evacuation uncertainty with Eq. D.20. Then, the metamodel relatively integrates the evacuation uncertainty with Eq. D.14. Both steps are supposed to solve this issue and make the metamodel applicable on response surfaces with large spatial variations in the aleatory uncertainties.

But another issue arises from the relative evacuation uncertainty, esp. in combination with a low spatial sensitivity. For instance, the mean result of a RSM at an arbitrary point $\widetilde{x}$ is elevated $\bar{\xi} > 0$ and the corresponding combined relative sample considers several neighbours in a large region. Hence, the combined relative sample can contain a data point $\vec{x}_i$ with a small mean result $\bar{\xi}_i^c \approx 0$ and therewith potentially high values $\widehat{\xi}_{i,j}^c \gg 0$ in the replications of its relative ORS $\widehat{\xi}_{i,j}^c \in \widehat{\xi}_i^c$. As a consequence, Eq. D.20 might draw a high relative evacuation uncertainty $\widetilde{\epsilon} \gg 0$, i.e. an outlier among results $\widetilde{\boldsymbol{\epsilon}}$ of multiple arbitrary points $\widetilde{x} \in \widetilde{X}$. In the end, the high relative evacuation uncertainties together with the elevated mean result at the arbitrary point $\bar{\xi} > 0$ contribute in Eq. D.14 to the result of the metamodel with $\widetilde{\xi}^{\epsilon} > 1$. But this result contradicts the system model as outlined in Subs. 'Intermediate nodes' (p. 19).

Two factors can prevent this drawback of the relative evacuation uncertainty. First, the number of neighbours adapts the spatial sensitivity of the evacuation uncertainty, in other words, the region around an arbitrary point where data points are considered. Hence, decreasing the number of neighbours should also reduce possible differences among the mean results of their ORSs. Correspondingly, a sufficient spatial sensitivity limits the probability for high relative evacuation uncertainties. Second, the direct approach limits data points with small mean results. More precisely, if the mean result of a data point $\vec{x}_i$ is below the parameter $\bar{\xi}_i^c \leq \bar{\xi}_{lim}^c$, all values in its relative ORS are manipulated to $\widehat{\xi}_i^c = \vec{1}$. These values drawn for the evacuation uncertainty will not affect the result of the metamodel in Eq. D.14. Beside these manipulations, $\widehat{\xi}_i^c = \vec{1}$ originates also from ORSs with $\widetilde{\xi}_i^c = \vec{0}$ or by chance directly from a replication $\widehat{\xi}_{i,j}^c \in \widehat{\xi}_i^c$.

Calibration and validation of the evacuation uncertainty

The definition of outliers in relative evacuation uncertainties $\widetilde{\boldsymbol{\epsilon}}$ of arbitrary points $\widetilde{X}$ derives from the interquartile range [64, p. 26]. In detail, the relative evacuation uncertainty at an arbitrary point $\widetilde{\epsilon}(\widetilde{x})$ is an outlier if $\widetilde{\epsilon}(\widetilde{x}) > 10 \cdot (\widetilde{\boldsymbol{\epsilon}}_{q99} - \widetilde{\boldsymbol{\epsilon}}_{q01}) + \widetilde{\boldsymbol{\epsilon}}_{q99}$ where $\widetilde{\boldsymbol{\epsilon}}_{q01}$ and $\widetilde{\boldsymbol{\epsilon}}_{q99}$ are the 1% and 99%-quantiles among all relative evacuation uncertainties $\widetilde{\boldsymbol{\epsilon}}$. In case of an outlier, its value is set to $\widetilde{\epsilon}(\widetilde{x}) = 10 \cdot (\widetilde{\boldsymbol{\epsilon}}_{q99} - \widetilde{\boldsymbol{\epsilon}}_{q01}) + \widetilde{\boldsymbol{\epsilon}}_{q99}$. Accordingly, the direct approach identifies and alters only very clear outliers.

The combination of ORSs, the relevance of the spatial sensitivity as well as the occurrence of outliers in the relative evacuation uncertainty demands a calibration of the direct approach for the metamodel. The calibration bases on the relative evacuation uncertainties $\widetilde{\boldsymbol{\epsilon}}$ of multiple arbitrary points $\widetilde{X}$ and directs at: first, the effects of the parameter $\bar{\xi}_{lim}^c$ on the frequency distribution of the relative evacuation uncertainties $\widetilde{\boldsymbol{\epsilon}}$, esp. the number of arbitrary points equal to one $\|\widetilde{\boldsymbol{\epsilon}} = 1\|$; second, on the number of outliers $\|\text{outliers}\|$; and third, on the spatial

sensitivity, esp. the number of arbitrary points with $\left\|\widetilde{\boldsymbol{\xi}}^{\boldsymbol{\epsilon}} > 1\right\|$. Finally, the calibration specifies the default combination mode as well as the default parameters to limit the data points $\bar{\xi}^c_{lim}$ as well as the number of neighbours N_{nb}.

Looking on the validation of the evacuation uncertainty, the direct approach has to reproduce the ORS of a data point $\vec{x}_i$. Therefore, it directly draws a result from the relative ORS $\widehat{\xi}^c_i$. So, for multiple arbitrary points $\widetilde{X}$, multiple results are drawn with replacement from this relative ORS, and of course also from other data points. As a result, the relative evacuation uncertainty $\widetilde{\boldsymbol{\epsilon}}$ comprises a bootstrap sample of the relative ORS $\widehat{\xi}^c_i$. Concluding, the approach in Subs. 'Evaluation of ORSs' (p. 26) evaluates the reproduction of ORSs also with bootstrap samples and for this reason it allows at the same time the evaluation whether the direct approach represents an ORS. Additionally, the evaluation of arbitrary points with the relative evacuation uncertainty $\widetilde{\boldsymbol{\epsilon}} = 1$ as well as of the spatial sensitivity of the combination modes contribute to the validation. The former ones are mostly linked to ORSs with results equal to zero $\widetilde{\xi}^c = \vec{0}$.

D.4 Approaches for the integration and evaluation of the metamodel

The setup of the metamodel consists of sequential refinement steps outlined in Subs. 'Metamodel' (p. 23) of Section B.4 as well as in Section C.3. Each refinement step comprises the setup of a RSM according to Subs. 'Calibration algorithm' (p. 45) of Section D.2. Next, the metamodel applies Eq. D.22 on each result of the RSM $\bar{y}_0 \in \bar{\boldsymbol{Y}}$ for the combined integration of the metamodel uncertainty and the evacuation uncertainty. More precisely, this equation first determines the unknown result of the deterministic complex model $\widetilde{y}^m_0$ and then employs the relative evacuation uncertainty $\widetilde{\epsilon}_0$. Therewith, it amalgamates Eq. D.10 as well as Eq. D.14 and finally yields the result of the metamodel $\widetilde{y}_0 \in \widetilde{\boldsymbol{Y}}$.

$$\widetilde{y}_0 = \widetilde{y}^m_0 \cdot \widetilde{\epsilon}_0 = (\bar{y}_0 + \delta\widetilde{y}^m_0) \cdot \widetilde{\epsilon}_0 \tag{D.22}$$

However, this result, i.e. the FF $\widetilde{\xi}_0 \in \widetilde{\boldsymbol{\xi}}$, does not represent a physical quantity within the system model as outlined in Subs. 'Intermediate nodes' (p. 19). Hence, the results of the metamodel have to be clipped to $0 \leq \widetilde{\Xi} \leq 1$ for the integration into the system model. Tab. D.3 provides an overview on the notation for the FF in the system model on the basis of the metamodel. Merely the symbol Ξ^* denotes the FF in the system model which is still unclipped and without specifications of the metamodel.

Table D.3: Notation for the FF used in the system model.

system model	metamodel	remarks
$0 \leq \widetilde{\Xi} \leq 1$	$\widetilde{\boldsymbol{\xi}}$ as Eq. D.22	metamodel uncertainty, evacuation uncertainty
$0 \leq \widetilde{\Xi}^m \leq 1$	$\widetilde{\boldsymbol{\xi}}^{\boldsymbol{m}}$ as Eq. D.10	no evacuation uncertainty, i.e. $\widetilde{\boldsymbol{\epsilon}} = \vec{1}$
$0 \leq \widetilde{\Xi}^{\epsilon} \leq 1$	$\widetilde{\boldsymbol{\xi}}^{\boldsymbol{\epsilon}}$ as Eq. D.14	no metamodel uncertainty, i.e. $\boldsymbol{\delta}\widetilde{\boldsymbol{\xi}}^m = \vec{0}$
$0 \leq \bar{\Xi} \leq 1$	$\bar{\boldsymbol{\xi}}$	RSM
Ξ^*	$\left\{\bar{\boldsymbol{\xi}}, \widetilde{\boldsymbol{\xi}}^{\boldsymbol{m}}, \widetilde{\boldsymbol{\xi}}^{\boldsymbol{\epsilon}}, \widetilde{\boldsymbol{\xi}}\right\}$	unclipped, without specification of the metamodel

After the integration into the system model, it follows the evaluation of the metamodel in each refinement step. The evaluation directs esp. on the convergence of the results of the RSM as well as of the prediction variance $\boldsymbol{s}^2$ during the sequential refinement. As soon as

both results converge, the metamodel does not require additional data points in the data base. So, the default RSM in the consequence model of the system model, shortly default RSM, can be specified together with the final refinement step.

The evaluation directs at the comparison of results of different metamodels and mainly comprises three approaches. For the first two approaches, the symbol $\boldsymbol{\Upsilon}$ represents a sample of a measure at arbitrary points $\widetilde{X}$, e.g. the result of the RSM $\bar{\boldsymbol{\xi}}$ or the relative evacuation uncertainty $\widetilde{\boldsymbol{\epsilon}}$. Also, $\boldsymbol{\Upsilon}_{q_i}$ denotes the i%th quantile and the terms 'lower' and 'upper quantiles' are either subjected to small or high values of $i \in \{1, \ldots, 99\}$. One approach, the quantile plot, juxtaposes the frequency distributions of two samples $\boldsymbol{\Upsilon}^0$ and $\boldsymbol{\Upsilon}^1$ of the same measure. Namely, its horizontal and the vertical axes both show the quantiles of the samples $\boldsymbol{\Upsilon}^0$ and $\boldsymbol{\Upsilon}^1$ respectively. A smaller dispersion of the sample $\boldsymbol{\Upsilon}^1$ leads to lower quantiles above and upper quantiles below the diagonal in the quantile plot, and vice versa for a larger dispersion. The quantile plot is first exemplified in Fig. E.18a on p. 80 and resembles the normal probability plot introduced in Section D.1.1. Together with the quantile plot, the euclidean relative difference $\mathrm{erd}_q\left(\boldsymbol{\Upsilon}^1, \boldsymbol{\Upsilon}^0\right)$ [71] quantifies the difference between both samples based on 1000 quantiles. Next, the relative quantile plot, e.g. depicted in Fig. E.21 (p. 86), is similar to the quantile plot. But its vertical axis shows the relative difference between the quantiles $\boldsymbol{\Upsilon}^1_{q_i} / \boldsymbol{\Upsilon}^0_{q_i} - 1$ of both samples and thus emphasises the differences between both frequency distributions more clearly. Last but not least, the quantification of differences between two metamodels bases on $\|X^{\mathrm{FFD}}\| \geq 10^5$ evaluation points. The evaluation points are identical with the fixed points in Subs. 'Integration of MLS models into the system model' (p. 45) and provide either the mean results of the RSM $\bar{\boldsymbol{Y}}$ or the prediction variances $\boldsymbol{s}^2$ of the RSMs. With regard to the mean results $\bar{\boldsymbol{Y}}$, the euclidean relative difference erd determines the difference between to RSMs. And for the prediction variance $\boldsymbol{s}^2$, the comparison of RSMs concentrates on their 90%-quantile $\boldsymbol{s}^2_{q90}$.

E Evaluation of the innovative methodology for risk analysis

Section B.3 and Section B.4 introduce the metamodel within the system model which serves for the methodology for risk analysis and Chapter C and Chapter D provide the details. So, subsequent to the scrutiny of the metamodel in App. G.6, now, the evaluation of the entire methodology follows. Hence, the results within the system model are in terms of the FF and still subjected to certain aleatory uncertainties. But these aleatory uncertainties do not affect the conclusions in this chapter.

The evaluation first covers all integral parts of the metamodel. Namely, the EDs and the data bases are described in Section E.1 and in Section E.2 the response surface method is examined together with the metamodel uncertainty. Then, the evacuation uncertainty is scrutinised in Section E.3. This entire assessment is based on system model simulations differentiated to risk analyses in Section B.5. Section B.5 also introduces different approaches to evaluate risk analyses. With these methods, the risk analysis described in Section B.2 is finally examined in Section E.4.

E.1 Data bases for the system model

The evaluation of the methodology for risk analysis applies different data bases for the system model. For each data base, the ED X specifies the data points outlined in Section B.4. Section C.3 sketches the selection process for the ED X which considers multiple EDs $\{X_1^{mima}, \ldots\}$ and bases on the distance measures $d_{minimax}$, $d_{maximin}$ and d_{cov} introduced in Section C.1. Each ED X^{mima} was built with the methods described in Section C.2. Accordingly, the total number of EDs considered in the selection process for one data base with the ED X, i.e. comprising all minimax and nested maximin optimisations for all X^{mima}, was in the order of magnitude of 4 or 5.

The main focus during the selection process was different for fire scenarios and evacuation scenarios. With regard to fire scenarios of the ED X^{fire}, the focus was on $d_{maximin}$ to get clearly different values of risk factors causing different interactions. And with regard to evacuation scenarios of the ED X^{evac}, the focus was on the minimisation of d_{cov} to guarantee an even distribution of data points on the entire domain. The mere optimisation of $d_{minimax}$ or $d_{maximin}$ would have little effect due to the higher number of evacuation scenarios in comparison to fire scenarios. Additionally, if the data base was sought for sequential refinement, the selection process focused less on $d_{minimax}$ due to possible improvements in subsequent refinement steps. Also, different focus was on the complete LHD- and PA-condition. On the one hand for fire scenarios of the ED X^{fire}, most EDs for the setup of X^{mima}, and consequently also the ED X^{mima}, had complete LHD- and PA-conditions. As a consequence, the selection process put little focus on both conditions. On the other hand, the setup and the selection process of EDs for evacuation scenarios of the ED X^{evac} considered continuously the LHD- and PA-condition: in particular during the maximin optimisation, in detail the approach to prevent the fail of PA- and LHD-condition outlined in Subs. 'Sequential refinement' (p. 35); and during the combination of EDs with the mode 'combination' outlined in

Table E.1: Parameters for data bases used in the system model; X_{new} and X_{i-1} add up to X_i according to Eq. C.6 (p. 35); the notations for the ORSs $\widetilde{\boldsymbol{\xi}}^c$ in the data base and the mean results $\bar{\boldsymbol{\xi}}$ follow the same conventions.

data base	X_i	X_{i-1}	$\left\|X^{\text{fire}}\right\|$	$\|X^{\text{evac}}\|$	$p_{stretch}\,(X_{new})$	N_{rep}
$\widetilde{\boldsymbol{\xi}}^c_{X_0}$	X_0	–	4	16	–	200
$\widetilde{\boldsymbol{\xi}}^c_{X_1}$	X_1	X_0	6	48	1.0	200
$\widetilde{\boldsymbol{\xi}}^c_{X_2}$	X_2	X_1	10	96	0.1	200
$\widetilde{\boldsymbol{\xi}}^c_{X_3}$	X_3	X_2	14	144	0.01	200
$\widetilde{\boldsymbol{\xi}}^c_{X_{1a}}$	X_{1a}	X_0	6	48	1.0	200
$\widetilde{\boldsymbol{\xi}}^c_{X_b}$	X_b	X_0	10	96	1.0	200

Subs. 'Combination of EDs' (p. 36). Finally, the selection of the final ED X was based on a visual comparison of few EDs X^{mima}. The visual comparison identified only small variations in their data points. For this reason, the setup of the ED X led to reproducible results meaning that the number of minimax and maximin optimisations was sufficient.

After the selection process, EDs specify the data points of the data bases for the system model. The data bases used in the evaluation of the methodology for risk analysis have three different foci. The first focus is on the sequential refinement of the metamodel with the data bases $\bar{\boldsymbol{\xi}}^c_{X_0}$, $\bar{\boldsymbol{\xi}}^c_{X_1}$, $\bar{\boldsymbol{\xi}}^c_{X_2}$ and $\bar{\boldsymbol{\xi}}^c_{X_3}$. The EDs are respectively $X_0 = X^{\text{FF2}}$ which is a two-level FFD, X_1, X_2 and X_3 as illustrated in Fig. E.1a and Fig. E.1b. The stretching parameter was $p_{stretch} = 1$ in the first refinement step to the ED X_1. Then, the evaluation of prediction variances $\boldsymbol{s}^2$ of the RSMs $\bar{\boldsymbol{\xi}}_{X_1}$ and $\bar{\boldsymbol{\xi}}_{X_2}$ exemplified in Fig. E.4 as well as preliminary results, e.g. in Subs. 'Comparison to the Kim 2008 [28]' (p. G-20) indicated increased prediction variances at the outer vertices. Hence, the focus was set to the outer vertices for the subsequent refinement steps to the EDs X_2 and X_3. Second, the evaluation focuses on the sensitivity of the RSM to variations in the ED. This evaluation applies the data base $\bar{\boldsymbol{\xi}}^c_{X_{1a}}$ with data points specified in the ED X_{1a} shown in Fig. E.2a and Fig. E.2b. To be equivalent to the ED X_1, both EDs comprise the same number of data points. Third, the interest lies on the batch design with the data base $\bar{\boldsymbol{\xi}}^c_{X_b}$ and the corresponding ED X_b depicted in Fig. E.3a and Fig. E.3b.

This data base has two purposes: first, to juxtapose the default RSM $\bar{\boldsymbol{\xi}}_{X_2}$ and the batch RSM $\bar{\boldsymbol{\xi}}_{X_b}$ based on sequential refinement and the batch design, respectively; second, to analyse the sensitivity of the RSM to variations in the ED. Consequently, the batch design X_b has the same number of data points as the ED X_2. To summarise, Tab. E.1 provides an overview on all data bases for the system model and App. G.7 shows all fire and evacuation scenarios in these data bases.

The data bases comprise results, i.e. the ORSs or the mean FF, of the evacuation scenarios with $N_{\text{rep}} = 200$ replications which was increased in successive steps during the evaluation of the methodology for risk analysis. The evaluation in this chapter puts large interest in the RSMs and metamodels. Two separate RSMs for scenarios with TA and FA result from the same ED X^{evac} as reasoned in Subs. 'Metamodel' (p. 23). Hence as basis for the subsequent sections, Tab. E.2 provides an overview on the RSMs and their MLS attributes according to the calibration algorithm of MLS in Subs. 'Calibration algorithm' (p. 45).

E.2 Response surface method and metamodel uncertainty

In Subs. 'Metamodel' (p. 23) it is stated that the ED, the data base and the RSM are integral parts of the metamodel. Additionally, the metamodel comprises the metamodel uncertainty

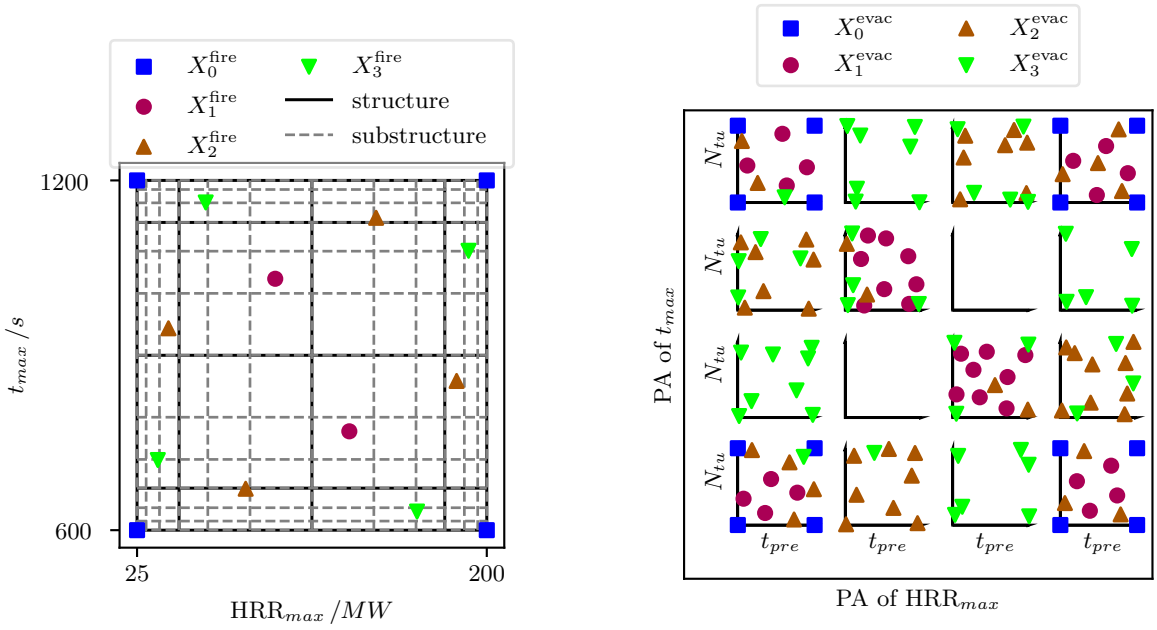

(a) fire scenarios **(b)** evacuation scenarios

Figure E.1: EDs of data bases shown in Tab. E.1 with focus on sequential refinement; the structures of the PADs belong to X_3^{fire} and X_3^{evac}.

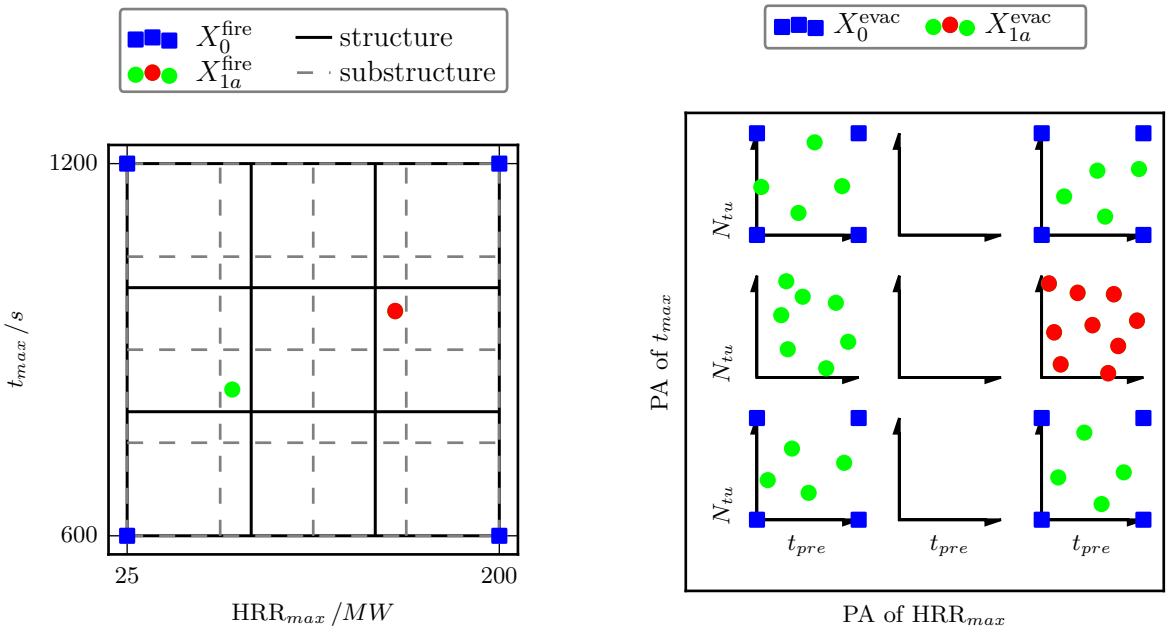

(a) fire scenarios **(b)** evacuation scenarios

Figure E.2: EDs of data bases shown in Tab. E.1 with focus on variations in the ED; the red data points exemplify the combination of EDs, multiple evacuation scenarios (right) aggregate in the region of the fire scenario (left) with the corresponding PA.

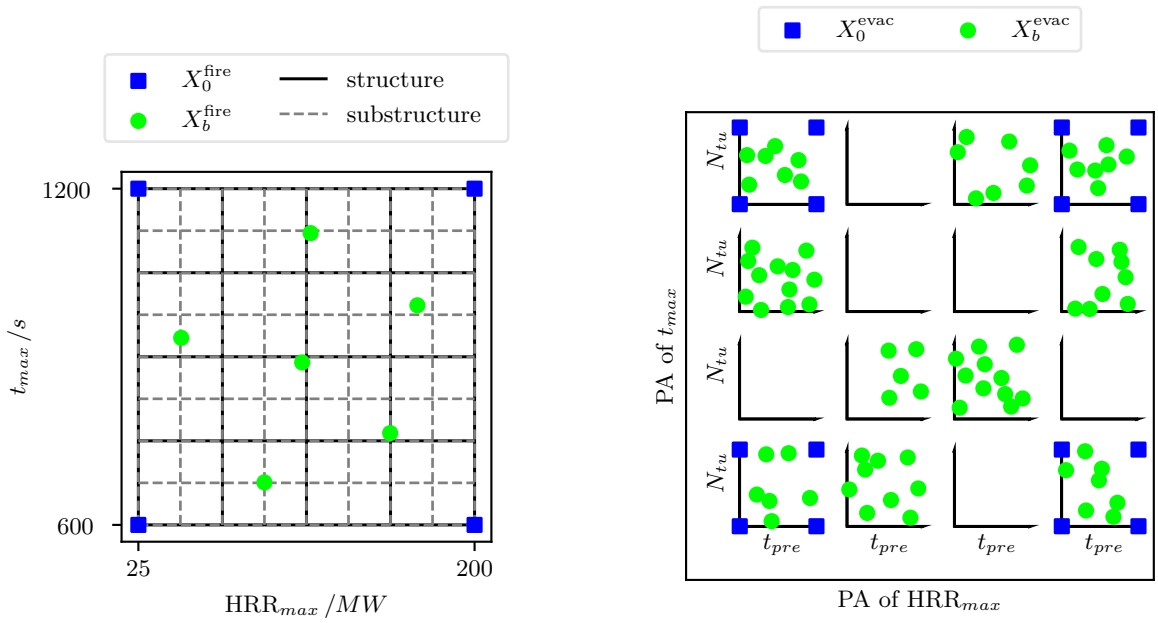

(a) fire scenarios

(b) evacuation scenarios

Figure E.3: EDs of data bases shown in Tab. E.1 with focus on the batch design.

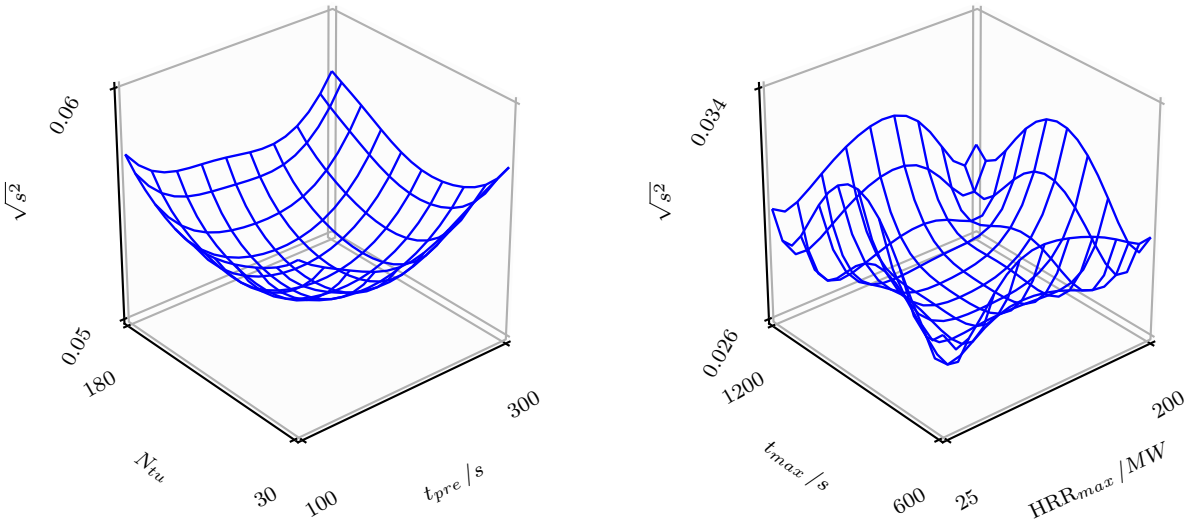

(a) for the RSM $\bar{\boldsymbol{\xi}}_{X_1}$ on evacuation risk factors (FA)

(b) for the RSM $\bar{\boldsymbol{\xi}}_{X_2}$ on fire risk factors (TA)

Figure E.4: Elevated prediction variance at outer vertices of the domain in the region of sc(97 MW, 882 s, 124 s, 48, $fa = -$); the scales differ between both figures.

Table E.2: MLS attributes of all RSMs used in the system model for scenarios with TA (above) and FA (below); the default RSM is denoted with $\bar{\boldsymbol{\xi}}_{X_2}$; the batch RSM is denoted with $\bar{\boldsymbol{\xi}}_{X_b}$.

RSM	data base	weighting type	polynomial degree	parameter ω
$\bar{\boldsymbol{\xi}}_{X_{0,0}}$	$\bar{\boldsymbol{\xi}}^c_{X_{0,0}}$	w_p	1	1.768
$\bar{\boldsymbol{\xi}}_{X_{1,0}}$	$\bar{\boldsymbol{\xi}}^c_{X_{1,0}}$	w_g	1	0.432
$\bar{\boldsymbol{\xi}}_{X_{2,0}}$	$\bar{\boldsymbol{\xi}}^c_{X_{2,0}}$	w_p	2	1.206
$\bar{\boldsymbol{\xi}}_{X_{3,0}}$	$\bar{\boldsymbol{\xi}}^c_{X_{3,0}}$	w_p	2	0.984
$\bar{\boldsymbol{\xi}}_{X_{1a,0}}$	$\bar{\boldsymbol{\xi}}^c_{X_{1a,0}}$	w_g	1	0.356
$\bar{\boldsymbol{\xi}}_{X_{b,0}}$	$\bar{\boldsymbol{\xi}}^c_{X_{b,0}}$	w_g	2	0.748
$\bar{\boldsymbol{\xi}}_{X_{0,1}}$	$\bar{\boldsymbol{\xi}}^c_{X_{0,1}}$	w_p	1	1.760
$\bar{\boldsymbol{\xi}}_{X_{1,1}}$	$\bar{\boldsymbol{\xi}}^c_{X_{1,1}}$	w_g	1	0.477
$\bar{\boldsymbol{\xi}}_{X_{2,1}}$	$\bar{\boldsymbol{\xi}}^c_{X_{2,1}}$	w_q	2	0.160
$\bar{\boldsymbol{\xi}}_{X_{3,1}}$	$\bar{\boldsymbol{\xi}}^c_{X_{3,1}}$	w_q	2	0.489
$\bar{\boldsymbol{\xi}}_{X_{1a,1}}$	$\bar{\boldsymbol{\xi}}^c_{X_{1a,1}}$	w_g	1	0.330
$\bar{\boldsymbol{\xi}}_{X_{b,1}}$	$\bar{\boldsymbol{\xi}}^c_{X_{b,1}}$	w_q	2	0.538

as well as the evacuation uncertainty. In Section E.1 the ED and the data bases are established. Accordingly, the RSM and the metamodel uncertainty come next to be examined. The examination splits up in following steps, all based on system model simulations described in Section B.5: Section E.2.1 aims at the model adequacy checking of MLS and the prediction interval method; Section E.2.2 copes with the sequential refinement of the metamodel and the default RSM is specified as well as juxtaposed with the batch RSM; the prediction interval method is validated in comparison to the accuracy of the RSM in Section E.2.3; the shape of the RSM is studied and MLS is validated with focus on the global objective in Section E.2.4; and, other response surface methods with regard to the application in risk analysis are investigated in Section E.2.5 which finalises the validation of MLS. The subsequent system model simulations as well as the risk analyses often apply the indirect mode over fixed points introduced in Subs. 'Integration of MLS models into the system model' (p. 45). As a prerequisite, Subs. 'Integration of the RSM into the system model' (p. G-34) in App. G.8 proved the accuracy of the indirect mode in comparison to the direct mode. Consequently, the notation in this dissertation does not differentiate between the two modes.

E.2.1 MLS and prediction interval method

At the beginning, MLS is examined in App. G.6, its calibration algorithm with the three weighting types as well as the prediction interval method. As a result, both methods are successfully verified and it is stated that MLS with the calibration algorithm leads to adequate results. In a next step, this section directs at the evaluation of all RSMs shown in Tab. E.2 and therewith follows three aims: first, to evaluate the residuals as part of model adequacy checking outlined in Section D.1.1; second, to select the variance estimator, either σ^2_X or σ^2_{-i}, to be used in the prediction variance of the prediction interval method; and third, to discuss the spatial sensitivity of the prediction interval method described in Subs. 'Validation of the prediction interval method' (p. 42). Finally, this section is concluded by stating the adequacy of MLS and the importance of the metamodel uncertainty and therefore this section contributes to the validation of the metamodel.

Table E.3: Results of the split-sample validation with $n = 100$ replications for the default RSM $\bar{\boldsymbol{\xi}}_{X_2}$ for TA (above) and FA (below): the empirical confidence level α^*_{mean} of the prediction interval method depends on the confidence level α as well as on the prediction variance with the variance estimators σ^2_X or σ^2_{-i}.

RSM	α	$\alpha^*_{mean}\left(\sigma^2_X\right)$	$\alpha^*_{mean}\left(\sigma^2_{-i}\right)$
$\bar{\boldsymbol{\xi}}_{X_{2,0}}$	0.50	0.48	0.78
$\bar{\boldsymbol{\xi}}_{X_{2,0}}$	0.75	0.63	0.89
$\bar{\boldsymbol{\xi}}_{X_{2,0}}$	0.90	0.77	0.95
$\bar{\boldsymbol{\xi}}_{X_{2,0}}$	0.95	0.81	0.97
$\bar{\boldsymbol{\xi}}_{X_{2,1}}$	0.50	0.21	0.74
$\bar{\boldsymbol{\xi}}_{X_{2,1}}$	0.75	0.36	0.91
$\bar{\boldsymbol{\xi}}_{X_{2,1}}$	0.90	0.53	0.97
$\bar{\boldsymbol{\xi}}_{X_{2,1}}$	0.95	0.62	0.98

The model adequacy checking of the RSMs used in the system model bases on the evaluation of normal probability plots according to Section D.1.1. Nearly every RSM corresponds to the results of the default RSM depicted in Fig. E.5a and Fig. E.5b. Namely, their residuals revealed no apparent deviation from the normal distribution. Except, the RSM $\bar{\boldsymbol{\xi}}_{X_3}$ for TA deviated more strongly at the lowest quantiles of the residuals in Fig. E.5c but its other residuals appeared to be normally distributed. Concluding, with these few exceptions in mind, all RSMs used in the system model fit adequately to their data bases.

The split-sample validation outlined in Subs. 'Validation of the prediction interval method' (p. 42) was used to choose between the variance estimators σ^2_X or σ^2_{-i} in Eq. D.7 (p. 40) of the prediction variance (Eq. D.12, p. 42). For this, the empirical confidence level α^*_{mean} in Eq. D.13 (p. 43) based on 100 repetitions with following specifications: $\bar{\boldsymbol{Y}}_{X_{eval}} \in \bar{\boldsymbol{\xi}}_{X_2}$ and $\bar{\boldsymbol{Y}}^* \in \bar{\boldsymbol{\xi}}^c_{X_2}$ were both based on the subsets of their data base; and $\bar{\boldsymbol{Y}}_{X_{eval}}$ served to analyse $\alpha^*_{mean}\left(\sigma^2_X\right)$ and $\alpha^*_{mean}\left(\sigma^2_{-i}\right)$. As general outcome, the empirical confidence levels of all RSMs of the system model were in line with the results of the RSM provided in Tab. E.3. In more detail, the prediction intervals based on the variance estimator σ^2_X showed small predictive capabilities. And in case of the variance estimator σ^2_{-i}, the prediction intervals were always slightly conservative and thus comparable to the results in Kim 2008 [28, Tab. 1]. These results are in contrast to Subs. 'Comparison to the Kim 2008 [28]' (p. G-20) in App. G.6.1 where σ^2_X led to good predictive capabilities and σ^2_{-i} led to too conservative prediction intervals. Despite these differences, the prediction variance of the prediction interval method applies the variance estimator σ^2_{-i} since it leads to adequate results with regard to the system model.

With view on the spatial sensitivity of the prediction interval method, all RSMs used in the system model led to similar results as in Fig. E.6a and Fig. E.6b for the default RSM. These figures illustrate that the prediction variance is independent to residuals at data points. Essentially, because the prediction variance in Eq. D.12 considers residuals globally by the variance estimator σ^2 of Eq. D.7. Moreover, Fig. G.2 on p. G-19 and Fig. G.3 confirm these results. Nota bene, Fig. E.6c and Fig. E.6d emphasise a characteristic of the prediction variance exemplarily for the RSM $\bar{\boldsymbol{\xi}}_{X_1}$. Namely, the prediction variances at data points clearly split up into two groups. A detailed analysis uncovers that the elevated prediction variances belong to data points located at the outer vertices of the domain. Concluding, the prediction variance is independent to the residuals only with differences between data points at the centre and the outer vertices. In other words, the prediction interval method is not spatially sensitive and hence, does not depend on the shape of the RSM.

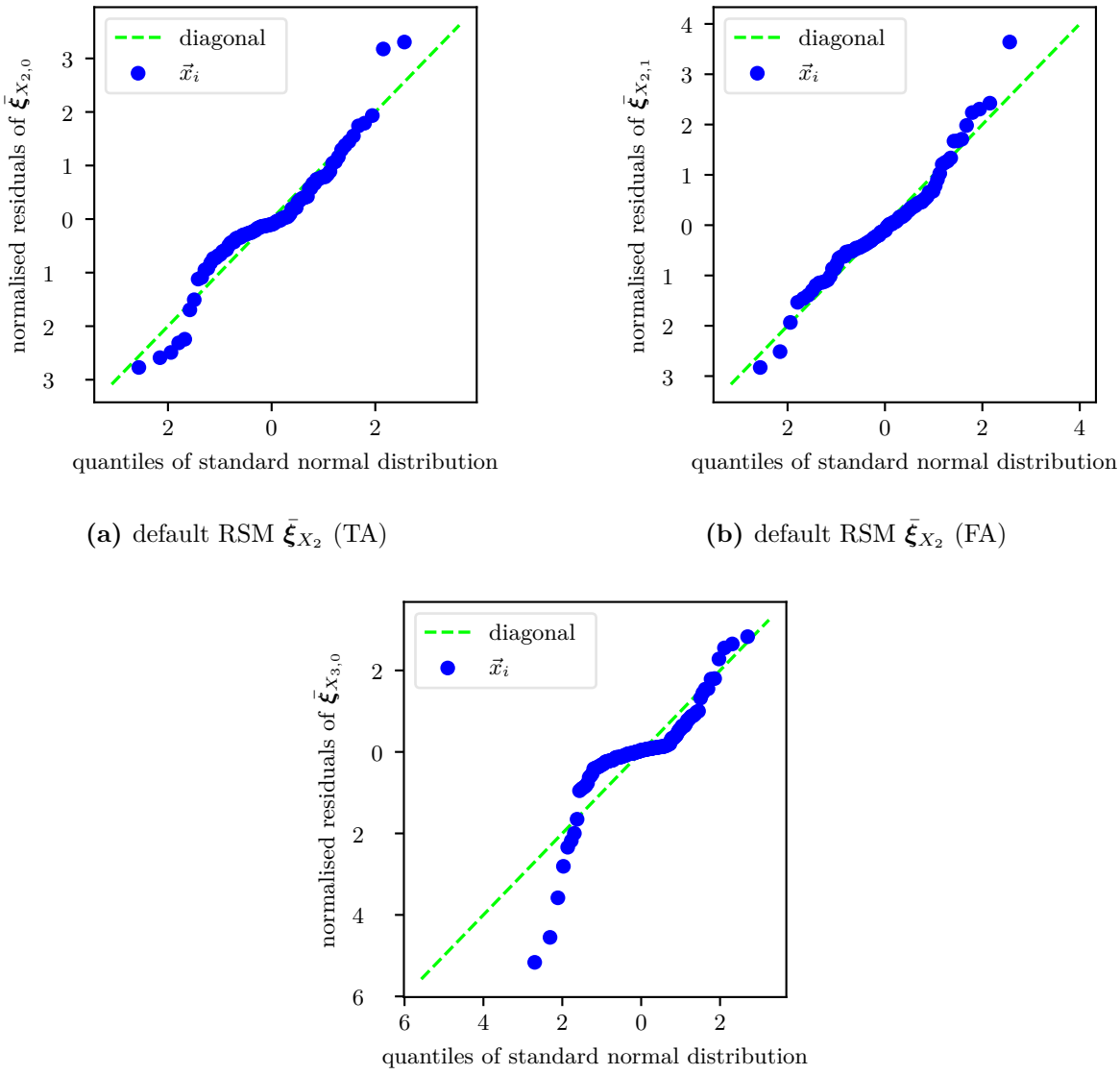

(a) default RSM $\bar{\boldsymbol{\xi}}_{X_2}$ (TA)

(b) default RSM $\bar{\boldsymbol{\xi}}_{X_2}$ (FA)

(c) RSM $\bar{\boldsymbol{\xi}}_{X_3}$ (TA)

Figure E.5: Frequency distributions of the residuals of RSMs; the residuals of the default RSM $\bar{\boldsymbol{\xi}}_{X_2}$ fit to a normal distribution (above) whereas the residuals of the RSM $\bar{\boldsymbol{\xi}}_{X_3}$ (TA) show some deviations (below); the scales differ between the figures.

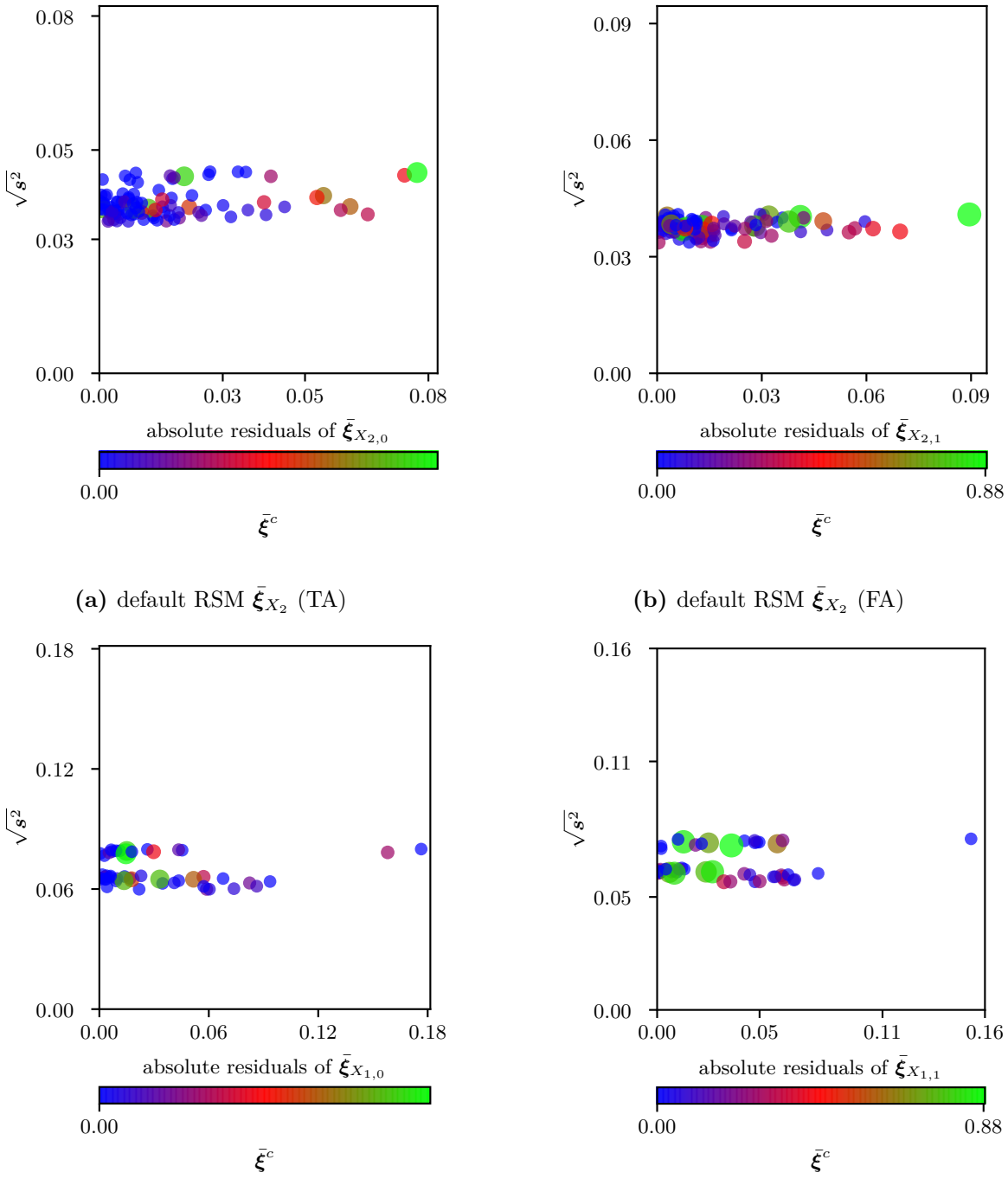

(a) default RSM $\bar{\xi}_{X_2}$ (TA)

(b) default RSM $\bar{\xi}_{X_2}$ (FA)

(c) RSM $\bar{\xi}_{X_1}$ (TA)

(d) RSM $\bar{\xi}_{X_1}$ (FA)

Figure E.6: Correlation of the prediction variance to residuals for the default RSM $\bar{\xi}_{X_2}$ (above) and the RSM $\bar{\xi}_{X_1}$ (below) at all their data points; the scales differ between both figures.

As a consequence, the prediction interval method reveals a drawback at vast plain response surfaces of the FF close to zero $\bar{\xi} \approx 0$, e.g. depicted in Fig. E.13a on p. 71. In this region, the metamodel uncertainty is expected to be small because of two reasons: first, since the results of all data points in this region are close to zero, i.e. $\bar{\xi}^c \approx 0$, the residuals should also be small; second, the results of the RSM should be close to zero, i.e. $\bar{\xi} \approx 0$ because

of the results of neighbouring data points. But the prediction variance, and thus also the metamodel uncertainty based on the prediction interval method, in this region is elevated as shown in Fig. E.14a. Additionally, the non-relative integration of the metamodel uncertainty into the metamodel with Eq. D.10 (p. 41) transfers this drawback of the prediction interval method to the results of the metamodel.

But two approaches might improve the metamodel uncertainty. First, the metamodel uncertainty could consider local residuals. Since residuals are spatially sensitive to the shape of the RSM as discussed in Subs. 'Validation of the prediction interval method' (p. 42), the metamodel uncertainty would be sensitive to the shape of the response surface too. Accordingly, the metamodel uncertainties would be small in regions with small second derivatives of the RSM, e.g. with the FF close to zero, i.e. $\bar{\boldsymbol{\xi}} \approx 0$, as in Fig. E.13a. In conclusion, this metamodel uncertainty is expected to be less conservative. Second, additional data points could reduce the metamodel uncertainty. For this approach, the assumption in Subs. 'Metamodel' (p. 23) that scenarios with $\mathrm{HRR}_{max} < 25\,\mathrm{MW}$ do not cause fatalities could be expanded to an additional region. This additional region could be specified with the knowledge on results of the complex model of previous refinement steps. Then, the data base of the RSM could be manually extended with data points to decrease the prediction variance in this region. These manual data points $\vec{x}_i \in X_{manual}$ have a FF equal to zero $\widetilde{\xi}^c_{manual} = \vec{0}$. To sum up, App. G.9 shortly outlines this second approach and illustrates its effects.

To conclude, MLS with the calibration algorithm and the prediction interval method using the variance estimator σ^2_{-i} lead to adequate results in the system model. Hence, MLS adequately represents the deterministic results of the complex model. However, the validation process identified one potential drawback of the prediction interval method, in detail, not to be spatially sensitive. But the integration of the metamodel uncertainty into the metamodel is important unrelated to the underlying method as exemplified in Subs. 'Basic characteristics' (p. G-19) in App. G.6.1. Thus, MLS and the metamodel uncertainty provide the basis for objective 1 (metamodel).

E.2.2 Sequential refinement

The focused sequential refinement and the combination of EDs to achieve an efficient metamodel were introduced in Subs. 'Metamodel' (p. 23) of Section B.4. Subs. 'Focus on regions of the domain' (p. 35), Subs. 'Sequential refinement' (p. 35) and Subs. 'Combination of EDs' (p. 36) in Section C.2 provide the details and Tab. E.1 on p. 53 in Section E.1 establishes the data bases for the sequential refinement. Now, the evaluation of the sequential refinement of the metamodel targets at: first, the convergence of the results of the RSM and the prediction variance during sequential refinement leading to the default RSM of the system model in Subs. 'Convergence of the RSM and the prediction variance' (p. 60); and second, the comparison of the default RSM to the batch RSM in Subs. 'Focused sequential refinement in comparison to the batch design' (p. 66) to identify advantages of the sequential refinement. To complete the discussion of the efficiency, Berchtold 2018 [9] highlighted the contribution of the combination of EDs to the efficiency.

Convergence of the RSM and the prediction variance

The convergence of the results of the RSM $\bar{\boldsymbol{\xi}}$ and the prediction variance $\boldsymbol{s}^2$ is important for the setup of the metamodel as outlined in Section D.4. The evaluation of the convergence bases on the RSMs $\bar{\boldsymbol{\xi}}_{X_0}$, $\bar{\boldsymbol{\xi}}_{X_1}$, $\bar{\boldsymbol{\xi}}_{X_2}$ and $\bar{\boldsymbol{\xi}}_{X_3}$. In more detail, the system model simulations $\mathcal{S}_0$, $\mathcal{S}_1$, $\mathcal{S}_2$ and $\mathcal{S}_3$, described in Section B.5, produced the following results with $N_{\mathrm{mcs}} = 10^4$ random scenarios.

Tab. E.4 shows the euclidean relative difference erd of all RSMs relative to the RSM $\bar{\boldsymbol{\xi}}_{X_3}$ as well as their prediction variances $\boldsymbol{s}^2_{q90}$. The sequential refinement achieved a monotonic decrease of the euclidean relative difference and a mostly monotonic decrease of the prediction variance. Additionally, Fig. E.7 illustrates the convergence of the results between the RSMs $\bar{\boldsymbol{\xi}}_{X_2}$ and $\bar{\boldsymbol{\xi}}_{X_3}$ and Fig. E.8 shows the convergence of the FF $\bar{\Xi}$ in the system model simulations. These results have already been published by Berchtold 2018 [9], the next paragraphs will discuss them in detail.

Table E.4: Prediction variance $\boldsymbol{s}^2_{q90}$ and euclidean relative difference erd $\left(\bar{\boldsymbol{\xi}}_{X_i}, \bar{\boldsymbol{\xi}}_{X_3}\right)$ for the RSMs of the sequential refinement (TA: above, FA: below).

RSM	$\sqrt{\boldsymbol{s}^2_{q90}}$	erd
$\bar{\boldsymbol{\xi}}_{X_{0,0}}$	0.163	0.54
$\bar{\boldsymbol{\xi}}_{X_{1,0}}$	0.061	0.30
$\bar{\boldsymbol{\xi}}_{X_{2,0}}$	0.031	0.10
$\bar{\boldsymbol{\xi}}_{X_{3,0}}$	0.032	0.00
$\bar{\boldsymbol{\xi}}_{X_{0,1}}$	0.155	0.24
$\bar{\boldsymbol{\xi}}_{X_{1,1}}$	0.053	0.14
$\bar{\boldsymbol{\xi}}_{X_{2,1}}$	0.031	0.05
$\bar{\boldsymbol{\xi}}_{X_{3,1}}$	0.037	0.00

The refinement steps achieve a convergence between the results of the RSMs $\bar{\boldsymbol{\xi}}_{X_2}$ and $\bar{\boldsymbol{\xi}}_{X_3}$. With a closer look, the euclidean relative difference between the RSMs $\bar{\boldsymbol{\xi}}_{X_2}$ and $\bar{\boldsymbol{\xi}}_{X_3}$ is larger for scenarios with TA than for scenarios with FA, namely erd $\left(\bar{\boldsymbol{\xi}}_{X_{2,0}}, \bar{\boldsymbol{\xi}}_{X_{3,0}}\right) >$ erd $\left(\bar{\boldsymbol{\xi}}_{X_{2,1}}, \bar{\boldsymbol{\xi}}_{X_{3,1}}\right)$. The rationale for the larger euclidean relative difference originates in the complexity of the response surface defined in Subs. 'Complex model within the system model' (p. 22). Scenarios with TA lead to a more complex shape of the response surface than scenarios with FA as discussed in Section B.3. The juxtaposed figures Fig. E.7a vs. Fig. E.7c (p. 62), Fig. E.11a vs. Fig. E.11b (p. 67), Fig. E.12a vs. Fig. E.12b (p. 68) as well as Fig. E.13a vs. Fig. E.13b (p. 71) exemplify this statement. As a consequence, the RSM for scenarios with FA requires less data points to reach convergence than the RSM for scenarios with TA. Therefore, the RSM for scenarios with TA is still subjected to differences, i.e. erd, between $\bar{\boldsymbol{\xi}}_{X_{2,0}}$ and $\bar{\boldsymbol{\xi}}_{X_{3,0}}$ in contrast to $\bar{\boldsymbol{\xi}}_{X_{2,1}}$ and $\bar{\boldsymbol{\xi}}_{X_{3,1}}$. However, Fig. E.8 shows good convergence between the FF $\bar{\Xi}_2$ and $\bar{\Xi}_3$ in the system model simulations $\mathcal{S}_2$ and $\mathcal{S}_3$ which consider scenarios with both TA and FA. With regard to the prediction variance $\boldsymbol{s}^2_{q90}$, the RSMs $\bar{\boldsymbol{\xi}}_{X_2}$ and $\bar{\boldsymbol{\xi}}_{X_3}$ show small differences. In case of scenarios with TA, the prediction variance of $\bar{\boldsymbol{\xi}}_{X_{2,0}}$ and $\bar{\boldsymbol{\xi}}_{X_{3,0}}$ even increases again. To summarise, this discussion leads to following conclusions: first, the difference in the results of risk analyses $\mathcal{R}$ using the FF Ξ^*_2 and Ξ^*_3 are expected to be small; and second, subsequent refinement steps of the RSM $\bar{\boldsymbol{\xi}}_{X_2}$, esp. for FA, will cause only small differences in the results. Hence, additional sequential refinement for the RSM $\bar{\boldsymbol{\xi}}_{X_2}$ is not required.

One interesting result in the convergence of the prediction variance is the increase of the prediction variance $\boldsymbol{s}^2_{q90}$ between the RSMs $\bar{\boldsymbol{\xi}}_{X_{2,1}}$ and $\bar{\boldsymbol{\xi}}_{X_{3,1}}$ for scenarios with FA. In contrast, the RSMs $\bar{\boldsymbol{\xi}}_{X_{2,0}}$ and $\bar{\boldsymbol{\xi}}_{X_{3,0}}$ for scenarios with TA lead similar prediction variances. And again the reason lies in the complexity of the response surfaces. As outlined before, scenarios with TA lead to more complex response surfaces. Consequently, the weighting parameter ω decreased between $\bar{\boldsymbol{\xi}}_{X_{2,0}}$ and $\bar{\boldsymbol{\xi}}_{X_{3,0}}$ whereas the other MLS attributes remained equal as shown in Tab. E.2. Therefore, the spatial sensitivity of the RSM increases which allows the adaptation to new data points as illustrated in Fig. E.9. The increase in the spatial sensitivity leads also to similar prediction variances between the RSMs $\bar{\boldsymbol{\xi}}_{X_{2,0}}$ and $\bar{\boldsymbol{\xi}}_{X_{3,0}}$ for

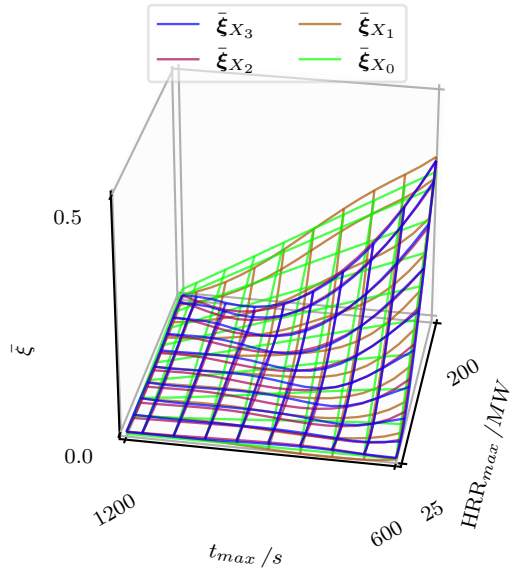

(a) results of the RSM (TA)

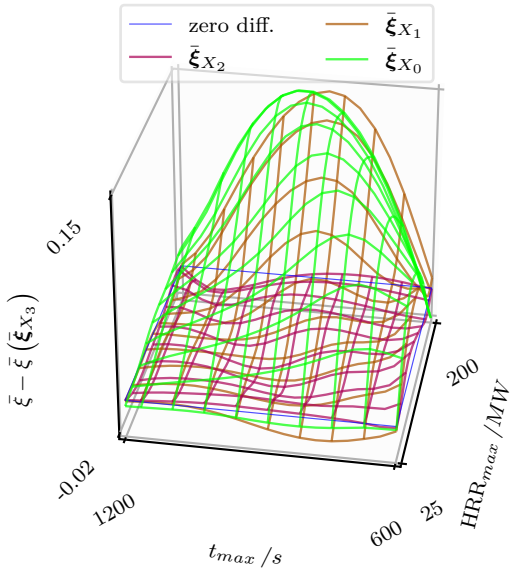

(b) difference to $\bar{\boldsymbol{\xi}}_{X_3}$ (TA)

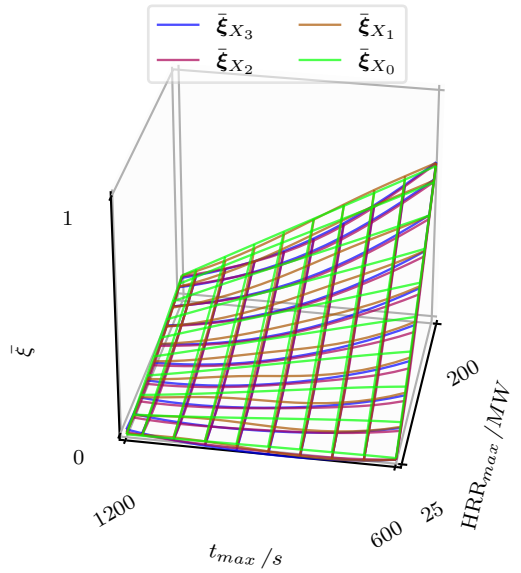

(c) results of the RSM (FA)

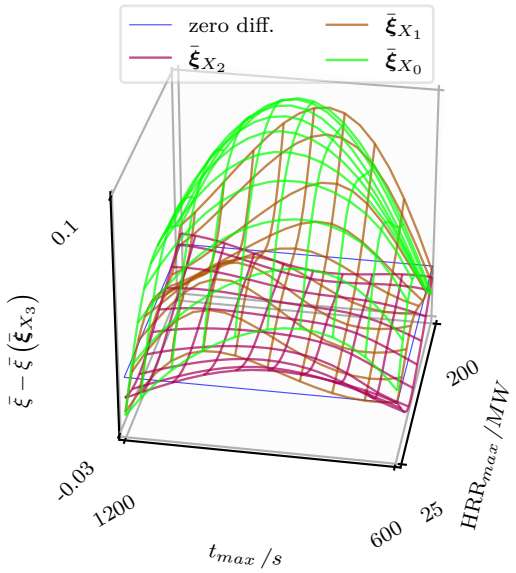

(d) difference to $\bar{\boldsymbol{\xi}}_{X_3}$ (FA)

Figure E.7: Convergence of the results of RSMs during the sequential refinement in the region of sc(−MW, −s, 124 s, 101, fa = −) (above: TA, below: FA); the scales differ between the figures.

scenarios with TA. On the other hand, scenarios with FA cause less complex response surfaces. Thus, the RSMs $\bar{\boldsymbol{\xi}}_{X_{2,1}}$ and $\bar{\boldsymbol{\xi}}_{X_{3,1}}$ become less spatially sensitive, i.e. the weighting parameter ω increases and the other MLS attributes do not change, which again results in an increase of the prediction variance $\boldsymbol{s}^2$ of the RSM $\bar{\boldsymbol{\xi}}_{X_{2,1}}$ compared to the RSM $\bar{\boldsymbol{\xi}}_{X_{3,1}}$. To explain this in detail: new data points elevate the variance estimator σ^2_{-i} when their results are different to the RSM with low spatial sensitivity because the RSM does not adapt to the new data points. Correspondingly, the prediction variance $\boldsymbol{s}^2$ increases globally. In summary, the increase of

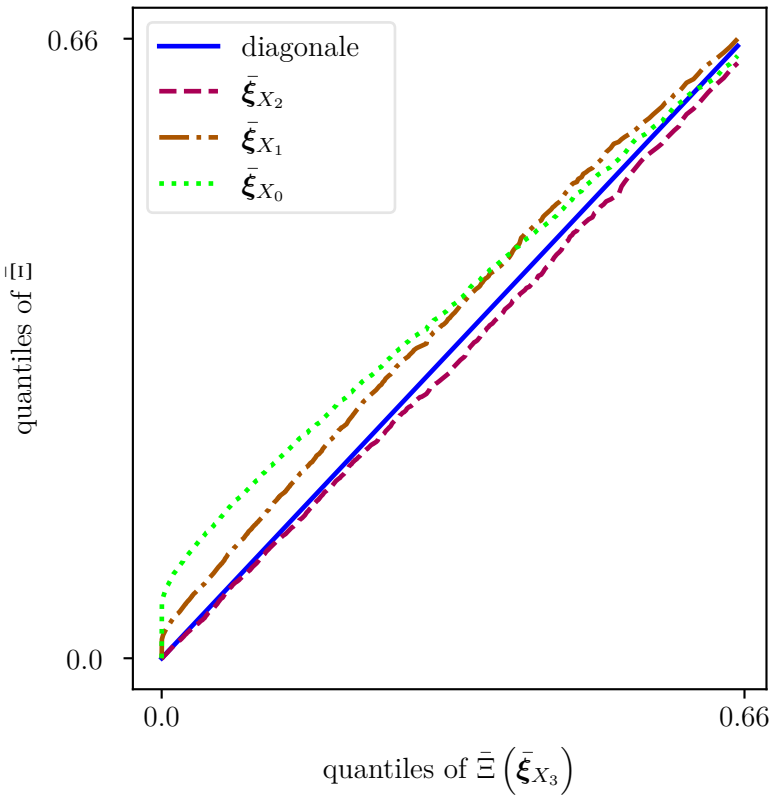

Figure E.8: Difference of the frequency distributions of the FFs $\bar{\Xi}_0$, $\bar{\Xi}_1$, $\bar{\Xi}_2$, $\bar{\Xi}_3$ relative to the FF $\bar{\Xi}_3$; the FFs show convergence between $\bar{\Xi}_2$ and $\bar{\Xi}_3$; the FFs stem from system model simulations subjected to the RSMs $\bar{\xi}_{X_0}$, $\bar{\xi}_{X_1}$, $\bar{\xi}_{X_2}$ and $\bar{\xi}_{X_3}$ using the indirect mode over fixed points.

prediction variance between the RSMs $\bar{\xi}_{X_{2,0}}$ and $\bar{\xi}_{X_{3,0}}$ of scenarios with TA can be reasoned by the complexity of the response surface.

Another aspect is the prediction variance of a RSM subjected to an 'infinite' number of data points. In this case, the residuals, using leave-one-out, are expected to be very small because of very close neighbours. Hence, the variance estimator σ^2_{-i} and prediction variance $\boldsymbol{s}^2$ might be small depending on aleatory uncertainties in the results of the complex model $\bar{\boldsymbol{\xi}}^c$. Subs. 'Calibration algorithm' (p. G-22) in App. G.6.1 provides an example of a RSM subjected to no aleatory uncertainties. In conclusion, the final convergence of the prediction variance depends on the aleatory uncertainties in the results of the complex model $\bar{\boldsymbol{\xi}}^c$.

Fig. E.10a uncovers one more interesting result: the prediction variance $\boldsymbol{s}^2$ of $\bar{\boldsymbol{\xi}}_{X_1}$ is clearly elevated close to data points in the centre of the domain. The preliminary discussion in Subs. 'Basic characteristics' (p. G-19) in App. G.6.1 mentioned only a slight elevation of the prediction variance at data points. The subsection further reasoned the strong elevation of the prediction variance of an arbitrary point at the outer vertices of the domain with the larger distance to most data points. But now, the rationale for the elevated prediction variances is mainly rooted in the combination of the EDs for fire and evacuation scenarios X^{fire} and X^{evac} described in Subs. 'Combination of EDs' (p. 36). The combination leads to an aggregation of multiple evacuation scenarios $\{\vec{x}^{\text{evac}} \in X^{\text{evac}}, \ldots\}$ on a single fire scenario $\vec{x}^{\text{fire}} \in X^{\text{fire}}$. Thus, a random scenario $\widetilde{x}$, varied on fire risk factors with constant values in the evacuation risk factors, can be close to multiple evacuation scenarios $\{\vec{x}^{\text{evac}} \in X^{\text{evac}}, \ldots\}$ all having equal values in the fire risk factors. In that case, the weighting matrix $\boldsymbol{W}$ in Eq. D.12

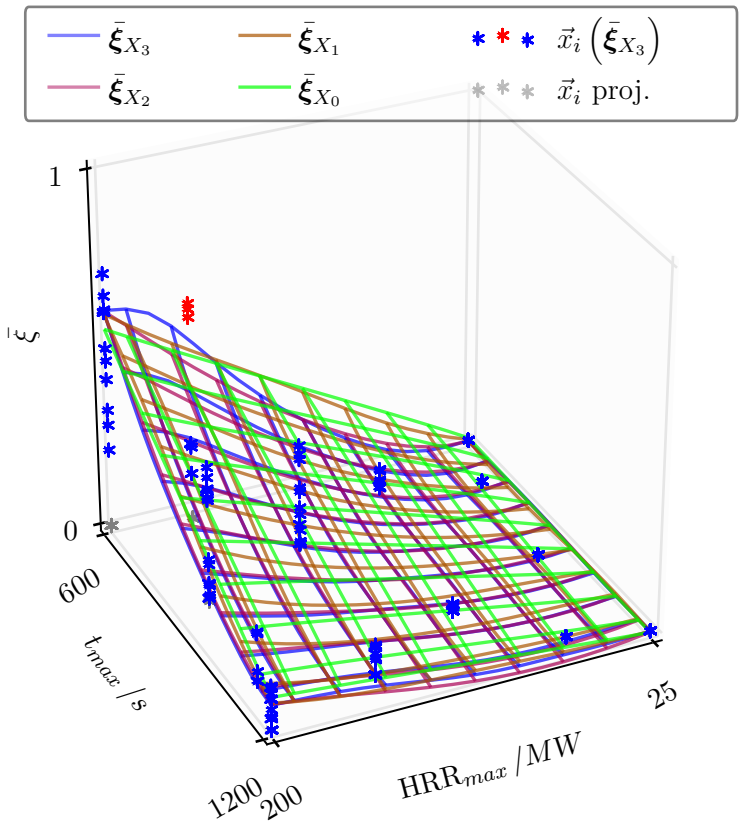

Figure E.9: Results of RSMs during the sequential refinement shown in the region of sc(− MW, − s, 241 s, 118, $fa = 0$); the RSM $\bar{\xi}_{X_3}$ adapts to new data points related to the fire scenario sc(165.1 MW, 631.9 s, − s, −, $fa = 0$) (highlighted red); the data points are projected (proj.) to the bottom of the figure.

(p. 42) is subjected to higher values which this time leads to the elevated prediction variances in the local region of $\widetilde{x}$ shown in Fig. E.10a. A similar effect was not obvious in Subs. 'Basic characteristics' (p. G-19). Differently, a random scenario $\widetilde{x}$, varied on evacuation risk factors but with constant values in the fire risk factors, has rather similar distances to evacuation scenarios $\{\bar{x}^{\text{evac}} \in X^{\text{evac}}, \ldots\}$ which again have identical values in the fire risk factors. As a consequence, the random scenario $\widetilde{x}$ has rather constant, but elevated, prediction variances in its local region as can be seen in Fig. E.10b. Further results, e.g. in Fig. E.10c, indicate that the refinement step from $\bar{\xi}_{X_1}$ to $\bar{\xi}_{X_2}$ reduces the central elevated prediction variances. Finally, three conclusions originate in these observations. First, the combination of EDs leads to stronger elevation of the prediction variance in the region of data points in the centre of the domain. From this result, it is expected that sequential refinement with only new evacuation scenarios $\|X_i^{\text{evac}}\| > \|X_{i-1}^{\text{evac}}\|$ but without new fire scenarios $\left\|X_i^{\text{fire}}\right\| = \left\|X_{i-1}^{\text{fire}}\right\|$ would not be efficient in decreasing the prediction variance. Second, the argumentation for the elevated prediction variance at outer vertices in Subs. 'Basic characteristics' (p. G-19) is still valid. Hence, the focused sequential refinement on the outer vertices remains important for the metamodel used in the system model. And third, the sequential refinement does not only lead to global effects as shown in Tab. E.4, but also to local effects as illustrated in Fig. E.10a and Fig. E.10c.

To finally emphasise the conclusions from the sequential refinement: first, the results of the RSM and the prediction variance s^2_{q90} converge between the RSMs $\bar{\xi}_{X_2}$ to $\bar{\xi}_{X_3}$; second, the focused sequential refinement achieves a sufficient data base for the metamodel with ten

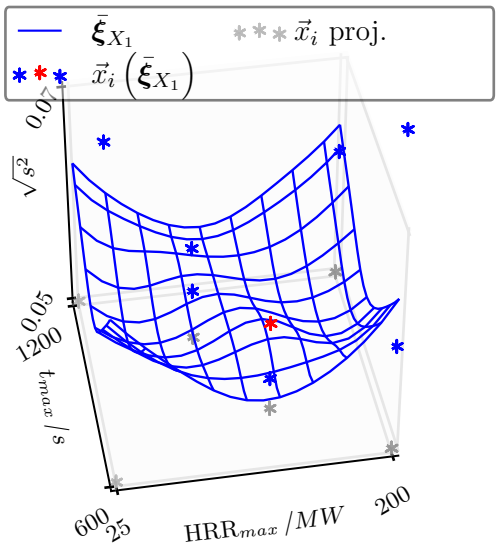

(a) for the RSM $\bar{\xi}_{X_1}$ on fire risk factors

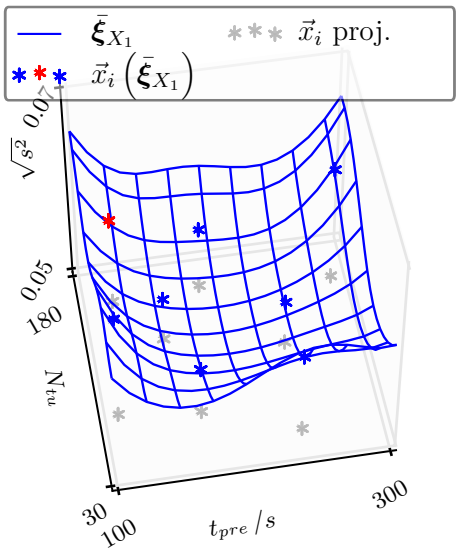

(b) for the RSM $\bar{\xi}_{X_1}$ on evacuation risk factors

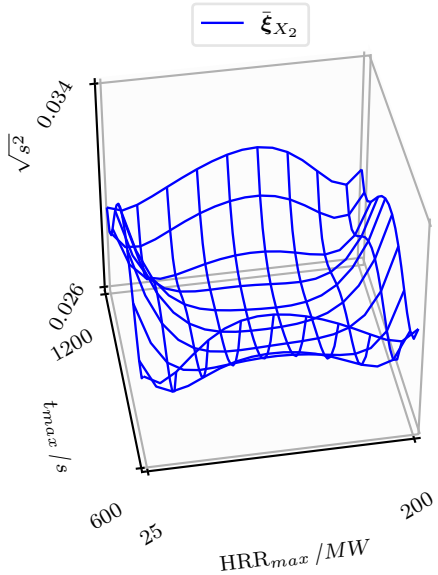

(c) for the RSM $\bar{\xi}_{X_2}$ on fire risk factors

Figure E.10: Elevated prediction variance $\sqrt{s^2}$ in the region of sc(131 MW, 770 s, 121 s, 155, $fa = 1$) (highlighted red in Fig. E.10a and Fig. E.10b) based on fire scenario sc(131 MW, 770 s, − s, −, fa = −) of $\bar{\xi}_{X_1}$; comparison to the prediction variance of the RSM $\bar{\xi}_{X_2}$; the scales differ between the figures.

Table E.5: Prediction variance $\boldsymbol{s}^2$ and euclidean relative difference erd $\equiv$ erd $\left(\bar{\boldsymbol{\xi}}_{X_i}, \bar{\boldsymbol{\xi}}_{X_2}\right)$ for the RSMs $\bar{\boldsymbol{\xi}}_{X_2}$ and $\bar{\boldsymbol{\xi}}_{X_b}$.

RSM	$\sqrt{\boldsymbol{s}^2_{q90}}$	erd
$\bar{\boldsymbol{\xi}}_{X_{2,0}}$	0.031	0.00
$\bar{\boldsymbol{\xi}}_{X_{b,0}}$	0.039	0.147
$\bar{\boldsymbol{\xi}}_{X_{2,1}}$	0.031	0.00
$\bar{\boldsymbol{\xi}}_{X_{b,1}}$	0.031	0.059

simulations of fire scenarios and $2 \cdot 96$ simulations of evacuation scenarios considering TA and FA; and third, the RSM $\bar{\boldsymbol{\xi}}_{X_2}$ is specified as default RSM used in the system model. Hence, the default RSM is supposed to be sufficient for risk analysis.

Focused sequential refinement in comparison to the batch design

Subs. 'Metamodel' (p. 23) describes the contribution of the focused sequential refinement to the efficiency of the metamodel. To further evaluate the efficiency, this section quantifies and discusses the prediction variance of the default RSM $\bar{\boldsymbol{\xi}}_{X_2}$ in comparison to the batch RSM $\bar{\boldsymbol{\xi}}_{X_b}$ shown in Tab. E.2.

Tab. E.5, Fig. E.11 and Fig. E.12 provide an overview on the results of the RSMs $\bar{\boldsymbol{\xi}}_{X_2}$ and $\bar{\boldsymbol{\xi}}_{X_b}$. The euclidean relative differences erd between both RSMs were only slightly elevated in relation to the differences between the RSMs $\bar{\boldsymbol{\xi}}_{X_2}$ and $\bar{\boldsymbol{\xi}}_{X_3}$ in Tab. E.4. And again, scenarios with FA caused smaller differences compared to scenarios with TA due to the lower complexity of the response surface, namely erd $\left(\bar{\boldsymbol{\xi}}_{X_{b,1}}, \bar{\boldsymbol{\xi}}_{X_{2,1}}\right) <$ erd $\left(\bar{\boldsymbol{\xi}}_{X_{b,0}}, \bar{\boldsymbol{\xi}}_{X_{2,0}}\right)$. Thus, to great extent, both RSMs $\bar{\boldsymbol{\xi}}_{X_2}$ and $\bar{\boldsymbol{\xi}}_{X_b}$ led to similar shapes with the largest differences at the outer vertices. The latter observation seems to justify the increased prediction variance at the outer vertices demonstrated in Fig. E.10 and indicates that the focus on the outer vertices during sequential refinement is useful.

With regard to the prediction variance $\boldsymbol{s}^2_{q90}$, the default RSM and the batch RSM had similar results for scenarios with FA, i.e. $\boldsymbol{s}^2_{q90}\left(\bar{\boldsymbol{\xi}}_{X_{2,1}}\right) \approx \boldsymbol{s}^2_{q90}\left(\bar{\boldsymbol{\xi}}_{X_{b,1}}\right)$. But for scenarios with TA, the default RSM was subjected to a smaller prediction variance than the batch RSM with $\boldsymbol{s}^2_{q90}\left(\bar{\boldsymbol{\xi}}_{X_{2,0}}\right) < \boldsymbol{s}^2_{q90}\left(\bar{\boldsymbol{\xi}}_{X_{b,0}}\right)$. The reason for this outcome is not immediately obvious but the adapted batch RSM $\bar{\boldsymbol{\xi}}_{X_{b^*,0}}$ allows the insight. But the first important fact is that the data base $\bar{\boldsymbol{\xi}}^c_{X_b}$ of the batch RSM provides more data points in the centre of the domain than the data base $\bar{\boldsymbol{\xi}}^c_{X_2}$ of the default RSM. Also, the complexity of the response surface, i.e. the second derivative, is higher in the centre than at the outer vertices which is exemplified by Fig. E.11a. Coming now to the adapted batch RSM $\bar{\boldsymbol{\xi}}_{X_{b^*,0}}$, it is subjected to the same data base $\bar{\boldsymbol{\xi}}_{X_{b,0}}$ as the batch RSM but the weighting type is w_p (Eq. D.17 on p. 45) instead of w_g. Due to this alteration, the adapted batch RSM and the default RSM $\bar{\boldsymbol{\xi}}_{X_{2,0}}$ both base on the same weighting type. As result, the corresponding weighting parameters reveal that the adapted batch RSM $\bar{\boldsymbol{\xi}}_{X_{b^*,0}}$, and thus presumably also the batch RSM $\bar{\boldsymbol{\xi}}_{X_{b,0}}$, is less spatially sensitive than the default RSM which is the second important fact. The two facts derived here lead to increased residuals for the variance estimator σ^2_{-i} which consequently causes the higher prediction variance $\boldsymbol{s}^2_{q90}$ of the batch RSM $\bar{\boldsymbol{\xi}}_{X_{b,0}}$ in comparison to the default RSM $\bar{\boldsymbol{\xi}}_{X_{2,0}}$.

Some conclusions can be drawn from these results. First, variations in the ED of the default RSM have small effects on the RSM $\bar{\boldsymbol{\xi}}_{X_2}$ in comparison to $\bar{\boldsymbol{\xi}}_{X_b}$. Second, the sequential refinement can lead to smaller metamodel uncertainties, i.e. prediction variances, compared to a

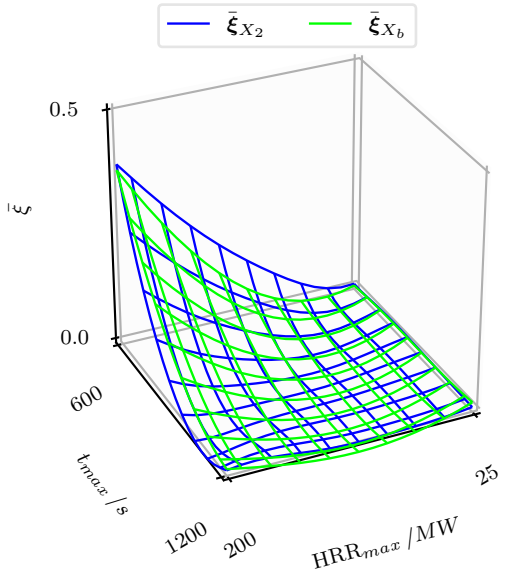

(a) results of the RSM (TA)

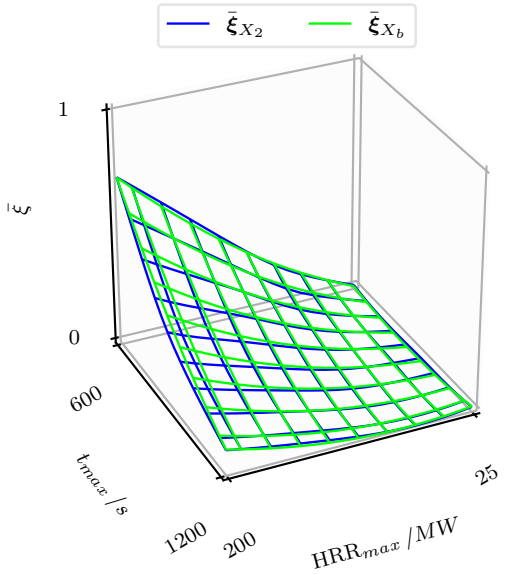

(b) results of the RSM (FA)

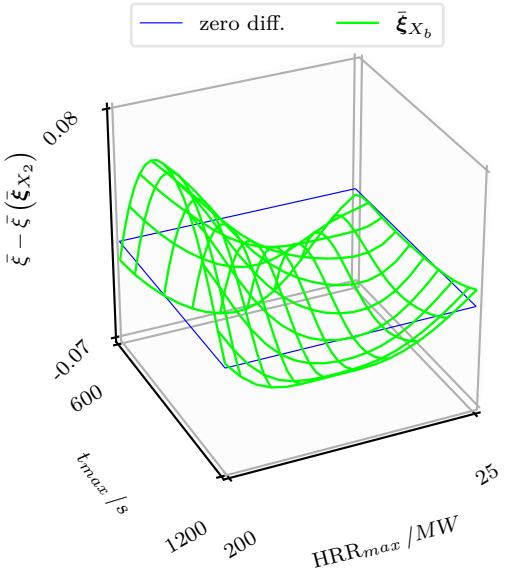

(c) difference to $\bar{\xi}_{X_2}$ (TA)

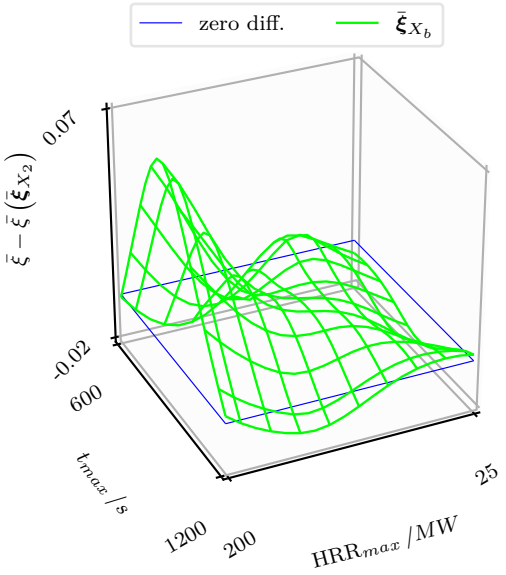

(d) difference to $\bar{\xi}_{X_2}$ (FA)

Figure E.11: Comparison of the results of the default RSM $\bar{\xi}_{X_2}$ with results of the batch RSM $\bar{\xi}_{X_b}$ for sc(− MW, − s, 124 s, 154, fa = −); the scales differ between both figures.

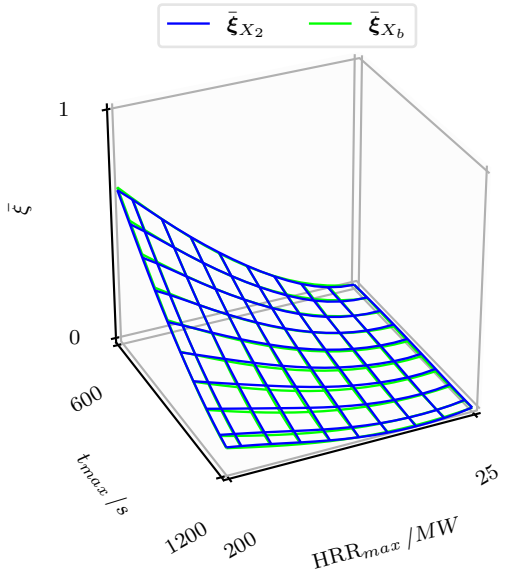

(a) results of the RSM (TA)

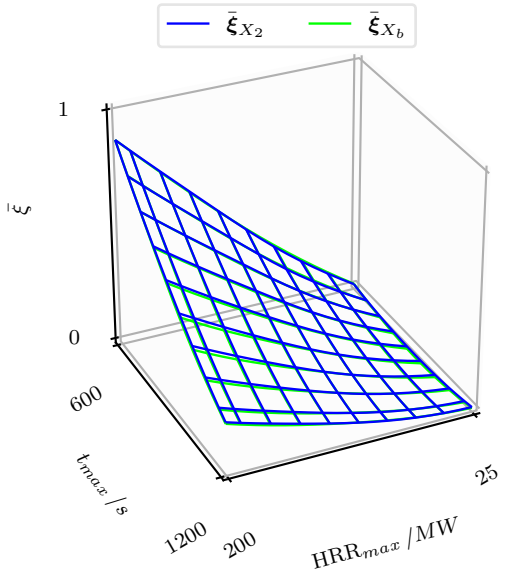

(b) results of the RSM (FA)

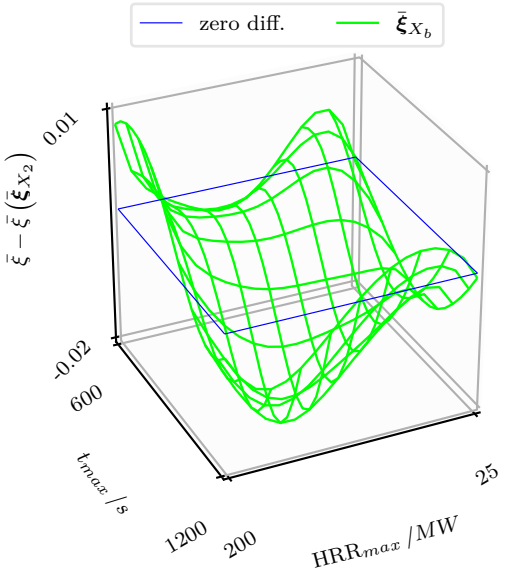

(c) difference to $\bar{\xi}_{X_2}$ (TA)

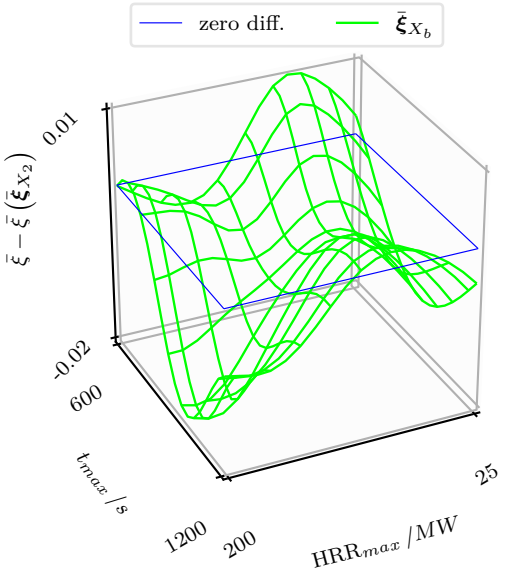

(d) difference to $\bar{\xi}_{X_2}$ (FA)

Figure E.12: Comparison of the results of the default RSM $\bar{\xi}_{X_2}$ with results of the batch RSM $\bar{\xi}_{X_b}$ for sc(− MW, − s, 276 s, 101, fa = −); the scales differ between both figures.

Table E.6: Empirical confidence level α^* according to complete-sample validation for the RSMs $\bar{\boldsymbol{\xi}}_{X_1}$ and $\bar{\boldsymbol{\xi}}_{X_2}$ depending on the confidence level α.

$\bar{\boldsymbol{Y}}_{X_{eval}}$	$\bar{\boldsymbol{Y}}^*$	$\alpha = 0.50$	$\alpha = 0.75$	$\alpha = 0.90$	$\alpha = 0.95$
$\bar{\boldsymbol{\xi}}_{X_{1,0}}$	$\bar{\boldsymbol{\xi}}_{X_{1a,0}}$	0.90	0.99	1.00	1.00
$\bar{\boldsymbol{\xi}}_{X_{1,0}}$	$\bar{\boldsymbol{\xi}}_{X_{2,0}}$	0.65	0.87	0.96	0.99
$\bar{\boldsymbol{\xi}}_{X_{1,0}}$	$\bar{\boldsymbol{\xi}}_{X_{3,0}}$	0.66	0.88	0.96	0.99
$\bar{\boldsymbol{\xi}}_{X_{1,1}}$	$\bar{\boldsymbol{\xi}}_{X_{1a,1}}$	0.78	0.95	1.00	1.00
$\bar{\boldsymbol{\xi}}_{X_{1,1}}$	$\bar{\boldsymbol{\xi}}_{X_{2,1}}$	0.60	0.91	0.98	1.00
$\bar{\boldsymbol{\xi}}_{X_{1,1}}$	$\bar{\boldsymbol{\xi}}_{X_{3,1}}$	0.64	0.93	0.99	1.00
$\bar{\boldsymbol{\xi}}_{X_{2,0}}$	$\bar{\boldsymbol{\xi}}_{X_{b,0}}$	0.73	0.91	0.97	0.98
$\bar{\boldsymbol{\xi}}_{X_{2,0}}$	$\bar{\boldsymbol{\xi}}_{X_{3,0}}$	0.93	0.97	0.98	0.99
$\bar{\boldsymbol{\xi}}_{X_{2,1}}$	$\bar{\boldsymbol{\xi}}_{X_{b,1}}$	0.87	0.96	0.99	1.00
$\bar{\boldsymbol{\xi}}_{X_{2,1}}$	$\bar{\boldsymbol{\xi}}_{X_{3,1}}$	0.91	0.98	0.99	1.00

batch design. And third, the focus on outer vertices of the domain seems to be useful for three reasons: the elevated prediction variance at the outer vertices; the larger differences in the shapes of the RSMs $\bar{\boldsymbol{\xi}}_{X_2}$ and $\bar{\boldsymbol{\xi}}_{X_b}$ at the outer vertices; and, the local effects of the sequential refinement discussed in Subs. 'Convergence of the RSM and the prediction variance' (p. 60). Moreover, the sequential refinement until convergence is reached avoids a 'conservative guess' for the number of data points as discussed by Berchtold 2018 [9]. To illustrate this advantage, the default RSM required ten simulations of fire scenarios and $2 \cdot 96$ evacuation scenarios for TA and FA shown in Tab. E.1 (p. 53) but the risk analysis in Berchtold 2016 [8] applies a batch RSM subjected to 20 fire scenarios and $2 \cdot 400$ evacuation scenarios. Consequently, this advantage and the previous conclusions demonstrate that the focused sequential refinement increases the efficiency of the metamodel. Accordingly, the PAD with sequential refinement and focus contributes to objective 2 (efficiency).

E.2.3 Predictive capability of the prediction interval method

A drawback of the prediction interval method is identified in Section E.2.1 but Subs. 'Basic characteristics' (p. G-19) in App. G.6.1 illustrates the importance of the metamodel uncertainty. As a consequence, it is important to validate the prediction interval method which is used for the metamodel uncertainty. In the validation, it is examined whether the prediction interval method is able to predict the 'value of a single future observation' [28, p. 4] as outlined in Subs. 'Prediction interval method' (p. 42). With this aim, the study considers subsequent refinement steps, i.e. the RSMs $\bar{\boldsymbol{\xi}}_{X_1}$, $\bar{\boldsymbol{\xi}}_{X_2}$ and $\bar{\boldsymbol{\xi}}_{X_3}$ as well as variations in the ED with the RSMs $\bar{\boldsymbol{\xi}}_{X_{1a}}$ and $\bar{\boldsymbol{\xi}}_{X_b}$ being equivalent to the RSMs $\bar{\boldsymbol{\xi}}_{X_1}$ and $\bar{\boldsymbol{\xi}}_{X_2}$ respectively. To quantify the predictive capability of the prediction interval method, the complete-sample validation in Subs. 'Validation of the prediction interval method' (p. 42) is applied. It serves to evaluate the empirical confidence level α^* according to Eq. D.13 (p. 43). Eq. D.13 is specified with $\bar{\boldsymbol{Y}}_{X_{eval}}$ and $\bar{\boldsymbol{Y}}^*$ both shown in Tab. E.6 where $\bar{\boldsymbol{Y}}^*$ provides results at the evaluation points representing the arbitrary points $\widetilde{X}$.

Tab. E.6 presents the empirical confidence levels. First, the evaluation of subsequent refinement steps considers the pairs of RSMs $\bar{\boldsymbol{\xi}}_{X_1}$ to $\bar{\boldsymbol{\xi}}_{X_2}$ and $\bar{\boldsymbol{\xi}}_{X_2}$ to $\bar{\boldsymbol{\xi}}_{X_3}$. The RSM $\bar{\boldsymbol{\xi}}_{X_0}$ comprises only data points at the outer vertices and consequently its prediction interval is exceptionally conservative with empirical confidence levels of $\alpha^* = 1.00$ for all confidence levels $\alpha \geq 0.5$. Concerning the RSM $\bar{\boldsymbol{\xi}}_{X_1}$, its prediction interval is conservative with values for the empirical confidence level comparable to the values in Kim 2008 [28, Tab. 1]. And for the RSM $\bar{\boldsymbol{\xi}}_{X_2}$ the

prediction interval is again more conservative due to convergence between the results of the RSMs $\bar{\boldsymbol{\xi}}_{X_2}$ and $\bar{\boldsymbol{\xi}}_{X_3}$. Second, with regard to the variations in the EDs, the prediction intervals of the RSMs $\bar{\boldsymbol{\xi}}_{X_1}$ and $\bar{\boldsymbol{\xi}}_{X_2}$ are very conservative to the RSM $\bar{\boldsymbol{\xi}}_{X_{1a}}$ in the former case and still fairly conservative in the latter case. The reason for the latter result is the similarity between the RSMs $\bar{\boldsymbol{\xi}}_{X_2}$ and $\bar{\boldsymbol{\xi}}_{X_b}$ as illustrated in Subs. 'Focused sequential refinement in comparison to the batch design' (p. 66). To sum up, the increased conservativeness of the prediction interval method might be related to its drawback. Accordingly, the approaches to improve the metamodel uncertainty discussed in Section E.2.1 could reduce the conservativeness for even better predictive capabilities.

Concluding, the prediction interval method based on variance estimator σ^2_{-i} leads to conservative results which confirms the results in Section E.2.1. But more important, the validation was successful in reference to 'predicting the interval of the value of a single future observation' [28, p. 4]. This conclusion is in particular true for subsequent refinement steps as well as to variations in the ED. In other words, the accuracy of the RSM with regard to unknown results of the complex model corresponds to the prediction interval.

E.2.4 Risk factors, discrete events and global objective

In Section A.1 it is explained that the risk analysis directs at complex scenarios with the global objective. Then, Section B.3 presents the complex scenarios which consider multiple risk factors, i.e. the parent nodes of the node FF, and discrete events. A short discussion of the effect of discrete events on the shape of the response surface follows in Subs. 'Complex model within the system model' (p. 22) in Section B.4. To extend this discussion, the shape of the RSM is explored with attention to, firstly, the correlation of risk factors and secondly, the effect of discrete events. Moreover, Section D.1.3 describes that MLS is suitable for the global objective. Accordingly, thirdly, MLS is validated with focus on the global objective. For these analyses, a visual evaluation of the RSM $\bar{\boldsymbol{\xi}}_{X_3}$ serves as basis. Additionally, the SoM model $\bar{\boldsymbol{\xi}}^{\mathrm{SoM}}_{X_3}$, with the background in Subs. 'FoM and SoM models in the metamodel' (p. 45), shall emphasise the difference of the MLS model to a global quadratic polynomial.

Fig. E.13 and Fig. E.14 act as example for this study. Furthermore, Fig. E.13a and Fig. E.14a show the increased prediction variance in a region where the FF is close to zero, i.e. $\bar{\boldsymbol{\xi}} \approx 0$. Therefore, these figures illustrate the reason for the approaches to improve the metamodel uncertainty outlined in Section E.2.1. Also, Fig. E.13a confirms the assumption in Subs. 'Metamodel' (p. 23) in Section B.4 that the number of fatalities is zero for scenarios with a maximum HRR of $\mathrm{HRR}_{max} < 25\,\mathrm{MW}$.

The risk factors maximum HRR HRR_{max}, time to maximum HRR t_{max}, maximum pre-evacuation time t_{pre} and number of tunnel users N_{tu}, i.e. parent nodes of the node FF, caused different correlations to the results of the RSM. First, the correlation between HRR_{max} and the results of the RSM $\bar{\boldsymbol{\xi}}_{X_3}$ is more complex than a global quadratic polynomial as depicted in Fig. E.13a. Second, t_{max} shows a correlation that is more complex than a global linear but less complex than a global quadratic polynomial according to Fig. E.13b and Fig. E.13d. And third, Fig. E.14c and Fig. E.14d demonstrate the more or less linear correlation of t_{pre}. These figures also illustrate that the RSM $\bar{\boldsymbol{\xi}}_{X_3}$ is only subjected to small effects of N_{tu}. For completeness, Fig. E.15 changes the perspective and exemplifies the correlation between the 'time' risk factors t_{max} and t_{pre}. Concluding, the implementation of the PAD could be improved with reference to Subs. 'Focus on regions of the domain' (p. 35). Currently, all risk factors are subjected to the same number of strata. But since, the risk factors contribute differently to the complexity in the shape of the RSM, different numbers of data points are required to reproduce their correlations. Consequently, the number of strata could be

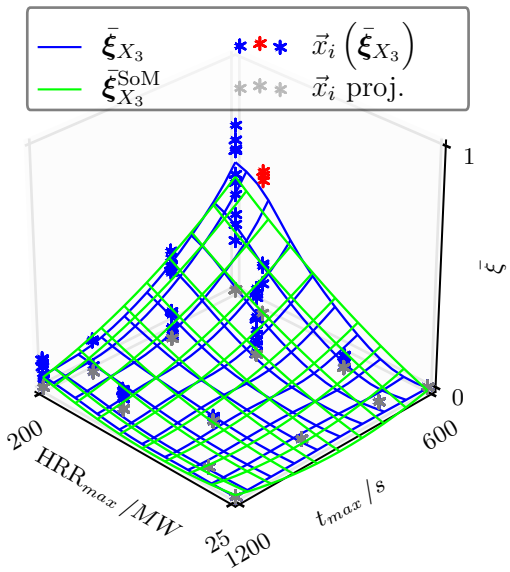

(a) results of the RSM (TA)

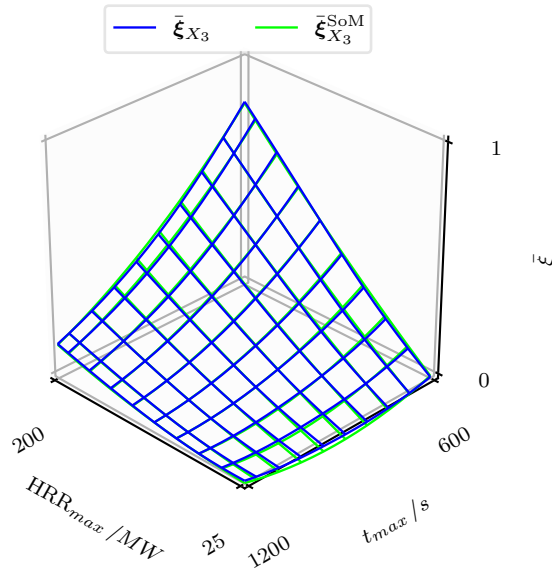

(b) results of the RSM (FA)

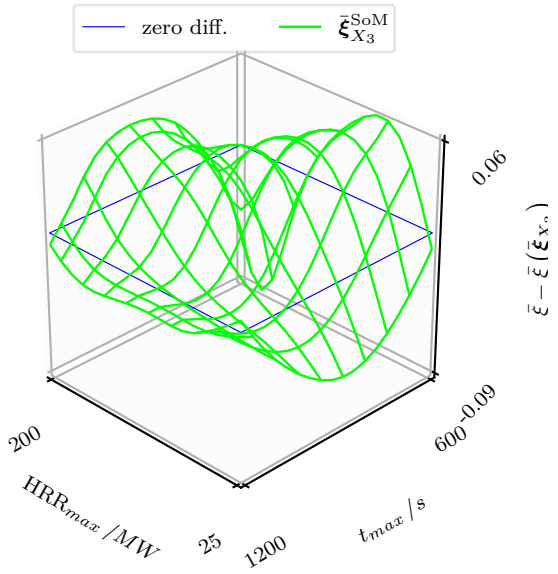

(c) difference to $\bar{\xi}_{X_3}$ (TA)

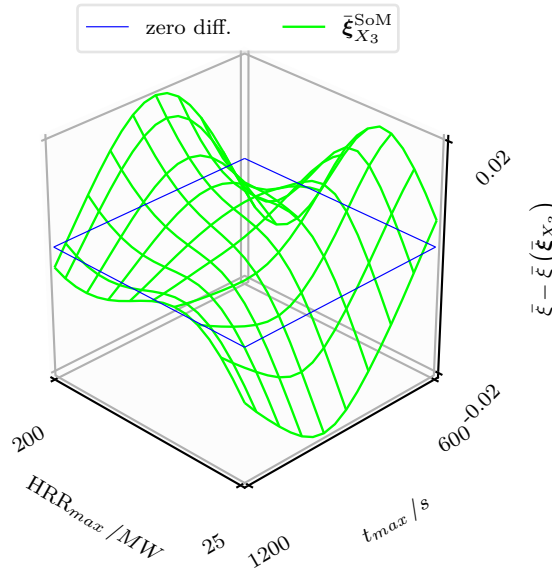

(d) difference to $\bar{\xi}_{X_3}$ (FA)

Figure E.13: Correlations between risk factors and the results of the RSM $\bar{\xi}_{X_3}$ in the region of sc(−MW, −s, 194 s, 171, $fa = -$) in comparison to the RSM $\bar{\xi}^{\mathrm{SoM}}_{X_3}$; the RSM $\bar{\xi}_{X_3}$ adapts to new data points (highlighted red) in Fig. E.13a; the scales differ between the figures.

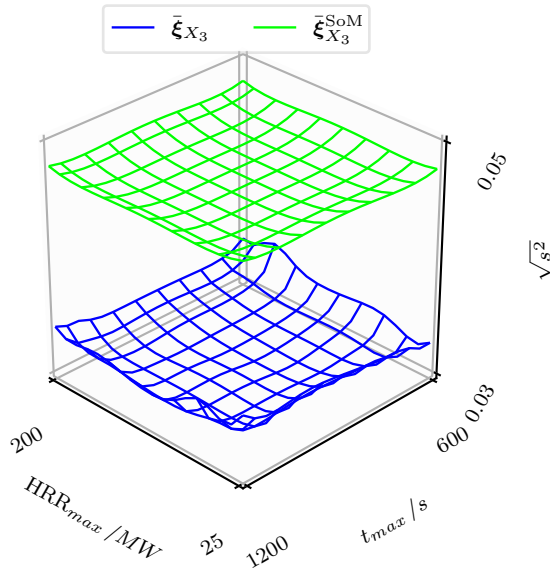

(a) prediction variance $\sqrt{s^2}$ (TA)

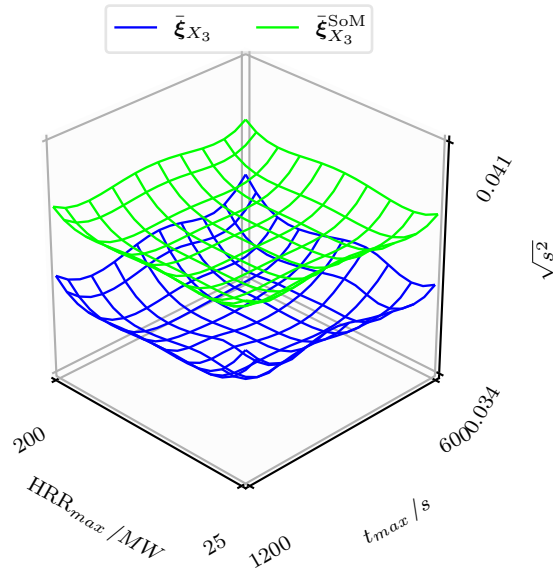

(b) prediction variance $\sqrt{s^2}$ (FA)

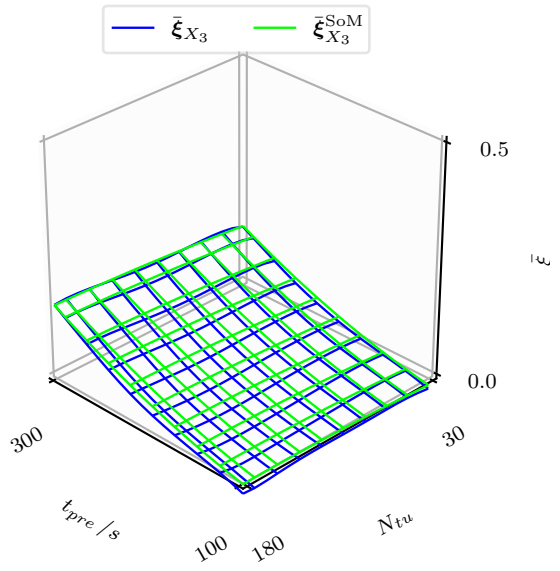

(c) results of the RSM on evacuation risk factors (TA)

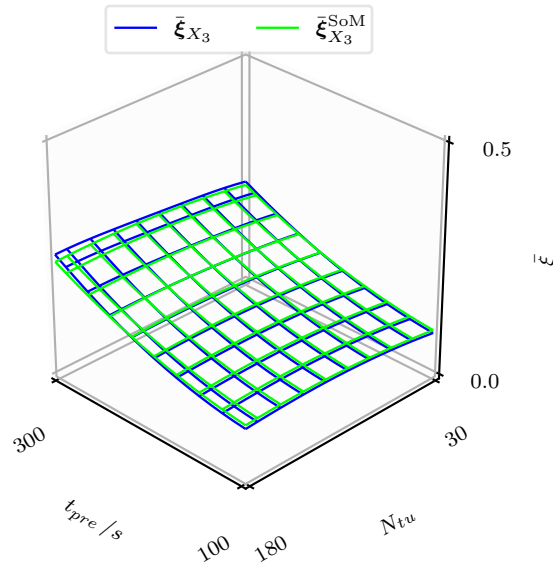

(d) results of the RSM on evacuation risk factors (FA)

Figure E.14: Correlations between risk factors and the results of the RSM $\bar{\boldsymbol{\xi}}_{X_3}$ in the region of sc(118 MW, 882 s, 194 s, 171, $fa = -$) in comparison to the RSM $\bar{\boldsymbol{\xi}}^{\mathrm{SoM}}_{X_3}$; Fig. E.14a uncovers the drawback of the prediction interval method: the prediction variance should be small in the region where the results of the data base and of the RSM are close to zero, i.e. $\bar{\boldsymbol{\xi}}^{c}_{X_3} \approx 0$ and $\bar{\boldsymbol{\xi}}_{X_3} \approx 0$ according to Fig. E.13a; the scales differ between the figures.

specified individually for each risk factor in the PAD. This adaption could further increase the efficiency of the metamodel.

The jam of tunnel users at emergency exits and the tunnel alarm are discrete events in the system model which raises the question on their effects on the shape of the RSM. First, the shape of the RSM $\bar{\boldsymbol{\xi}}_{X_3}$ reveals no hints on jams because of the rather small number of tunnel users in the evacuation area. But with regard to the tunnel alarm, an effect is recognisable. The tunnel alarm depends on HRR_{max} and t_{max}, accordingly the effect appears on the fire risk factors. Juxtaposing Fig. E.13a and Fig. E.13b, the second derivative of the response surface along the diagonal between the outer vertices ($\mathrm{HRR}_{max} = 25\,\mathrm{MW}, t_{max} = 600\,\mathrm{s}$) and ($\mathrm{HRR}_{max} = 200\,\mathrm{MW}, t_{max} = 1200\,\mathrm{s}$) seems to be higher for scenarios with TA than for scenarios with FA. This interpretation bases on the larger plain response surface for TA in comparison to the steady increase right from the axes at $t_{max} = 1200\,\mathrm{s}$ and $\mathrm{HRR}_{max} = 25\,\mathrm{MW}$. In more detail, the event of tunnel alarm alerts multiple TUs at the same time narrowing the period when the TUs reach the emergency exit. As a consequence, the tunnel alarm causes a steep increase of the FF, i.e. if the alarm was not early enough. Of course, the individual pre-evacuation times as well as the individual positions of TUs blur this increase leading to a differentiable response surface. In case of FA, the individual alarm of TUs depends on the smoke spread and the positions of the TUs. This interaction widens the period for arriving at the emergency exit and additionally blurs the increase of the FF.

Finally, Fig. E.13a highlights two characteristics concerning the global objective of MLS. First, the MLS model $\bar{\boldsymbol{\xi}}_{X_3}$ is able to adapt to data points as can be also seen in Fig. E.9 on p. 64. And, MLS reproduces the large horizontal response surface, i.e. $\bar{\boldsymbol{\xi}}^{c} \approx 0$ for small HRR_{max} and high t_{max}, together with an adjacent high gradient in the response surface. Thus, these two observations support the conclusion that MLS adequately reproduces complex response surfaces on the entire domain.

E.2.5 Response surface methods

The study in Section E.2.4 proved that MLS is suitable for risk analysis which directs at complex response surfaces with the global objective. Since other response surface methods, namely FoM, SoM, LIn and LIl are also used in risk analysis as outlined in Section D.1.2, this study extends Section E.2.4 accordingly. For this, the focus lies on first, the bias and variance error of the RSMs of the different response surface methods, second, their shapes and third, their effects on results of risk analysis. The RSMs are denoted with $\bar{\boldsymbol{\xi}}^{\mathrm{MLS}}$, $\bar{\boldsymbol{\xi}}^{\mathrm{FoM}}$, $\bar{\boldsymbol{\xi}}^{\mathrm{SoM}}$, $\bar{\boldsymbol{\xi}}^{\mathrm{LIn}}$, $\bar{\boldsymbol{\xi}}^{\mathrm{LIl}}$. It has to be kept in mind, that the RSMs of FoM and SoM are equal for the data bases $\bar{\boldsymbol{\xi}}^{c}_{X_0}$ and $\bar{\boldsymbol{\xi}}^{c}_{X_1}$ as outlined in Subs. 'FoM and SoM models in the metamodel' (p. 45) with $\bar{\boldsymbol{\xi}}^{\mathrm{FoM}} \equiv \bar{\boldsymbol{\xi}}^{\mathrm{SoM}}$. Furthermore, Subs. 'Metamodel uncertainty for LIn and LIl models' (p. 46) of Section D.2 states that the variance estimators of LIn and LIl are identical for the data base $\bar{\boldsymbol{\xi}}^{c}_{X_0}$, written $\sigma^2_{-i}\left(\bar{\boldsymbol{\xi}}^{\mathrm{LIl}}_{X_0}\right) \equiv \sigma^2_{-i}\left(\bar{\boldsymbol{\xi}}^{\mathrm{LIn}}_{X_0}\right)$. At last, the study aims at the final validation of MLS models, esp. the default RSM.

Bias error and variance error of the RSM

Response surface methods naturally affect the bias and variance error of their RSMs. Consequently, model adequacy checking in this dissertation comprises the evaluation of the bias and variance error in comparison to other response surface methods. Section D.1.1 describes the background for model adequacy checking. Accordingly, the generalisation error provides information on bias error and variance error and can be represented by the variance estimator σ^2_{-i}. Additionally, the variance error expresses qualitatively the sensitivity of the RSM to variations in the ED. Hence, the euclidean relative difference at the evaluation points of two

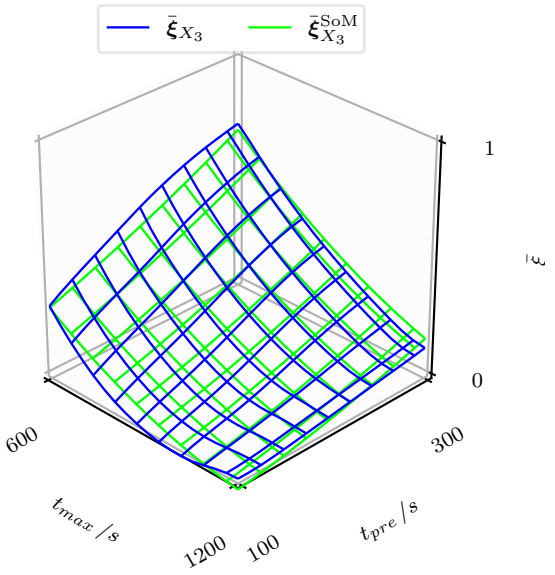

(a) results of the RSM (TA)

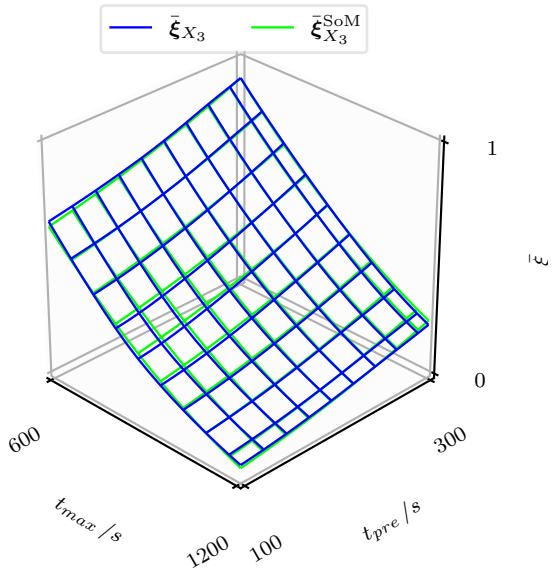

(b) results of the RSM (FA)

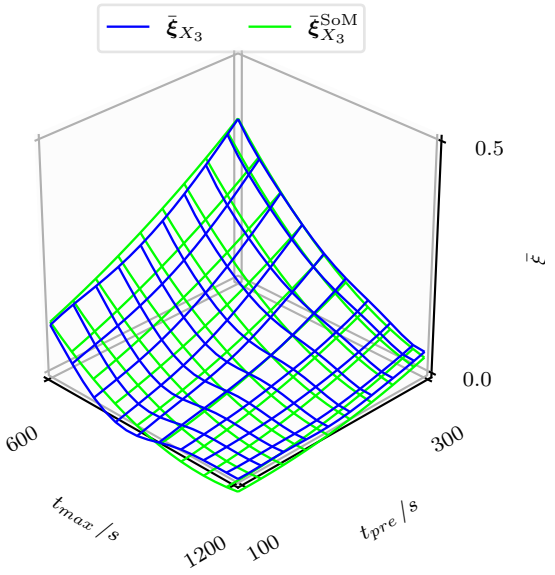

(c) results of the RSM (TA)

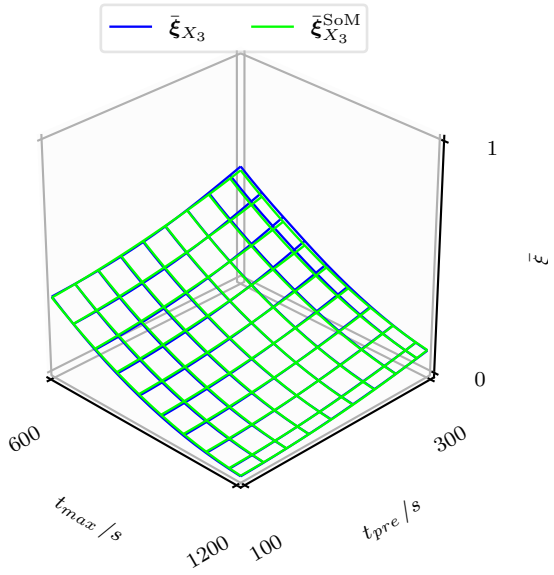

(d) results of the RSM (FA)

Figure E.15: Correlation between t_{max} as well as t_{pre} and their effect on the results of the RSM based on the data base $\bar{\boldsymbol{\xi}}^{c}_{X_3}$ in sc(190 MW, − s, − s, 171, $fa = -$) (above) and sc(118 MW, − s, − s, 171, $fa = -$) (below); the scales differ between the figures.

Table E.7: Variance estimator σ^2_{-i} for RSM of different response surface methods subjected to the data bases of all refinement steps (TA: above, FA: below).

data base	$\sigma^2_{-i}\left(\bar{\boldsymbol{\xi}}^{\mathrm{MLS}}\right)$	$\sigma^2_{-i}\left(\bar{\boldsymbol{\xi}}^{\mathrm{FoM}}\right)$	$\sigma^2_{-i}\left(\bar{\boldsymbol{\xi}}^{\mathrm{SoM}}\right)$	$\sigma^2_{-i}\left(\bar{\boldsymbol{\xi}}^{\mathrm{LIn}}\right)$	$\sigma^2_{-i}\left(\bar{\boldsymbol{\xi}}^{\mathrm{LIl}}\right)$
$\bar{\boldsymbol{\xi}}^c_{X_{0,0}}$	0.14	0.24	–	0.29	–
$\bar{\boldsymbol{\xi}}^c_{X_{1,0}}$	0.05	0.14	–	0.06	0.06
$\bar{\boldsymbol{\xi}}^c_{X_{2,0}}$	0.03	0.12	0.05	0.05	0.04
$\bar{\boldsymbol{\xi}}^c_{X_{3,0}}$	0.03	0.11	0.05	0.05	0.04
$\bar{\boldsymbol{\xi}}^c_{X_{0,1}}$	0.13	0.29	–	0.37	–
$\bar{\boldsymbol{\xi}}^c_{X_{1,1}}$	0.05	0.16	–	0.04	0.04
$\bar{\boldsymbol{\xi}}^c_{X_{2,1}}$	0.03	0.13	0.03	0.05	0.04
$\bar{\boldsymbol{\xi}}^c_{X_{3,1}}$	0.03	0.13	0.04	0.05	0.04

RSMs based on two equivalent data bases allows a qualitative comparison of the variance error. The equivalent data bases are $\bar{\boldsymbol{\xi}}^c_{X_1}$ and $\bar{\boldsymbol{\xi}}^c_{X_{1a}}$ as well as $\bar{\boldsymbol{\xi}}^c_{X_2}$ and $\bar{\boldsymbol{\xi}}^c_{X_b}$.

Tab. E.7 provides an overview on the variance estimators of the different RSMs. In particular, FoM led to an increased variance estimator. In detail, the variance estimator of the RSMs of $\bar{\boldsymbol{\xi}}^{\mathrm{FoM}}$ are higher than the RSMs of SoM because of the smaller polynomial degree in FoM. Comparing LIn and LIl, LIl considers more data points, i.e. neighbours to an arbitrary point, than LIn which concentrates on the closest neighbour. As a consequence, the variance estimators of the RSMs $\bar{\boldsymbol{\xi}}^{\mathrm{LIl}}_{X_2}$ and $\bar{\boldsymbol{\xi}}^{\mathrm{LIl}}_{X_3}$ were slightly lower than for the RSMs $\bar{\boldsymbol{\xi}}^{\mathrm{LIn}}_{X_2}$ and $\bar{\boldsymbol{\xi}}^{\mathrm{LIn}}_{X_3}$. MLS caused the lowest variance estimator with an exception for $\bar{\boldsymbol{\xi}}^c_{X_{1,1}}$ due to the quadratic polynomial and the local weighting of all data points. Furthermore, MLS could still reduce the generalisation error by using the variance estimator as measure in the calibration algorithm instead of the prediction variance $\boldsymbol{s}^2_{q90}$.

The sensitivity of the RSMs to variations in their EDs is shown by the euclidean relative difference erd in Tab. E.8. The results depend on the spatial sensitivity of the RSMs. Accordingly, LIn led to the highest variations which is emphasised with Fig. E.16a and Fig. E.16b. These variations cause high uncertainties in the results of the RSM esp. for small numbers of data points. LIl and MLS are roughly comparable in their spatial sensitivity, also depicted in Fig. E.16c and Fig. E.16d. And finally, FoM and SoM models are subjected to the smallest spatial sensitivities. Thus, the global least squares regression methods cause the lowest variance error.

Summing up, MLS focuses on the global objective and is for this reason more spatially sensitive than global least squares regression methods. As a result, MLS models, using the calibration algorithm, cause an increased variance error but are able to reduce the bias error. Therefore, among FoM, SoM, LIn and LIl, MLS achieves the highest accuracy of RSMs with respect to the generalisation error.

Shape of the RSM

Beside from the bias and variance error, the validation of the MLS model comprises the evaluation of the MLS model with respect to the shape of the response surface. The response surface is, according to Subs. 'Complex model within the system model' (p. 22) continuous, differentiable and rather complex in its shape. But the RSMs of the response surface methods are attributed to different spatial sensitivities as sketched in Section D.1.2, and are for this reason differently suitable for the response surface. Thus, the shapes of the RSMs are qualitatively juxtaposed in Fig. E.17 and compared quantitatively with the euclidean relative

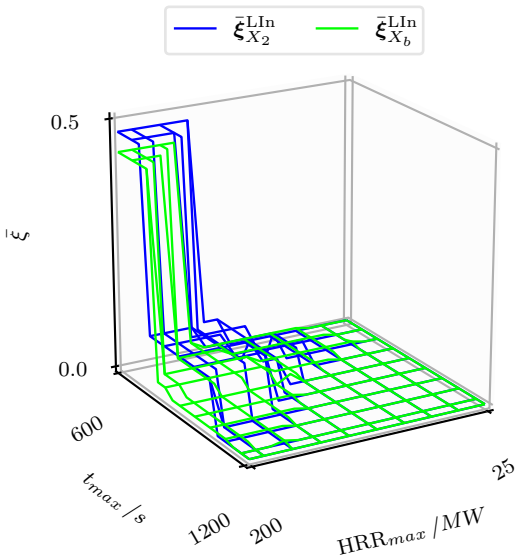

(a) results of the RSM $\bar{\boldsymbol{\xi}}^{\mathrm{LIn}}$

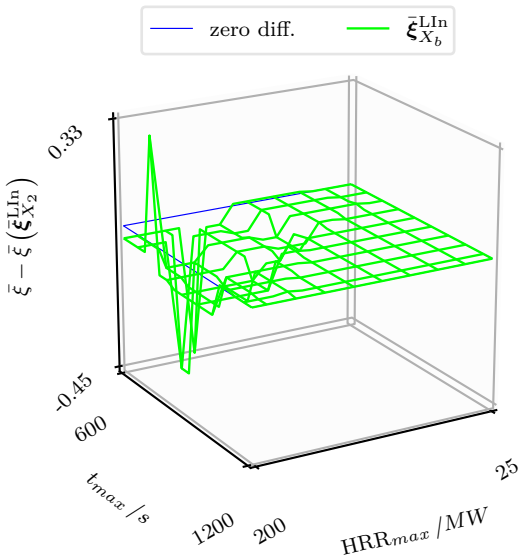

(b) difference to $\bar{\boldsymbol{\xi}}^{\mathrm{LIn}}_{X_2}$

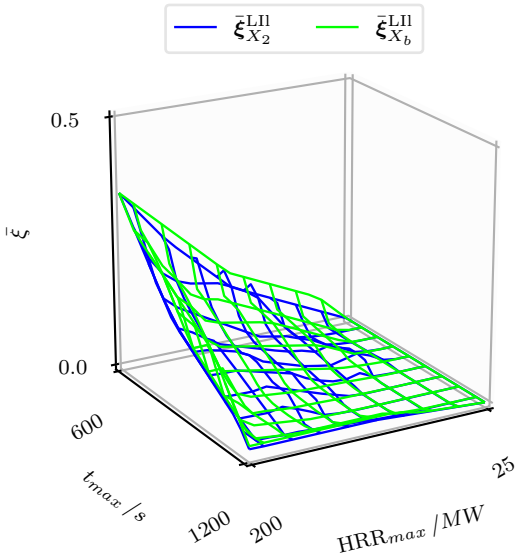

(c) results of the RSM $\bar{\boldsymbol{\xi}}^{\mathrm{LIl}}$

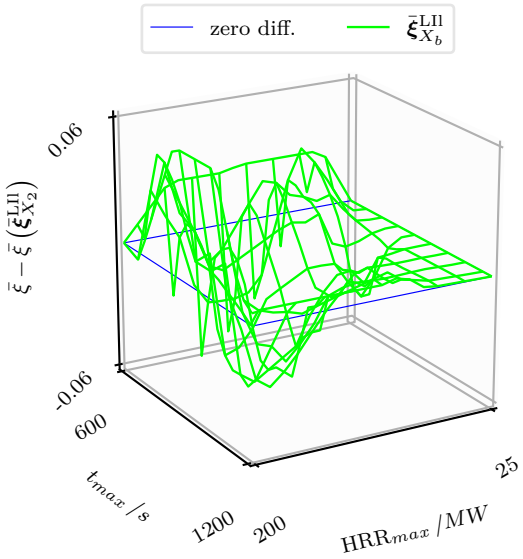

(d) difference to $\bar{\boldsymbol{\xi}}^{\mathrm{LIl}}_{X_2}$

Figure E.16: Sensitivity of RSMs of LIn (above) and LIl (below) to variations in the ED: comparison of results of the RSM subjected to the EDs X_2 and X_b in the region of sc($-$ MW, $-$ s, 147 s, 39, $fa = 0$); the scales differ between the figures.

Table E.8: Sensitivity of RSMs subjected to different response surface methods to variations in the ED: quantified with the euclidean relative difference erd between X_1 and X_{1a} (above) and between X_2 and X_b (below).

	TA	FA
$\text{erd}\left(\bar{\boldsymbol{\xi}}^{\text{MLS}}_{X_1}, \bar{\boldsymbol{\xi}}^{\text{MLS}}_{X_{1a}}\right)$	0.14	0.10
$\text{erd}\left(\bar{\boldsymbol{\xi}}^{\text{FoM}}_{X_1}, \bar{\boldsymbol{\xi}}^{\text{FoM}}_{X_{1a}}\right)$	0.08	0.08
$\text{erd}\left(\bar{\boldsymbol{\xi}}^{\text{SoM}}_{X_1}, \bar{\boldsymbol{\xi}}^{\text{SoM}}_{X_{1a}}\right)$	–	–
$\text{erd}\left(\bar{\boldsymbol{\xi}}^{\text{LIn}}_{X_1}, \bar{\boldsymbol{\xi}}^{\text{LIn}}_{X_{1a}}\right)$	0.72	0.61
$\text{erd}\left(\bar{\boldsymbol{\xi}}^{\text{LIl}}_{X_1}, \bar{\boldsymbol{\xi}}^{\text{LIl}}_{X_{1a}}\right)$	0.14	0.07
$\text{erd}\left(\bar{\boldsymbol{\xi}}^{\text{MLS}}_{X_2}, \bar{\boldsymbol{\xi}}^{\text{MLS}}_{X_b}\right)$	0.15	0.06
$\text{erd}\left(\bar{\boldsymbol{\xi}}^{\text{FoM}}_{X_2}, \bar{\boldsymbol{\xi}}^{\text{FoM}}_{X_b}\right)$	0.04	0.04
$\text{erd}\left(\bar{\boldsymbol{\xi}}^{\text{SoM}}_{X_2}, \bar{\boldsymbol{\xi}}^{\text{SoM}}_{X_b}\right)$	0.10	0.04
$\text{erd}\left(\bar{\boldsymbol{\xi}}^{\text{LIn}}_{X_2}, \bar{\boldsymbol{\xi}}^{\text{LIn}}_{X_b}\right)$	0.48	0.39
$\text{erd}\left(\bar{\boldsymbol{\xi}}^{\text{LIl}}_{X_2}, \bar{\boldsymbol{\xi}}^{\text{LIl}}_{X_b}\right)$	0.11	0.07

difference erd at the evaluation points relative to the RSM $\bar{\boldsymbol{\xi}}^{\text{MLS}}$. First, the RSMs of MLS and LIl were able to reproduce large horizontal response surfaces adjacent to high gradients exemplified in Fig. E.17a. This ability is additionally emphasised for MLS in Fig. E.13a on p. 71. Next, Fig. E.17c demonstrates that LIn was also reproduces the large horizontal shape but it causes discontinuities which lack of real analogies in the response surface. In contrast, the RSM of FoM could not replicate the horizontal shape but led to FF below zero. The same yields for SoM but in a less distinct way as shown in Fig. E.17d. Concluding, these results indicate sufficient spatial sensitivity of the RSMs of MLS and LIl whereas the other response surface methods fail to meet real analogies in the response surface.

Tab. E.9 reveals in combination with Fig. E.13c and Fig. E.13d on p. 71 that SoM was subjected to the smallest euclidean relative difference to MLS. This similarity was in particular pronounced for scenarios with FA because of the less complex response surface. But MLS still causes a smaller variance error shown in Tab. E.7. Accordingly, the increased spatial sensitivity of MLS models show advantages with regard to the global objective. More clearly, Fig. E.17d expresses this advantage in the sc(25 MW, 1200 s, − s, −, $fa = 0$) with a FF close to zero: MLS approximated the FF to zero at this scenario whereas SoM led to increased results with $\bar{\boldsymbol{\xi}}^{c}_{X_2} \approx 0$; $\bar{\boldsymbol{\xi}}^{\text{MLS}}_{X_2} \approx \bar{\boldsymbol{\xi}}^{c}_{X_2}$; $\bar{\boldsymbol{\xi}}^{\text{SoM}}_{X_2} > \bar{\boldsymbol{\xi}}^{c}_{X_2}$.

Also, the RSMs of LIl and MLS resulted in a small euclidean relative difference which corresponds to the qualitative evaluation. In more detail, the RSM $\bar{\boldsymbol{\xi}}^{\text{MLS}}_{X_1}$ is subjected to a linear polynomial similar to LIl, whereas the RSM $\bar{\boldsymbol{\xi}}^{\text{MLS}}_{X_2}$ bases on a quadratic polynomial. Therefore, the RSM $\bar{\boldsymbol{\xi}}^{\text{LIl}}_{X_1}$ is closer to $\bar{\boldsymbol{\xi}}^{\text{MLS}}_{X_1}$ than $\bar{\boldsymbol{\xi}}^{\text{LIl}}_{X_2}$ to $\bar{\boldsymbol{\xi}}^{\text{MLS}}_{X_2}$ because of the same polynomial degree with $\text{erd}\left(\bar{\boldsymbol{\xi}}^{\text{MLS}}_{X_1}, \bar{\boldsymbol{\xi}}^{\text{LIl}}_{X_1}\right) < \text{erd}\left(\bar{\boldsymbol{\xi}}^{\text{MLS}}_{X_2}, \bar{\boldsymbol{\xi}}^{\text{LIl}}_{X_2}\right)$. But as downside of LIl, its RSMs are not differentiable at data points, e.g. shown in Fig. E.17b, which might cause discrepancies to very complex response surfaces. Fig. E.17b displays another discrepancy of the RSM of LIl, namely the particular shape of an elevated FF at the outer vertices of the domain. The particular shape originates in the method using unstructured data points and contributes to the higher euclidean relative difference between LIl and MLS in comparison to SoM and MLS.

Finally, the RSMs of LIn, FoM and SoM miss real analogies to the response surface e.g. with respect to discontinuous, global linear or quadratic shapes. Quantitatively, MLS, SoM and LIl lead to similar results of their RSMs. But the medium spatial sensitivity of MLS

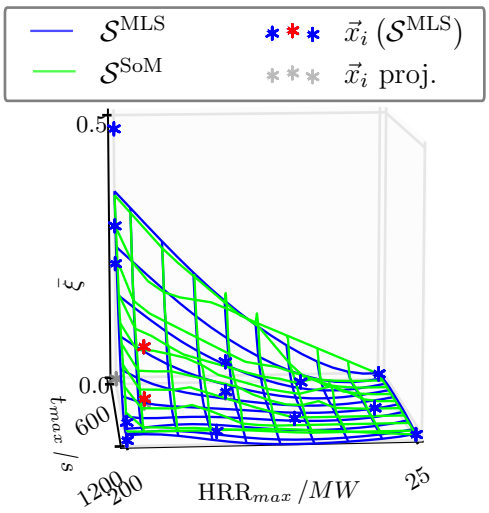

(a) results for MLS and LIl on fire risk factors

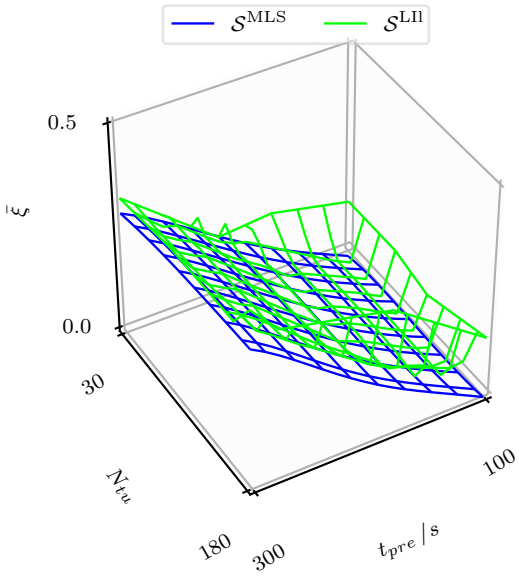

(b) results for MLS and LIl on evacuation risk factors

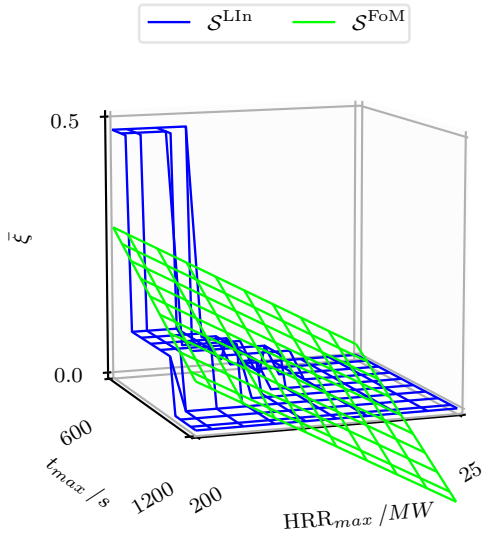

(c) results for LIn and FoM on fire risk factors

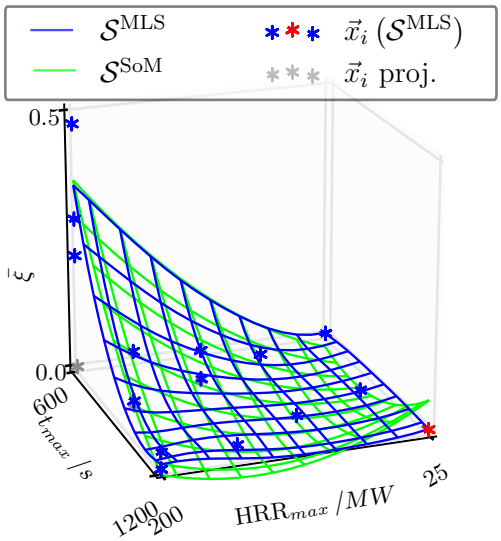

(d) results for MLS and SoM on fire risk factors

Figure E.17: Shapes of the RSMs in the region of sc(179 MW, 882 s, 147 s, 39, $fa = 0$) for different response surface methods and the data base X_2; Fig. E.17a indicates that the RSM of LIl is not differentiable at data points (highlighted red); Fig. E.17d illustrates that MLS is able to approximate to sc(25 MW, 1200 s, − s, −, $fa = 0$) whereas SoM is not (highlighted red).

Table E.9: Euclidean relative difference erd between RSMs of different response surface methods and the MLS model for all refinement steps (TA: above, FA: below); brief notation for erd $\left(\bar{\boldsymbol{\xi}}^{\mathrm{SoM}}\right) = \mathrm{erd}\left(\bar{\boldsymbol{\xi}}^{\mathrm{MLS}}, \bar{\boldsymbol{\xi}}^{\mathrm{SoM}}\right)$.

data base	erd $\left(\bar{\boldsymbol{\xi}}^{\mathrm{FoM}}\right)$	erd $\left(\bar{\boldsymbol{\xi}}^{\mathrm{SoM}}\right)$	erd $\left(\bar{\boldsymbol{\xi}}^{\mathrm{LIn}}\right)$	erd $\left(\bar{\boldsymbol{\xi}}^{\mathrm{LIl}}\right)$
$\bar{\boldsymbol{\xi}}^{c}_{X_{0,0}}$	0.25	–	0.82	0.32
$\bar{\boldsymbol{\xi}}^{c}_{X_{1,0}}$	0.38	–	0.49	0.15
$\bar{\boldsymbol{\xi}}^{c}_{X_{2,0}}$	0.53	0.20	0.49	0.34
$\bar{\boldsymbol{\xi}}^{c}_{X_{3,0}}$	0.54	0.21	0.44	0.31
$\bar{\boldsymbol{\xi}}^{c}_{X_{0,1}}$	0.20	–	0.69	0.21
$\bar{\boldsymbol{\xi}}^{c}_{X_{1,1}}$	0.26	–	0.38	0.10
$\bar{\boldsymbol{\xi}}^{c}_{X_{2,1}}$	0.29	0.05	0.35	0.16
$\bar{\boldsymbol{\xi}}^{c}_{X_{3,1}}$	0.29	0.03	0.33	0.15

achieves the smallest generalisation error discussed in Subs. 'Bias error and variance error of the RSM' (p. 73). Consequently, models of MLS and LIl most reasonably represent the response surface and thus show advantages for the global objective.

Results of risk analysis

The methodology for risk analysis applies the system model as well as the metamodel in the consequence model both described in Section B.3 and Section B.4. Hence, the differences in the shapes of the RSMs caused by the response surface methods suggest effects on the results of risk analysis. To examine these effects, system model simulations produce results for $N_{\mathrm{mcs}} = 10^6$ random scenarios. Each system model simulation uses one of the response surface methods as well as the data base $\bar{\boldsymbol{\xi}}^{c}_{X_2}$. Tab. E.10 introduces the notation of the system model simulations $\mathcal{S}$ and the FF in the system model $\bar{\Xi}$. The following comparison uses the system model simulation $\mathcal{S}^{\mathrm{MLS}}$ as reference.

Table E.10: Effects of different response surface methods on the individual risk of system model simulations with the data base $\bar{\boldsymbol{\xi}}^{c}_{X_2}$.

response surface method	MLS	FoM	SoM	LIn	LIl
$\mathcal{S}$	$\mathcal{S}^{\mathrm{MLS}}$	$\mathcal{S}^{\mathrm{FoM}}$	$\mathcal{S}^{\mathrm{SoM}}$	$\mathcal{S}^{\mathrm{LIn}}$	$\mathcal{S}^{\mathrm{LIl}}$
$\mathcal{R}^{ind} / \left(10^{-3} \frac{1}{year}\right)$	4.5	6.7	5.0	4.8	5.9

Tab. E.10, Fig. E.18a and Fig. E.18b provide the results of risk analysis, namely the individual risk $\mathcal{R}^{ind}$, the FF in the system model $\bar{\Xi}$, and the societal risk curve. The FF $\bar{\Xi}$ disregard the metamodel uncertainty and the evacuation uncertainty to clearly evaluate the effect of the shapes of the RSMs. Opposite to Subs. 'Shape of the RSM' (p. 75), the results reveal no effects of local differences in the RSMs but global effects on the entire domain for random scenarios with TA and FA at the same time. Nonetheless, some global effects can be reasoned with local differences.

The RSM $\bar{\boldsymbol{\xi}}^{\mathrm{LIn}}$ resulted in elevated FF e.g. in the region of the sc(200 MW, 600 s, − s, −, $fa = 0$) in Fig. E.17c. With respect to the results of the system model simulation $\mathcal{S}^{\mathrm{LIn}}$, this result is apparent in the upper quantiles of $\bar{\Xi}^{\mathrm{LIn}}$ in Fig. E.18a. More precisely, more random scenarios lead to high FF compared to $\bar{\Xi}^{\mathrm{MLS}}$ which again contribute to an increased upper part of the societal risk curve in Fig. E.18b.

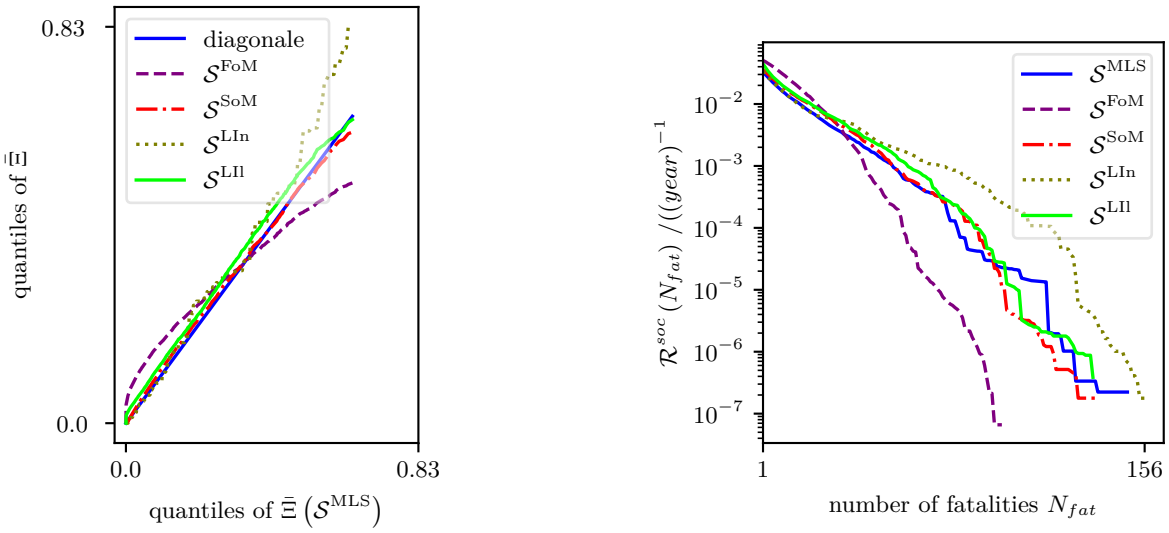

(a) quantile plot of $\bar{\Xi}$ relative to $\bar{\Xi}^{\mathrm{MLS}}$

(b) societal risk curves

Figure E.18: Effect of different response surface methods on results of system model simulations with the data base $\bar{\boldsymbol{\xi}}^{c}_{X_2}$.

Examining Fig. E.18a, fewer random scenarios with FF close to zero $\bar{\Xi}^{\mathrm{FoM}}$ happened in the system model simulation $\mathcal{S}^{\mathrm{FoM}}$ relative to $\mathcal{S}^{\mathrm{MLS}}$. This characteristic contributes to an increased individual risk since random scenarios with a high frequency f_{sc} have elevated FF. Also, there are less scenarios with high FF which reduces the upper part in the societal risk curve.

Most random scenarios in the system model simulation $\mathcal{S}^{\mathrm{LIl}}$ had a slightly increased FF $\bar{\Xi}^{\mathrm{LIl}}$ in comparison to the results of $\bar{\Xi}^{\mathrm{MLS}}$ with reference to Fig. E.18a. The particular shape at the outer vertices of the RSM $\bar{\boldsymbol{\xi}}^{\mathrm{LIl}}$ might be a factor to this outcome. Consequently, fewer random scenarios with a FF close to zero occur which results in an increased individual risk and a small increase in the societal risk curve.

The system model simulations $\mathcal{S}^{\mathrm{SoM}}$ and $\mathcal{S}^{\mathrm{MLS}}$ came to a similar frequency distribution in the FF of random scenarios $\bar{\Xi}$. Accordingly, their individual risks and societal risk curves deviated only slightly. This similarity stems from the quantitative similar shapes of the RSMs discussed in Subs. 'Shape of the RSM' (p. 75). But Subs. 'Shape of the RSM' (p. 75) also emphasised some advantages of MLS with regard to the global objective and some fails of SoM in local real analogies to the response surface.

As expected, these results prove that the choice of the response surface method affects the results of risk analysis. Another implication is, that the mere evaluation of the global results of risk analysis might not be enough to get adequate results for local random scenarios. For this, it might be beneficial to investigate the shape of the RSM in detail.

Summary and conclusion

The response surface methods represent differently the complex response surface on the entire domain. First, the shapes of the RSMs of FoM and SoM have little real analogies and FoM reveals the highest generalisation error. Accordingly, the global least squares regression methods are less suitable for the global objective together with complex response surfaces. Second, LIn produces RSMs with discontinuous shapes which miss real analogies and clearly affect the results of risk analysis. Also, the high variance error of LIn models leads to

increased uncertainties in the RSMs, in particular in case of data bases with a small number of scenarios. This might be true for methodologies for risk analysis of road tunnels which are based on few discrete scenarios, i.e. LIn, as outlined in Section A.1. At last, LIl models are comparable to MLS models with regard to the bias and variance error as well as the shape of the RSMs. Exceptions are the particular shapes at the outer vertices of the domain which lack for real analogies in the response surface and contribute to increased results of risk analysis. However, available methods for LIl allow a simple setup. Accordingly, it might be advisable to use LIl instead of LIn for risk analysis due to its higher accuracy and better real analogy to the response surface.

Summing up, MLS is favourable for risk analysis in comparison to other response surface methods. Some advantages are the small generalisation error as well as the representation of the complex response surface, esp. with regard to the continuous and differentiable shape. Together with following earlier results in: Subs. 'Convergence of the RSM and the prediction variance' (p. 60) in Section E.2.2 which proved the convergence of the results of the RSM; Section E.2.3 which demonstrated that the accuracy of the RSM corresponds to the prediction interval; and Section E.2.4 which illustrated the adequate reproduction of complex response surfaces on the entire domain; it is concluded that the results of the default RSM represent the deterministic results of the complex model and that MLS is able to direct at the global objective. Finally, these conclusions prove the successful validation of the default RSM. Thereby, MLS contributes to objective 1 (metamodel).

E.3 Evacuation uncertainty

The integral parts of the metamodel as well as the metamodel uncertainty were already examined in Section E.1 and Section E.2. But the complex model, providing results for the data base of the metamodel, comprises an evacuation model which causes the evacuation uncertainties. Therefore, the evacuation uncertainty comes at last in the assessment of the metamodel. First, the ORSs in the data base, i.e. the results of all replications of each scenario computed with the complex model, are evaluated in Section E.3.1. Then, the direct approach used to integrate the evacuation uncertainty at arbitrary points into the metamodel is scrutinised in Section E.3.2.

E.3.1 Observed random samples of the complex model

Looking at the ORSs, two questions arise. First, how many replications are required to reproduce the unknown probability distributions behind the ORSs, i.e. the evacuation uncertainty of the complex model? Second, does a particular distribution type, e.g. the normal distribution, fit to the ORSs? To answer both question, the evaluation considers the data bases of the three different foci $\widetilde{\xi}_i^c \in \left\{\widetilde{\boldsymbol{\xi}}_{X_3}^c, \widetilde{\boldsymbol{\xi}}_{X_{1a}}^c, \widetilde{\boldsymbol{\xi}}_{X_b}^c\right\}$ which comprise 512 data points in total. But for obvious reasons, all ORSs equal to zero, namely $\widetilde{\xi}_i^c = \vec{0}$, are excluded which leaves 316 data points.

Number of replications

Subs. 'Evaluation of ORSs' (p. 26) describes the approach used to determine the required number of replications in the ORSs. The approach bases on a quantitative and a qualitative comparison of an ORS with bootstrap samples. The quantitative comparison provides results of the largest absolute difference $\mathrm{D}\widetilde{\xi}_q^c$ according to Eq. B.6 on p. 27. For this, 10^4 bootstrap

samples were sufficient to get reproducible results. In case of the qualitative comparison, a figure juxtaposes the frequency distribution of a bootstrap sample and the ORS.

First, less than five, the exact number depends on the randomness in the bootstrap samples, of the 316 ORSs led to largest absolute differences with $\mathrm{D}\widetilde{\xi}_q^c > 0.03$. In particular, the lower and the upper quantiles were responsible for these results. The visual analysis, exemplified in Fig. E.19a and Fig. E.19b, revealed that their maximum values lied clearly apart to the central part of the frequency distribution. The bootstrap samples rarely reproduced the extrema but showed small differences in other quantiles. Second, around 20 ORSs resulted in largest absolute differences of $0.02 < \mathrm{D}\widetilde{\xi}_q^c < 0.03$. Again, mostly the lower and upper quantiles caused these values whereas the other quantiles differed only to small extent as depicted in Fig. E.19c and Fig. E.19d. Third, the other bootstrap samples had also essentially the same frequency distribution as their ORSs. As a result, the ORSs and the bootstrap samples were mostly similar in all data points.

In addition, the mean and variance of the ORSs converged with $N_{\mathrm{rep}} = 200$ replications. This conclusion derives from the approach published by Ronchi 2014 [43] which resembles the approach outlined in Section B.5, i.e. Eq. B.7 on p. 28. In consequence, mean and variance of the FF can be regarded as deterministic which corroborates the assumption in Subs. 'Complex model within the system model' (p. 22) in Section B.4.

In summary, the bootstrap samples could reproduce the ORSs in most data points. This result implies that 200 replications are sufficient to reproduce the unknown probability distributions for results of the complex model. Of course, for many data points, less replications could suffice. Therefore, an individual number of replications depending on the largest absolute difference could reduce the number of replications in many data points.

Distribution type

Often, a frequency distribution of a sample is assumed to be normally distributed. This assumption might be also one choice for the ORSs with regard to the application in the evacuation uncertainty. To question this assumption, the one-sample Kolmogorov-Smirnoff test, outlined in Subs. 'Evaluation of ORSs' (p. 26), was used with the null hypothesis stating that the ORSs are normally distributed. The test comprised all ORSs unequal to zero and used the confidence level $\alpha = 0.05$, the test statistic $d_{KS,crit} = 0.096$ and the sample size equal to the number of replications $N_{\mathrm{rep}} = 200$.

As a result, the null hypothesis had to be rejected for 149 of 316 data points. The ORSs in these data points had two main characteristics. First, the modal of the ORS was zero. Consequently, the normal distribution resulted in values below zero, e.g. for sc(79 MW, 671 s, 288 s, 34, $fa = 0$) in Fig. E.20a. Second, the ORS consisted only of a small number of discrete values as for sc(94 MW, 1031 s, 285 s, 80, $fa = 0$) in Fig. E.20d which contradicts the continuous normal distribution. But also ORSs of scenarios like sc(165 MW, 632 s, 106 s, 50, $fa = 1$) depicted in Fig. E.20e and Fig. E.20f were rejected although they had none of these characteristics. Additionally, the assumption of a Rayleigh distribution with the interval $[0; \infty]$ led to a similar number of rejections. And the beta distribution, because of the interval $[0; 1]$ often used for probabilities, brought less rejections but some data points with substantial differences between the ORS and the beta distribution.

These results indicate that, first, the variety of different frequency distributions of the ORSs are also subjected to different unknown probability distributions, and second, that the assumption of a normal distribution is not valid for many ORSs. Hence, they provide the basis for the direct approach to integrate the evacuation uncertainty into the metamodel.

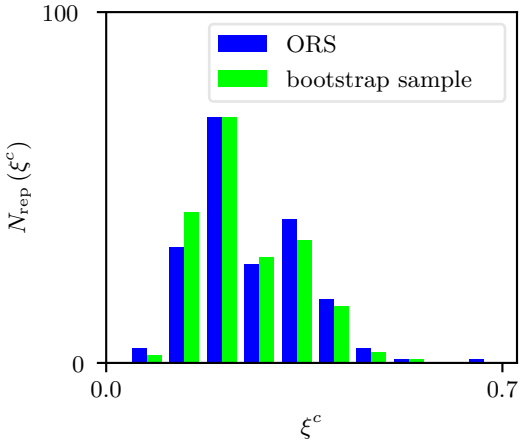

(a) $\mathrm{D}\widetilde{\xi}_q^c = 0.035$ for sc(200 MW, 600 s, 100 s, 30, $fa = 0$)

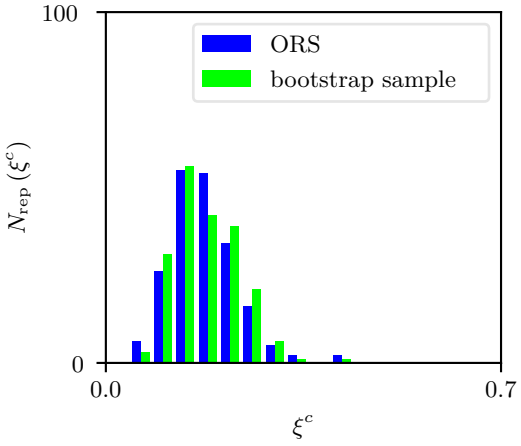

(b) $\mathrm{D}\widetilde{\xi}_q^c = 0.031$ for sc(91 MW, 676 s, 152 s, 56, $fa = 1$)

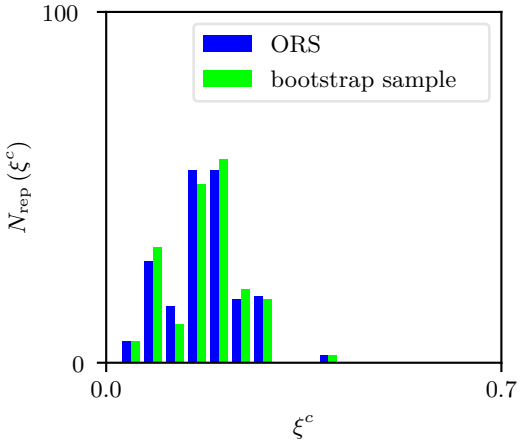

(c) $\mathrm{D}\widetilde{\xi}_q^c = 0.028$ for sc(145 MW, 1136 s, 292 s, 48, $fa = 1$)

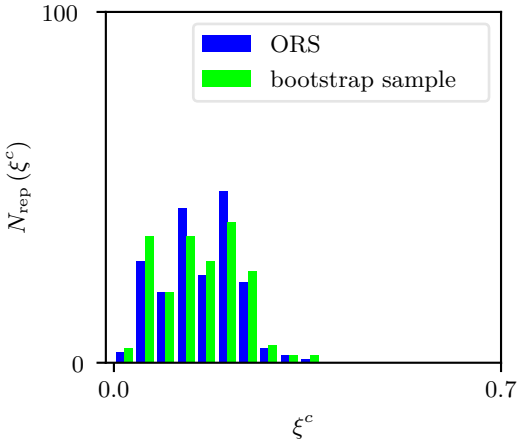

(d) $\mathrm{D}\widetilde{\xi}_q^c = 0.020$ for sc(165 MW, 632 s, 106 s, 50, $fa = 0$)

Figure E.19: Examples of a bootstrap sample in comparison to the ORS $\widetilde{\xi}_i^c$ for different data points with large absolute differences $\mathrm{D}\widetilde{\xi}_q^c$.

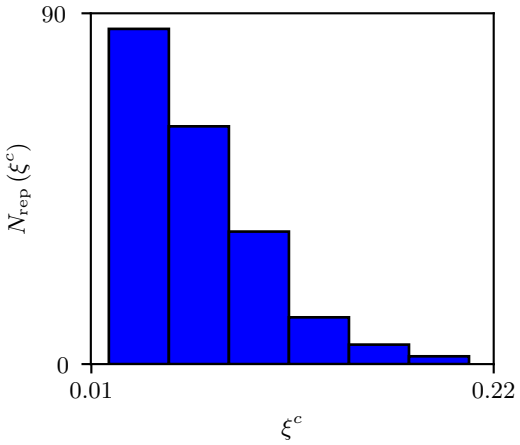

(a) sc(79 MW, 671 s, 288 s, 34, $fa = 0$)

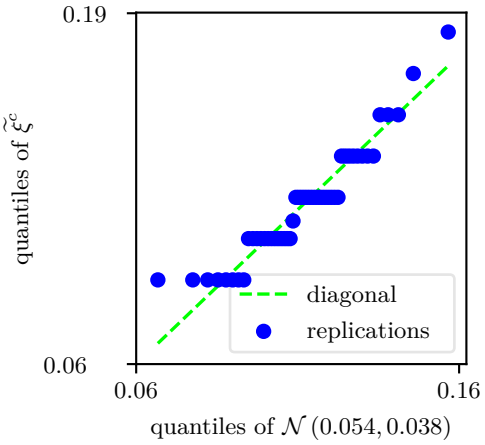

(b) sc(79 MW, 671 s, 288 s, 34, $fa = 0$)

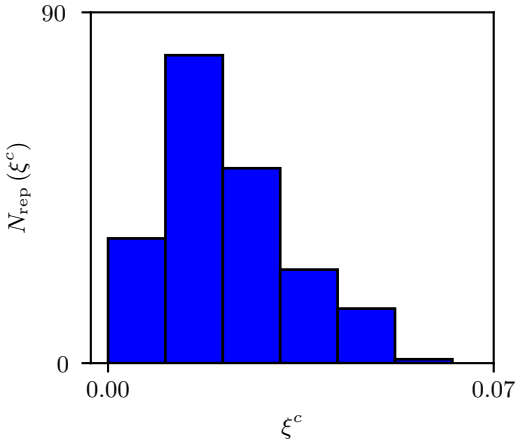

(c) sc(94 MW, 1031 s, 285 s, 80, $fa = 0$)

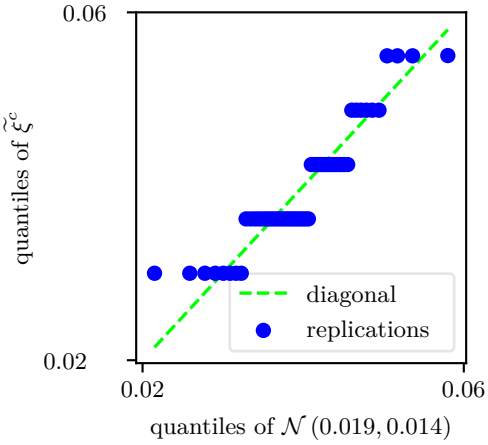

(d) sc(94 MW, 1031 s, 285 s, 80, $fa = 0$)

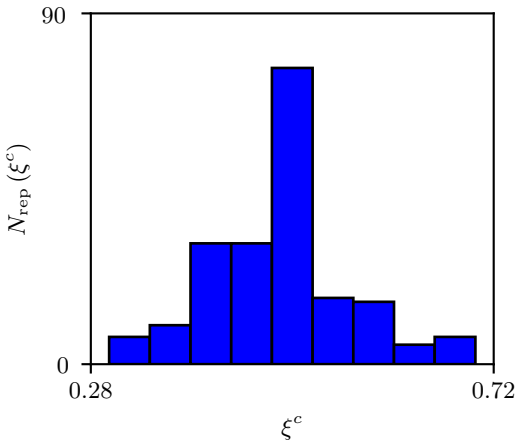

(e) sc(165 MW, 632 s, 106 s, 50, $fa = 1$)

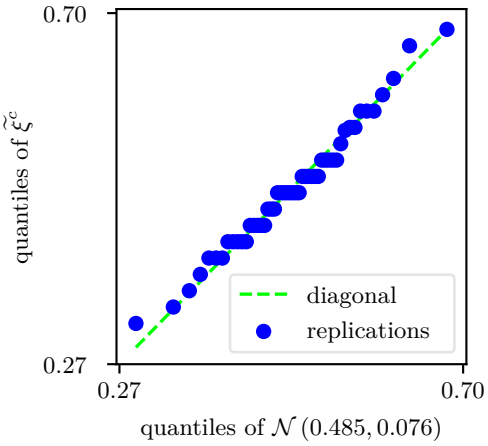

(f) sc(165 MW, 632 s, 106 s, 50, $fa = 1$)

Figure E.20: Examples for ORSs of different data points: frequency distribution of the ORS (left) with the number of bins to get at least five replications in each bin; normal probability plot of the ORS to the normal distribution $\mathcal{N}(\mu, \sigma)$ (right); the scales differ between the figures.

E.3.2 Direct approach

Section D.1.5 provides the background for the evacuation uncertainty as well as the averaged variance and Section D.3 describes the direct approach which was developed during this dissertation to integrate the evacuation uncertainty into the metamodel. The verification went hand in hand with the implementation of the direct approach. The next steps in the development are the calibration and the validation. They both base on system model simulations with the data base $\widetilde{\boldsymbol{\xi}}^{c}_{X_2}$. With regard to the definition of 'validation' in Subs. 'Terms related to the evaluation of the accuracy of models' (p. G-2), the data base can be regarded as the 'real world' because its ORSs shall be represented. The system model simulations apply results of the metamodel $\widetilde{\boldsymbol{\xi}}^{\boldsymbol{\epsilon}}$ in $N_{\mathrm{mcs}} = 10^6$ random scenarios. For this, the metamodels disregard the metamodel uncertainty but for obvious reasons consider the evacuation uncertainty with the direct approach attributed to the default parameters: combination mode linear; $\bar{\xi}^{c}_{lim} = 10^{-4}$ for the limit for data points; $N_{\mathrm{nb}} = 5 \cdot N_{\mathrm{rf}} = 20$ as initial number of neighbours for the automatic reduction in the combination mode linear according to the averaged variance in Section D.1.5; and $N_{\mathrm{rep}} = 200$, i.e. all replications in the ORSs.

The following subsections describe the calibration, in other words the specification of the default parameters, and outline the validation. The validation demonstrates that the results of the direct approach require only little manipulations and correspond to real analogies, i.e. the different frequency distributions of the ORSs identified in Subs. 'Distribution type' (p. 82). For this, the subsections discuss the spatial sensitivity of the results, for instance the number of random scenarios with $\left\|\widetilde{\boldsymbol{\xi}}^{\boldsymbol{\epsilon}} > 1\right\|$, and evaluate the number of random scenarios with $\|\widetilde{\boldsymbol{\epsilon}} = 1\|$ which might originate from manipulations to limit outliers. At the end, the direct approach should achieve a sufficient spatial sensitivity as stated in Section D.1.5. And, it should represent the evacuation uncertainty of the complex model for random scenarios.

Reproducibility of results

Eq. D.20 on p. 47 emphasises that the relative evacuation uncertainty $\widetilde{\epsilon}$ of one scenario is subjected to aleatory uncertainties. Naturally, relative evacuation uncertainties $\widetilde{\boldsymbol{\epsilon}}$ of N_{mcs} random scenarios in a Monte-Carlo simulation are subjected to even more aleatory uncertainties resulting in an individual frequency distribution of $\widetilde{\boldsymbol{\epsilon}}$. Hence, six system model simulations $\mathcal{S}_0, \ldots, \mathcal{S}_5$ with identical parameters, models and modes, esp. in the direct approach serve to quantify the effects of the aleatory uncertainties on the frequency distribution. This assessment allows to judge the reproducibility e.g. of the frequency distribution of $\widetilde{\boldsymbol{\epsilon}}$ and of risk measures to be able to identify effects of other parameters or modes in the direct approach.

Fig. E.21a depicts the relative differences in the frequency distributions of $\widetilde{\boldsymbol{\epsilon}}$ for all system model simulations. As a result, the relative difference between quantiles of $\widetilde{\boldsymbol{\epsilon}}$ are mostly below 0.02 with exceptions at the lower and upper quantiles. With regard to the risk measures, the individual risk was essentially the same with $\mathcal{R}^{ind} = 1.5 \cdot 10^{-2} \frac{1}{year}$ and Fig. E.21b shows variations in the upper part of the societal risk curve.

These results suggest that relative differences between quantiles of $\widetilde{\boldsymbol{\epsilon}}$ of less than 0.02 as well as the variations in the societal risk curve are caused by aleatory uncertainties in the relative evacuation uncertainty itself or by random scenarios in Monte-Carlo simulations. Therefore, larger variations in the frequency distribution of $\widetilde{\boldsymbol{\epsilon}}$ or in risk measures are likely to stem from modes or parameters in the direct approach used in the system model simulations of the following subsections.

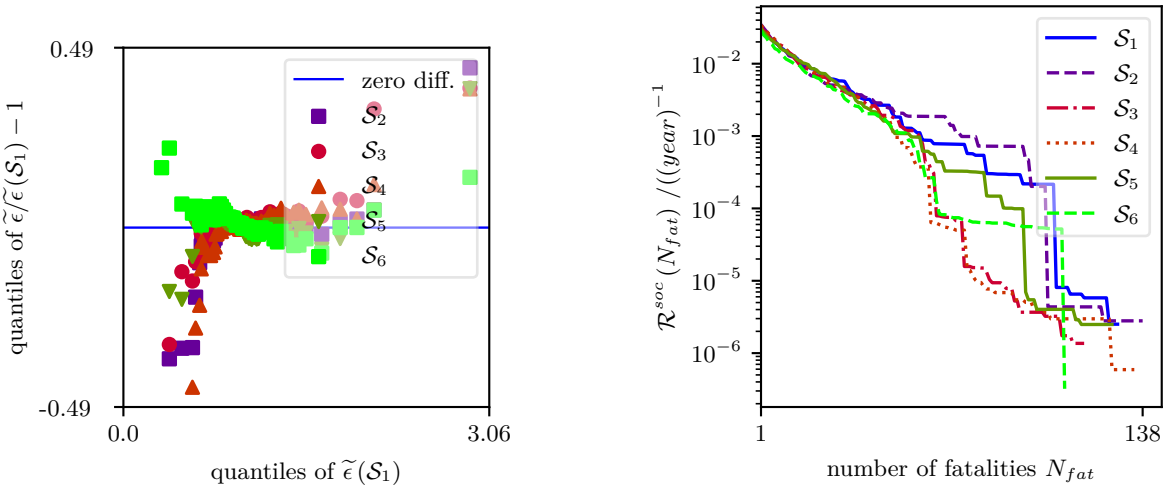

(a) relative quantile plot of $\widetilde{\boldsymbol{\epsilon}}$ relative to $\widetilde{\boldsymbol{\epsilon}}(\mathcal{S}_0)$

(b) societal risk curves

Figure E.21: Reproducibility of the relative evacuation uncertainty $\widetilde{\boldsymbol{\epsilon}}$ in six system model simulations with identical parameters.

Combination mode

The direct approach considers the combination modes uniform, closest and linear for the combination of neighbouring ORSs. Since the combination modes diverge in their spatial sensitivity and the spatial sensitivity is relevant to represent the ORSs, the combination mode is selected accordingly. The selection bases on three system model simulations with the combination modes uniform, closest and linear denoted with $\mathcal{S}_{uni}$, $\mathcal{S}_{clo}$, $\mathcal{S}_{lin}$. All system model simulations do not limit their data points with the parameter $\bar{\xi}^c_{lim} = 0$ to clearly show all effects on the relative evacuation uncertainty.

The system model simulations provide the results of the relative evacuation uncertainty $\widetilde{\boldsymbol{\epsilon}}$ and of the metamodel $\widetilde{\boldsymbol{\xi}}^{\boldsymbol{\epsilon}}$. First, the different combination modes had no clear effect on the number of random scenarios with $\|\widetilde{\boldsymbol{\epsilon}} = 1\|$, in other words, they account specific regions of the domain in the same way, for instance where the ORSs are equal to zero. But the system model simulations $\mathcal{S}_{clo}$ and $\mathcal{S}_{lin}$ led to higher dispersions in $\widetilde{\boldsymbol{\epsilon}}$ than $\mathcal{S}_{uni}$ as displayed in Fig. E.22. Additionally, the combination mode uniform had also an effect on $\left\|\widetilde{\boldsymbol{\xi}}^{\boldsymbol{\epsilon}} > 1\right\|$ which was ten times higher than for the combination modes closest and linear. These results of the metamodel require adaptions to meet the FF in the system model as outlined in Section B.3. But even for the combination mode uniform, $\left\|\widetilde{\boldsymbol{\xi}}^{\boldsymbol{\epsilon}} > 1\right\|$ is far lower than the number of random scenarios with results of the RSM below zero, namely $\left\|\bar{\boldsymbol{\xi}} < 0\right\|$, causing adaptions, too. So, the direct approach is responsible for only a small number of adaptions in the results of the metamodel.

The elevated value in $\left\|\widetilde{\boldsymbol{\xi}}^{\boldsymbol{\epsilon}} > 1\right\|$ clearly emphasises the lowest spatial sensitivity of the combination mode uniform which can be reasoned with the highest number of neighbours. On the contrary, the combination mode closest is most spatially sensitive but also spatially discontinuous. However spatial discontinuities in the evacuation uncertainty miss real analogies in the response surface. At last, the spatial sensitivity of the combination mode linear depends on the euclidean distance between a random scenario and its neighbours. On the one hand, if a random scenario is equal to a data point, i.e. $\widetilde{\epsilon}(\widetilde{x}) \equiv \widehat{\xi}^c(\vec{x}_i)$ if $\widetilde{x} = \vec{x}_i$, the relative evacuation uncertainty represents exactly the relative ORS because the number of neighbours shrinks

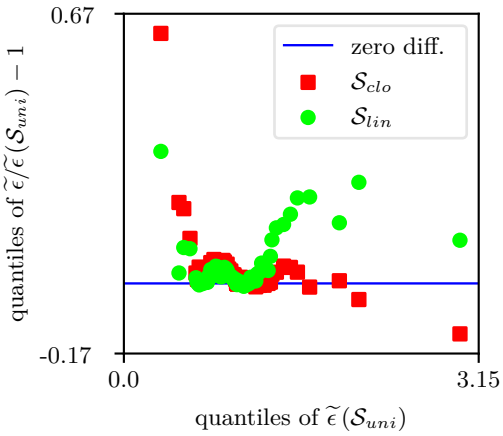

Figure E.22: Effects of the combination modes uniform, closest and linear ($\mathcal{S}_{uni}$,$\mathcal{S}_{clo}$, $\mathcal{S}_{lin}$ respectively) on $\widetilde{\boldsymbol{\epsilon}}$; relative quantile plot relative to $\mathcal{S}_{uni}$.

to $N_{\text{nb}} = 1$. This behaviour is prescribed by the equation used for the linear weighting of neighbours. On the other hand, if a random scenario has rather equal distances to its neighbours, the linear weighting takes more ORSs into account, i.e. up to the initial number of neighbours. Additionally, the combination modes linear and closest result in much the same frequency distribution of $\widetilde{\boldsymbol{\epsilon}}$ except for the lower quantiles as shown in Fig. E.22. This result proves the high spatial sensitivity of the combination mode linear.

Finally, the combination mode linear is highly spatially sensitive. As a consequence, the direct approach uses the combination mode linear as default weighting mode.

Outliers in the relative evacuation uncertainty

Outliers in the relative evacuation uncertainty have their origin in large values in combined relative samples, in more detail in ORS with very small mean FF, i.e. $\bar{\xi}^c \approx 0$. They can lead to results of the metamodel with $\widetilde{\xi}^{\epsilon} > 1$ which contradicts the real analogy in the response surface. To avoid such contradictions, the prevention of outliers bases on the limitation of data points with $\bar{\xi}^c < \bar{\xi}^c_{lim}$. The determination of the parameter $\bar{\xi}^c_{lim}$ comprises two steps. First, the evaluation of the mean FF in ORSs to narrow the range of $\bar{\xi}^c_{lim}$. This evaluation considers all ORSs of the three data bases $\widetilde{\xi}^c_i \in \left\{\widetilde{\boldsymbol{\xi}}^c_{X_3}, \widetilde{\boldsymbol{\xi}}^c_{X_{1a}}, \widetilde{\boldsymbol{\xi}}^c_{X_b}\right\}$. And second, the precise specification of $\bar{\xi}^c_{lim}$ with system model simulations. The system model simulations $\mathcal{S}_{1e-5}$, $\mathcal{S}_{1e-4}$, $\mathcal{S}_{5e-3}$, $\mathcal{S}_{1e-3}$ and $\mathcal{S}_{1e-2}$ are subjected to different parameters for $\bar{\xi}^c_{lim}$ as shown in Tab. E.11. Finally, the aim is to specify $\bar{\xi}^c_{lim}$ to reduce the number of outliers in the relative evacuation uncertainty without large effects on its frequency distribution.

First, Tab. E.11 shows the number of data points with $\bar{\xi}^c \leq \bar{\xi}^c_{lim}$ denoted with $\|X_{limited}\|$. As a result, one ORS had a mean FF of $0 < \bar{\xi}^c \leq 10^{-4}$ and six additional ORSs had $10^{-4} < \bar{\xi}^c \leq 10^{-3}$. Then, the number of data points $\|X_{limited}\|$ increased monotonically with $\bar{\xi}^c_{lim}$. Consequently, the parameter $\bar{\xi}^c_{lim}$ should be in the range of $10^{-5} < \bar{\xi}^c_{lim} < 10^{-3}$.

Second, according to Fig. E.23a and Tab. E.11, outliers in the relative evacuation uncertainty $\widetilde{\boldsymbol{\epsilon}}$ only occurred in the system model simulation $\mathcal{S}_{1e-5}$ and hence were linked to ORSs with $\bar{\xi}^c \leq 10^{-4}$. The outliers had values of $\widetilde{\epsilon} \approx 100$ and were sometimes in conjunction with random scenarios with $\bar{\xi} > 0.01$. These outliers lead to results of the metamodel with $\widetilde{\xi}^{\epsilon} > 1$

Table E.11: Effects of $\bar{\xi}^c_{lim}$ on: data points in data bases $\widetilde{\boldsymbol{\xi}}^c_{X_3}$, $\widetilde{\boldsymbol{\xi}}^c_{X_{1a}}$, $\widetilde{\boldsymbol{\xi}}^c_{X_b}$ (left part); results of system model simulations (right part).

$\bar{\xi}^c_{lim}$	$\|X_{limited}\|$	$\mathcal{S}$	$\|\text{outliers}\|$	$\left\|\widetilde{\boldsymbol{\xi}}^{\boldsymbol{\epsilon}} > 1\right\|$	$\|\widetilde{\boldsymbol{\epsilon}} = 1\|$
$\leq 10^{-5}$	196	$\mathcal{S}_{1e-5}$	≈ 100	≈ 140	≈ 295000
$\leq 10^{-4}$	197	$\mathcal{S}_{1e-4}$	0	≈ 100	≈ 305000
$\leq 10^{-3}$	203	$\mathcal{S}_{1e-3}$	0	≈ 60	≈ 311000
$\leq 5 \cdot 10^{-3}$	218	$\mathcal{S}_{5e-3}$	0	≈ 15	≈ 321000
$\leq 10^{-2}$	228	$\mathcal{S}_{1e-2}$	0	≈ 10	≈ 343000

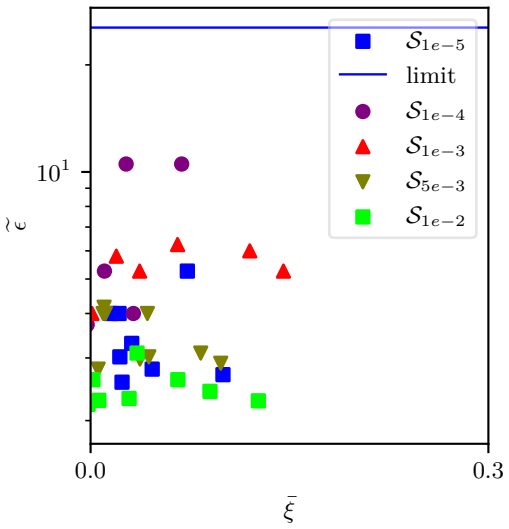

(a) outliers in $\widetilde{\boldsymbol{\epsilon}}$ for random scenarios with $\widetilde{\epsilon} > \widetilde{\epsilon}_{q99}$; the limits for outliers of all system model simulations are close to the limit of $\mathcal{S}_{1e-5}$;

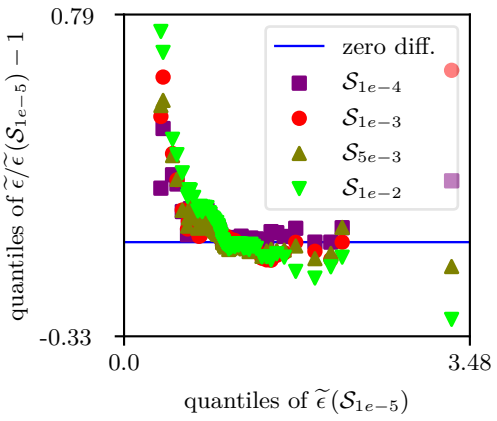

(b) relative quantile plot of $\widetilde{\boldsymbol{\epsilon}}$ relative to $\widetilde{\boldsymbol{\epsilon}}(\mathcal{S}_{1e-5})$

Figure E.23: Effects of $\bar{\xi}^c_{lim} \in \{10^{-5}, 10^{-4}, 5 \cdot 10^{-3}, 10^{-3}, 10^{-2}\}$ ($\mathcal{S}_{1e-5}$, $\mathcal{S}_{1e-4}$, $\mathcal{S}_{5e-3}$ and $\mathcal{S}_{1e-2}$ respectively) on $\widetilde{\boldsymbol{\epsilon}}$.

as a consequence from Eq. D.14 on p. 43. Regarding to the number of random scenarios with $\left\|\widetilde{\boldsymbol{\xi}}^{\boldsymbol{\epsilon}} > 1\right\|$, the parameter $\bar{\xi}^c_{lim}$ showed clear effects. This result confirms the purpose of the limitation of data points, namely to avoid large values in the relative ORS $\widehat{\xi}^c$ by setting $\widehat{\xi}^c = \vec{1}$ in case of $\bar{\xi}^c \leq \bar{\xi}^c_{lim}$. Therefore, the parameter $\bar{\xi}^c_{lim}$ substantially influences the number of random scenarios with $\|\widetilde{\boldsymbol{\epsilon}} = 1\|$ and at the same time the frequency distribution of $\widetilde{\boldsymbol{\epsilon}}$ as highlighted in Fig. E.23b. Hence, with the aim to avoid large effects on the frequency distribution of $\widetilde{\boldsymbol{\epsilon}}$, it is reasonable to set $\bar{\xi}^c_{lim}$ as small as possible.

Concluding, the default parameter for the limit for data points is $\bar{\xi}^c_{lim} = 10^{-4}$. This default parameter allows to remove outliers and at the same time to limit the manipulations in the frequency distribution of the relative evacuation uncertainty.

Number of neighbours

The number of neighbours N_{nb} is crucial for the spatial sensitivity of the direct approach as already seen in Subs. 'Combination mode' (p. 86). For this reason, this subsection deals with its reasoned specification. But the default combination mode linear automatically reduces the

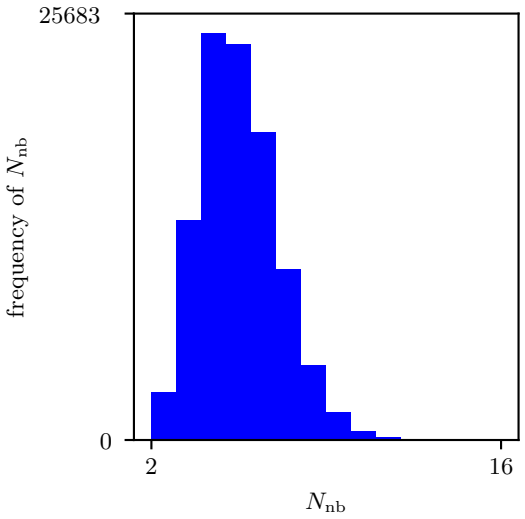

Figure E.24: Frequency distribution of the adapted number of neighbours $\boldsymbol{N}_{\mathrm{nb}}$ after the automatic reduction in the combination mode linear of $N_{\mathrm{mcs}} = 10^6$ random scenarios in $\mathcal{S}_{lin}$; the initial number of neighbours was $N_{\mathrm{nb}} = 96$.

number of neighbours as exemplified in Fig. E.24 for the system model simulation $\mathcal{S}_{lin}$. For this reason, the system model simulations $\mathcal{S}_5$, $\mathcal{S}_{10}$, $\mathcal{S}_{20}$, $\mathcal{S}_{48}$, $\mathcal{S}_{96}$ apply the combination mode uniform with the respective numbers of neighbours and generate results for the specification.

Tab. E.12 presents the relative evacuation uncertainty $\widetilde{\boldsymbol{\epsilon}}$ and the results of the metamodel $\widetilde{\boldsymbol{\xi}}^{\boldsymbol{\epsilon}}$ for the different numbers of neighbours N_{nb}. First, the number of random scenarios with $\left\|\widetilde{\boldsymbol{\xi}}^{\boldsymbol{\epsilon}} > 1\right\|$ was small for system model simulations with $N_{\mathrm{nb}} \leq 20$ and increased for $N_{\mathrm{nb}} \geq 48$ which gives a first hint on the spatial sensitivity. Second, the numbers of random scenarios with $\|\widetilde{\boldsymbol{\epsilon}} = 1\|$ were rather constant for $N_{\mathrm{nb}} \leq 20$. This result corresponds to Tab. E.11 and indicates that the random scenarios with $\widetilde{\epsilon} = 1$ are linked to ORSs with $\widetilde{\xi}^c = \vec{0}$ and thus have real analogies. Above $N_{\mathrm{nb}} \geq 20$, the number of random scenarios with $\|\widetilde{\boldsymbol{\epsilon}} = 1\|$ increased which proves the decreasing spatial sensitivity of the relative evacuation uncertainty. To be more specific, data points with $\bar{\xi}^c < \bar{\xi}^c_{lim}$ and i.e. $\widehat{\xi}^c = \vec{1}$ are only located at the outer vertices of the domain with a low maximum HRR and a high time to maximum HRR. Hence, a lower spatial sensitivity, in other words a larger region around a random scenario, increases the frequency of these data points within the combined relative sample and thus increases the frequency of random scenarios with $\widetilde{\epsilon} = 1$. Third, the frequency distribution of the relative evacuation uncertainty reacted in accordance with the number of random scenarios with $\|\widetilde{\boldsymbol{\epsilon}} = 1\|$. The effects are not shown explicitly but are similar to Fig. E.23b of Subs. 'Outliers in the relative evacuation uncertainty' (p. 87). Finally, the system model simulation $\mathcal{S}_{lin}$ with the number of neighbours shown in Fig. E.24 led to results in line with the system model simulations using the combination mode uniform.

Looking at the averaged variance outlined in Section D.1.5, the number of neighbours N_{nb} should be high enough to reduce the uncertainties of the variance estimates at data points. For this, $N_{\mathrm{nb}} = 5 \cdot N_{\mathrm{rf}}$ is suggested which depends on the number of risk factors. In contrast, the number of neighbours in the direct approach should be low enough to achieve sufficient spatial sensitivity. Since the spatial sensitivity depends on the number of neighbours along each risk factor, the number of neighbours for the direct approach also depends on the number of risk factors and is independent to the number of data points in the data base.

Table E.12: Effects of N_{nb} in system model simulations with combination mode uniform (above); results of system model simulation with combination mode linear (below).

$\mathcal{S}$	N_{nb}	$\|\widetilde{\boldsymbol{\epsilon}} = 1\|$	$\left\|\widetilde{\boldsymbol{\xi}}^{\boldsymbol{\epsilon}} > 1\right\|$
$\mathcal{S}_5$	5	≈ 304000	≈ 200
$\mathcal{S}_{10}$	10	≈ 310000	≈ 400
$\mathcal{S}_{20}$	20	≈ 310000	≈ 900
$\mathcal{S}_{48}$	48	≈ 324000	≈ 2000
$\mathcal{S}_{96}$	96	≈ 386000	≈ 2000
$\mathcal{S}_{lin}$	linear	≈ 304000	≈ 100

To sum up, the direct approach with the combination mode uniform and a number of neighbours of $N_{\text{nb}} = 5 \cdot N_{\text{rf}} = 20$ is sufficiently spatially sensitive. Fig. E.24 shows that the combination mode linear considers virtually always more than one and less than 20 neighbours. This result implies that it is even more spatially sensitive as the combination mode uniform as discussed in Subs. 'Combination mode' (p. 86) without being spatially discontinuous. Consequently, $N_{\text{nb}} = 20$ is used as default initial number of neighbours in the combination mode linear.

Number of replications

Subs. 'Number of replications' (p. 81) established that ORSs with $N_{\text{rep}} = 200$ replications are sufficient to reproduce the unknown probability distributions of the complex model. In this case, as is deduced in Section D.3, the direct approach is likely to represent the ORSs. This rationale is now questioned with respect to results of system model simulations. On the one hand, system model simulations with different numbers of replications $N_{\text{rep}} \in \{200, 150, 100, 50, 10\}$ in their ORSs, e.g. denoted with $\mathcal{S}_{200}$, direct at the sensitivity of their results to the number of replications in the ORSs. The ORSs in these system model simulations uses only the first consecutive N_{rep} results of all 200 replications of the original ORSs. On the other hand, five system model simulations $\mathcal{S}_{150,0}, \ldots, \mathcal{S}_{150,4}$, all with $N_{\text{rep}} = 150$ replications in their ORSs, serve to assess the reproducibility of the relative evacuation uncertainty. But still, the ORSs of the same data points differ among the system model simulations because each ORS consists of $N_{\text{rep}} = 150$ randomly drawn results without replacement of the original ORS.

Fig. E.25a and Fig. E.25b depict the results of the system model simulations $\mathcal{S}_{200}, \ldots, \mathcal{S}_{10}$. The frequency distributions of the relative evacuation uncertainty $\widetilde{\boldsymbol{\epsilon}}$ in the system model simulation $\mathcal{S}_{150}$ revealed only small effects in comparison to $\mathcal{S}_{200}$ but system model simulations with $N_{\text{rep}} \leq 100$ replications in the ORSs led to considerable effects. The individual risk of $\mathcal{R}^{ind} = 1.5 \cdot 10^{-2} \frac{1}{year}$ was similar for all system model simulations but the societal risk curve was subjected to increased variations in the upper part for system model simulations with $N_{\text{rep}} \leq 100$ replications in the ORSs. System model simulation $\mathcal{S}_{10}$ led by hazard to similar results as system model simulation $\mathcal{S}_{200}$. A similar approach as for the reproducibility of results with $N_{\text{rep}} = 150$ replications would highlight the uncertainties in the results. The latter result has to be seen with respect to Fig. E.21b of Subs. 'Reproducibility of results' (p. 85). Accordingly, the direct approach with $N_{\text{rep}} \geq 150$ replications in the ORSs has small effects on the results of system model simulations.

Fig. E.26 demonstrates the reproducibility of the relative evacuation uncertainty $\widetilde{\boldsymbol{\epsilon}}$ of the system model simulations $\mathcal{S}_{150,0}, \ldots, \mathcal{S}_{150,4}$. The differences of the frequency distribution of the relative evacuation uncertainty are mostly below 0.03 except for the lower and upper

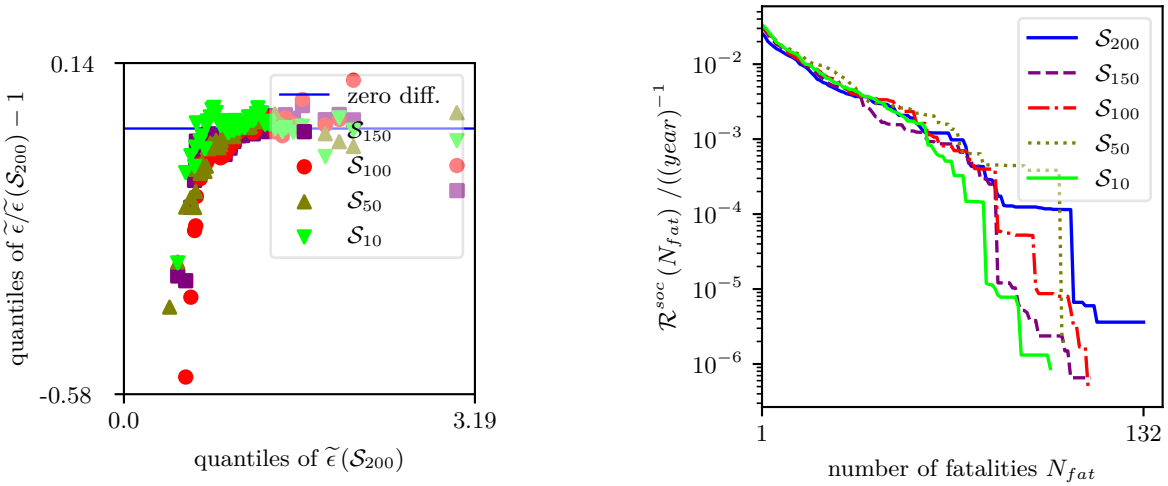

(a) relative quantile plot of $\widetilde{\epsilon}$ relative to $\mathcal{S}_{200}$

(b) societal risk curves

Figure E.25: Effects of $N_{\text{rep}} \in \{200, 150, 100, 50, 10\}$ on results of the system model simulations; the system model simulations $\mathcal{S}$ are denoted correspondingly.

quantiles. These differences are hardly higher than in Fig. E.21a of Subs. 'Reproducibility of results' (p. 85). Thus, ORSs with $N_{\text{rep}} = 150$ replications are sufficient to reproduce the frequency distribution of the relative evacuation uncertainty in system model simulations.

Lastly, these results approve the conclusion in Subs. 'Number of replications' (p. 81) in Section E.3.1: $N_{\text{rep}} = 200$ replications are sufficient for the results of system model simulations.

Summary and conclusions

It is stated in Subs. 'Combination mode' (p. 86) and Subs. 'Number of neighbours' (p. 88) that the direct approach using the combination mode linear with $N_{\text{nb}} = 20$ replications is highly spatially sensitive without being spatially discontinuous. Furthermore, the parameter $\bar{\xi}^{c}_{lim} = 10^{-4}$ is specified in Subs. 'Outliers in the relative evacuation uncertainty' (p. 87) to remove all outliers in the relative evacuation uncertainty. And finally, with $N_{\text{rep}} = 200$ replications in the ORSs according to Subs. 'Number of replications' (p. 90), the calibration and validation ensured that the direct approach is sufficiently spatially sensitive and reduces the manipulations in the evacuation uncertainty. As a consequence, the direct approach represents the ORSs and more general also the evacuation uncertainties of the complex model for random scenarios. For this reason the direct approach contributes to objective 1 (metamodel).

E.4 Risk analysis

After the examination of the metamodel with system model simulations in Section E.1, Section E.2 and Section E.3, now follows the evaluation of the risk analyses conducted with the methodology developed in this dissertation. The differentiation between system model simulation and risk analysis originates in Section B.5. The evaluation comprises: the effects of the metamodel uncertainty and the evacuation uncertainty in Section E.4.1; the convergence during sequential refinement in Section E.4.2; the effects of risk factors in the system model in Section E.4.3; and the final scrutiny of the results of risk analysis in Section E.4.4. As a result

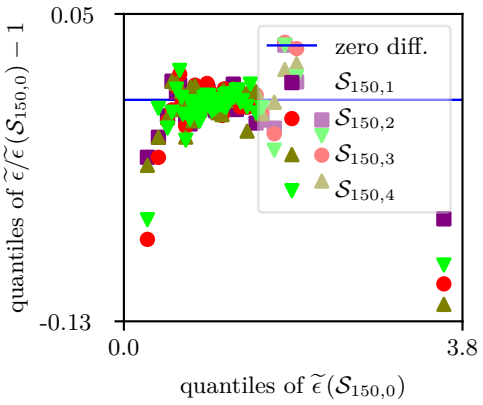

Figure E.26: Reproducibility of $\widetilde{\boldsymbol{\epsilon}}$ in five system model simulations with identical parameters and $N_{\text{rep}} = 150$: relative quantile plot for $\widetilde{\boldsymbol{\epsilon}}$ relative to $\mathcal{S}_{150,0}$.

of Subs. 'Convergence of risk measures during Monte-Carlo simulation' (p. G-34) in App. G.8, the risk analyses base on the defaults $N_{\text{mcs}} = 10^6$ random scenarios as well as importance sampling in the risk factors HRR_{max} and fa. These defaults ensure the convergence of risk measures.

E.4.1 Metamodel uncertainty and evacuation uncertainty

Subs. 'Metamodel' (p. 23) of Section B.4 explains the integration of the results of the metamodel into the system model and Section D.4 particularly focuses on the combined integration of the metamodel uncertainty and the evacuation uncertainty. After the prediction interval and the direct approach were examined in Section E.2 and Section E.3, now follows the assessment of their effects on the results of risk analysis. This assessment combines two perspectives and for this specifies the risk analyses in Tab. E.13 subjected to different metamodels with and without metamodel uncertainty or evacuation uncertainty. The first perspective concentrates on the FF in the system model of the single risk analysis $\mathcal{R}_{m,\epsilon}$ as denoted in Tab. D.3 on p. 50. It further considers only random scenarios with $\text{HRR}_{max} > 25\,\text{MW}$ which is the lower limit in the ED defined in Subs. 'Metamodel' (p. 23). To begin with the details, the FF of the RSM $\bar{\boldsymbol{\xi}}$ of all random scenarios in $\mathcal{R}_{m,\epsilon}$ forms the basis. These results are combined with the metamodel uncertainties $\boldsymbol{\delta}\widetilde{\boldsymbol{\xi}}^m$ and the relative evacuation uncertainties $\widetilde{\boldsymbol{\epsilon}}$ according to Eq. D.22 on p. 50. One yields the different FFs of the different metamodels in Tab. E.13 by fixing the results for the metamodel uncertainty or the evacuation uncertainty in the manner: $\bar{\boldsymbol{\xi}}$ with $\boldsymbol{\delta}\widetilde{\boldsymbol{\xi}}^m = \vec{0}$ and $\widetilde{\boldsymbol{\epsilon}} = \vec{1}$; $\widetilde{\boldsymbol{\xi}}^{\boldsymbol{m}}$ with $\widetilde{\boldsymbol{\epsilon}} = \vec{1}$; $\widetilde{\boldsymbol{\xi}}^{\boldsymbol{\epsilon}}$ with $\boldsymbol{\delta}\widetilde{\boldsymbol{\xi}}^m = \vec{0}$; and $\widetilde{\boldsymbol{\xi}}$ with the results for $\boldsymbol{\delta}\widetilde{\boldsymbol{\xi}}^m$ and $\widetilde{\boldsymbol{\epsilon}}$ directly of the risk analyses $\mathcal{R}_{m,\epsilon}$. Finally, the FF of the metamodels $\bar{\boldsymbol{\xi}}$, $\widetilde{\boldsymbol{\xi}}^{\boldsymbol{m}}$, $\widetilde{\boldsymbol{\xi}}^{\boldsymbol{\epsilon}}$ and $\widetilde{\boldsymbol{\xi}}$ are all clipped to $[0, \ldots, 1]$ to be in accordance with the FF in the system model. This approach guarantees that the metamodels $\bar{\boldsymbol{\xi}}$, $\widetilde{\boldsymbol{\xi}}^{\boldsymbol{m}}$, $\widetilde{\boldsymbol{\xi}}^{\boldsymbol{\epsilon}}$ and $\widetilde{\boldsymbol{\xi}}$ are based on the same random scenarios of $\mathcal{R}_{m,\epsilon}$. Consequently, the different FFs of the metamodels of each random scenario are directly comparable without effects of the aleatory uncertainties in the system model. The second perspective is less sophisticated. It plainly compares the risk measures of the risk analyses $\mathcal{R}_0$, $\mathcal{R}_m$, $\mathcal{R}_\epsilon$, $\mathcal{R}_{m,\epsilon}$ all with different random scenarios.

Table E.13: Risk analyses with different integration of the metamodel uncertainty and the evacuation uncertainty and their results of the individual risk $\mathcal{R}^{ind}$.

$\mathcal{R}$	metamodel	metamodel uncertainty	evacuation uncertainty	$\mathcal{R}^{ind}$ / $\frac{10^{-5}}{\text{year}}$
$\mathcal{R}_0$	$\bar{\boldsymbol{\xi}}$	no	no	1.1
$\mathcal{R}_m$	$\widetilde{\boldsymbol{\xi}}^{\boldsymbol{m}}$	yes	no	8.3
$\mathcal{R}_\epsilon$	$\widetilde{\boldsymbol{\xi}}^{\boldsymbol{\epsilon}}$	no	yes	1.1
$\mathcal{R}_{m,\epsilon}$	$\widetilde{\boldsymbol{\xi}}$	yes	yes	8.2

The results are jointly discussed from both perspectives in the following paragraphs. The discussion refers to the results depicted in Fig. E.27a and Fig. E.27b for the first perspective and to the individual risk in Tab. E.13 as well as the societal risk curve in Fig. E.27c for the second perspective. But first, the FF of the metamodel was below one for all random scenarios, $\Xi^* \leq 1$, for all risk analyses because the risk factor maximum HRR now obtains values of $\text{HRR}_{max} \leq 100\,\text{MW}$ in contrast to the system model simulations in the earlier sections. On the other side, around 40% of the FF of the metamodel were below zero and had to be clipped to be conform with the FF in the system model. It is to be noted, that neither the metamodel uncertainty nor the evacuation uncertainty much affected the number of random scenarios that had to be clipped in their results.

With respect to the metamodel $\widetilde{\boldsymbol{\xi}}^{\boldsymbol{m}}$ only with the metamodel uncertainty, the effects on the results of the risk analysis $\mathcal{R}_m$ are twofold. Random scenarios with small FF $\bar{\boldsymbol{\xi}} \approx 0$ led to high metamodel uncertainties in Fig. E.27a. This result stems from the drawback of the prediction interval method discussed in Section E.2.1 which is transferred into the system model by the non-relative integration with Eq. D.10 (p. 41). Next, random scenarios with high FF had similar frequency distributions in $\bar{\boldsymbol{\xi}}$ and $\widetilde{\boldsymbol{\xi}}^{\boldsymbol{m}}$ as illustrated in the upper part of the quantile plot in Fig. E.27b. In other words, the metamodel uncertainty had small effects. To sum up, the effects of the metamodel uncertainty on the results of the risk analysis $\mathcal{R}_m$ are: a large increase of the individual risk and of the lower part of societal risk curve in Tab. E.13 and Fig. E.27c resulting from random scenarios with small FF; and small effects on the upper part of the societal risk curve due to random scenarios with high FF.

Coming to the metamodel $\widetilde{\boldsymbol{\xi}}^{\boldsymbol{\epsilon}}$ only with the evacuation uncertainty and the risk analysis $\mathcal{R}_\epsilon$, it caused a larger dispersion in the frequency distribution of the FF $\widetilde{\boldsymbol{\xi}}^{\boldsymbol{\epsilon}}$ compared to $\bar{\boldsymbol{\xi}}$ in Fig. E.27b. e.g. Fig. E.27a displays that the evacuation uncertainty reduces many random scenarios with a FF from clearly above zero $\bar{\xi}_i > 0$ to zero $\widetilde{\xi}_i^{\epsilon} = 0$. This reduction derives directly from replications in relative ORSs equal to zero as a result of the direct approach introduced in Section D.3, $\widetilde{\epsilon} = \widehat{\xi}_{i,j}^{c} = 0$ with $\widehat{\xi}_{i,j}^{c} \in \widehat{\xi}_i^{c}$ at a data point $\vec{x}_i$. Also, random scenarios with the relative evacuation uncertainty $\widetilde{\epsilon} = 1$, i.e. lying on the diagonal in Fig. E.27a, are mostly the direct result of the ORSs as proved in Subs. 'Number of neighbours' (p. 88). Additionally, Fig. E.27a and Fig. E.27c demonstrate general effects on the results of risk analysis as a consequence of the relative integration of the evacuation uncertainty. In detail, the evacuation uncertainty had small effects at random scenarios with small FF $\bar{\boldsymbol{\xi}}$ leading to small effects on the individual risk and at the lower part of the societal risk curve. But the relative integration of the evacuation uncertainty contributed to large effects at random scenarios with high FF $\bar{\boldsymbol{\xi}}$ which resulted in large effects on the upper part of the societal risk curve.

Lastly, Fig. E.27c shows the united effects of the combined integration of the metamodel uncertainty and the evacuation uncertainty in the risk analysis $\mathcal{R}_{m,\epsilon}$. In particular, the metamodel uncertainty affected the lower part of the societal risk curve and the evacuation

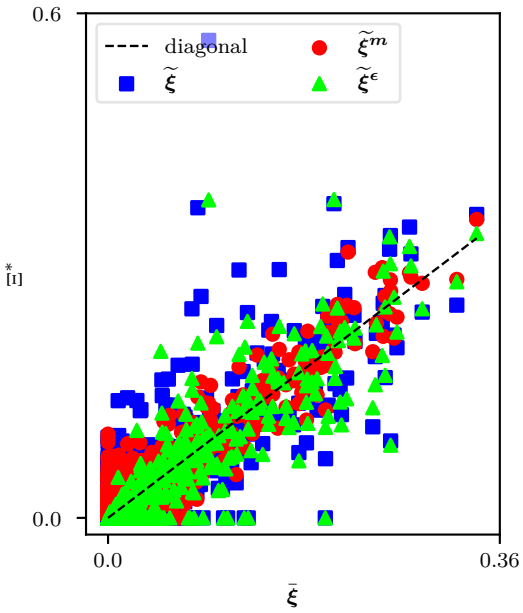

(a) effect on $\bar{\boldsymbol{\xi}}$ (clipped to $[0,\ldots,1]$) in $N_{\text{mcs}} = 10^4$ random scenarios

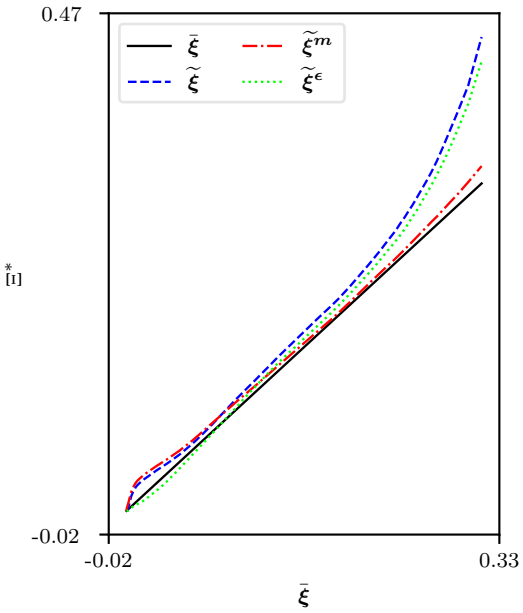

(b) frequency distributions of $\bar{\boldsymbol{\xi}}$, $\widetilde{\boldsymbol{\xi}}$, $\widetilde{\boldsymbol{\xi}}^{\boldsymbol{m}}$, $\widetilde{\boldsymbol{\xi}}^{\boldsymbol{\epsilon}}$ (clipped to $[0,\ldots,1]$): quantile plot relative to $\bar{\boldsymbol{\xi}}$

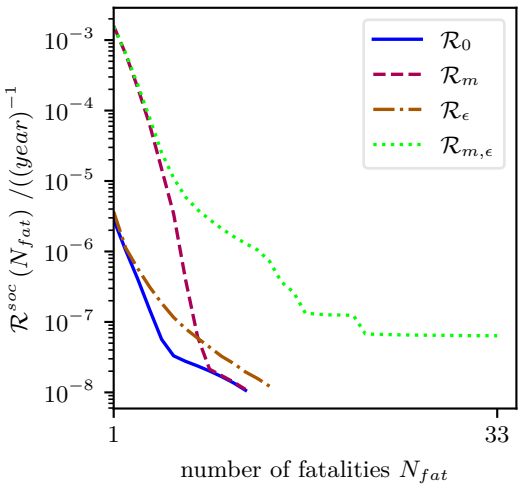

(c) societal risk curves

Figure E.27: Effect of the integration of metamodel uncertainty and evacuation uncertainty on the results of risk analyses: results of a single risk analysis $\mathcal{R}_{m,\epsilon}$ (above); results of different risk analyses $\mathcal{R}_0$, $\mathcal{R}_m$, $\mathcal{R}_\epsilon$, $\mathcal{R}_{m,\epsilon}$ (below).

uncertainty affected the upper part of the societal risk curve. Both effects correspond to the combined integration with Eq. D.22 on p. 50.

These results prove that the metamodel uncertainty and the evacuation uncertainty clearly affect the results of risk analysis. They further lead to the statement that the combined integration of metamodel uncertainty and evacuation uncertainty is important for risk analysis which is necessary for assumption 2 (plausibility). This statement is further strengthened with: the importance of the metamodel uncertainty illustrated in Subs. 'Basic characteristics' (p. G-19) in App. G.6.1 and despite the drawback of the prediction interval method; and the realistic representation of the ORSs in the evacuation uncertainty highlighted in Subs. 'Summary and conclusions' (p. 91).

E.4.2 Convergence of risk measures during sequential refinement

In Section B.1 a metamodel for the methodology for risk analysis was demanded which is suitable for sequential refinement and directs at the global objective. Obviously, the sequential refinement affects the results of risk analysis. Coping with this fact, Subs. 'Convergence of the RSM and the prediction variance' (p. 60) in Section E.2.2 specified the default RSM and supposed that the default RSM is sufficient for risk analysis. The global objective of risk analysis led to the choice of the response surface method MLS as explained in Section D.1.2. But a comparison of different response surface methods in Subs. 'Bias error and variance error of the RSM' (p. 73) identified that MLS models are attributed to an increased variance error to favour the global objective. These two findings, the specification of the default RSM and the increased variance error, call for: the confirmation that the metamodel with the default RSM, the metamodel uncertainty and the evacuation uncertainty is sufficient for risk analyses; and the evaluation of the effect of the increased variance error on the results of risk analysis, i.e. the sensitivity of the results to variations in the ED as described in Section D.1.1. Therefore, the risk analyses in Tab. E.14 are assessed in this section. These risk analyses either use the metamodel $\widetilde{\boldsymbol{\xi}}$ with the metamodel uncertainty and the evacuation uncertainty or the metamodel $\widetilde{\boldsymbol{\xi}}^{\boldsymbol{\epsilon}}$ without the metamodel uncertainty. The latter risk analyses with the metamodel $\widetilde{\boldsymbol{\xi}}^{\boldsymbol{\epsilon}}$ are intended to exclude the drawback of the prediction interval.

Table E.14: Risk analyses $\mathcal{R}$ based on the metamodel $\widetilde{\boldsymbol{\xi}}$ (with metamodel uncertainty and evacuation uncertainty) and $\widetilde{\boldsymbol{\xi}}^{\boldsymbol{\epsilon}}$ (without metamodel uncertainty); results of the individual risk $\mathcal{R}^{ind}$ and the euclidean relative difference erd_q of the quantile plot in Fig. E.28a; erd_q is relative to $\mathcal{R}_3$ or $\mathcal{R}_{3,\epsilon}$, with the short notations for $\mathrm{erd}_q(\mathcal{R}_i, \mathcal{R}_3)$ and $\mathrm{erd}_q(\mathcal{R}_{i,\epsilon}, \mathcal{R}_{3,\epsilon})$.

data base	$\widetilde{\boldsymbol{\xi}}$	$\widetilde{\boldsymbol{\xi}}^{\boldsymbol{\epsilon}}$	$\mathcal{R}^{ind}(\mathcal{R}_i)\ /\frac{1}{\mathrm{year}}$	$\mathrm{erd}_q(\mathcal{R}_i)$	$\mathcal{R}^{ind}(\mathcal{R}_{i,\epsilon})\ /\frac{1}{\mathrm{year}}$	$\mathrm{erd}_q(\mathcal{R}_{i,\epsilon})$
$\underline{\boldsymbol{\xi}}^c_{X_0}$	$\mathcal{R}_0$	$\mathcal{R}_{0,\epsilon}$	$47 \cdot 10^{-5}$	1.7	$49 \cdot 10^{-6}$	0.92
$\underline{\boldsymbol{\xi}}^c_{X_1}$	$\mathcal{R}_1$	$\mathcal{R}_{1,\epsilon}$	$15 \cdot 10^{-5}$	0.50	$6.7 \cdot 10^{-6}$	0.41
$\underline{\boldsymbol{\xi}}^c_{X_2}$	$\mathcal{R}_2$	$\mathcal{R}_{2,\epsilon}$	$8.3 \cdot 10^{-5}$	0.05	$11 \cdot 10^{-6}$	0.05
$\underline{\boldsymbol{\xi}}^c_{X_3}$	$\mathcal{R}_3$	$\mathcal{R}_{3,\epsilon}$	$7.8 \cdot 10^{-5}$	0.00	$4.6 \cdot 10^{-6}$	0.00
$\underline{\boldsymbol{\xi}}^c_{X_{1a}}$	$\mathcal{R}_{1a}$	$\mathcal{R}_{1a,\epsilon}$	$8.0 \cdot 10^{-5}$	0.22	$3.1 \cdot 10^{-6}$	0.27
$\underline{\boldsymbol{\xi}}^c_{X_b}$	$\mathcal{R}_b$	$\mathcal{R}_{b,\epsilon}$	$9.8 \cdot 10^{-5}$	0.07	$10 \cdot 10^{-6}$	0.08

For questioning the default RSM, Fig. E.28a, Tab. E.14 and Fig. E.28b inform on the results of the FF in the system model, the individual risk and the societal risk curves respectively for the risk analyses using the metamodel $\widetilde{\boldsymbol{\xi}}$. At the beginning, the risk analysis $\mathcal{R}_0$ markedly deviated to the other risk analyses in the FF as well as in the risk measures. Then, both risk measures decreased monotonically during the sequential refinement from the risk analysis $\mathcal{R}_0$

to $\mathcal{R}_3$. Between the risk analyses $\mathcal{R}_2$ and $\mathcal{R}_3$, the difference in the FFs was reasonably small, esp. in comparison to the former refinement step between $\mathcal{R}_1$ and $\mathcal{R}_2$. Hence, the individual risks of $\mathcal{R}_2$ and $\mathcal{R}_3$ are similar in relation to the variations in the accepted risk measures of an order of magnitude of two as outlined in Section B.5. And also the societal risk curves resemble each other in particular in the maximum number of fatalities. So, the results of risk analysis converged between the risk analyses $\mathcal{R}_2$ and $\mathcal{R}_3$.

The results of the risk analyses $\mathcal{R}_1$ and $\mathcal{R}_{1a}$, subjected to variations in their EDs, differed considerably. In contrast, the risk analyses using the metamodels $\bar{\boldsymbol{\xi}}_{X_2}$ and $\bar{\boldsymbol{\xi}}_{X_b}$ led to close results in the FF in the system model and consequently led to similar risk measures. These results imply that the risk analysis $\mathcal{R}_2$ is less sensitive to variations in the ED than the risk analysis $\mathcal{R}_1$.

Two outcomes are relevant after juxtaposing the risk analyses subjected to metamodels $\widetilde{\boldsymbol{\xi}}^{\boldsymbol{\epsilon}}$ disregarding the metamodel uncertainty with the other risk analyses. During sequential refinement, the effect of the metamodel uncertainty was strikingly if one compares the differences between the risk analyses $\mathcal{R}_0$ and $\mathcal{R}_3$ with the differences between $\mathcal{R}_{0,\epsilon}$ and $\mathcal{R}_{3,\epsilon}$. In particular Fig. E.28a and Fig. E.28c as well as Fig. E.28b and Fig. E.28d highlight this effect for the FF in the system model as well as the societal risk curve. Additionally, Tab. E.14 quantifies it with the euclidean relative differences between $\widetilde{\Xi}(\mathcal{R}_0)$ and $\widetilde{\Xi}(\mathcal{R}_3)$ as well as $\widetilde{\Xi}(\mathcal{R}_{0,\epsilon})$ and $\widetilde{\Xi}(\mathcal{R}_{3,\epsilon})$. With regard to the sensitivity to variations in the ED, the risk analyses $\mathcal{R}_2$ and $\mathcal{R}_b$ as well as $\mathcal{R}_{2,\epsilon}$ and $\mathcal{R}_{3,\epsilon}$ reveal that the metamodel uncertainty reduces the sensitivity of the FFs. The sensitivity to variations in the ED between $\widetilde{\Xi}(\mathcal{R}_2)$ and $\widetilde{\Xi}(\mathcal{R}_b)$ is indirectly shown over $\widetilde{\Xi}(\mathcal{R}_3)$: $\mathrm{erd}_q\left(\widetilde{\Xi}(\mathcal{R}_2), \widetilde{\Xi}(\mathcal{R}_3)\right) \approx \mathrm{erd}_q\left(\widetilde{\Xi}^{\epsilon}(\mathcal{R}_{2,\epsilon}), \widetilde{\Xi}^{\epsilon}(\mathcal{R}_{3,\epsilon})\right)$ and $\mathrm{erd}_q\left(\widetilde{\Xi}(\mathcal{R}_b), \widetilde{\Xi}(\mathcal{R}_3)\right) = 0.072 < \mathrm{erd}_q\left(\widetilde{\Xi}^{\epsilon}(\mathcal{R}_{b,\epsilon}), \widetilde{\Xi}^{\epsilon}(\mathcal{R}_{3,\epsilon})\right) = 0.08$. Summing up, the metamodel uncertainty contributes strongly to the risk measures and it further decreases the sensitivity to variations in the ED.

The latter conclusions substantiate Section E.4.1 where it is stated that the metamodel uncertainty and the evacuation uncertainty are important for risk analysis. But more important, the risk measures converged with the risk analyses $\mathcal{R}_2$. Thus, the results confirm the conclusions on the default RSM in Subs. 'Convergence of the RSM and the prediction variance' (p. 60) and of Berchtold 2018 [9] which does not consider the evacuation uncertainty. Moreover, referring to the conclusions of Subs. 'Bias error and variance error of the RSM' (p. 73), risk measures of the risk analysis $\mathcal{R}_2$ have small sensitivity to variations in the ED. This result has following implications: the increased variance error of MLS has little effect on results of risk analysis; accordingly, the selection of the ED outlined in Section C.3 and detailed for the system model in Section E.1 is less important. In summary, the metamodel with the default RSM, the metamodel uncertainty and the evacuation uncertainty is sufficiently accurate for risk analysis. So, together with the conclusions in App. G.8, this section proves that the methodology for risk analysis using the metamodel $\widetilde{\boldsymbol{\xi}}_{X_2}$, more precisely the default RSM, the metamodel uncertainty and the evacuation uncertainty, leads to reproducible results. At last, the methodology for risk analysis contributes to objective 1 (metamodel).

E.4.3 Risk factors

In Section A.1 is shown that methodologies for risk analysis of road tunnels apply different numbers of risk factors. For this reason, the system model in Section B.3 comprises also multiple risk factors which apparently have different effects on the risk measures. Section B.5 sketches two approaches to determine the effects: the Spearman's rank correlation coefficient; and the relative effect on the individual risk and on the societal risk curve. The effects are

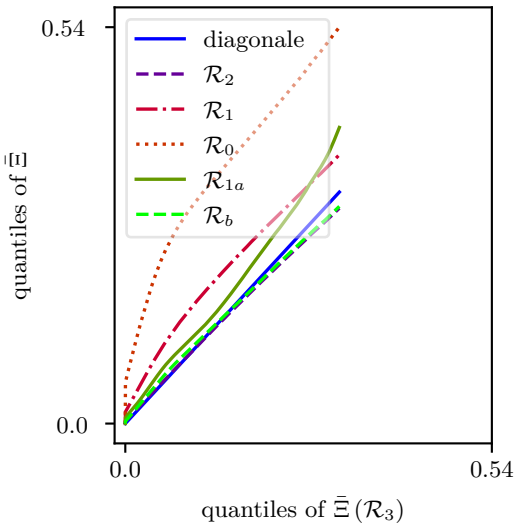

(a) quantile plot of $\widetilde{\Xi}$ relative to $\widetilde{\Xi}(\mathcal{R}_3)$

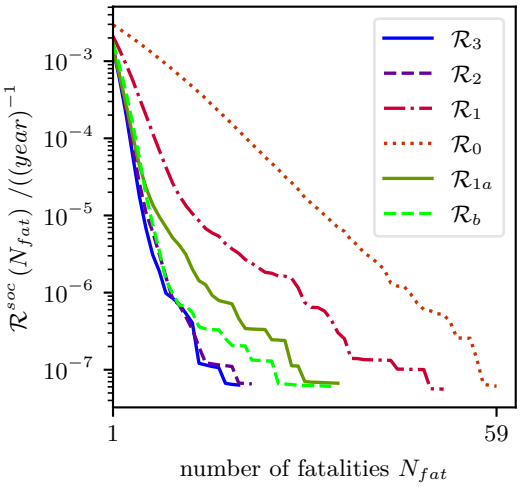

(b) societal risk curves

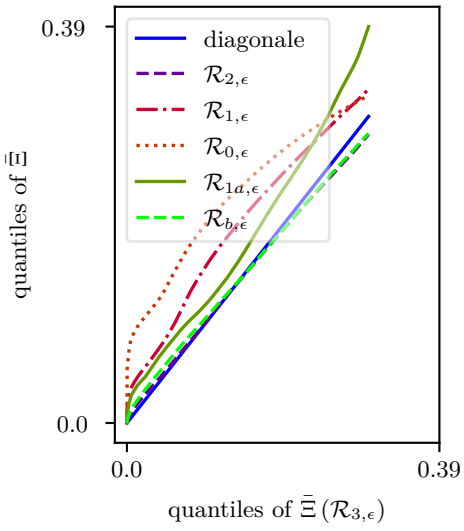

(c) quantile plot of $\widetilde{\Xi}$ relative to $\widetilde{\Xi}(\mathcal{R}_{3,\epsilon})$

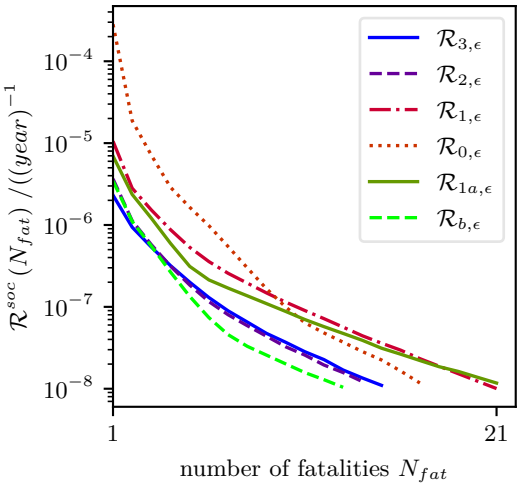

(d) societal risk curves

Figure E.28: Effects of the ED on results of the risk analyses $\mathcal{R}$ in Tab. E.14 based on a metamodel without metamodel uncertainty ($\widetilde{\boldsymbol{\xi}}$: above); with metamodel uncertainty and evacuation uncertainty ($\widetilde{\boldsymbol{\xi}}^{\epsilon}$: below); the scales differ between the figures.

discussed in the next subsections and finally the most important risk factors in the system model are defined. The discussion bases on results of the risk analysis $\mathcal{R}_{def} \equiv \mathcal{R}_{def,1}$ with the default methods, modes and parameters including the metamodel uncertainty and the evacuation uncertainty. An exception is the increased number of random scenarios with $N_{\text{mcs}} = 10^7$ since the relative effect on the individual risk splits the domain of a risk factor into ten equally spaced intervals. The risk analysis $\mathcal{R}_{def,2}$, which is equal to $\mathcal{R}_{def,1}$, indicated the reproducibility of the effects of the risk factors on the FF in the system model and on the individual risk but gave hints on dissimilarities in the societal risk curve.

Effects on the FF in the system model

Fig. E.29 depicts the correlation to the FF in the system model of the risk factors maximum HRR HRR_{max}, time to maximum HRR t_{max}, maximum pre-evacuation time t_{pre} and number of tunnel users N_{tu}. These risk factors are parent nodes of the node FF. In general, the results approved the discussion in Section E.2.4. Furthermore, Tab. E.15 provides an overview on the correlation coefficients for all risk factors and therewith gives also a qualitative impression on the effect on the FF.

Table E.15: Correlation coefficient ρ^{sp} between results of risk factors and the FF in the system model of the risk analysis $\mathcal{R}_{def}$; the p-value is zero due to the large variations in the FFs.

risk factor	notation	ρ^{sp}
maximum HRR	HRR_{max}	0.46
time to maximum HRR	t_{max}	−0.26
maximum pre-evacuation time	t_{pre}	0.14
failure of tunnel alarm	fa	0.14
number of tunnel users	N_{tu}	−0.05
average daily traffic volume	$\dot{N}_{adtv}$	−0.01
ratio of HGV	χ_{HGV}	0.00
tunnel length	l_{tunnel}	0.00

First of all, the risk factors HRR_{max} and t_{max} had clear effects on the FF in the system model. The pre-evacuation time of tunnel users should have similar effects as t_{max} but the risk factor t_{pre} is the maximum pre-evacuation time among all tunnel users. Hence, the individual tunnel users have smaller, distributed, pre-evacuation times. In consequence, the effect of t_{pre} was smaller as also illustrated in Fig. E.15 (p. 74).

The risk factor failure of tunnel alarm fa caused a similar correlation coefficient to the FF as t_{pre}. Since the alarm of tunnel users is either initiated individually by smoke or by the tunnel alarm, the latter one establishes the upper limit. Hence, the individual time of alarm of a tunnel user is limited by the intermediate node 'time of tunnel alarm' and thus, also by the risk factor fa. Hence, the risk factor fa is similar to the risk factor t_{pre} which constitutes the upper limit of the individual pre-evacuation time of a tunnel user. This similarity leads to the comparable effects of t_{pre} and fa on the FF and also to the reduced effect with respect to the risk factors HRR_{max} and t_{max}. But still, Fig. E.13a and Fig. E.13b (p. 71) or Fig. E.14c and Fig. E.14d on p. 72 highlight the differences between FFs of random scenarios with TA or FA. So, the event of 'failure of tunnel alarm' is important in the scenario of the system model.

According to Fig. E.29d, showing the effect of the number of tunnel users N_{tu} on the FF, the random scenarios split up into two groups. These two groups depend on the risk factor fa with the distinct events TA and FA. The TA prevents vehicles from entering the tunnel and

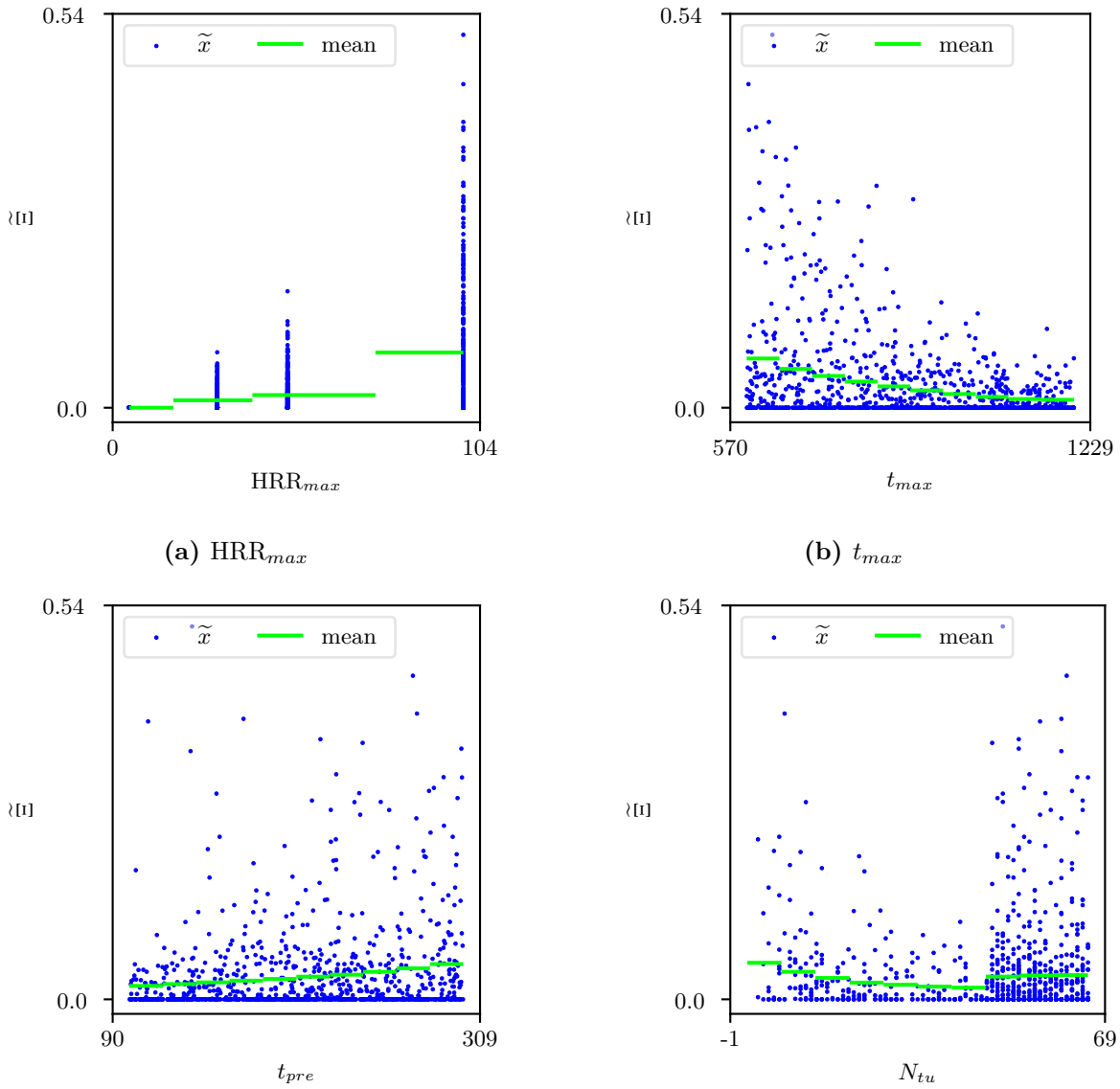

(a) HRR_{max} **(b)** t_{max}

(c) t_{pre} **(d)** N_{tu}

Figure E.29: Correlation between the FF in the system model $\widetilde{\Xi}$ and the results of the parent nodes of the node FF for $N_{\mathrm{mcs}} = 10^3$ random scenarios of the risk analysis $\mathcal{R}_{def}$; the mean was calculated for every bin of $N_{\mathrm{mcs}} = 10^6$ random scenarios which led to similar results as $N_{\mathrm{mcs}} = 10^7$.

keeps the 'number of vehicles' as well as the N_{tu} low, esp. in case of a fast fire growth. At the same time, the TA reduces the individual pre-evacuation time which leads to the effect on the FF. This rationale states that the effect of the risk factor N_{tu} on the FF is caused by the effect of the risk factor fa on the pre-evacuation time of tunnel users. In other words, the N_{tu} in a random scenario has small direct effect on the FF because of few interactions among tunnel users, e.g. there are no hint on jams at emergency exits in Section E.2.4.

Relative effect on the individual risk

The relative effects of risk factors on the individual risk derive from Eq. B.8 on p. 28. Tab. E.16 summarises the results for all risk factors.

Table E.16: Relative effects of risk factors on: individual risk η^{ind} which is similar for $\mathcal{R}_{def,1}$ and $\mathcal{R}_{def,2}$ (left); societal risk η^{soc} in qualitative order of the risk factors for both $\mathcal{R}_{def,1}$ and $\mathcal{R}_{def,2}$ (right).

risk factor	η^{ind}	$\mathcal{R}_{def,1}\,(\eta^{soc})$	$\mathcal{R}_{def,2}\,(\eta^{soc})$
HRR_{max}	3.3	HRR_{max}	HRR_{max}
fa	2.0	fa	fa
$\dot{N}_{adtv}$	1.3	t_{pre}	$\dot{N}_{adtv}$
N_{tu}	1.1	t_{max}	t_{pre}
χ_{HGV}	1.1	$\dot{N}_{adtv}$	t_{max}
$\dot{f}_{fire}$	1.1	N_{tu}	N_{tu}
l_{tunnel}	1.0	l_{tunnel}	χ_{HGV}
t_{max}	0.3	χ_{HGV}	$\dot{f}_{fire}$
t_{pre}	0.2	$\dot{f}_{fire}$	l_{tunnel}

The risk factors HRR_{max} and fa led to the highest relative effects on the individual risk. Beside the FF, both risk factors also influence the frequency of a random scenario f_{sc} used to determine the individual risk with Eq. B.3 on p. 15. The frequency of a random scenario depends on the probability distributions of both risk factors described in Tab. B.3 (p. 19). In a nutshell: the smaller the probability of a certain value of a risk factor in a random scenario, the smaller is the contribution of the random scenario to the individual risk. This effect counteracts a potentially increased FF. For instance, random scenarios with FA contribute less to the individual risk than random scenarios with TA due to their smaller frequency and despite their higher FF. Section B.3 addresses this issue in more detail. Concluding, the probability distribution of the risk factors HRR_{max} and fa also contributed to effects on the individual risk.

The parent nodes of the node f_{sc} $\dot{N}_{adtv}$, $\dot{f}_{fire}$ and l_{tunnel} as well as the risk factor χ_{HGV} apply general models. But despite these models, their relative effect on the individual risk was smaller in comparison to the risk factors HRR_{max} and fa. And tunnel specific models would even reduce this effect.

Next, the risk factor N_{tu} has small effects on the FF and no direct effect on the frequency of a random scenario. Consequently, its effect on the individual risk is mostly indirect originating from the risk factor fa.

Lastly, the risk factors t_{max} and t_{pre} are neither subjected to general models nor depend on other risk factors but base on uniform distributions which means no effect on the frequency of a random scenario. This fact resulted in far smaller relative effects on the individual risk, even for the risk factor t_{max} strongly affecting the FF in the system model. With reference to Eq. B.8, fixed values for t_{max} cause an absolute difference between the minimum and the

maximum individual risk smaller than an order of magnitude of two, i.e. the variations in the accepted individual risk with $\mathcal{R}^{ind}$ between $\mathcal{R}^{ind}_{min} = 6.6 \cdot 10^{-5} \frac{1}{\text{year}}$ and $\mathcal{R}^{ind}_{max} = 9.3 \cdot 10^{-5} \frac{1}{\text{year}}$. This result further emphasises its small contribution.

Relative effect on the societal risk curve

Eq. B.9 on p. 29 produced the relative effects of the risk factors on the societal risk curve. But, in contrast to the FF in the system model and the individual risk, the relative effects were hardly reproducible e.g. $\eta^{soc}\left(\text{HRR}_{max}\right) = \{3.1, 2.2\}$, $\eta^{soc}\left(\dot{N}_{adtv}\right) = \{1.1, 1.6\}$. Actually, the steps to increase the reproducibility introduced in Section B.5 did not succeed. However, more restrictions like further reducing the maximum number of fatalities would obliterate the information content of the societal risk curve. For this reason, Tab. E.16 now includes the qualitative order of the risk factors for both risk analyses $\mathcal{R}_{def,1}$ and $\mathcal{R}_{def,2}$.

At least remain some concluding remarks. The risk factors HRR_{max} and fa led constantly to the largest relative effects on the societal risk curve. These outcomes suggest their importance thereon. The risk factor N_{tu} has small direct effect on the FF and no direct effect on the frequency f_{sc} of a random scenario. But it affected at least the societal risk curve to some extent. This effect stems from the definition of the societal risk in Eq. B.4 (p. 15): N_{tu} is directly linked to the number of fatalities in Eq. B.1 on p. 14 and thus also directly linked to the societal risk. Accordingly, a detailed model for the frequency distribution of the N_{tu} seems to be relevant for risk analysis.

Summary and conclusions on the most important risk factors

The final evaluation of the effects of risk factors mostly considers the FF and the individual risk because of the limited information gained from the societal risk curve. To begin, the risk factor HRR_{max} is most important for risk analysis due to its influence on the FF as well as on the frequency of a random scenario and the ensuing relevance for both risk measures. Next, the risk factor fa revealed a smaller correlation coefficient to the FF of the system model but still influences the frequency of a random scenario which increases the effect on the individual risk. It further has clear effects on the FF between equal random scenarios with TA and FA. Hence, the event of tunnel alarm and its failure is also important for risk analysis. On the other side, the risk factor t_{max} does not contribute to the frequency of a random scenario. But its strong correlation to the FF of a random scenario emphasises its importance in the consequence model and thus also for risk analysis, esp. with regard to scenarios with rare events and high consequences. Finally, the risk factors $\dot{N}_{adtv}$, $\dot{f}_{fire}$, l_{tunnel} and χ_{HGV} are less important for the individual risk than HRR_{max} or fa. Additionally, their importance will decrease in case of tunnel specific models ranking them fourth for the most important risk factors.

The risk factors N_{tu} and t_{pre} contribute little to the individual risk but their results provide insights to the choice of the fire model and the evacuation model. The risk factor t_{pre} has larger effects on the FF in the system model in comparison to N_{tu}. This result implies, that the evacuation model should focus on the pre-evacuation time whereas modelling interactions among tunnel users is less important because of few interactions throughout the scenario. Therefore, microscopic evacuation models are not necessarily required for risk analysis of road tunnels. This conclusion corroborates the one-dimensional evacuation models used in methodologies for risk analysis of road tunnels outlined in Section A.1 but conflicts with assumption 1 (complex scenarios) with regard to microscopic evacuation models. Moreover, the focus on the pre-evacuation time raises another implication. Since, the risk factors fa and t_{max} are important for risk analysis, also the individual alarm of tunnel users is important,

Table E.17: Most important risk factors in risk analysis $\mathcal{R}_{def}$.

risk factor	notation	remark
maximum HRR	HRR_{max}	
failure of tunnel alarm	fa	
time to maximum HRR	t_{max}	due to the effect on the FF
parent nodes of f_{sc}	$\dot{N}_{adtv}$, $\dot{f}_{fire}$, l_{tunnel}, χ_{HGV}	regarding tunnel specific models

e.g. in case of FA. For this, CFD methods are advantageous, i.e. for the interactions between the fire source, the emergency ventilation and the tunnel users which this time confirms assumption 1 (complex scenarios) with respect to the CFD method.

The previous rationale results in the most important risk factors highlighted in Tab. E.17. The three most important risk factors are parent nodes of the node FF and thus directly linked to the complex model as depicted in Fig. B.1 on p. 16. Consequently, multiple risk factors are required for the interactions in complex scenarios which again confirms assumption 1 (complex scenarios). Later on, the development of the system model should concentrate on the nodes of the most important risk factors in order to reproduce the interactions in real tunnel fires. The models in these nodes could be refined with subsystems of multiple risk factors as parent nodes, e.g. discussed in Berchtold 2016 [8] and suggested by Haimes 2018 [4]. Or, the risk factor HRR_{max} now applies a discrete distribution in case of risk analyses due to the lack of more detailed models. But effects of discrete scenarios in the RSM, i.e. by the use of LIn, illustrated in Subs. 'Shape of the RSM' (p. 75) and Subs. 'Results of risk analysis' (p. 79) show the demand for an improvement with a continuous probability distribution.

E.4.4 Scrutiny

Section A.1 motivates the final scrutiny of the results of the methodology for risk analysis in the following subsections. First, Section E.4.3 and Section E.4.2 are revisited in Section E.4.3 and Section E.4.2 respectively where the reproducibility of the results is questioned. Then, in Subs. 'Plausibility of risk measures' (p. 105) the emphasis is put on the effects of the metamodel uncertainty and the evacuation uncertainty with reference to Section E.4.1. And finally, Subs. 'The effect of the risk analyst' (p. 106) closes with the discussion of further epistemic uncertainties from the perspective of the risk analyst.

For the scrutiny, the subsections juxtapose different risk analyses shown in Tab. E.18. These risk analyses either derive from the methodology for risk analysis developed in this dissertation and are indexed with D or from the methodology for risk analysis in Berchtold 2016 [8] with the index I. Whereas the system models are equal for both cases, the differences lie in the metamodels detailed in Tab. E.18 and Tab. E.19. In case of the risk analysis $\mathcal{R}_I$, the data base has not been available and accordingly $\mathcal{R}_I$ could not be used to produce quantitative results. As a consequence, the risk analysis $\mathcal{R}_{I,r}$ reproduces the results of $\mathcal{R}_I$ with a different data base of a later research step. This data base deviates to the data base of $\mathcal{R}_I$ in two points: first, in the number of data points and second, in the domain of the risk factor HRR_{max} in the ED as described in Tab. E.19. Despite these differences, the results of both risk analyses, i.e. the individual risk with $\mathcal{R}^{ind}(\mathcal{R}_I) = 2.4 \cdot 10^{-7} \frac{1}{\text{year}}$, $\mathcal{R}^{ind}(\mathcal{R}_{I,r}) = 8.5 \cdot 10^{-7} \frac{1}{\text{year}}$. and the societal risk, were comparable. Hence, the results of the risk analysis $\mathcal{R}_{I,r}$ represent the results of $\mathcal{R}_I$.

Reproducibility of the most important risk factors

The most important risk factors are defined in Subs. 'Summary and conclusions on the most

Table E.18: Risk analyses based on different metamodels with their results on the individual risk $\mathcal{R}^{ind}$.

$\mathcal{R}$	methodology	metamodel	background	$\mathcal{R}^{ind}/\frac{1}{\text{year}}$
$\mathcal{R}_D$	dissertation	$\widetilde{\boldsymbol{\xi}}$	with metamodel uncertainty and evacuation uncertainty as concluded in Section E.4.1	$8.3 \cdot 10^{-5}$
$\mathcal{R}_{D,\epsilon}$	dissertation	$\widetilde{\boldsymbol{\xi}}^{\boldsymbol{\epsilon}}$	only evacuation uncertainty to avoid drawback of the prediction interval method	$1.1 \cdot 10^{-5}$
$\mathcal{R}_{D,f}$	dissertation	$\bar{\boldsymbol{\xi}}$	neither metamodel uncertainty nor evacuation uncertainty to be close to $\mathcal{R}_I$	$1.1 \cdot 10^{-5}$
$\mathcal{R}_{D,LIl}$	dissertation	$\bar{\boldsymbol{\xi}}^{\text{LIl}}$	as $\mathcal{R}_{D,f}$ but with response surface method LIl similar to $\mathcal{R}_I$	$0.7 \cdot 10^{-5}$
$\mathcal{R}_I$	ISTSS 2016	$\bar{\boldsymbol{\xi}}^{\text{LIl}}$	based on methodology in Berchtold 2016 [8]	$2.4 \cdot 10^{-7}$
$\mathcal{R}_{I,r}$	ISTSS 2016	$\bar{\boldsymbol{\xi}}^{\text{LIl}}$	reproduction of $\mathcal{R}_I$	$8.5 \cdot 10^{-7}$

Table E.19: Parameters of the RSMs used in the risk analyses $\mathcal{R}_D$, $\mathcal{R}_I$ and $\mathcal{R}_{I,r}$; the number of fire scenarios and evacuation scenarios in the data base are denoted with $\left\|X^{\text{fire}}\right\|$ and $\|X^{\text{evac}}\|$.

	$\mathcal{R}_D$	$\mathcal{R}_I$	$\mathcal{R}_{I,r}$
$\left\|X^{\text{fire}}\right\|, \|X^{\text{evac}}\|$	10, 96	20, 400	18, 157
domain of HRR_{max} /MW in the ED	$[25 \dots 200]$	$[25 \dots 100]$	$[25 \dots 200]$
response surface method	MLS	LIl	LIl

important risk factors' (p. 101) using the risk analysis $\mathcal{R}_D$. Also, Berchtold 2016 [8] presented most important risk factors derived from the risk analysis $\mathcal{R}_I$. These findings now allow to briefly discuss the reproducibility of the results of risk analyses. Apart from the metamodels in both risk analyses, also the approach to evaluate the relative effect of risk factors on risk measures in $\mathcal{R}_I$ differed to the approach outlined in Section B.5. Although the approach for $\mathcal{R}_I$ still applied Eq. B.8 and Eq. B.9 on p. 28, the relative effect of a risk factor derived from a screening of multiple risk analyses, each with a fixed value for the risk factor. Furthermore, the nodes N_{tu}, probability for failure of the TA, $\dot{f}_{fire}$ and 'traffic speed', which is an analytical function in the risk analysis $\mathcal{R}_D$, used independent uniform distributions during the screening. But in spite of these differences, both approaches lead to qualitatively similar results in case of identical risk analyses.

Both risk analyses led to the most important risk factors: HRR_{max}, fa and t_{max} for the risk analysis $\mathcal{R}_D$; and HRR_{max}, N_{tu}, fa with t_{max} on the fourth rank for the risk analysis $\mathcal{R}_I$. On the one hand, the focus in this dissertation, i.e. the evaluation of $\mathcal{R}_D$, lies on the metamodel and not on the system model. For this reason, the risk factor N_{tu} is less important than other risk factors. On the other hand, the focus in case of $\mathcal{R}_I$ was on the system model and not on the metamodel. Accordingly, the risk factor N_{tu} was identified as one of the most important risk factors due to its direct link to the societal risk in Eq. B.5 on p. 15. But if the risk factor N_{tu} had not been considered, the third most important risk factor would have been the risk factor t_{max} leading to equal qualitative orders for the most important risk factors. With this rationale, the differences in the most important risk factors of both risk analyses can be

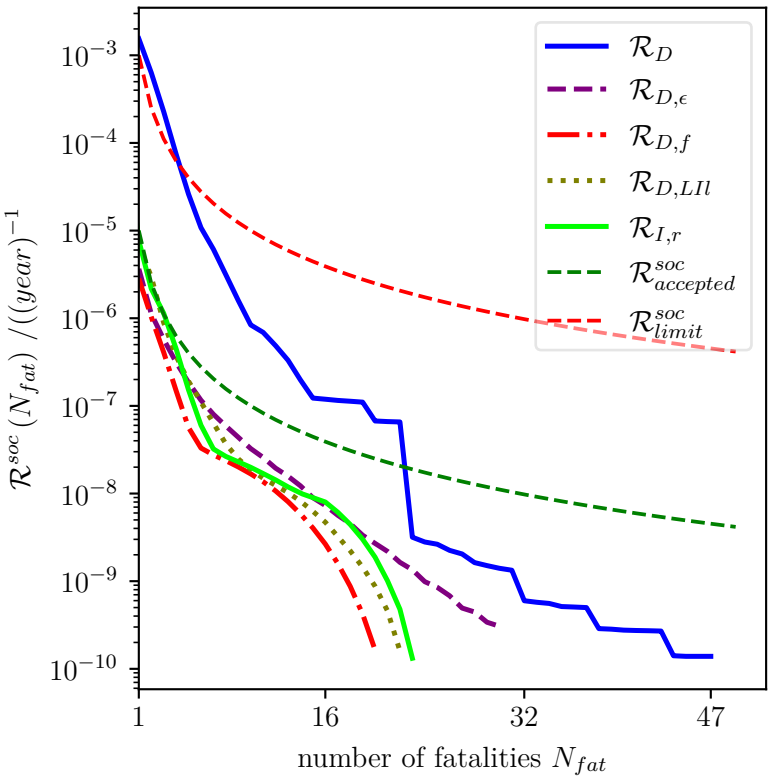

Figure E.30: Risk measures of risk analyses based on two different methodologies according to Tab. E.18: developed in this dissertation (for different metamodels); in Berchtold 2016 [8]; $\mathcal{R}^{soc}_{accepted}$ and $\mathcal{R}^{soc}_{limit}$ are the accepted and the limited societal risk curves introduced in Section B.5; the societal risk curve is limited to N_{fat} with $\mathcal{R}^{soc}(N_{fat}) > 10^{-10}\frac{1}{\text{year}}$ (as in Wahlström 2018 [67, Fig. 6]).

reasoned by different foci of the evaluations and not by qualitatively different results of the risk analyses.

Effects of the metamodel

In Section E.4.2 the effect of different refinement steps on the results of risk analysis was quantified and concluded that risk analyses using the default RSM, the metamodel uncertainty and the evacuation uncertainty lead to reproducible results. Following this conclusion, this subsection aims at the effects of different metamodels on the results of risk analysis with regard to differences: first, caused by variations in the ED and the response surface method LIl, i.e. $\mathcal{R}_{D,LIl}$ and $\mathcal{R}_I$; and second, caused by disparate response surface methods together with variations in the ED, namely $\mathcal{R}_{D,f}$ and $\mathcal{R}_I$. The results of both assessments are summarised in Tab. E.18 for the individual risk and in Fig. E.30 for the societal risk curve.

First, the risk analyses $\mathcal{R}_{D,LIl}$ and $\mathcal{R}_I$ resulted in comparable societal risk curves and in individual risks which is 30 times higher for $\mathcal{R}_{D,LIl}$ than for $\mathcal{R}_I$. To compare, the risk analyses $\mathcal{R}_2$ and $\mathcal{R}_b$ of Section E.4.2 led to similar individual risks. The metamodels of both risk analyses $\mathcal{R}_2$ and $\mathcal{R}_b$ also applied different data bases but considered the metamodel uncertainty and the evacuation uncertainty in contrast to the risk analyses $\mathcal{R}_{D,LIl}$ and $\mathcal{R}_I$. Additionally, Subs. 'Bias error and variance error of the RSM' (p. 73) revealed similar variance errors for the response surface methods MLS and LIl. Thus, this comparison suggests, that

the metamodel uncertainty and the evacuation uncertainty contributes to a reduction of the sensitivity to variations in the ED.

Second, the individual risk of the risk analysis $\mathcal{R}_{D,f}$ with MLS was about 45 times higher to the risk analysis $\mathcal{R}_I$ with LIl and both societal risk curves resembled each other. Also in case of the risk analyses $\mathcal{R}_{D,f}$ and $\mathcal{R}_{D,LIl}$, both with the same data base, MLS led to the increased individual risk. In contrast, according to Subs. 'Results of risk analysis' (p. 79) LIl caused higher individual risks in system model simulations than MLS. This disagreement originates from the default model of the risk factor HRR_{max} which leads to random scenarios with maximum HRRs of $\mathrm{HRR}_{max} \leq 100\,\mathrm{MW}$ in the risk analyses $\mathcal{R}_{D,f}$, $\mathcal{R}_{D,LIl}$ and $\mathcal{R}_I$. Consequently, the particular shape of $\bar{\boldsymbol{\xi}}^{\mathrm{LIl}}$ identified in Subs. 'Shape of the RSM' (p. 75) at the outer vertices of $\mathrm{HRR}_{max} \approx 200\,\mathrm{MW}$ has no effect. Accordingly, there is no contradiction to the conclusions in Subs. 'Summary and conclusion' (p. 80) that the particular shape of LIl raises the individual risks.

These results corroborate the conclusions in Section E.2.5 that MLS and LIl lead to similar results. They also confirm Section E.4.2 that the metamodel uncertainty and in this subsection also the evacuation uncertainty further reduce the sensitivity to variations in the ED. This conclusion again manifests that the metamodel uncertainty and evacuation uncertainty are important for risk analysis stated in Section E.4.1. Additionally, the results again exemplify that the selection of the ED is less important for risk analyses as already concluded in Section E.4.2. And finally, variations in the ED as well as different response surface methods together with variations in the ED cause smaller effects on risk measures than the variations of accepted risk measures discussed in Section B.5. In other words, differences in the design of the metamodel lead to variations in the results of risk analysis that seem to be acceptable with regard to general variations in risk measures described in literature. Therefore, the methodology for risk analysis leads to reproducible results and substantiates the conclusion in Section E.4.2.

Plausibility of risk measures

The scrutiny now culminates in the discussion of the plausibility of the risk measures. For this, the discussion follows the approach of falsification outlined in Section B.5, in more detail, the comparison to two observations: first, to the accepted risk measures, i.e. the accepted individual risk with $10^{-6}\frac{1}{\mathrm{year}} \leq \mathcal{R}^{ind}_{accepted} \leq 10^{-4}\frac{1}{\mathrm{year}}$ and the limiting $\mathcal{R}^{soc}_{limit}$ as well as the accepted societal risk curves $\mathcal{R}^{soc}_{accepted}$ depicted in Fig. E.30; and second, the societal risk curves of other risk analyses in Wahlström 2018 [67, Fig. 6], esp. random scenarios with more than $N_{fat} > 100$ fatalities. Furthermore, it has to be kept in mind that the focus on the upper evacuation area described in Section B.3 leads to elevated individual risks and the underestimation of high numbers of fatalities with effects on the societal risk curve. These two observations serve for the falsification of the results of a risk analysis. If the results clearly contradict the observations, then, the risk analysis seems not to be plausible, else, it could not be falsified. After the conclusions of Section E.4.1, the discussion focuses on the metamodel uncertainty and the evacuation uncertainty and hence, on the risk analyses $\mathcal{R}_{D,f}$, $\mathcal{R}_{D,\epsilon}$ and $\mathcal{R}_D$.

Tab. E.18 and Fig. E.30 provide the results of the individual risks and the societal risk curves. To begin, the risk analysis $\mathcal{R}_{D,f}$ disregarding the metamodel uncertainty and the evacuation uncertainty resulted in an individual risk within the accepted range. But the societal risk curve and above all the number of fatalities seem to be underestimated in comparison to both observations which is supposed to be a contradiction. Next, considering only the evacuation uncertainty, both risk measures of the risk analysis $\mathcal{R}_{D,\epsilon}$ seem to be in line with the observations. And at last, the risk analysis $\mathcal{R}_D$ noticeably overestimated random scenarios

with small numbers of fatalities. This outcome derives from the drawback of the prediction interval method and appears to contradict both observations on the societal risk curve.

To conclude, the results of the risk analyses $\mathcal{R}_{D,f}$ and $\mathcal{R}_D$ seem not to be plausible whereas the results of $\mathcal{R}_{D,\epsilon}$ could not be falsified. These results imply that the evacuation uncertainty increases the plausibility of the results of risk analysis whereas the metamodel uncertainty based on the current implementation of the prediction interval method counteracts. As a consequence, the results confirm the assumption 2 (plausibility) with regard to the evacuation uncertainty and refute it for the metamodel uncertainty. But Section E.2.1 describes two approaches to improve the metamodel uncertainty and App. G.9 exemplifies one. After an improvement, future results might finally also confirm assumption 2 (plausibility) with regard to the metamodel uncertainty.

The effect of the risk analyst

Section B.1 introduces epistemic uncertainties as result from lack of knowledge, e.g. with regard to the selection of the model by the developer of the risk analysis, shortly risk analyst. For instance, the risk analyses $\mathcal{R}_I$ and $\mathcal{R}_{D,f}$ were both based on reasonable assumptions in the point of view of the risk analyst, that is then for Berchtold 2016 [8] and now for this dissertation. These risk analyses had the same focus and accordingly the same assumptions on the metamodel uncertainty and the evacuation uncertainty. But the risk analyst decided to select different response surface methods and different EDs. Subs. 'Effects of the metamodel' (p. 104) fortunately uncovers that the risk analyses $\mathcal{R}_I$ and $\mathcal{R}_{D,f}$ lead to reproducible results.

Evidently, the risk analyst has more options in the setup of the metamodel and these options can of course affect the results of risk analyses. One example is the integration, or disregarding, of the metamodel uncertainty or the evacuation uncertainty into risk analysis as can be seen in other methodologies for risk analyses in fire safety engineering outlined in Section B.1. Possible effects on the results are illustrated in Fig. E.27 (p. 94). Another example is the selection of a different response surface method, e.g. LIn. Section A.1 outlines methodologies for risk analysis of road tunnels using LIn and Subs. 'Summary and conclusion' (p. 80) in Section E.2.5 summarises possible outcomes. The risk analyst has even more options in the system model, e.g. multiple models for nodes like the maximum HRR or the frequency of scenarios referenced in App. G.2 and in general a variety of different references for models for other risk factors. This variety of models also implies the use of approaches like imprecise probabilities discussed by Berner 2016 [48]. And all these different models might have unknown effects on the results of risk analysis.

At least, this issue is an interesting research topic referring to the validity of the results of risk analysis discussed in Goerlandt 2017 [24, p. 123]. A possible approach could be a systematic setup of a system model from small complexity to high complexity in its structure hand in hand with a continuous sensitivity analysis. For such a study, the methodology for risk analysis in this dissertation, with the graph structure for the system model, the efficiency of the metamodel and the identification of most important risk factors, provides a profound basis.

F Summary and conclusions

Section A.1 outlines the background for risk analysis of road tunnels and derives that the analysis of consequences in complex scenarios requires complex models as well as multiple risk factors (assumption 1). Assumption 1 can arise to a challenge for risk analyses, namely that the complex model and the global objective limit the number of risk factors as well as the number of scenarios computed with the complex model. These limitations again limit the complexity of scenarios considered in the risk analysis. The motivation of this dissertation is to overcome this challenge and to allow an increased complexity of scenarios in risk to take into account the increasing complexity of real fire scenarios.

For this reason, an innovative methodology for risk analysis of road tunnels was developed in this dissertation with two objectives: to introduce a metamodel in the methodology in order to integrate complex scenarios into risk analysis (objective 1); and to achieve an efficient metamodel to be able to focus on the complexity in scenarios (objective 2). Finally, the plausibility of the results of risk analysis was questioned under the assumption that the metamodel uncertainty and the evacuation uncertainty contribute to an increased plausibility of the results (assumption 2).

This chapter first outlines how both objectives of this dissertation were achieved and the assumptions either confirmed or refuted. Then, it draws the final conclusions of this dissertation and lastly discusses the expected impact.

Querying the assumptions and objectives of this dissertation

Assumption 1 (complex scenarios) states that the analysis of consequences in complex scenarios requires complex models as well as multiple risk factors. To question this assumption, this dissertation describes a complex scenario in the system model and discusses its complexity in Section B.3. Furthermore, the metamodel comprises the PAD as well as MLS methods which are both suitable for a high number of risk factors as discussed for MLS in Section D.1.3. Finally, it is concluded in Section E.4.3 that: firstly, microscopic evacuation models are not required because of only few interactions among the tunnel users; secondly, CFD models are important for risk analysis due to the individual alarm of tunnel users by the perception of smoke, e.g. influenced by the emergency ventilation; and thirdly, the most important risk factors, namely the maximum HRR, the failure of tunnel alarm and the time to the maximum HRR are directly linked to the complex model as shown in Fig. B.1 on p. 16 which shows the relevance of multiple risk factors in complex scenarios. In summary, these conclusions refute assumption 1 for microscopic evacuation models but confirm assumption 1 for CFD models as well as for multiple risk factors.

According to objective 1 (metamodel), the metamodel should be able to integrate complex scenarios into risk analysis. For this, PAD and MLS both direct at the global objective of risk analysis as outlined in Section C.1 and Section D.1.3. Furthermore, the verification and validation in Section E.2.1 show that MLS leads to adequate results and that the metamodel uncertainty is important for the metamodel despite the drawback of the prediction interval method. These conclusions provide the basis for objective 1. Objective 1 comprises three different parts which are outlined in the following three paragraphs. In the paragraphs it is deduced that: a) MLS, b) the direct approach and c) the metamodel and its integration into

risk analysis contribute to objective 1. Thus, these conclusions prove that the methodology for risk analysis with the metamodel achieves objective 1.

For objective 1a, it is concluded in Section E.2.5 that the default RSM represents the results of the complex model and is able to direct at the global objective of risk analysis. This conclusion bases also on: firstly, the specification of the default RSM in Subs. 'Convergence of the RSM and the prediction variance' (p. 60) in Section E.2.2; secondly, Section E.2.3 which states that the accuracy of the default RSM corresponds to the prediction interval; and finally, the results of Section E.2.4 deduce that MLS reproduces the results of complex response surfaces on the entire domain.

Objective 1b covers the reproduction of the evacuation uncertainty of the complex model within the metamodel. In order to reach this objective, the direct approach was originally developed in this dissertation based on the results in Subs. 'Distribution type' (p. 82) demonstrating the relevance of such approach. It follows the calibration and validation process of the direct approach, e.g. the limitation of outliers in the evacuation uncertainty in Subs. 'Outliers in the relative evacuation uncertainty' (p. 87). The calibrations in Subs. 'Combination mode' (p. 86) and Subs. 'Number of neighbours' (p. 88) lead to the high spatial sensitivity of the direct approach required for the realistic representation of the ORSs. In Subs. 'Number of replications' (p. 90) it is also concluded that 200 replications of evacuation scenarios are sufficient to reproduce the evacuation uncertainty which backs the conclusions in Subs. 'Number of replications' (p. 81). To end this argumentation, Section E.3.2 summarises that the direct approach represents the evacuation uncertainties of the complex model.

For the last part of objective 1, objective 1c claims that the methodology for risk analysis leads to reproducible results. Therefore, App. G.8 provides the necessary background stating that the integration of the RSM into the system model with indirect mode over fixed points is accurate and that the risk measures converge in Monte-Carlo simulations with 10^6 random scenarios. Then, the evaluation of the sequential refinement of the metamodel in Section E.4.2 leads to the conclusion that the default RSM is sufficiently accurate and that the methodology for risk analysis leads to reproducible results. Section E.4.4 corroborates this conclusion in Subs. 'Reproducibility of the most important risk factors' (p. 102) as well as further discussions in Subs. 'Effects of the metamodel' (p. 104).

Objective 2 (efficiency) is concerned with the efficiency of the metamodel. For this, two approaches within the PAD described in Section C.2 aim at the efficiency of the metamodel: the focused sequential refinement as well as the combination of EDs. Both approaches have been developed in this dissertation. To prove objective 2: firstly, it is stated in Subs. 'Convergence of the RSM and the prediction variance' (p. 60) of Section E.2.2 that the data base of the default RSM with simulations of ten fire scenarios with the CFD model and simulations of $2 \cdot 96$ evacuation scenarios for TA and FA with the microscopic evacuation model is sufficient for the convergence of the results of the RSM; secondly, the conclusion of Subs. 'Focused sequential refinement in comparison to the batch design' (p. 66) sais that the focused sequential refinement can reduce the metamodel uncertainty efficiently and prevents conservative guesses of the number of simulations with the complex model; and thirdly, Berchtold 2018 [9] highlights that the combination of EDs allows a small number of simulations with the CFD model. Nota bene, the convergence depends on the specific shape of the response surface. Additionally, the other response surface methods evaluated in Section E.2.5 lacked for real analogies in the response surface. For these reasons, the efficiency was not quantified in comparison to other response surface methods but the metamodel based on MLS and PAD achieves objective 2 esp. through the focused sequential refinement and the combination of EDs.

At last, assumption 2 claims that the metamodel uncertainty as well as the evacuation uncertainty are required to increase the plausibility of results of risk analysis. To question this assumption, Section B.5 describes the evaluation of the plausibility of risk measures by falsification. Then in a first step, it is concluded in Section E.4.1 that the combined integration of the metamodel uncertainty and the evacuation uncertainty is important for risk analysis which is necessary for the assumption 2. On top, the results in Section E.4.2 and Subs. 'Effects of the metamodel' (p. 104) of Section E.4.4 assert the importance of the metamodel uncertainty and evacuation uncertainty for risk analysis. Finally in Subs. 'Plausibility of risk measures' (p. 105), the risk measures are compared to accepted risk measures and societal risk curves of other risk analyses of road tunnels and it is concluded that: firstly, the evacuation uncertainty contributes to an increased plausibility; and secondly, the metamodel uncertainty might contribute to an increased plausibility. The effect of the metamodel uncertainty depends on its further improvement. Two potential improvements were outlined in Section E.2.1 and one is illustrated in App. G.9. Consequently, the results confirm assumption 2 with regard to the evacuation uncertainty but for now refute assumption 2 with regard to the metamodel uncertainty.

Closing conclusions

The metamodel, namely the RSM together with the metamodel uncertainty and the evacuation uncertainty, achieves both objectives of this dissertation. Though the efficiency was not compared to other response surface methods, Section E.2.5 reveals a lower generalisation error of MLS compared to LIn for the data base of the default RSM. This result proofs the increased efficiency of the metamodel in comparison to the direct use of discrete scenarios. Hence, it confirms the hypothesis that a metamodel constitutes a possible solution to the challenge stated in Section A.1. Summing up, the metamodel within the innovative methodology for risk analysis allows to consider an increased complexity of scenarios. Accordingly, the metamodel is suitable to reproduce all necessary interactions of real fire scenarios for the evaluation of safety measures, which seems of particular interest with regard to their growing complexity.

Section B.1 outlines the metamodels of other methodologies for risk analysis of road tunnels and in fire safety engineering. As a result, methodologies for risk analysis of road tunnels often use discrete scenarios in the consequence model whereas metamodels, like the mapping approach, are rarely applied. Methodologies for risk analysis in fire safety engineering more often apply metamodels. These metamodels are commonly used for deterministic models like fire models and their sequential refinement focuses on the local objective. Finally, the methodologies rarely consider the effect of the metamodel uncertainty on the results of risk analysis. In contrast: the metamodel developed in this dissertation is applicable on stochastic models; the sequential refinement directs at the global objective, in particular on regions of the domain with increased metamodel uncertainty; and the metamodel uncertainty is considered in the results of risk analysis. For these three reasons and with respect to the importance of the metamodel uncertainty and the evacuation uncertainty for the results of risk analysis, the metamodel is an advancement among methodologies for risk analysis of road tunnels and in general for fire safety engineering.

Expected impact of this dissertation

The advanced metamodel and the innovative methodology for risk analysis of this dissertation can have an impact in three different parts: firstly, risk analysis of road tunnels; secondly, risk analysis in fire safety engineering; and thirdly, on various other issues in engineering apart from the risk analysis. The metamodel and the methodology for risk analysis both employed

in these parts could finally lead to an economic and social impact because of an efficiently increased level of safety.

Firstly, other methodologies for risk analysis of road tunnels could adopt parts of this methodology as mentioned in Subs. 'Current state of methodologies for risk analysis of road tunnels' (p. 2). Esp. parts leading to the increased efficiency in the analysis of consequences might be useful: namely, the metamodel using MLS and PAD in general; and in particular, the PAD method with the sequential refinement, the focus on high metamodel uncertainties as well as, if required, the combination of EDs. Finally, these parts could help to consider more interactions during the evaluation of scenarios.

Secondly, as a consequence of the advanced metamodel, the methodology for risk analysis might be also interesting for risk analysis of other complex systems with focus on fire safety engineering. To facilitate the application on other complex systems, the methodology applies flexible methods. In particular, the structure of the system model, realised with a directed acyclic graph, has a clear structure and a high flexibility. The implementation of the directed acyclic graph is shortly outlined in App. G.3. Also, the CFD model FDS and the microscopic evacuation model FDS+Evac can be used in general for fire safety engineering.

Thirdly, the generic metamodel is widely applicable on other issues with similar challenges. In particular, the metamodel: is suitable for multiple control variables, also for more than four control variables as shown in this dissertation; can reproduce complex response surfaces with global objective as illustrated in Section E.2.4; and can use results of stochastic and deterministic complex models as data base. Consequently, the metamodel is also applicable for time consuming experiments with multiple control variables and global objective as they are common in the assessment of the safety of structures.

Last but not least, the direct approach can contribute to the impact because of three characteristics. One important characteristic is that the direct approach avoids assumptions on the distribution type which is important for ORSs subjected to different unknown probability distributions as depicted in Subs. 'Distribution type' (p. 82). Another important characteristic is its high spatial sensitivity which allows large variations in aleatory uncertainties in the results of different, also neighbouring, data points as discussed in Subs. 'Combination mode' (p. 86). The background for the high spatial sensitivity are the relative combination of ORSs and the relative integration into the metamodel described in Section D.3. Finally, the direct approach is also applicable on small number of replications as discussed in Subs. 'Number of replications' (p. 90). This characteristic might be useful for stochastic models with increased computational cost, e.g. microscopic evacuation models in comparison to one-dimensional evacuation models.

Bibliography

[1] Haukur Ingason. "New Challenges in Tunnel Fire Safety". In: *Fire Technology* 52.5 (2016), pp. 1445–1447. ISSN: 0015-2684.

[2] Nigel Casey, Michael A. Regan, and Asif Hassan. "A Methodology for Assessing Driver Behaviour and Improving Safety and Customer Experience in Long Urban Road Tunnels". In: *Eighth International Symposium on Tunnel Safety and Security (ISTSS): RISE Report 2018:13*. Ed. by RISE Research Institutes of Sweden. 2018, pp. 651–666. ISBN: 978-91-88695-48-2.

[3] Marius H. Raddum and Rolf Mellum. "Public Investigation of Fire in Tank Trailer in the Skate- Straum Tunnel in Sogn og Fjordane County on 15th of July 2015". In: *Eighth International Symposium on Tunnel Safety and Security (ISTSS): RISE Report 2018:13*. Ed. by RISE Research Institutes of Sweden. 2018, pp. 131–144. ISBN: 978-91-88695-48-2.

[4] Yacov Y. Haimes. "Risk Modeling of Interdependent Complex Systems of Systems: Theory and Practice". In: *Risk analysis : an official publication of the Society for Risk Analysis* 38.1 (2018), pp. 84–98. ISSN: 1539-6924.

[5] Anders Jensen and Terje Aven. "A new definition of complexity in a risk analysis setting". In: *Reliability Engineering & System Safety* 171 (2018), pp. 169–173. ISSN: 09518320.

[6] Ying Zhen Li. "Overview of tunnel fire research". In: *Eighth International Symposium on Tunnel Safety and Security (ISTSS): RISE Report 2018:13*. Ed. by RISE Research Institutes of Sweden. 2018, pp. 29–46. ISBN: 978-91-88695-48-2.

[7] European Parliament and the council of the European Union. "Directive 2004/54/EC of the European Parliament and of the Council of 29 April 2004 on minimum safety requirements for tunnels in the trans-European road network". In: *Official Journal of the European Union* (2004), pp. L201/56–76.

[8] Florian Berchtold et al. "Risk analysis in road tunnels - Most important risk indicators". In: *Seventh International Symposium on Tunnel Safety and Security (ISTSS)*. Ed. by SP Technical Research Institute of Sweden. 2016, pp. 637–648.

[9] Florian Berchtold et al. "Risk analysis for road tunnels - a metamodel to efficiently integrate complex fire scenarios". In: *Eighth International Symposium on Tunnel Safety and Security (ISTSS): RISE Report 2018:13*. Ed. by RISE Research Institutes of Sweden. 2018, pp. 349–360. ISBN: 978-91-88695-48-2.

[10] Thomas J. Santner, Brian J. Williams, and William I. Notz. *The Design and Analysis of Computer Experiments*. Springer Series in Statistics. New York, NY: Springer New York, 2003. ISBN: 978-1-4419-2992-1.

[11] National Institute of Standards and Technology. *Fire Dynamics Simulator (Version 6.3.1): User's Guide: NIST Special Publication 1019*. Gaithersburg, Maryland (USA), 2016.

[12] World Road Association. *Current practice for risk evaluation for road tunnels: Technical Committee C.4 Road Tunnel Operation: 2012R23EN*. Paris: World Road Association (PIARC), 2012. ISBN: 978-2-84060-290-3.

[13] Bundesanstalt für Straßenwesen (BASt). *Bewertung der Sicherheit von Strassentunneln*. Bremerhaven: Wirtschaftsverlag NW, Verlag für Neue Wissenschaft GmbH, 2009. ISBN: 978-3-86509-909-9.

[14] ILF Consulting Engineers. *Erweiterung und Vertiefung des österr. Tunnelmodells - TuRisMo 2: Arbeitsbericht zum Arbeitsausschuss Tunnel-Sicherheit: 31.03.2015*. Ed. by ILF Consulting Engineers. Linz, 31.03.2015.

[15] Matthias Schubert et al. *Development of a best practice methodology for risk assessment in road tunnels: Research project ASTRA 2009/001*. Bern, 2011.

[16] Rijkswaterstaat Bouwdienst. *Het RWSQRA-model voor wegtunnels: Versie 1.1, Definitief: RWS 4818-2006-0091*. Ed. by Rijkswaterstaat Bouwdienst. Rotterdam, 2006-04-28.

[17] Mirjam Nelisse and A. C. W. M. Vrouwenvelder. "Probability of a large fire in a road tunnel - a Bayesian approach". In: *Seventh International Symposium on Tunnel Safety and Security (ISTSS)*. Ed. by SP Technical Research Institute of Sweden. 2016, pp. 659–670.

[18] Florian Berchtold et al. "Review of road tunnel risk assessment - common aspects?" In: *Sixth International Symposium on Tunnel Safety and Security (ISTSS)*. Ed. by SP Technical Research Institute of Sweden. 2014, pp. 669–670.

[19] Oxford dictionary. *oxforddictionaries.com*. 2018. URL: `https://en.oxforddictionaries.com/` (visited on 06/14/2018).

[20] Raymond H. Myers and Douglas C. Montgomery. *Response surface methodology: Process and product optimization using designed experiments*. 2nd ed. Wiley series in probability and statistics. New York: J. Wiley, 2002. ISBN: 0-471-41255-4.

[21] Nestor V. Queipo et al. "Surrogate-based analysis and optimization". In: *Progress in Aerospace Sciences* 41.1 (2005), pp. 1–28. ISSN: 03760421.

[22] Saideep Nannapaneni and Sankaran Mahadevan. "Reliability analysis under epistemic uncertainty". In: *Reliability Engineering & System Safety* 155 (2016), pp. 9–20. ISSN: 09518320.

[23] Anders Lönnermark and Haukur Ingason. "Recent achievements regarding heat release and temperatures during fires in tunnels". In: *Safety in Infrastructure*. 2004.

[24] Floris Goerlandt, Nima Khakzad, and Genserik Reniers. "Special Issue: Risk Analysis Validation and Trust in Risk management". In: *Safety Science* 99 (2017), pp. 123–126. ISSN: 09257535.

[25] Jason L. Loeppky, Leslie M. Moore, and Brian J. Williams. "Projection array based designs for computer experiments". In: *Journal of Statistical Planning and Inference* 142.6 (2012), pp. 1493–1505. ISSN: 03783758.

[26] M. D. McKay, R. J. Beckman, and W. J. Conover. "A Comparison of Three Methods for Selecting Values of Input Variables in the Analysis of Output from a Computer Code". In: *Technometrics* 21.2 (1979), pp. 239–245. ISSN: 00401706. DOI: 10.2307/1268522.

[27] P. Lancaster and K. Salkauskas. "Surfaces Generated by Moving Least Squares Methods". In: *Mathematics of Computation* 37.155 (1981), p. 141. ISSN: 0025-5718.

[28] Chwail Kim and K. K. Choi. "Reliability-Based Design Optimization Using Response Surface Method With Prediction Interval Estimation". In: *Journal of Mechanical Design* 130.12 (2008), 121401:1–121401:12. ISSN: 10500472.

[29] Peter Salemi, Barry L. Nelson, and Jeremy Staum. "Moving Least Squares Regression for High-Dimensional Stochastic Simulation Metamodeling". In: *ACM Transactions on Modeling and Computer Simulation* 26.3 (2016), pp. 1–25. ISSN: 10493301.

[30] Cornelius Albrecht. "Quantifying life safety Part I: Scenario-based quantification". In: *Fire Safety Journal* 64 (2014), pp. 87–94. ISSN: 03797112.

[31] C. Albrecht and D. Hosser. "A Response Surface Methodology for Probabilistic Life Safety Analysis using Advanced Fire Engineering Tools". In: *Fire Safety Science* 10 (2011), pp. 1059–1072. ISSN: 18174299.

[32] Gianluca de Sanctis and Mario Fontana. "Risk-based optimisation of fire safety egress provisions based on the LQI acceptance criterion". In: *Reliability Engineering & System Safety* 152 (2016), pp. 339–350. ISSN: 09518320.

[33] Bart van Weyenberge et al. "Response surface modelling in quantitative risk analysis for life safety in case of fire". In: *Fire Safety Journal* 91 (2017), pp. 1007–1015. ISSN: 03797112.

[34] Bart van Weyenberge et al. "Development of a Risk Assessment Method for Life Safety in Case of Fire in Rail Tunnels". In: *Fire Technology* 52.5 (2016), pp. 1465–1479. ISSN: 0015-2684.

[35] Austin Anderson and Ofodike A. Ezekoye. "Quantifying Generalized Residential Fire Risk Using Ensemble Fire Models with Survey and Physical Data". In: *Fire Technology* 43.2 (2018), p. 127. ISSN: 0015-2684.

[36] M. Estecahandy et al. "Some acceleration methods for Monte Carlo simulation of rare events". In: *Reliability Engineering & System Safety* 144 (2015), pp. 296–310. ISSN: 09518320.

[37] International Organization for Standardization. *ISO 16732-1: Fire safety engineering - Fire risk assessment - Part 1: general*. Geneva, 2012.

[38] Qiang Meng et al. "Quantitative Risk Assessment Modeling for Nonhomogeneous Urban Road Tunnels". In: *Risk Analysis* 31.3 (2011), pp. 382–403. ISSN: 0272-4332.

[39] G. De Sanctis et al. "Combining engineering and data-driven approaches: Development of a generic fire risk model facilitating calibration". In: *Fire Safety Journal* 70 (2014), pp. 23–33. ISSN: 03797112.

[40] David A. Purser. "Toxicity Assessment of Combustion Products". In: *SFPE Handbook of Fire Protection Engineering*. Ed. by Philip J. DiNenno et al. Quincy Massachusetts, 2003, pp. 2/83–2/171.

[41] Armen Der Kiureghian and Ove Ditlevsen. "Aleatory or epistemic? Does it matter?" In: *Structural Safety* 31.2 (2009), pp. 105–112. ISSN: 01674730.

[42] Ciro Caliendo et al. "Simulation of People Evacuation in the Event of a Road Tunnel Fire". In: *Procedia - Social and Behavioral Sciences* 53 (2012), pp. 178–188. ISSN: 18770428.

[43] Enrico Ronchi, Paul A. Reneke, and Richard D. Peacock. "A Method for the Analysis of Behavioural Uncertainty in Evacuation Modelling". In: *Fire Technology* 50.6 (2014), pp. 1545–1571. ISSN: 0015-2684.

[44] Ruggiero Lovreglio, Enrico Ronchi, and Dino Borri. "The validation of evacuation simulation models through the analysis of behavioural uncertainty". In: *Reliability Engineering & System Safety* 131 (2014), pp. 166–174. ISSN: 09518320.

[45] Hans J. Pasman, William J. Rogers, and M. Sam Mannan. “Risk assessment: What is it worth? Shall we just do away with it, or can it do a better job?” In: *Safety Science* 99 (2017), pp. 140–155. ISSN: 09257535. DOI: 10.1016/j.ssci.2017.01.011.

[46] Terje Aven. *Foundations of risk analysis*. 2nd ed. New York: John Wiley & Sons, 2012. ISBN: 978-1-119-966975.

[47] Terje Aven and Bodil S. Krohn. “A new perspective on how to understand, assess and manage risk and the unforeseen”. In: *Reliability Engineering & System Safety* 121 (2014), pp. 1–10. ISSN: 09518320.

[48] C. Berner and R. Flage. “Strengthening quantitative risk assessments by systematic treatment of uncertain assumptions”. In: *Reliability Engineering & System Safety* 151 (2016), pp. 46–59. ISSN: 09518320.

[49] Sven Ove Hansson and Terje Aven. “Is Risk Analysis Scientific?” In: *Risk Analysis* 34.7 (2014), pp. 1173–1183. ISSN: 0272-4332.

[50] Forschungsgesellschaft für Straßen- und Verkehrswesen (FGSV). *Richtlinien für die Ausstattung und den Betrieb von Straßentunneln: RABT*. Ed. by Forschungsgesellschaft für Straßen- und Verkehrswesen (FGSV). Köln, 2006.

[51] Armin Seyfried et al. “New Insights into Pedestrian Flow Through Bottlenecks”. In: *Transportation Science* 43.3 (2009), pp. 395–406. ISSN: 0041-1655.

[52] Timo Korhonen and Simo Hostikka. *Fire Dynamics Simulator with Evacuation: FDS+Evac 2.2.1: Technical Reference and User’s Guide*. Ed. by VTT Technical Research Centre of Finland. 2009.

[53] Benjamin Schröder. *Multivariate Methods for Life Safety Analysis in Case of Fire*. Vol. 34. Schriften des Forschungszentrums Jülich IAS Series. Jülich: Forschungszentrum, Zentralbibliothek, 2016. ISBN: 978-3-95806-254-2.

[54] Benjamin Truchot and Guillaume Leroy. “Fire Safety Engineering Method Evaluation Based on a Real Tunnel Fire Case”. In: *Eighth International Symposium on Tunnel Safety and Security (ISTSS): RISE Report 2018:13*. Ed. by RISE Research Institutes of Sweden. 2018, pp. 515–526. ISBN: 978-91-88695-48-2.

[55] Miho Seike, Nobuyoshi Kawabata, and Masato Hasegawa. “Quantitative assessment method for road tunnel fire safety: Development of an evacuation simulation method using CFD-derived smoke behavior”. In: *Safety Science* 94 (2017), pp. 116–127. ISSN: 09257535.

[56] Enrico Ronchi. “Testing the predictive capabilities of evacuation models for tunnel fire safety analysis”. In: *Safety Science* 59 (2013), pp. 141–153. ISSN: 09257535.

[57] Weichen Liao et al. “Validation of FDS+Evac for Pedestrian Simulations in Wide Bottlenecks”. In: *IEEE 17th International Conference on Intelligent Transportation Systems (ITSC)*. 2014, pp. 554–559.

[58] Haukur Ingason. “Design fire curves for tunnels”. In: *Fire Safety Journal* 44.2 (2009), pp. 259–265. ISSN: 03797112.

[59] Centre d’Études des Tunnels. *Guide to Road Tunnel Safety Documentation: Booklet 4: Specific Hazard Investigations*. Bron (France), 2003.

[60] Jeremy Fraser-Mitchell and David A. Charters. “Human Behaviour in Tunnel Fire Incidents”. In: *Eighth International Symposium on Fire Safety Science*. Ed. by International Association for Fire Safety Science. 2005, pp. 543–554.

[61] World Road Association. *Fire and Smoke Control in Road Tunnels: PIARC Committee on Road tunnels C.5: 05.05.B*. Ed. by World Road Association. Paris, 1999.

[62] Enrico Ronchi et al. “Representation of the Impact of Smoke on Agent Walking Speeds in Evacuation Models”. In: *Fire Technology* 49.2 (2013), pp. 411–431. ISSN: 0015-2684.

[63] Bradley Efron. “Nonparametric estimates of standard error: The jackknife, the bootstrap and other methods”. In: *Biometrika* 68.3 (1981), pp. 589–599. ISSN: 0006-3444.

[64] Daniel Zwillinger and Stephen Kokoska. *Standard probability and statistics tables*. Boca Raton, Fla.: Chapman & Hall, 1999. ISBN: 1-58488-059-7.

[65] B. J. Arends et al. “Evaluation of tunnel safety: towards an economic safety optimum”. In: *Reliability Engineering & System Safety* 90 (2005), pp. 217–228. ISSN: 09518320.

[66] J. K. Vrijling, W. van Hengel, and R.J Houben. “Acceptable risk as a basis for design”. In: *Reliability Engineering & System Safety* 59.1 (1998), pp. 141–150. ISSN: 09518320.

[67] Bo Wahlström et al. “Common life safety targets in traffic tunnels”. In: *Eighth International Symposium on Tunnel Safety and Security (ISTSS): RISE Report 2018:13*. Ed. by RISE Research Institutes of Sweden. 2018, pp. 175–185. ISBN: 978-91-88695-48-2.

[68] T. Bedford and Roger M. Cooke. *Probabilistic risk analysis: Foundations and methods*. Cambridge et al.: Cambridge University Press, 2001. ISBN: 0521773202.

[69] Michael D. Shields et al. “Refined Stratified Sampling for efficient Monte Carlo based uncertainty quantification”. In: *Reliability Engineering & System Safety* 142 (2015), pp. 310–325. ISSN: 09518320.

[70] Thomas Most and Christian Bucher. “New concepts for moving least squares: An interpolating non-singular weighting function and weighted nodal least squares”. In: *Engineering Analysis with Boundary Elements* 32.6 (2008), pp. 461–470. ISSN: 09557997.

[71] Richard D. Peacock, William D. Reneke, and Walter W. Jones Davis. “Quantifying fire model evaluation using functional analysis”. In: *Fire Safety Journal* 33 (1999), pp. 167–184. ISSN: 03797112.

G Appendix

G.1 Definition of terms

Terms related to risk analysis

The understanding of the term **risk** in this dissertation bases on: first, the meaning of Kaplan with 'The notion of risk, therefore, involves both uncertainty and some kind of loss or damage that might be received.' [72, p. 12]; second and more recently, 'Risk is often expressed in terms of combination of the consequences of an event (including changes in circumstances) and the associated likelihood of occurrence' [73, p. 1]; and third, with regard to fire risk analysis [74, p. 6], fire risk combines the expected frequency of a scenario and its expected damages. **Consequences** are the 'outcome of an event affecting objectives' [73, p. 1–6]. To be noted, the term **event** in this dissertation means a 'thing that happens or takes place, especially one of importance' [19], for instance the tunnel alarm, and therewith is in contrast to 'incident' or 'accident' (Note 3) [73, p. 4]. To complete, a scenario is understood as 'a postulated sequence or development of events' [19]. To sum up, 'risk' in this dissertation means the combination of frequencies and consequences of scenarios.

Risk analysis is the 'process to comprehend the nature of risk and to determine the level of risk' [73, p. 5]. Hence, the quantitative risk analysis quantifies the frequency of scenario and the possible damages, or fatalities, and further considers the effects of safety measures [74, p. 16, 44]. Often, the term 'risk assessment' is used equally to 'risk analysis'. But this dissertation distinguishes between both terms. Hence, **risk assessment** is the 'overall process of risk identification, risk analysis, and risk evaluation' [73, p. 4].

Term risk factor

Section A.1 introduces 'factors which have effects on risks' to specify scenarios. There are at least two common options to briefly name these factors: **risk indicator** or **risk factor**. With regard to the Oxford dictionary, an 'indicator' is a 'thing that indicates the state or level of something' and a factor is a 'circumstance, fact, or influence that contributes to a result' [19]. WebOfScience revealed about 300 articles for 'risk indicator' and 31000 articles for 'risk factor' according to the search detailed in Tab. G.1. On the one hand, the term 'risk indicator' had different interpretations among these publications. For instance, a risk indicator is, first, a factor that indicates the risk in a system like the fatality rate [75, p. 97] or second, they 'characterise the system [...] and are input variables for the risk model. Risk indicators x are defined as any observable or measurable characteristic of the system influencing the risk' [76, p. 18]. The former use is in the meaning of **risk measure**; the latter use would be similar to the 'factors which have effects on risks' in this dissertation. On the other hand, the term 'risk factor' had consistent interpretations in several articles, e.g. 'factor that contributes to risks (in a Bayesian network)' [77, p. 515ff]. To conclude, 'risk factor' is more common and more specific than 'risk indicator'. Consequently, this dissertation applies the term risk factor for 'factors which have effects on risks' despite the former use of risk indicator in Berchtold 2016 [8] and Berchtold 2018 [9].

Furthermore, it is important to differentiate between risk factor and **variable**. A risk factor is a variable within the system model outlined in Section B.3. In particular, the term 'risk

Table G.1: Search items to get publications on 'risk indicator' and 'risk factor' (results from 2015).

item	risk indicator	risk factor
title	risk NEAR/0 indicator	risk NEAR/0 factor
data base	WebOfScience	WebOfScience
research field	Science Technology	Science Technology
type	Article	Article
research area	mathematics, engineering, physics, transportation, nuclear science technology	mathematics, engineering, physics
number of articles	292	31675

factor' emphasises the relation of a variable to risk analysis. Hence, it is similar to **control variable** of Subs. 'Distinction between deterministic and stochastic models' (p. G-2), i.e. its value has an effect on the risk of a scenario. With regard to Monte-Carlo simulations, the value of a risk factor depends on a probabilistic model causing aleatory uncertainties but this is not in the meaning of an **environmental variable**. To sum up, this dissertation mainly applies the term 'risk factor' in the meaning of control variables, only Chapter D uses the term 'control variable' to emphasise its general applicability and to be consistent with more general publications.

At last, risk factors allow to differentiate between scenarios quantitatively. E.g. the maximum pre-evacuation time among all tunnel users is a risk factor whereas the individual pre-evacuation time of one tunnel user cannot be used to differentiate between scenarios. Hence, the latter one is not a risk factor or control variable.

Terms related to the evaluation of the accuracy of models

In general, a model is a 'simplified description of a system' whereas a method is a 'particular procedure' [19]. The simplifications in a model demand the evaluation of its accuracy. Referring to fire safety engineering [78, p. 3f], the evaluation comprises: the **verification**, which is the 'process of determining that a calculation method implementation accurately represents the developer's conceptual description of the calculation method and the solution to the calculation method'; and the **validation**, namely the 'process of determining the degree to which a calculation method is an accurate representation of the real world from the perspective of the intended uses of the calculation method'. These, definitions for instance apply to the fire model or the evacuation model. And in the same line but in a more general context, Nannapaneni 2016 [22, p. 9] parts the evaluation into: the model **calibration** to 'estimate model parameters based on input / output data'; the model verification to 'quantify numerical solution errors'; and the model **validation** to 'identify model form errors [uncertainties] by comparison with physical observations'. To conclude, this dissertation rather relates to the latter definitions for the evaluation of the accuracy of the metamodel.

Distinction between deterministic and stochastic models

The description of models first requires the definition of variables. In the mathematical meaning, a **variable** is a 'quantity which during a calculation is assumed to vary or be capable of varying in value' [19]. In more detail, Santner 2003 [10, p. 15] differentiates between: **control variables** 'control the product or process'; and **environmental variables** 'depend on specific user or on the environment at the time the item is used', thus, environmental variables are 'random with a distribution that is known or unknown'. And to complete, Santner

2003 [10, p. 15] names 'model variables' which cause the 'uncertainty in the mathematical modelling that relates other inputs to outputs'. However, the latter term is not used in this dissertation.

Myers 2002 [20, p. 481] refers to two types of models, the deterministic model and the stochastic model. Accordingly, the results of a **deterministic model**, e.g. a fire model based on the CFD method or a zone model, mostly depend on control variables whereas environmental variables have only small effects. The latter statement relies on the experience with fire models that time dependent variations in local quantities like the temperature are small in comparison to the effects originating from variations in risk factors. Next, in case of a **stochastic model**, like an evacuation model, environmental variables prevail. Examples for environmental variables are the individual position or the individual pre-evacuation time of tunnel users. As a consequence, the results of stochastic models are subjected to aleatory uncertainties.

Remarks on the mathematical notation

The results of the consequence model are equally expressed in terms of the FF denoted with ξ as well as with the general symbol y. This ambiguity has mainly two reasons: first, y emphasises the general applicability of the metamodel, i.e. it is not limited to the FF of the consequence model; and second, y corresponds to other literature. Accordingly, the general notation with y is mainly used in Chapter D. To sum up, it yields $y \equiv \xi$ in this dissertation where both symbols follow the same conventions and hence, the nomenclature shows only symbols for the FF.

This dissertation applies a **bold symbols** for results of the consequence model. The bold notation highlights multiple results structured in column vectors or matrices in contrast to a single result. It serves to clarify mathematical functions. For instance, $\bar{\boldsymbol{\xi}}$ comprises results of the RSM at multiple arbitrary points whereas $\bar{\xi}$ denotes the result at a single arbitrary point. But the notation is not entirely consistent for better legibility in some parts, e.g. the symbol for the ED X is not bold.

Terms related to spatial

The term spatial is not limited to physical space but refers to an arbitrary space in the domain, i.e. the unit hypercube, of the ED. Two terms are also directly connected to spatial: **local** means spatially close or in a small region of the domain; and **global** labels a large region or the entire domain.

The term **shape of the response surface** describes the form of the response surface, e.g. with second derivatives or discontinuities. **Spatial sensitivity** has mainly two meanings related to: first, the correlation between a measure, e.g. the prediction variance, and the shape of the response surface; and second, the different effects of data points on the result of the RSM at an arbitrary point depending on their euclidean distances. Salemi 2016 [29, p. 8f] exemplifies the latter meaning with the '**prediction window**' outside which data points have no effect on a result of the result of the RSM.

The spatial sensitivity can be either low, high or even lead to discontinuities. First, the consideration of data points in a large region around an arbitrary point for a result leads to its low spatial sensitivity. An example is a global RSM where the regression coefficients are identical on the entire domain leading to equal effects of all data points. Second, the result of a highly spatially sensitive RSM considers only local data points to its arbitrary point. In other words, close data points have large effects on the result and data points with a large euclidean distance to the arbitrary point have only small effects. At last, **spatially discontinuous** is the discontinuous transition of a measure in the domain.

Terms related to data point or discrete scenarios

A **data point** represents a **discrete scenario** in an ED as well as its result simulated with the complex model. The term scenario is used with regard to risk analysis and to distinguish between fire scenarios and evacuation scenarios. The term data point: first, signalises the flexibility of the methods for other applications; second, emphasises simulations with the complex models and their results; and third, is used for abstract purposes, e.g. for the euclidean distance within the domain.

The terms neighbour and arbitrary point are closely related to data point. **Arbitrary point** denotes a scenario with random or arbitrary values of risk factors together with its result, e.g. determined with the metamodel. A **neighbour** is a data point of a subset of an ED $X_s \in X$ within a small euclidean distance around an arbitrary point.

G.2 Background for the system model

Section B.3 introduces the road tunnel, the risk factors and the intermediate nodes of the scenario in the system model. Now, this section provides the background together with the literature. To begin, the system model and in particular the tunnel geometry is not based on a particular tunnel but generally represents a common road tunnel in Germany.

G.2.1 Road tunnel

The tunnel geometry is mainly determined by its slope, its cross-section and the tunnel length and corresponds to German legislation [50, p. 11ff]. German legislation allows slopes in road tunnels of up to five percent. Thus, the system model assumes a slope of one percent to take into account its effect on the smoke spread, but still to be representative for other road tunnels. Also with regard to other road tunnels, the cross-section agrees with the common tunnel type 10.5 T, i.e. with a width of 9.5 m and the height of 4.5 m, for two lanes and bi-directional traffic. The evacuation paths in this tunnel type have a width of 1.5 m which already includes the safety margin to the road. However, the evacuation paths in the evacuation scenario of FDS+Evac described in Subs. 'Discrete scenario in FDS and FDS+Evac' (p. 20) have a width of two metres to enable tunnel users to overtake each other. At last, the tunnel length in the system model is set with the corresponding risk factor in App. G.2.2.

The layout of the road tunnel in the system model comprises: first, emergency exits; second, the emergency ventilation system; and third, the systems for fire detection and tunnel alarm. First, road tunnels with a length of more than 400 m are obliged to have emergency exits at least every 300 m [50, p. 35, 40]. Hence, the emergency exit in the system model lies in a distance of 150 m to the fire source and has a width of one metre. Second, German legislation allows longitudinal emergency ventilation systems until tunnel lengths of 1200 m [50, p. 22ff]. The system model comprises this ventilation system despite its risk factor can reach values of up to 3000 m. But the ventilation system is reasoned with: its conservativeness for tunnel lengths of more than 400 m because of its little sophistication; its suitability for the tunnel length within the complex model; and its suitability for tunnel lengths of up to 3000 m in case of uni-directional traffic. During the self-rescue phase, the longitudinal emergency ventilation system directs downward the road tunnel and maintains a gas velocity of less than 1.5 $\frac{\mathrm{m}}{\mathrm{s}}$ to not disturb the smoke layer. For the same reason, the fans are switched off within the smoke layer. And third, App. G.2.3 describes the remaining safety systems of the layout together with the intermediate nodes time of fire detection and time of tunnel alarm.

G.2.2 Risk factors

Second, the models of all risk factors are shortly summarised in Tab. B.2 on p. 16.

Maximum HRR HRR_{max} /MW

The default model of the maximum HRR stems from the methodology for risk analysis for road tunnels in Germany and is therewith valid for fully-developed fires ignited either as a consequence of accidents or by technical defects [13, p. 30]. To be noted, it excludes fires of dangerous goods vehicles and does not differentiate between cars and HGVs. In detail, the model comprises a discrete distribution for values of the maximum HRR from five to 100 MW. The default model was chosen for its application in Germany, but of course, other models are available: e.g. for Austria [14, p. 15] based on statistical data [79, p. 17], or for France [59, Apdx. C].

Other publications consider fires in road tunnels with maximum HRRs larger than 300 MW [61, p. 61; 80, p. 31; 81, p. 33]. Even more, Section A.1 mentions a real tunnel fire with an estimated maximum HRR of about 400 MW [3]. However, these publications mostly refer to fire scenarios related to dangerous goods vehicles. But an experiment in a road tunnel similar to the system model measures maximum HRRs of until 200 MW. And to complete, fires of cars in road tunnels commonly reach less than ten MW [23, p. 3; 61, p. 61; 82, p. A-1ff; 83, p. 2]. Concluding, the uniform distribution of the maximum HRR has the limits 25 MW and 200 MW for fires without dangerous goods where Subs. 'Metamodel' (p. 23) reasons the lower limit.

Time to maximum HRR t_{max} /s

Only few information on the time to maximum HRR of HGV fires in road tunnels exist. For instance, Lönnermark 2004 [23, p. 3] summarises ten experiments with the time to maximum HRR between eight and 18 minutes. Also, the French guide on specific hazard investigations in road tunnels [59, Apdx. C.1] suggests values of more than ten minutes for fire scenarios with maximum HRRs larger than 30 MW. According to these results, the default model for the time to maximum HRR bases on a uniform distribution between ten and 20 minutes.

Maximum pre-evacuation time t_{pre} /s

The pre-evacuation time begins with the alarm of tunnel users and ends when they start to move. Several studies on the pre-evacuation time of tunnel users are available, e.g. publications [60; 84; 85]. In particular, publications [59, Apdx. E.2; 86, p. 462; 87, p. 26] report short maximum pre-evacuation times of about 100 s. In contrast, other publications [61, p. 31; 88, p. 75] state large maximum pre-evacuation times of about 300 s. Summing up, the maximum pre-evacuation time of the system model is defined with a uniform distribution between 100 s and 300 s to cover the large range of possible values. But, this model does not consider tunnel users who stay in their vehicles.

Section B.3 establishes the uniform distribution of individual pre-evacuation times among tunnel users between zero and the maximum pre-evacuation time of a scenario. Therewith, it complies with a recommendation in RiMEA 2009 [89, p. 22]. However, RiMEA 2009 also recommends a normal distribution as well as Ronchi 2012 [88, p. 75] uses it. Additionally, Norén 2003 [90, p. 32ff] applies the normal distribution for the time to leave the car as well as for the 'hesitation time'. However, an evaluation of the pre-evacuation times mentioned in the previous paragraph uncovered clear variations in their standard deviation and in particular in their coefficient of variations. Furthermore, a screening in the evacuation scenario of

FDS+Evac identified strong effects of these parameters on the results of the simulations. The screening also implied that the uniform distribution leads to similar results as the normal distribution. For these reasons, the system model favours the uniform distribution.

Number of tunnel users N_{tu}

This risk factor comprises all tunnel users within the upper evacuation area next to the fire source. Its default model derives from BASt 2009 [91, p. 12] and depends on the risk factor ratio of HGV and on the intermediate node number of vehicles. The results of these nodes lead to the number of cars, HGVs and buses which are not rounded because of the small fraction of buses. Furthermore, BASt 2009 assumes that cars, HGVs and buses are occupied with 1.5, 1.1 and 40 tunnel users respectively. Finally, the number of tunnel users of all vehicles types sums up to the total number of tunnel users.

Next to the default model, the risk factor also comprises a uniform distribution with the limits of 30 and 180 tunnel users. These values respectively derive from the assumptions that, first, 30 cars, each with one occupant, line up over the entire length of the upper evacuation area, and second, that there are three buses and the rest of cars with a mean of about two tunnel users.

Failure of tunnel alarm fa

There are only few information on the probability of the failure of tunnel alarm in a road tunnel. Hence, it is supposed to be equal to the probability of failure of the fire detection system. This system fails in one percent of its demand assumed in the methodology of Germany [13, p. 30]. Also, a screening in the system model revealed that a variation of this probability within reasonable ranges had little effects on the results of risk analysis. Accordingly, the probability is a fix value which leads to FA in one percent of all scenarios.

Ratio of HGV χ_{HGV}

Different publications report the ratio of HGV of: twelve percent for Switzerland and Norway according to Schubert 2011 [15, p. 34]; 14% in Norway in 2014 [92, p. 104]; and 14% to 31% in Italian road tunnels in 2011 [93, p. 169]. With regard to Germany, the ratio of HGV with buses and dangerous goods vehicles varied between five and 45% on motorways in 2011 [94]. The ratio of buses among HGV is about five percent [91, p. 12]. Consequently, the risk factor adopts a uniform distribution between five percent and 45% including five percent of buses and therewith constitutes a general model to account for arbitrary road tunnels.

Average daily traffic volume $\dot{N}_{adtv}$ / $\frac{\text{veh.}}{\text{day}}$

As for the ratio of HGV, the average daily traffic volume also strongly depends on the section of a road. For example, two- and three-lane road tunnels in Italy are respectively used by 4500 to 40761 and by 11439 to 32260 vehicles per day [93, p. 169]. Additionally, Tab. G.2 exemplifies some values for German highways and federal roads with two lanes in 2011 [94]. As a result, the average daily traffic volume in Caliendo 2012 [93, p. 169] seems to be reasonable for the general model of the road tunnel in the system model with its two lanes and the bi-directional traffic. For this reason, the uniform distribution in this risk factor has the limits of 5000 $\frac{\text{veh.}}{\text{day}}$ and 40000 $\frac{\text{veh.}}{\text{day}}$ vehicles per day. To be noted, the values of this risk factor always yield for both directions.

Table G.2: Tunnel length l_{tunnel} and average daily traffic volume $\dot{N}_{adtv}$ for road tunnels in Germany with bi-directional traffic and two lanes based on BASt 2011 [94]; the roads are either abbreviated with 'A' for highway or 'B' for federal road; some information beside from the traffic data are based on wikipedia.de.

name	road	section	l_{tunnel} /km	$\dot{N}_{adtv}$/, $\frac{\text{veh.}}{\text{day}}$
Malbergtunnel	B260	Fachbach-Bad Ems	1.6	10000
Bürgerwaldtunnel	A98	Tiengen-West - Lauchringen	1.435	9500
Gmünder Einhorn Tunnel	B29	Haupttunnel [95]	1.687	19600
Saukopftunnel	B38	LG Saukopftunnel - L3408	2.715	15200
Michaelstunnel	B500	Tunnel Baden-Baden - L500 KVP Cite Baden-Baden	2.544	31200
Heslacher Tunnel	B14	Vaihingen - Heslach West	2.300	33200

Tunnel length l_{tunnel} /km

The tunnel length derives from values of BASt 2011 [94] exemplified in Tab. G.2. Thus, the general model of the risk factor applies a uniform distribution between one and three kilometres.

G.2.3 Intermediate nodes

Third, the section continues with the background to the intermediate nodes which were introduced in Section B.3.

Frequency of scenarios f_{sc} / $\frac{1}{\text{year}}$

The model for the frequency of scenarios bases on CETU 2003 [59, Apdx. B.1]. It considers fires ignited in case of accidents or due to technical defects and is valid for road tunnels with two lanes, bi-directional traffic, as well as no additional access roads. Furthermore, it assumes that vehicles after their ignition can leave the tunnel within a distance of 200 m in the direction to the tunnel portals. However, vehicles can not leave the tunnel in case of accidents which occurs in one of 30 scenarios. According to these assumptions, Eq. G.1 includes a reduction factor and also considers the risk factors average daily traffic volume as well as tunnel length.

$$f_{sc} = \dot{f}_{fire}\left(\chi_{HGV}\right) \cdot \left(\frac{29}{30} \cdot \left(1 - \frac{0.2\,\text{km}}{l_{tunnel}}\right) + \frac{1}{30}\right) \cdot l_{tunnel} \cdot \dot{N}_{adtv} \cdot 365\,\frac{\text{days}}{\text{year}} \tag{G.1}$$

Moreover, Eq. G.1 indirectly introduces the risk factor ratio of HGV together with the variable specific frequency of fire $\dot{f}_{fire}$, i.e. the frequency of fire per driven vehicle kilometre. More precisely, the specific frequency of fire differs between cars and HGVs. For cars, the value is given with $2 \cdot 10^{-8} \cdot 0.05$ /(veh. km) where the second factor was adopted of the methodology of Germany [13, p. 28] to exclude self-extinguishing fires. HGVs are subjected to a value of $1.5 \cdot 10^{-8}$ /(veh. km) which is valid for fires not brought under control and for 'trunk roads' with regard to the bi-directional traffic. Accordingly, the specific frequency of fire in Eq. G.1 derives from the average of both values weighted with the ratio of HGV. Nota bene, it is possible to average both values since both fire risk factors with effects on the HRR are supposed to be independent from the risk factor ratio of HGV.

Of course, the values for the specific frequency of fire are subjected to uncertainties, e.g. CETU 2003 [59, Apdx. B.1] provides a wider range of values besides from trunk roads. For this reason, several different models to describe the frequency of scenarios exist, e.g. in methodology of Germany [13, p. 27ff] or in Schubert 2011 [15, p. 55].

Detection time of fire

The guideline for German road tunnels demands the detection of a pool fire with a HRR of five MW within 60 s [50, p. 24]. Accordingly, the fire detection system in the system model detects the fire as soon as it reaches a HRR of five MW. Thus, the detection time of fire derives from the exponential function in Eq. G.2 (p. G-11). Additionally, the methodology of Germany [13, p. 30] assumes a failure of the fire detection system in one percent of all fires. However, the system model does not consider the failure of fire detection. This simplification originates in the screening during the setup of the fire and the evacuation scenario. The screening uncovered that a failure of fire detection and consequently no emergency ventilation had little effect on the outcome of the scenario.

Of course, the fire detection depends on many different factors [96, p. 705ff], e.g. the type of the detection system, detection by tunnel users, or the type and location of the fire source. With the knowledge on the importance of the alarm of tunnel users, a further refinement of the system model could begin with this intermediate node.

Time of tunnel alarm

There are few information on the time of tunnel alarm, e.g. that it ranges between 120 s and 300 s [61, p. 31]. For this reason, the tunnel alarm of the fire alarm system is directly linked to the intermediate node time of fire detection. However, the time of tunnel alarm additionally considers the risk factor failure of tunnel alarm. Namely, the time of tunnel alarm does not affect the evacuation scenario in case of FA.

Number of vehicles $N_{vehicle}$

The model for the number of vehicles derives from CETU 2003 [59, Apdx. E.1]. It is valid for free-flowing traffic and focuses on the upper evacuation area. According to CETU 2003 , the model splits up into two phases, i.e. before and after the time of tunnel alarm. Before, the vehicles line up in a tailback beginning directly after the fire source. Afterwards, the vehicles stop immediately and hence have the same front-to-front distances as in free-flowing traffic. Consequently, this intermediate node depends on the risk factor average daily traffic volume as well as on the intermediate nodes traffic speed and time of tunnel alarm.

Traffic speed

According to BASt 2009 [91, p. 12], vehicles drive with the speed allowed by the speed limits. For HGV, the speed limit is 80 km/h [91, p. 12]. And for cars, the speed limit is commonly 80 km/h but in some cases up to 100 km/h [50, p. 29ff]. The system model assumes the latter value of 100 km/h. Hence, this intermediate node results in the averaged speed for cars and HGV, i.e. 100 km/h and 80 km/h, weighted with the ratio of HGV.

G.3 Python modules

Section B.3 and Section B.4 introduce the system model and the consequence model with focus on the metamodel. Now, this section sketches the different classes written in Python

to realise the methodology for risk analysis developed in this dissertation. It also highlights some details with regard to the implementation of the nodes in the system model.

Fig. G.1 provides an overview on the different classes and data bases used in the methodology. First, the class MLS refers to the data bases for the system model containing FFs at discrete scenarios. The discrete scenarios were specified with an ED of the class ED as described in Section C.3. Their results were simulated with FDS and FDS+Evac according to Subs. 'Discrete scenario in FDS and FDS+Evac' (p. 20). The class MLS establishes the metamodel according to its inputs, i.e. the specific data base as well as further options, as detailed in Section D.1.3, Section D.1.4 and Section D.2. The MLS attributes of each metamodel are saved in a data base and can be reloaded for equal inputs. Second, the node FF integrates the results of the metamodel into the system model via two modes. Section D.4 describes the integration and Subs. 'Integration of MLS models into the system model' (p. 45) of Section D.2 introduces the modes. In case of the direct mode, the node FF directly applies a metamodel to get the FFs at the random scenarios of a Monte-Carlo simulation. In case of the indirect mode, the node FF derives the FFs from the data base for the fixed points. This data base contains results of the FF at the fixed points precalculated for various metamodels with different inputs. Finally, the class GRAPH initiates a system model object with its graph depicted in Fig. B.1 on p. 16. The graph also initiates the Monte-Carlo simulation in the system model and receives the results of risk analysis determined according to Section B.2.

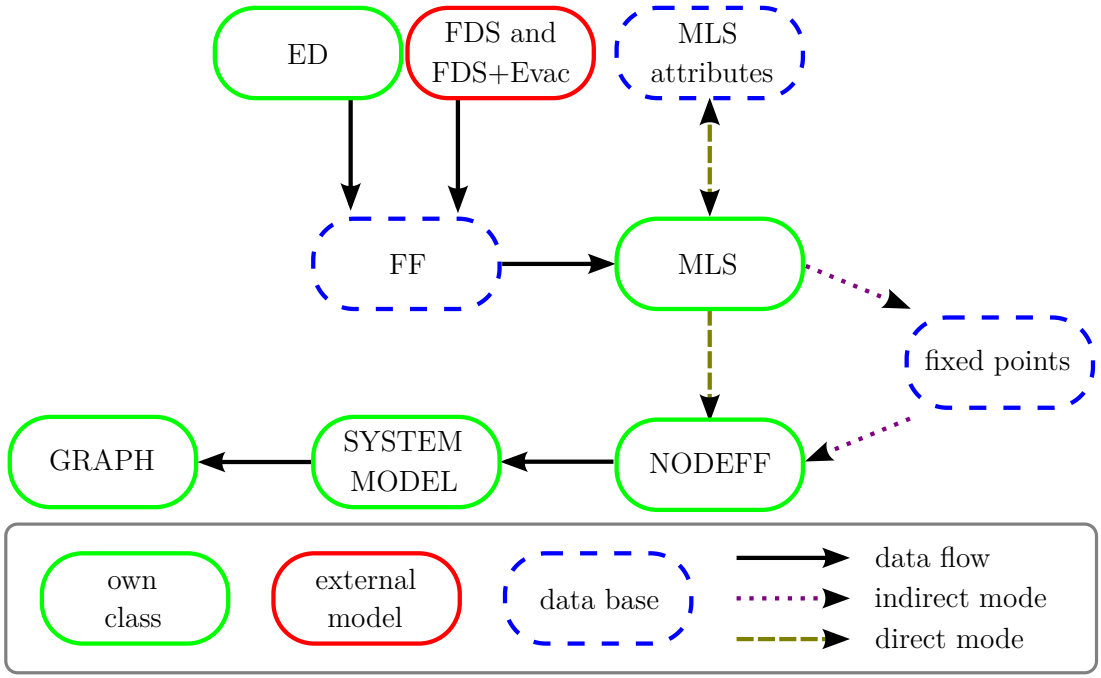

Figure G.1: Data flow between the classes developed in this dissertation, the external models and data bases used to reduce the computational effort.

The different classes of the nodes in the system model all inherit from the same class NODE written in the following reduced code. The graph object initiates only a single node which serves to quantify the risk measures. Subsequently, this node initiates its parent nodes, namely the frequency of scenarios and the node FF. These two nodes continue the graph as depicted in Fig. B.1. Generally, the entire graph is set up with a bottom-up approach. Namely, each node initiates its parent nodes which are defined in corresponding list of their classes. Equally, each node triggers its parent nodes to produce the results for a Monte-Carlo simulation. Consequently, neither the graph object nor the nodes contain the information on

the entire graph. Moreover, there is no connection from a parent node to a child node. For this reason, each node is directly linked to the graph object to facilitate the transfer of the results of a Monte-Carlo simulation for the final evaluation in the graph object.

```
class NODE(object,metaclass=Singleton):
    def __init__(self,g=None):
        self._parents=[]#list for parent nodes defined in each node
               self._result=None#updated after _run_sim()
               self._graph=g#link to the graph object g

   def _run_sim(self): #method triggers the parent nodes to produce results
        self._result=np.nan#specific model for each node
```

The bottom-up approach produces a specific issue when a parent node has multiple child nodes, for instance the maximum HRR. In this case, the class of the parent node is initiated by every child node which would lead to multiple node objects each producing different results during a Monte-Carlo simulation. To prevent the existence of multiple objects of one class, the class node derives from the metaclass SINGLETON shown in the following reduced code. The SINGLETON always returns the object of its first initialisation during all subsequent initialisations of its class.

```
class SINGLETON(type):
    _instances={}
    def __call__(self, *args, **kwargs):
        if self not in self._instances:
            self._instances[self] = super(SINGLETON, self).__call__(*args, **kwargs)
        return self._instances[self]
```

Furthermore, the class NODEFF applies another metaclass because it had to be revised completely during the development of the methodology for risk analysis. The aim of the revision was to establish a completely new class using MLS but still to be able to apply the deprecated class with its local interpolation methods. Additionally, the parent nodes of the node FF should call the node FF object always in the same way independent from its specific class. To achieve these objectives, the class NODEFF derives from the metaclass FFSPLIT as shown in the following reduced code. This metaclass simply reads the options specified in the graph object during its initialisation and accordingly selects either the new or the deprecated class. Then, it returns the corresponding object to the class NODEFF. As a result, the object of the node FF always stems from the same class NODEFF.

```
class FFSPLIT(type):#metaclass for the node FF
    def __call__(self,*args,**kwargs):#is executed before the __init__ method
        g=args[0]
        specs=g._get_options('FF')['S']#reads options defined in the graph object g
        if 'deprecated' in specs:#switches between different classes depending on
            the option in graph
            return FFLIN(g)#object of the deprecated class using local interpolation
        else:
            return FFMLS(g)#object of the class using MLS

class NODEFF(metaclass=FFSPLIT):#Node FF represented either by the deprecated or
    current class
    def __init__(self,g):#initiated in the graph object g
```

```
pass
```

G.4 Complex model

Subs. 'Discrete scenario in FDS and FDS+Evac' (p. 20) describes the fire and evacuation scenarios simulated with FDS and FDS+Evac. To complement the description, this section first defines the time-dependent HRR curve applied in the complex model which is crucial for the FF. In the same subsection, it also gives some background to the fire source. Subsequently, it provides the input files for the simulations with FDS and FDS+Evac. The second input file additionally comprises the option to consider a second emergency exit as well as the evacuation to the upper tunnel portal for a more flexible exit selection. Moreover, it already describes variables to include mobility-impaired occupants.

Exponential HRR curve of the fire source

The time-dependent HRR $\dot{Q}(t)$ in MW follows the exponential function Eq. G.2 according to Ingason 2009 [58, p. 260]. However, more recently, Ingason 2015 [97, p. 136] uncovered a linear increase of the HRR in road tunnels. The exponential function therewith comprises the growth and the decay period of the fire. For this purpose, Eq. G.2 applies the parameters $k = \frac{\mathrm{HRR}_{max}}{Q} \cdot r$ and $r = \left(1 - \frac{1}{n}\right)^{1-n}$ where Q in MJ is the calorific value of the fire source, i.e. the HGV. The fire source in the complex model is subjected to the assumption that a HGV with a small calorific value automatically leads to a smaller maximum HRR HRR_{max} than a HGV with a high calorific value. In other words, the maximum HRR linearly correlates with the calorific value. According to the median values of experiments in road tunnels [23, p. 3], HGVs with a heat capacity of about $Q \approx 75 \cdot 10^3\, MJ$ led to fires with a maximum HRR of $\mathrm{HRR}_{max} \approx 50\, MW$. These results together with the linear correlation result in the calorific value of the fire source of $Q = \frac{75 \cdot 10^3\, MJ}{50\, MW} \cdot \mathrm{HRR}_{max}$ depending on the risk factor maximum HRR. At last, the parameter n in Eq. G.2 derives from Eq. G.3 with the risk factor time to maximum HRR t_{max} in s.

$$\dot{Q}(t) = \mathrm{HRR}_{max} \cdot n \cdot r \left(1 - e^{-kt}\right)^{n-1} \cdot e^{-kt} \tag{G.2}$$

$$t_{max} = \frac{\ln(n)}{\frac{\mathrm{HRR}_{max}}{Q}\left(1 - \frac{1}{n}\right)^{1-n}} \tag{G.3}$$

Next, the fire source in the fire scenario of FDS bases on a user-specified fuel in the simple chemistry model to generally represent fires in road tunnels. At the beginning, a screening in the fire scenario uncovered clear effects on the FF of following parameters: first, the heat of combustion; second and third, the yields for soot $\frac{\dot{m}_{soot}}{\dot{m}_{fuel}}$ and carbon monoxide $\frac{\dot{m}_{\mathrm{CO}}}{\dot{m}_{\mathrm{CO_2}}}$. $\dot{m}$ are the corresponding combustion and production rates in mass per time. As a consequence, first, the user-specified fuel bases on acetone $\mathrm{C_3H_6O}$ with a heat of combustion of 28560 $\frac{kJ}{kg}$ [98, p. 3440]. The heat of combustion is neither low nor high and thus should represent other fuels in road tunnels. However, acetone itself is not representative with regard to the other parameters. Thus, they were specified independently to the actual values of acetone. Second, there are little information on the soot yield of fires in road tunnels. For instance, Mulholland 2003 [99, p. 2/259] describes values in the range of $\frac{\dot{m}_{soot}}{\dot{m}_{fuel}} = \{0.01 \ldots 0.19\}\ \frac{kg_{soot}}{kg_{fuel}}$.

Hence, the fire scenario in FDS adopts a medium soot yield of $\frac{\dot{m}_{soot}}{\dot{m}_{fuel}} = 0.1\,\frac{kg_{soot}}{kg_{fuel}}$. And third, according to PIARC 1999 [61, p. 65], the ratio between carbon monoxide and carbon dioxide is $\frac{\dot{m}_{CO}}{\dot{m}_{CO_2}} \approx 0.05\,\frac{kg_{CO}}{kg_{CO}}$. This value results in the carbon monoxide yield of $\frac{\dot{m}_{CO}}{\dot{m}_{CO_2}} = 0.1221\,\frac{kg_{CO}}{kg_{fuel}}$ following the simple chemistry model in the FDS user guide [11, p. 131f]. Summing up, these three parameters were determined to generally represent fuels in road tunnels but they are not subjected to epistemic or aleatory uncertainties despite their clear effects on the FF. For this reason, the variation of these parameters throughout the system model could reveal interesting results.

FDS input file

```
Overview on variables (to set up simulations automatically):
<<name>> : <<<name>>>
<<template_name>> : <<<template_name>>>
<<HRR_max>> : <<<HRR_max>>>
<<t_HRR_max>> : <<<t_HRR_max>>>
<<t_vent>> : <<<t_vent>>>
<<HRR_PUA>> : <<<HRR_PUA>>>
<<HRR_string>> : see at HRR_curve

Legend:
name : name of fire simulation
HRR_max /MW : maximum HRR (risk factor)
t_HRR_max /s : time to maximum HRR (risk factor)
t_vent /s : begin of ventilation
HRR_PUA /(kW/,m^2) : HRR_max / 162.5 m^2 * 1000
HRR_string : string to describe the time-dependent HRR in FDS

&HEAD CHID='<<<name>>>', TITLE='FDSF-SyMo based on template <<<template_name>>>.' /
&MISC
       RESTART=.FALSE.,
       TMPA=10.0,
       GVEC=-0.098095,0,-9.8095,
       U0=1.0,
       EVACUATION_DRILL=.FALSE.,
       EVACUATION_MC_MODE=.FALSE.,
       NO_EVACUATION=.FALSE.,
       EVAC_PRESSURE_ITERATIONS=50,
       EVAC_TIME_ITERATIONS=50, /
&MESH IJK=2600,40,18, XB=-200.0,450.0,0.0,10.0,0.0,4.5, /
&TIME T_END=1200.0 /1200
&DUMP NFRAMES=2400, DT_HRR=1., DT_DEVC=1, DT_RESTART=5.0, /
&PRES MAX_PRESSURE_ITERATIONS=20, /

==========FIRE GEOMETRY==========
----------Activation time of ventilation----------
&DEVC ID='TimerVent', QUANTITY='TIME', SETPOINT=<<<t_vent>>>, INITIAL_STATE=.FALSE.,
     XYZ=0,0,0, /
----------FIRE SOURCE:----------
&SURF ID='FIRE', HRRPUA=<<<HRR_PUA>>>, COLOR='RED', RAMP_Q='HRR_curve'/
&OBST XB=-10.0,10.0,3.5,6.0,0.5,3.0, SURF_IDS='FIRE','FIRE','INERT', EVACUATION=.
    FALSE., /
```

```
&OBST XB=-10.0,10.0,3.5,6.0,0.0,0.5, SURF_ID='INERT', COLOR='BLACK', EVACUATION=.
    FALSE., /
&RAMP ID='HRR_curve', T=0.0, F=0.0000,/
<<<HRR_string>>>
&REAC ID='model',
       FUEL = 'ACETONE',
       HEAT_OF_COMBUSTION = 28560.0,
       FORMULA = 'C3H6O',
       CO_YIELD=0.1221,
       SOOT_YIELD=0.1, /
----------TUNNEL BOUNDARIES----------
&VENT MB='ZMIN', SURF_ID='ROAD' / road surface
&VENT MB='XMIN', SURF_ID='OPEN' / Portal 1
&VENT MB='XMAX', SURF_ID='OPEN' / Portal 2
&VENT MB='ZMAX', SURF_ID='TUNNEL WALL' /
&VENT MB='YMIN', SURF_ID='TUNNEL WALL' /
&VENT MB='YMAX', SURF_ID='OPEN' /
&OBST XB=-200.0,450.0,9.5,10.0,0.0,4.5, SURF_ID='TUNNEL WALL', EVACUATION=.FALSE.,/
    tunnel wall
&HOLE XB=-125.5,-124.5,9.49,10.01,4.0,4.5, /
&HOLE XB=-25.5,-24.5,9.49,10.01,4.0,4.5, /
&HOLE XB=274.5,275.5,9.49,10.01,4.0,4.5, /
&HOLE XB=374.5,375.5,9.49,10.01,4.0,4.5, /
&SURF ID='TUNNEL WALL', MATL_ID='CONCRETE', THICKNESS=1.0, BACKING='INSULATED',
    COLOR='GRAY', TRANSPARENCY=0.0, /
&SURF ID='ROAD', MATL_ID='ASPHALT', THICKNESS=1.0, BACKING='INSULATED', COLOR='DIM
    GRAY', /
------------VENTILATION------------
JET FAN at -150 lower y: u at 60 m, switches of at -90 m
&OBST XB=-150.0,-149.5,0.0,1.5,3.0,4.5, COLOR='GOLDENROD'/
&VENT XB=-150.0,-150.0,0.0,1.5,3.0,4.5, SURF_ID='HVAC',ID='in-15018',COLOR='BLACK'/
    Inlet
&VENT XB=-149.5,-149.5,0.0,1.5,3.0,4.5, SURF_ID='HVAC',ID='out-15018',COLOR='BLACK'/
    Outlet
&HVAC ID='in-15018',TYPE_ID='NODE',DUCT_ID='fan-15018',VENT_ID='in-15018',/
&HVAC ID='out-15018',TYPE_ID='NODE',DUCT_ID='fan-15018',VENT_ID='out-15018',/
&HVAC ID='fan-15018', TYPE_ID='DUCT', NODE_ID='in-15018','out-15018', VOLUME_FLOW
    =55.575, AREA=2.25, RAMP_ID='vent-150', DAMPER=.TRUE., CTRL_ID='DampCTRL-150', /
&OBST XB=-151.0,-148.0,0.0,0.0,3.0,4.5, COLOR='GOLDENROD'/
&OBST XB=-151.0,-148.0,1.5,1.5,3.0,4.5, COLOR='GOLDENROD'/
&OBST XB=-151.0,-148.0,0.0,1.5,3.0,3.0, COLOR='GOLDENROD'/
&OBST XB=-151.0,-148.0,0.0,1.5,4.5,4.5, COLOR='GOLDENROD'/
JET FAN at -150 upper y: u at 60 m, switches of at -90 m
&OBST XB=-150.0,-149.5,8.0,9.5,3.0,4.5, COLOR='GOLDENROD'/
&VENT XB=-150.0,-150.0,8.0,9.5,3.0,4.5, SURF_ID='HVAC',ID='in-15098',COLOR='BLACK'/
    Inlet
&VENT XB=-149.5,-149.5,8.0,9.5,3.0,4.5, SURF_ID='HVAC',ID='out-15098',COLOR='BLACK'/
    Outlet
&HVAC ID='in-15098',TYPE_ID='NODE',DUCT_ID='fan-15098',VENT_ID='in-15098',/
&HVAC ID='out-15098',TYPE_ID='NODE',DUCT_ID='fan-15098',VENT_ID='out-15098',/
&HVAC ID='fan-15098', TYPE_ID='DUCT', NODE_ID='in-15098','out-15098', VOLUME_FLOW
    =55.575, AREA=2.25, RAMP_ID='vent-150', DAMPER=.TRUE., CTRL_ID='DampCTRL-150', /
&OBST XB=-151.0,-148.0,8.0,8.0,3.0,4.5, COLOR='GOLDENROD'/
&OBST XB=-151.0,-148.0,9.5,9.5,3.0,4.5, COLOR='GOLDENROD'/
&OBST XB=-151.0,-148.0,8.0,9.5,3.0,3.0, COLOR='GOLDENROD'/
&OBST XB=-151.0,-148.0,8.0,9.5,4.5,4.5, COLOR='GOLDENROD'/
JET FAN at 420 lower y: u at 300 m, switch off at 300 m
```

```
&OBST XB=420.0,420.5,0.0,1.5,3.0,4.5, COLOR='GOLDENROD'/
&VENT XB=420.0,420.0,0.0,1.5,3.0,4.5, SURF_ID='HVAC',ID='in42018',COLOR='BLACK'/
    Inlet
&VENT XB=420.5,420.5,0.0,1.5,3.0,4.5, SURF_ID='HVAC',ID='out42018',COLOR='BLACK'/
    Outlet
&HVAC ID='in42018',TYPE_ID='NODE',DUCT_ID='fan42018',VENT_ID='in42018',/
&HVAC ID='out42018',TYPE_ID='NODE',DUCT_ID='fan42018',VENT_ID='out42018',/
&HVAC ID='fan42018', TYPE_ID='DUCT', NODE_ID='in42018','out42018', VOLUME_FLOW
    =55.575, AREA=2.25, RAMP_ID='vent+420', DAMPER=.TRUE., CTRL_ID='DampCTRL420', /
&OBST XB=419.0,422.0,0.0,0.0,3.0,4.5, COLOR='GOLDENROD'/
&OBST XB=419.0,422.0,1.5,1.5,3.0,4.5, COLOR='GOLDENROD'/
&OBST XB=419.0,422.0,0.0,1.5,3.0,3.0, COLOR='GOLDENROD'/
&OBST XB=419.0,422.0,0.0,1.5,4.5,4.5, COLOR='GOLDENROD'/
JET FAN at 420 upper y: u at 300 m, switch off at 300 m
&OBST XB=420.0,420.5,8.0,9.5,3.0,4.5, COLOR='GOLDENROD'/
&VENT XB=420.0,420.0,8.0,9.5,3.0,4.5, SURF_ID='HVAC',ID='in42098',COLOR='BLACK'/
    Inlet
&VENT XB=420.5,420.5,8.0,9.5,3.0,4.5, SURF_ID='HVAC',ID='out42098',COLOR='BLACK'/
    Outlet
&HVAC ID='in42098',TYPE_ID='NODE',DUCT_ID='fan42098',VENT_ID='in42098',/
&HVAC ID='out42098',TYPE_ID='NODE',DUCT_ID='fan42098',VENT_ID='out42098',/
&HVAC ID='fan42098', TYPE_ID='DUCT', NODE_ID='in42098','out42098', VOLUME_FLOW
    =55.575, AREA=2.25, RAMP_ID='vent+420', DAMPER=.TRUE., CTRL_ID='DampCTRL420', /
&OBST XB=419.0,422.0,8.0,8.0,3.0,4.5, COLOR='GOLDENROD'/
&OBST XB=419.0,422.0,9.5,9.5,3.0,4.5, COLOR='GOLDENROD'/
&OBST XB=419.0,422.0,8.0,9.5,3.0,3.0, COLOR='GOLDENROD'/
&OBST XB=419.0,422.0,8.0,9.5,4.5,4.5, COLOR='GOLDENROD'/
----------BI-DIRECTIONAL TRAFFIC----------
&RAMP ID='vent-150', T=-3.0, F=1.0, DEVC_ID='FUV+06055'/left end of evacuation area
&RAMP ID='vent-150', T=3.0, F=-1.0, /
&RAMP ID='vent+420', T=-3.0, F=1.0, DEVC_ID='FUV+30055'/right end of evacuation area
&RAMP ID='vent+420', T=3.0, F=-1.0, /
&CTRL ID='DampCTRL-150', INITIAL_STATE=.FALSE., FUNCTION_TYPE='ALL', INPUT_ID='
    TimerVent','FOD-09059', LATCH=.FALSE., /
&CTRL ID='DampCTRL420', INITIAL_STATE=.FALSE., FUNCTION_TYPE='ALL', INPUT_ID='
    TimerVent','FOD+36059', LATCH=.FALSE., /
----------TUNNEL MATERIALS----------
&MATL  ID = 'ASPHALT',
               EMISSIVITY=0.7,
               DENSITY=2100,
               SPECIFIC_HEAT=1.000,
               CONDUCTIVITY=0.7, /
&MATL  ID = 'CONCRETE',
               EMISSIVITY=0.7,
               DENSITY=2400,
               SPECIFIC_HEAT=1.000,
               CONDUCTIVITY=1.111, /
==========EVAC GEOMETRY===========
&MESH
       IJK=900,24,1,
       XB=0,450,0.0,12.0,0.5,1.5,
       EVAC_Z_OFFSET=1.00,
       EVACUATION=.TRUE.,
       EVAC_HUMANS=.TRUE.,
       ID='MainEvacGrid', /
The exact geometry for evac is not relevant in case of the fire scenario.
...
```

```
==========Output of computed data:==========
The exact output is not relevant here.
...
&TAIL /
```

FDS+Evac input file

```
Overview on variables:
<<name>> : <<<name>>>
<<template_name>> : <<<template_name>>>
<<fire_name>> : <<<fire_name>>>
<<HRR_max>> : <<<HRR_max>>>
<<t_HRR_max>> : <<<t_HRR_max>>>
<<t_reac_max>> : <<<t_reac_max>>>
<<n_tu>> : <<<n_tu>>>
<<f_alm_tu>> : <<<f_alm_tu>>>
<<t_alm_tu>> : <<<t_alm_tu>>>
<<xi_mip>> : <<<xi_mip>>>
<<n_ad>> : <<<n_ad>>>
<<n_mi>> : <<<n_mi>>>

Legend:
name : name of evacuation simulation
template_name : name of template
fire_name : name of fire simulation (fire)
HRR_max /MW : maximum HRR (fire risk factor)
t_HRR_max /s : time to maximum HRR (fire risk factor)
t_reac_max /s : maximum pre-evacuation time (evacuation risk factor)
n_tu : number of tunnel users (evacuation risk factor)
f_alm_tu : failure of tunnel alarm (evacuation risk factor)
t_alm_tu /s : time of tunnel alarm (depends on HRR, 1200 in case of failure of
    tunnel alarm)
xi_mip : ratio of mobility-impaired persons
n_ad : number of adults
n_mi : number of mobility-impaired persons

&HEAD CHID='<<<name>>>', TITLE='FDSE-SyMo based on template <<<template_name>>>.' /
&MISC
       EVACUATION_DRILL=.FALSE.,
       EVACUATION_MC_MODE=.TRUE.,
       NO_EVACUATION=.FALSE.,
       EVAC_PRESSURE_ITERATIONS=50,
       EVAC_TIME_ITERATIONS=50, /
&TIME T_END=1200 /1200
&DUMP NFRAMES=2400, /
&MESH
       IJK=900,24,1,
       XB=0,450,0.0,12.0,0.5,1.5,
       EVAC_Z_OFFSET=1.00,
       EVACUATION=.TRUE.,
       EVAC_HUMANS=.TRUE.,
       ID='MainEvacGrid', /
&PERS ID='Adult',
```

```
      DEFAULT_PROPERTIES='Adult',
          HUMAN_SMOKE_HEIGHT=1.6,
          OUTPUT_SPEED=.TRUE.,
          OUTPUT_FED=.TRUE.,
          COLOR_METHOD=5,
          SMOKE_MIN_SPEED=0.25,
          TDET_SMOKE_DENS=0.000001,
          FED_DOOR_CRIT=1.0,
          DET_EVAC_DIST=0,
          DET_MEAN=<<<t_alm_tu>>>,
          PRE_EVAC_DIST=1,
          PRE_LOW=0,
          PRE_HIGH=<<<t_reac_max>>>, /
&PERS ID='MobilityImpaired',
      DEFAULT_PROPERTIES='Elderly',
          HUMAN_SMOKE_HEIGHT=1.6,
          OUTPUT_SPEED=.TRUE.,
          OUTPUT_FED=.TRUE.,
          COLOR_METHOD=5,
          DET_EVAC_DIST=0,
          DET_MEAN=<<<t_alm_tu>>>,
          PRE_EVAC_DIST=1,
          PRE_LOW=0,
          PRE_HIGH=<<<t_reac_max>>>, /
&EVAC ID = 'AD',
      NUMBER_INITIAL_PERSONS = <<<n_ad>>>,
          XB =30.0,270.0,0.0,9.5,0.5,1.5,
      AVATAR_COLOR = 'BLUE',
      PERS_ID = 'Adult',
          AGENT_TYPE=2,
          KNOWN_DOOR_NAMES='EmOut1+', /
&EVAC ID = 'MI',
      NUMBER_INITIAL_PERSONS = <<<n_mi>>>,
          XB =30.0,270.0,0.0,9.5,0.5,1.5,
      AVATAR_COLOR = 'RED',
      PERS_ID = 'MobilityImpaired',
          AGENT_TYPE=2,
          KNOWN_DOOR_NAMES='EmOut1+', /
&OBST XB=0.0,450.0,9.5,12.0,0.5,1.5, SURF_ID='Evac Wall', EVACUATION=.TRUE., OUTLINE
    =.TRUE.,/wall
&OBST XB=0.0,300.0,2.0,7.5,0.5,1.5, SURF_ID='INERT', COLOR='WHITE', EVACUATION=.TRUE
    ., TRANSPARENCY=0.1, /cars
&EVHO XB=155.0,145.0,0.9,9.1,0.5,1.5, /emergency exit
&HOLE XB=155.0,145.0,0.9,9.1,0.5,1.5, EVACUATION=.TRUE., /EmEx1+ (passage to
    emergency exit)
&HOLE XB=155.0,145.0,9.4,12.0,0.5,1.5, EVACUATION=.TRUE., /EmEx1+ (compartment)
&OBST XB=155.0,150.5,9.3,9.3,0.5,1.5, SURF_ID='Evac Wall', EVACUATION=.TRUE., /EmEx1
    + (wall)
&OBST XB=149.5,145.0,9.3,9.3,0.5,1.5, SURF_ID='Evac Wall', EVACUATION=.TRUE., /EmEx1
    + (wall)
&EXIT
       ID='EmEx1+',
       XB=150.5,149.5,10.0,10.0,0.5,1.5,
       HEIGHT=2.0,
       SHOW=.TRUE.,
       IOR=2,
       COUNT_ONLY=.TRUE.,
```

```
       COLOR='GREEN', /
&EXIT
       ID='EmOut1+',
       XB=155.0,145.0,12.0,12.0,0.5,1.5,
       XYZ=150,9.0,4.0,
       HEIGHT=4.0,
       SHOW=.TRUE.,
       IOR=2,
       COUNT_ONLY=.FALSE.,
       COLOR='GREEN', /
&HOLE XB=445.0,435.0,0.9,9.1,0.5,1.5, EVACUATION=.TRUE., /EmEx2+ (passage)
&HOLE XB=445.0,435.0,9.4,12.0,0.5,1.5, EVACUATION=.TRUE., /EmEx2+ (compartment)
&OBST XB=445.0,440.5,9.3,9.3,0.5,1.5, SURF_ID='Evac Wall', EVACUATION=.TRUE., /EmEx2
    + (wall)
&OBST XB=439.5,435.0,9.3,9.3,0.5,1.5, SURF_ID='Evac Wall', EVACUATION=.TRUE., /EmEx2
    + (wall)
&EXIT
       ID='EmEx2+',
       XB=440.5,439.5,10.0,10.0,0.5,1.5,
       HEIGHT=2.0,
       SHOW=.TRUE.,
       IOR=2,
       COUNT_ONLY=.TRUE.,
       COLOR='RED', /
&EXIT
       ID='EmOut2+',
       XB=445.0,435.0,12.0,12.0,0.5,1.5,
       XYZ=440,9.0,4.0,
       HEIGHT=4.0,
       SHOW=.TRUE.,
       IOR=2,
       COUNT_ONLY=.FALSE.,
       COLOR='RED', /
&TAIL /
```

G.5 Background to the prediction interval method

Section D.1.4 introduces the prediction interval method used for the metamodel uncertainty in this dissertation. Now, this section derives the prediction interval in accordance with Kim 2008 [28]. To begin, it later refers to following transformations:

1. $\mathrm{var}\left(\boldsymbol{b}^T\boldsymbol{B}\right) = \boldsymbol{b}^T \cdot \mathrm{var}\left(\boldsymbol{B}\right)\boldsymbol{b}$;
2. $\mathrm{cov}\left(\boldsymbol{A},\boldsymbol{A}\right) = \mathrm{var}\left(\boldsymbol{A}\right)$ with respect to the notation in [28, Eq. 7] $\mathrm{cov}\left(a\right) = \mathrm{cov}\left(a,a\right)$;
3. $\left(\boldsymbol{AB}\right)^T = \boldsymbol{B}^T\boldsymbol{A}^T$; $\left(\boldsymbol{A}^T\right)^{-1} = \left(\boldsymbol{A}^{-1}\right)^T$; $\left(c \cdot \boldsymbol{A}\right)^T = c \cdot \boldsymbol{A}^T$; and $\boldsymbol{W}^T = \boldsymbol{W}$.

Where $\boldsymbol{A}$, i.e. a, as well as $\boldsymbol{B}$ are matrices, $\boldsymbol{b}$ is a column vector, c is a scalar and $\boldsymbol{W}$ is the diagonal matrix in Eq. D.8 (p. 41) for MLS.

The prediction interval originates in the variance of the deterministic result of MLS with Eq. G.4. More precisely: $\mathrm{var}\left(\bar{y}_0\right) = \mathrm{var}\left(\widetilde{\wp}_0^T b_0\right) = \widetilde{\wp}_0^T \mathrm{var}\left(b_0\right)\widetilde{\wp}_0 = \widetilde{\wp}_0^T \mathrm{cov}\left(b_0\right)\widetilde{\wp}_0$ with Eq. D.9 [28, Eq. 12], transformation 1, and transformation 2, respectively.

$$\mathrm{var}\left(\bar{y}_0\right) = \widetilde{\wp}_0^T \mathrm{cov}\left(b_0\right)\widetilde{\wp}_0 \tag{G.4}$$

Then, $\operatorname{cov}(b_0)$ in Eq. G.4 becomes with Eq. D.8 [28, Eq. 6] and transformation 1:

$$\begin{aligned}\operatorname{cov}(b_0) &= \operatorname{cov}\left(\left(\boldsymbol{P}^T\boldsymbol{W}_0\boldsymbol{P}\right)^{-1}\boldsymbol{P}^T\boldsymbol{W}_0\bar{\boldsymbol{Y}}^c\right)\\ &= \left(\left(\boldsymbol{P}^T\boldsymbol{W}_0\boldsymbol{P}\right)^{-1}\boldsymbol{P}^T\boldsymbol{W}_0\right)\cdot\operatorname{cov}\left(\bar{\boldsymbol{Y}}^c\right)\cdot\left(\left(\boldsymbol{P}^T\boldsymbol{W}_0\boldsymbol{P}\right)^{-1}\boldsymbol{P}^T\boldsymbol{W}_0\right)^T\end{aligned}$$

In this term, it yields $\operatorname{cov}\left(\bar{\boldsymbol{Y}}^c\right) = \operatorname{cov}(\boldsymbol{P}\cdot\boldsymbol{\beta}+\boldsymbol{\delta y}) = 0+\operatorname{cov}(\boldsymbol{\delta y}) = \operatorname{var}(\boldsymbol{\delta y}) = \sigma^2$ with the transformation 2 where $\boldsymbol{\delta y}$ is the approximation error in Subs. 'Global least squares regression method' (p. 38) and its latter factor becomes with transformation 3:

$$\begin{aligned}\left(\left(\boldsymbol{P}^T\boldsymbol{W}_0\boldsymbol{P}\right)^{-1}\boldsymbol{P}^T\boldsymbol{W}_0\right)^T &= \left(\boldsymbol{P}^T\boldsymbol{W}_0\boldsymbol{P}\right)^{-1}\left(\boldsymbol{P}^T\boldsymbol{W}_0\right)^T\\ &= \boldsymbol{W}_0^T\boldsymbol{P}\left(\boldsymbol{P}^T\boldsymbol{W}_0\boldsymbol{P}\right)^{-1}\\ &= \boldsymbol{W}_0\boldsymbol{P}\left(\boldsymbol{P}^T\boldsymbol{W}_0\boldsymbol{P}\right)^{-1}\end{aligned}$$

Altogether, the transformations conform to [28, Eq. 7] which leads with Eq. G.4 to the confidence interval in Eq. G.5 [28, Eq. 14].

$$\operatorname{var}(\bar{y}_0) = \sigma^2\left(\widetilde{\varphi}_0\right)^T\left(\boldsymbol{P}^T\boldsymbol{W}_0\boldsymbol{P}\right)^{-1}\boldsymbol{P}^T\boldsymbol{W}_0\boldsymbol{W}_0\boldsymbol{P}\left(\boldsymbol{P}^T\boldsymbol{W}_0\boldsymbol{P}\right)^{-1}\widetilde{\varphi}_0 \tag{G.5}$$

'The confidence interval is for estimating the interval of the mean response. However, the prediction interval is for predicting the interval of the value of a single future observation at a point.' [28, p. 4] 'The expected value of the prediction error is' zero [28, p. 4] and the prediction variance is:

$$\begin{aligned}\operatorname{var}\left(\bar{y}_0^c-\bar{y}_0\right) &= \operatorname{var}\left(\bar{y}_0^c\right)+\operatorname{var}\left(\bar{y}_0\right)-2\cdot\operatorname{cov}\left(\bar{y}_0^c,\bar{y}_0\right)\\ &= \operatorname{var}\left(\bar{y}_0^c\right)+\operatorname{var}\left(\bar{y}_0\right)-0 = \sigma^2+\sigma^2\left(\ldots\right)\end{aligned}$$

Hence, the prediction variance finally results in Eq. D.12 on p. 42. Concluding, Eq. D.12 states the mathematical background for the prediction interval $\Delta\bar{y}^m$.

G.6 Scrutiny of MLS and the prediction interval method

Prior to the final evaluations of the system model in Chapter E, this section scrutinises the implementation of MLS together with its calibration algorithm as well as the prediction interval method. First, App. G.6.1 describes the verification and first validation of both methods with different RSMs. The RSMs use results of analytical functions, representing the complex model, as data base. And finally, App. G.6.2 discusses the effects of weighting types on the default RSM introduced in Tab. E.2 on p. 56.

G.6.1 Verification and first validation

This section aims at the verification and first validation of the implementations of MLS and the prediction interval method using analytical functions. For this: Subs. 'Basic characteristics' (p. G-19) evaluates qualitatively a RSM; Subs. 'Comparison to the Kim 2008 [28]' (p. G-20) quantifies the predictive capability of the prediction interval method; and Subs. 'Calibration algorithm' (p. G-22) analyses RSMs based on different numbers of data points. Finally, Subs. 'Conclusions' (p. G-23) states the successful verification of MLS and the prediction interval method.

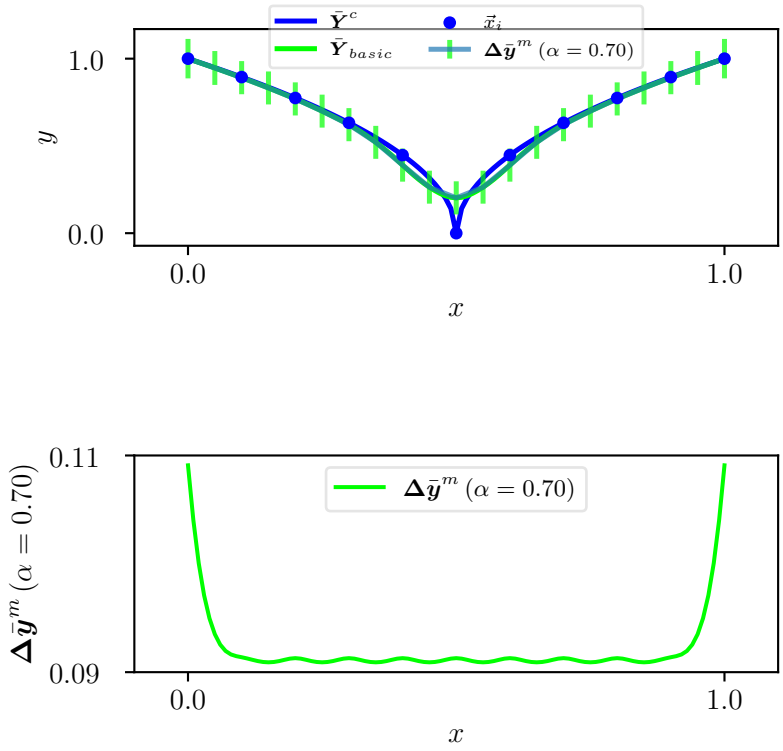

Figure G.2: Symmetrical and differentiable shape of the results of the RSM $\bar{\boldsymbol{Y}}_{basic}$ and the prediction interval $\boldsymbol{\Delta}\bar{\boldsymbol{y}}^m$ for the analytical function $\bar{\boldsymbol{Y}}^c$ in Eq. G.6.

Basic characteristics

At the start, this evaluation exemplifies some basic characteristics of MLS and the prediction interval method and serves as a first verification of their implementations. For this, the analytical function Eq. G.6 with the control variable $x \in [0, \ldots, 1]$ represents the complex model. It provides results for the data base of the RSM at eleven data points evenly spread on the entire domain. The function is symmetric and has one non-differentiable point. The calibration algorithm of MLS described in Subs. 'Calibration algorithm' (p. 45) results in the RSM $\bar{\boldsymbol{Y}}_{basic}$ subjected to a linear polynomial, the polynomial function w_p of Eq. D.17 (p. 45) and the weighting parameter $\omega = 0.23$. The prediction interval method bases on the prediction variance in Eq. D.12 (p. 42) with the variance estimator σ_X^2 in Eq. D.7 (p. 40).

$$\bar{y}^c = |2x - 1|^{0.5} \tag{G.6}$$

Fig. G.2 illustrates the results of the RSM and the prediction interval with a confidence level of $\alpha = 0.7$. The visual evaluation led to three observations: first, that the shape of the RSM and the prediction interval is symmetrical which is analogous to the analytical equation; second, that the RSM is differentiable, esp. in the region of the non-differentiable point; and third, that the prediction interval qualitatively corresponds to the confidence level. Furthermore, a quantitative inspection of the matrices esp. in Eq. D.8 on p. 41 for MLS and in Eq. D.12 for the prediction variance revealed no hints on numerical instabilities.

As another result, the prediction interval at data points is slightly elevated. But more apparent, the prediction interval increases at the outer vertices of the domain. Scrutiny of numerical values in Eq. D.12 uncovered that the weighting matrix $\boldsymbol{W}$ at an arbitrary point at

Table G.3: MLS attributes of different RSM for the analytical function in Eq. G.7 used for comparison to Kim 2008 [28, Fig. 5d].

RSM	weighting type	polynomial degree	parameter ω
$\bar{\boldsymbol{Y}}_{g,man}$	w_g	1	0.17
$\bar{\boldsymbol{Y}}_{p,man}$	w_p	1	0.39
$\bar{\boldsymbol{Y}}_{opt}$	w_p	2	0.34

the outer vertices comprises smaller values due to the large distances to most data points in comparison to the weighting matrix at an arbitrary point in the centre. This fact causes the increased prediction variance since the variance estimator is constant on the entire domain. To sum up, the weighting matrix and thus the distance to data points has clear effect on the prediction variance at the outer vertices. Thus, it appears that more data points close to the outer vertices will decrease the prediction interval in these regions.

To be noted, the prediction interval at data points is not zero which is in line with the prediction variance in Eq. D.12. This characteristic reflects that MLS does not interpolate but approximates to the data points which causes the residuals, i.e. the difference between the results of the RSM and the data points. Accordingly, the metamodel should consider the metamodel uncertainty to take this difference into account.

In summary, MLS and the prediction interval method lead to reasonable results. Furthermore, the results indicate that the metamodel uncertainty is important for the metamodel to represent the unknown results of the complex model.

Comparison to the Kim 2008 [28]

This subsection compares results of MLS with results shown in Kim 2008 [28, Fig. 5d]. It further validates the prediction interval method using either σ_X^2 or σ_{-i}^2 as variance estimator in Eq. D.7 of the prediction variance in Eq. D.12. Thus, both examinations contribute to the verification of the implementations of MLS and the prediction interval method and to the validation of the prediction interval method. The data base for the RSMs results from eleven evenly spread data points on $x \in [-1, \ldots, 1]$ of Eq. G.7 [28, Eq. 28]. Since Kim 2008 [28] does not provide information on the MLS attributes, the RSMs $\bar{\boldsymbol{Y}}_{g,man}$ and $\bar{\boldsymbol{Y}}_{p,man}$ base on the Gaussian function w_g in Eq. D.16 and the polynomial function w_p in Eq. D.17 (p. 45) respectively. Both RSMs are subjected to weighting parameters set manually in order to reproduce the RSM $\bar{\boldsymbol{Y}}_{pub}$ of Kim 2008 [28, Fig. 5d]. The optimised RSM $\bar{\boldsymbol{Y}}_{opt}$ is the result of the calibration algorithm in Subs. 'Calibration algorithm' (p. 45). To sum up, Tab. G.3 provides an overview on the MLS attributes of all RSMs.

$$\bar{y}^c = 0.5x^5 - 1.5x^4 - 2.5x^3 + 0.53x^2 + 1.3x + 2 \tag{G.7}$$

Fig. G.3 shows the results of the RSMs with a confidence level of $\alpha = 0.7$ for the prediction intervals. Both RSMs $\bar{\boldsymbol{Y}}_{g,man}$ and $\bar{\boldsymbol{Y}}_{p,man}$ resemble the RSM $\bar{\boldsymbol{Y}}_{pub}$ as it was the aim of their manual calibration. Also, both prediction intervals of the RSMs $\bar{\boldsymbol{Y}}_{g,man}$ and $\bar{\boldsymbol{Y}}_{p,man}$ are virtually identical. The RSM $\bar{\boldsymbol{Y}}_{opt}$, as result of the calibration algorithm, approximated well to Eq. G.7 on the entire domain. It further appears that the prediction interval of the RSM $\bar{\boldsymbol{Y}}_{opt}$ is smaller compared to the prediction intervals of the RSM $\bar{\boldsymbol{Y}}_{g,man}$ or $\bar{\boldsymbol{Y}}_{p,man}$. The small prediction interval of the RSM $\bar{\boldsymbol{Y}}_{opt}$ is reasonable since Eq. G.7 is entirely deterministic and not related to aleatory uncertainties which indicates that the calibration algorithm performs well. Again, the prediction intervals of all RSMs increase at the outer vertices which agrees with the results in Kim 2008 [28, Fig. 5d].

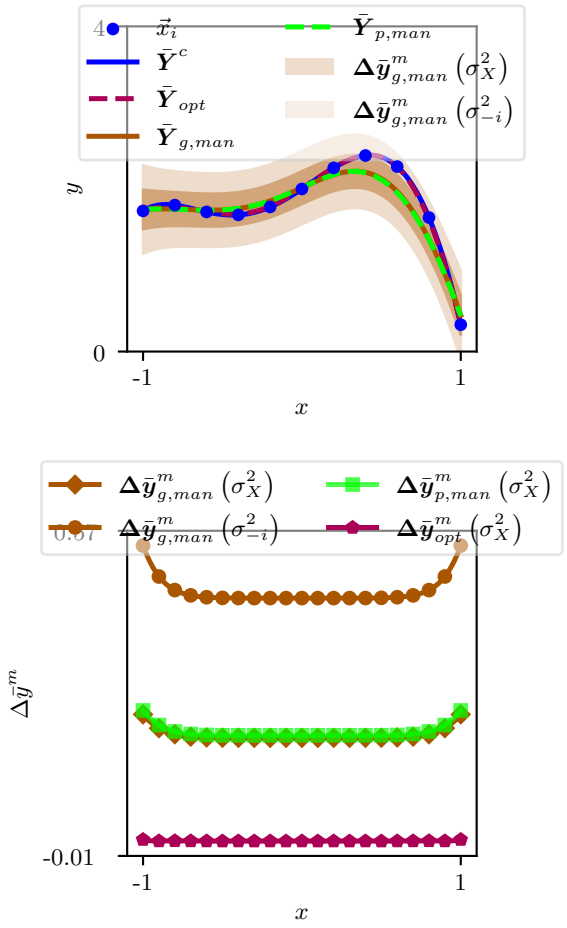

Figure G.3: Reproduction of the results $\bar{\boldsymbol{Y}}_{pub}$ of the RSM in Kim 2008 [28, Fig. 5d] with the RSMs $\bar{\boldsymbol{Y}}_{g,man}$ and $\bar{\boldsymbol{Y}}_{p,man}$ subjected to different weighting types; comparison to the RSM $\bar{\boldsymbol{Y}}_{opt}$ based on the calibration algorithm.

Finally, the complete-sample validation in Subs. 'Validation of the prediction interval method' (p. 42) determined the predictive capability of the prediction interval method either based on σ^2_X or σ^2_{-i}. The corresponding empirical confidence levels of Eq. D.13 (p. 43) are denoted with $\alpha^*\left(\sigma^2_X\right)$ and $\alpha^*\left(\sigma^2_{-i}\right)$. Eq. D.13 was further specified with: $\bar{\boldsymbol{Y}}_{X_{eval}} = \bar{\boldsymbol{Y}}_{opt}$ which is used to determine $\alpha^*\left(\sigma^2_X\right)$ and $\alpha^*\left(\sigma^2_{-i}\right)$; and $\bar{\boldsymbol{Y}}^* = \bar{\boldsymbol{Y}}^c_{X_{real}}$ which is the analytical function shown in Eq. G.7 providing results at 101 evenly spread data points, in more detail at $\widetilde{X} = X^{\mathrm{FFD}}$ with 101 levels in one dimension. With a confidence level of $\alpha = 0.7$ according to the Kim 2008 [28, Fig. 5d], Eq. D.13 led to: $\alpha^*\left(\sigma^2_X\right) = 0.77$ which is comparable to $\alpha^* = 0.82$ in Kim 2008 [28, Tab. 1]; and $\alpha^*\left(\sigma^2_{-i}\right) = 1.00$. From these results derives that σ^2_X leads to conservative prediction intervals with good predictive capability and σ^2_{-i} leads to too conservative prediction intervals, in other words small predictive capability.

In conclusion, the results did not reveal obvious problems in the implementation of MLS and the calibration algorithm or the prediction interval method. Also, they indicate a correspondence between the predictive capabilities of the predication interval method using σ^2_X and the results in Kim 2008 [28, Fig. 5d].

Table G.4: RSMs with their MLS attributes subjected to the analytical function in Eq. G.7 with different numbers of data points used to evaluate the calibration algorithm.

RSM	N_{dps}	weighting type	polynomial degree	parameter ω
$\bar{\boldsymbol{Y}}_{3,l}$	3	w_p	2	1
$\bar{\boldsymbol{Y}}_{3,g}$	3	w_p	2	1000
$\bar{\boldsymbol{Y}}_{6}$	6	w_p	2	0.75
$\bar{\boldsymbol{Y}}_{51}$	51	w_p	2	0.065

Calibration algorithm

The focus lies now on the performance of the calibration algorithm and also on MLS in case of overfitting. An overfitted RSM is caused by too many model parameters for a too small number of data points. It interpolates exactly to the data points and also reproduces aleatory uncertainties in the results of the complex model. But a deterministic RSM should not replicate aleatory uncertainties and hence, the residuals should not be zero.

This evaluation still applies Eq. G.7 representing the complex model. But the RSMs rely on different numbers of data points N_{dps} evenly spread on the domain, i.e. $X = X^{\text{FFD}}$ with the corresponding number of levels and one dimension. Tab. G.4 provides an overview on the MLS attributes of the different RSMs.

Three data points inevitably lead to overfitting of a quadratic polynomial. To evaluate MLS in case of overfitting, two RSMs are subjected to different manually set weighting parameters: $\bar{\boldsymbol{Y}}_{3,l}$, namely local, represents a MLS model with high spatial sensitivity; and $\bar{\boldsymbol{Y}}_{3,g}$, namely global, has low spatial sensitivity. For six data points, the RSM $\bar{\boldsymbol{Y}}_{6}$ results from the calibration algorithm and represents an intermediate step in the sequential refinement of the experimental design. Finally, the RSM $\bar{\boldsymbol{Y}}_{51}$, based on 51 data points and optimised with the calibration algorithm, serves to assess the results of MLS and the prediction interval method subjected to an 'infinite' number of data points.

The results of the RSMs are shown in Fig. G.4. The RSMs $\bar{\boldsymbol{Y}}_{3,l}$ and $\bar{\boldsymbol{Y}}_{3,g}$ both led to essentially the same results, in more detail a global quadratic polynomial, because the weighting matrix $\boldsymbol{W}$ is an identity matrix ensuing no effect of the weighting parameter. Thus, the global quadratic polynomial indicates overfitting of MLS. For six data points, the RSM $\bar{\boldsymbol{Y}}_{6}$ did not interpolate to the data points but approximated them demonstrating the trade-off between bias error and variance error in the calibration algorithm. At last, for the RSM $\bar{\boldsymbol{Y}}_{51}$ the calibration algorithm led to a small value of the weighting parameter which means a high spatial sensitivity with near interpolation to the data points and consequently small residuals. The small residuals again result in small prediction variances and prediction intervals. These results are reasonable since Eq. G.7 is not subjected to aleatory uncertainties.

The RSMs $\bar{\boldsymbol{Y}}_{3,l}$ and $\bar{\boldsymbol{Y}}_{3,g}$ illustrate the overfitting of MLS in case of an analytical equation which raises the question on overfitting of MLS using the data base for the system model. Since the mean results of the complex model used in the data base are considered to be deterministic with small aleatory uncertainties as outlined in Subs. 'Complex model within the system model' (p. 22), near interpolation of MLS is no sign for overfitting. However, a RSM subjected to overfitting can still be identified by the shape of a global linear or quadratic polynomial and small effects of the weighting parameter on the RSM. But in this dissertation, MLS is subjected to a linear polynomial, i.e. with a small number of polynomial terms, in case of a small number of data points as outlined in Subs. 'Calibration algorithm' (p. 45). Hence, overfitting of MLS in the system model is not expected.

The previous results lead to two conclusions. First, the calibration algorithm based on the prediction variance, i.e. also on the generalisation error, leads to a trade-off between bias

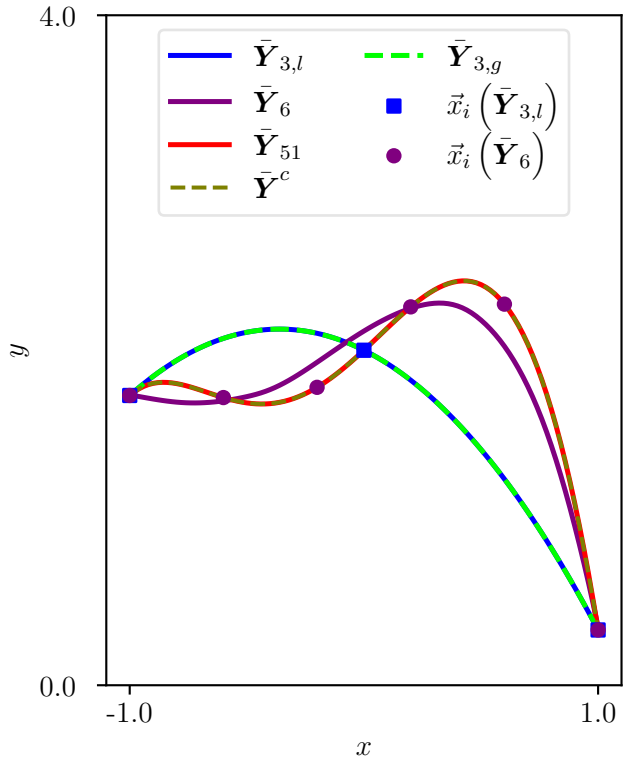

Figure G.4: Effect of different numbers of data points on the shapes of the RSMs in Tab. G.4; the data points $\vec{x}_i$ are only plotted for $\bar{\boldsymbol{Y}}_{3,l}$, $\bar{\boldsymbol{Y}}_{3,g}$ and $\bar{\boldsymbol{Y}}_{6}$.

error and variance error. The generalisation error serves for the same purpose as discussed in Section D.1.1 which corroborates this conclusion. Second, in case of an 'infinite' number of data points and small aleatory uncertainties, the metamodel uncertainty would be close to zero.

Conclusions

The results provided in this section give no hints on wrong implementation of MLS and the prediction interval method. Thus, this section adds to a successful verification of both methods. Moreover, MLS with the calibration algorithm leads to adequate results.

G.6.2 Weighting types in the calibration algorithm of MLS

The calibration algorithm of MLS comprises three different weighting types: w_g in Eq. D.16, w_p in Eq. D.17 and w_q in Eq. D.18 as described in Subs. 'Weighting functions' (p. 44). This section now questions the effect of these weighting types on the RSM by comparing different RSMs. The RSMs all use the data base of the default RSM in Tab. E.2 (p. 56) but apply different weighting types. For that reason, the calibration algorithm is restricted to specific weighting types and polynomial degrees for the RSMs but freely calibrates their weighting parameters ω. The default RSM bases on the unrestricted calibration algorithm and is denoted with $\bar{\boldsymbol{\xi}}_{X_{opt}} \equiv \bar{\boldsymbol{\xi}}_{X_{p,2}}$ for TA and $\bar{\boldsymbol{\xi}}_{X_{opt}} \equiv \bar{\boldsymbol{\xi}}_{X_{q,2}}$ for FA. Tab. G.5 provides an overview on the RSMs and their MLS attributes.

The complete-sample validation outlined in Subs. 'Validation of the prediction interval method' (p. 42) determined the predictive capability of the prediction interval of the default RSM. For this,

Table G.5: RSMs based on different weighting functions for TA with the weighting parameter ω (TA) and for FA with ω (FA); the default RSM is $\bar{\boldsymbol{\xi}}_{X_{opt}} \equiv \bar{\boldsymbol{\xi}}_{X_{p,2}}$ for scenarios with TA and $\bar{\boldsymbol{\xi}}_{X_{opt}} \equiv \bar{\boldsymbol{\xi}}_{X_{q,2}}$ for scenarios with FA; short notation for the euclidean relative difference erd $\equiv$ erd $\left(\bar{\boldsymbol{\xi}}_{X_i}, \bar{\boldsymbol{\xi}}_{X_{opt}}\right)$ with TA and FA in brackets.

RSM	weighting type	polynomial degree	ω (TA)	ω (FA)	erd (TA)	erd (FA)
$\bar{\boldsymbol{\xi}}_{X_{g,2}}$	w_g	2	0.522	0.792	0.02	0.02
$\bar{\boldsymbol{\xi}}_{X_{q,2}}$	w_q	2	0.004	0.160	0.06	0.00
$\bar{\boldsymbol{\xi}}_{X_{p,2}}$	w_p	2	1.206	1.140	0.00	0.04
$\bar{\boldsymbol{\xi}}_{X_{g,1}}$	w_g	1	0.271	0.305	0.17	0.08
$\bar{\boldsymbol{\xi}}_{X_{q,1}}$	w_q	1	0.004	0.004	0.24	0.10
$\bar{\boldsymbol{\xi}}_{X_{p,1}}$	w_p	1	0.729	0.768	0.18	0.08

Eq. D.13 (p. 43) for the empirical confidence level α^* specified: $\bar{\boldsymbol{Y}}_{X_{eval}} = \bar{\boldsymbol{\xi}}_{X_{opt}}$; and $\bar{\boldsymbol{Y}}^* = \bar{\boldsymbol{\xi}}_{X_i}$ with the RSMs $\bar{\boldsymbol{\xi}}_{X_i}$ shown in Tab. G.5 which provided results at the evaluation points representing the arbitrary points $\widetilde{X}$. As a result, the empirical confidence levels for all RSMs of the three weighting types with quadratic polynomials were close to $\alpha^* = 1.00$ for confidence levels $\alpha > 0.5$. Accordingly, all RSMs of the three weighting types with quadratic polynomials lay within the prediction interval of the default RSM. In other words, the prediction interval method covered the effect of the different weighting types on the RSMs.

The euclidean relative difference describes the effect of the weighting types on the RSMs more precisely. Tab. G.5 shows the euclidean relative difference between the different RSMs $\bar{\boldsymbol{\xi}}_{X_i}$ to the default RSM $\bar{\boldsymbol{\xi}}_{opt}$ at all evaluation points. Obviously, RSMs subjected to linear polynomials caused larger euclidean relative differences than RSMs with quadratic polynomials. Thus, the polynomial degree has more effect on the RSM than the weighting type.

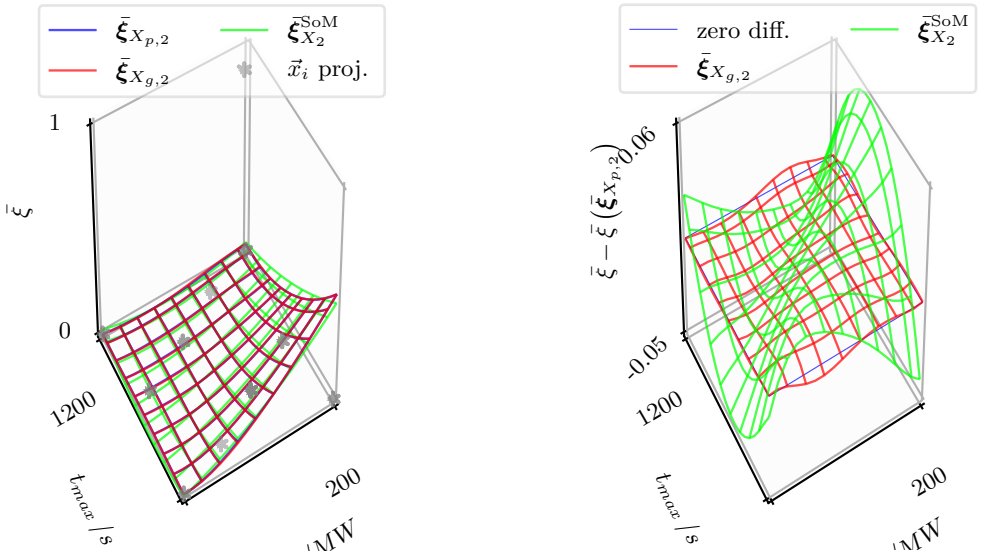

(a) result of RSM **(b)** difference to $\bar{\boldsymbol{\xi}}_{X_{opt}}$

Figure G.5: Difference between the result of the MLS models $\bar{\boldsymbol{\xi}}_{X_{p,2}}$ (default RSM), $\bar{\boldsymbol{\xi}}_{X_{g,2}}$ and the SoM model $\bar{\boldsymbol{\xi}}^{\mathrm{SoM}}_{X_2}$ for TA in the region of scenario sc($-$ MW, $-$ s, 194 s, 101, $fa = 0$); the figures display all data points $\vec{x}_i \in \bar{\boldsymbol{\xi}}^{c}_{X_2}$, for this reason, the results of the RSM are not close to all data points.

One result is worth discussing: the RSM $\bar{\boldsymbol{\xi}}_{X_{g,2}}$ fitted closely, i.e. with small euclidean relative difference, to the default RSM $\bar{\boldsymbol{\xi}}_{X_{opt}}$ for TA and FA. This result might indicate insufficient model adequacy of the RSM $\bar{\boldsymbol{\xi}}_{X_{g,2}}$ as discussed in Subs. 'Calibration algorithm' (p. G-22) for overfitting. But Fig. G.5 on p. G-24 exemplarily illustrates the difference of the RSM $\bar{\boldsymbol{\xi}}_{X_{g,2}}$ for TA to a SoM model $\bar{\boldsymbol{\xi}}_{X_2}^{\mathrm{SoM}}$. Because of this dissimilarity, there is no reason to assume insufficient model adequacy. In summary, the calibration algorithm using the three different weighting types leads to adequate RSMs.

G.7 Fire and evacuation scenarios of the data bases for the system model

The data bases introduced in Section E.1 comprise several fire scenarios and evacuation scenarios. The following two subsections provide information on each scenario, in detail: name, ED, as well as the risk factors maximum HRR HRR_{max}, time to maximum HRR t_{max}, maximum pre-evacuation time t_{pre}, number of tunnel users N_{tu}, and failure of tunnel alarm fa. Furthermore, the second subsection shows the arithmetic mean $\mu(\widetilde{\xi}^c)$ and the standard deviation $\sigma(\widetilde{\xi}_i^c)$ of the FFs of all 200 replications.

The simulations for fire and evacuation scenarios ran on different workstations using Windows 7 and the then current version of FDS and FDS+Evac. Furthermore, the JARA-HPC Vergabegremium and VSR commission on the supercomputer JURECA at Forschungszentrum Jülich granted additional run time on their clusters used for test purposes of the fire and evacuation scenarios.

List of fire scenarios in data bases

name	ED	$\mathrm{HRR}_{max}\,/MW$	$t_{max}\,/s$
FDSF0000	X_0^{fire}	25	600
FDSF0001	X_0^{fire}	200	600
FDSF0002	X_0^{fire}	25	1200
FDSF0003	X_0^{fire}	200	1200
FDSF0004	X_1^{fire}	94	1031
FDSF0005	X_1^{fire}	131	770
FDSF0006	X_{1a}^{fire}	151	962
FDSF0007	X_{1a}^{fire}	74	836
FDSF0008	X_2^{fire}	41	946
FDSF0009	X_2^{fire}	185	856
FDSF0010	X_2^{fire}	79	671
FDSF0011	X_2^{fire}	145	1136
FDSF0012	X_3^{fire}	165	632
FDSF0013	X_3^{fire}	35	720
FDSF0014	X_3^{fire}	191	1079
FDSF0015	X_3^{fire}	59	1162
FDSF0016	X_b^{fire}	115	1121
FDSF0017	X_b^{fire}	156	764
FDSF0018	X_b^{fire}	47	934
FDSF0019	X_b^{fire}	91	676
FDSF0020	X_b^{fire}	110	890
FDSF0021	X_b^{fire}	170	992

List of evacuation scenarios in data bases

name	ED	name (fire)	$\mathrm{HRR}_{max}\,/MW$	$t_{max}\,/s$	$t_{pre}\,/s$	N_{tu}	fa	$\mu(\widetilde{\xi^c})$	$\sigma(\widetilde{\xi^c})$
FDSE0000	X_0^{evac}	FDSF0000	25	600	100	30	FA	0.00	0.000
FDSE0001	X_0^{evac}	FDSF0001	200	600	100	30	FA	0.62	0.096
FDSE0002	X_0^{evac}	FDSF0002	25	1200	100	30	FA	0.00	0.000
FDSE0003	X_0^{evac}	FDSF0003	200	1200	100	30	FA	0.07	0.046
FDSE0004	X_0^{evac}	FDSF0000	25	600	300	30	FA	0.00	0.000
FDSE0005	X_0^{evac}	FDSF0001	200	600	300	30	FA	0.85	0.063
FDSE0006	X_0^{evac}	FDSF0002	25	1200	300	30	FA	0.00	0.000
FDSE0007	X_0^{evac}	FDSF0003	200	1200	300	30	FA	0.21	0.083
FDSE0008	X_0^{evac}	FDSF0000	25	600	100	180	FA	0.00	0.000
FDSE0009	X_0^{evac}	FDSF0001	200	600	100	180	FA	0.71	0.030
FDSE0010	X_0^{evac}	FDSF0002	25	1200	100	180	FA	0.00	0.000
FDSE0011	X_0^{evac}	FDSF0003	200	1200	100	180	FA	0.08	0.022
FDSE0012	X_0^{evac}	FDSF0000	25	600	300	180	FA	0.00	0.000
FDSE0013	X_0^{evac}	FDSF0001	200	600	300	180	FA	0.88	0.027
FDSE0014	X_0^{evac}	FDSF0002	25	1200	300	180	FA	0.00	0.000
FDSE0015	X_0^{evac}	FDSF0003	200	1200	300	180	FA	0.22	0.032
FDSE0016	X_1^{evac}	FDSF0003	200	1200	219	140	FA	0.17	0.036
FDSE0017	X_1^{evac}	FDSF0003	200	1200	134	111	FA	0.11	0.030
FDSE0018	X_1^{evac}	FDSF0004	94	1031	149	39	FA	0.01	0.017
FDSE0019	X_1^{evac}	FDSF0002	25	1200	216	164	FA	0.00	0.000
FDSE0020	X_1^{evac}	FDSF0002	25	1200	125	102	FA	0.00	0.000
FDSE0021	X_1^{evac}	FDSF0005	131	770	289	152	FA	0.42	0.052
FDSE0022	X_1^{evac}	FDSF0005	131	770	121	155	FA	0.23	0.035
FDSE0023	X_1^{evac}	FDSF0000	25	600	187	120	FA	0.00	0.000
FDSE0024	X_1^{evac}	FDSF0003	200	1200	276	87	FA	0.20	0.044
FDSE0025	X_1^{evac}	FDSF0004	94	1031	201	71	FA	0.04	0.022
FDSE0026	X_1^{evac}	FDSF0004	94	1031	206	170	FA	0.04	0.016
FDSE0027	X_1^{evac}	FDSF0005	131	770	110	75	FA	0.22	0.043
FDSE0028	X_1^{evac}	FDSF0005	131	770	240	48	FA	0.31	0.077
FDSE0029	X_1^{evac}	FDSF0001	200	600	177	58	FA	0.75	0.058
FDSE0030	X_1^{evac}	FDSF0004	94	1031	266	42	FA	0.07	0.042
FDSE0031	X_1^{evac}	FDSF0000	25	600	255	93	FA	0.00	0.000

name	ED	name (fire)	HRR_{max} /MW	t_{max} /s	t_{pre} /s	N_{tu}	fa	$\mu(\widetilde{\xi^c})$	$\sigma(\widetilde{\xi^c})$
FDSE0032	X_1^{evac}	FDSF0005	131	770	188	158	FA	0.28	0.036
FDSE0033	X_1^{evac}	FDSF0002	25	1200	227	63	FA	0.00	0.000
FDSE0034	X_1^{evac}	FDSF0000	25	600	171	53	FA	0.00	0.000
FDSE0035	X_1^{evac}	FDSF0001	200	600	143	116	FA	0.73	0.041
FDSE0036	X_1^{evac}	FDSF0003	200	1200	195	45	FA	0.15	0.055
FDSE0037	X_1^{evac}	FDSF0001	200	600	232	146	FA	0.84	0.032
FDSE0038	X_1^{evac}	FDSF0005	131	770	170	69	FA	0.26	0.054
FDSE0039	X_1^{evac}	FDSF0004	94	1031	159	175	FA	0.02	0.009
FDSE0040	X_1^{evac}	FDSF0002	25	1200	280	99	FA	0.00	0.000
FDSE0041	X_1^{evac}	FDSF0001	200	600	248	88	FA	0.83	0.037
FDSE0042	X_1^{evac}	FDSF0005	131	770	242	109	FA	0.34	0.054
FDSE0043	X_1^{evac}	FDSF0005	131	770	154	123	FA	0.26	0.040
FDSE0044	X_1^{evac}	FDSF0004	94	1031	141	130	FA	0.01	0.008
FDSE0045	X_1^{evac}	FDSF0004	94	1031	285	80	FA	0.08	0.031
FDSE0046	X_1^{evac}	FDSF0004	94	1031	264	135	FA	0.07	0.022
FDSE0047	X_1^{evac}	FDSF0000	25	600	115	81	FA	0.00	0.000
FDSE0048	X_0^{evac}	FDSF0000	25	600	100	30	TA	0.00	0.000
FDSE0049	X_0^{evac}	FDSF0001	200	600	100	30	TA	0.22	0.082
FDSE0050	X_0^{evac}	FDSF0002	25	1200	100	30	TA	0.00	0.000
FDSE0051	X_0^{evac}	FDSF0003	200	1200	100	30	TA	0.00	0.000
FDSE0052	X_0^{evac}	FDSF0000	25	600	300	30	TA	0.00	0.000
FDSE0053	X_0^{evac}	FDSF0001	200	600	300	30	TA	0.66	0.085
FDSE0054	X_0^{evac}	FDSF0002	25	1200	300	30	TA	0.00	0.000
FDSE0055	X_0^{evac}	FDSF0003	200	1200	300	30	TA	0.12	0.060
FDSE0056	X_0^{evac}	FDSF0000	25	600	100	180	TA	0.00	0.000
FDSE0057	X_0^{evac}	FDSF0001	200	600	100	180	TA	0.34	0.039
FDSE0058	X_0^{evac}	FDSF0002	25	1200	100	180	TA	0.00	0.000
FDSE0059	X_0^{evac}	FDSF0003	200	1200	100	180	TA	0.00	0.000
FDSE0060	X_0^{evac}	FDSF0000	25	600	300	180	TA	0.00	0.000
FDSE0061	X_0^{evac}	FDSF0001	200	600	300	180	TA	0.72	0.037
FDSE0062	X_0^{evac}	FDSF0002	25	1200	300	180	TA	0.00	0.000
FDSE0063	X_0^{evac}	FDSF0003	200	1200	300	180	TA	0.12	0.025
FDSE0064	X_1^{evac}	FDSF0003	200	1200	219	140	TA	0.06	0.022
FDSE0065	X_1^{evac}	FDSF0003	200	1200	134	111	TA	0.00	0.002
FDSE0066	X_1^{evac}	FDSF0004	94	1031	149	39	TA	0.00	0.000
FDSE0067	X_1^{evac}	FDSF0002	25	1200	216	164	TA	0.00	0.000
FDSE0068	X_1^{evac}	FDSF0002	25	1200	125	102	TA	0.00	0.000
FDSE0069	X_1^{evac}	FDSF0005	131	770	289	152	TA	0.26	0.049
FDSE0070	X_1^{evac}	FDSF0005	131	770	121	155	TA	0.01	0.008
FDSE0071	X_1^{evac}	FDSF0000	25	600	187	120	TA	0.00	0.000
FDSE0072	X_1^{evac}	FDSF0003	200	1200	276	87	TA	0.10	0.036
FDSE0073	X_1^{evac}	FDSF0004	94	1031	201	71	TA	0.00	0.000
FDSE0074	X_1^{evac}	FDSF0004	94	1031	206	170	TA	0.00	0.001
FDSE0075	X_1^{evac}	FDSF0005	131	770	110	75	TA	0.00	0.006
FDSE0076	X_1^{evac}	FDSF0005	131	770	240	48	TA	0.15	0.055
FDSE0077	X_1^{evac}	FDSF0001	200	600	177	58	TA	0.48	0.069
FDSE0078	X_1^{evac}	FDSF0004	94	1031	266	42	TA	0.01	0.017
FDSE0079	X_1^{evac}	FDSF0000	25	600	255	93	TA	0.00	0.000
FDSE0080	X_1^{evac}	FDSF0005	131	770	188	158	TA	0.09	0.026
FDSE0081	X_1^{evac}	FDSF0002	25	1200	227	63	TA	0.00	0.000
FDSE0082	X_1^{evac}	FDSF0000	25	600	171	53	TA	0.00	0.000
FDSE0083	X_1^{evac}	FDSF0001	200	600	143	116	TA	0.42	0.047
FDSE0084	X_1^{evac}	FDSF0003	200	1200	195	45	TA	0.03	0.027
FDSE0085	X_1^{evac}	FDSF0001	200	600	232	146	TA	0.62	0.045
FDSE0086	X_1^{evac}	FDSF0005	131	770	170	69	TA	0.06	0.029
FDSE0087	X_1^{evac}	FDSF0004	94	1031	159	175	TA	0.00	0.000
FDSE0088	X_1^{evac}	FDSF0002	25	1200	280	99	TA	0.00	0.000
FDSE0089	X_1^{evac}	FDSF0001	200	600	248	88	TA	0.61	0.059
FDSE0090	X_1^{evac}	FDSF0005	131	770	242	109	TA	0.17	0.048
FDSE0091	X_1^{evac}	FDSF0005	131	770	154	123	TA	0.04	0.020
FDSE0092	X_1^{evac}	FDSF0004	94	1031	141	130	TA	0.00	0.000
FDSE0093	X_1^{evac}	FDSF0004	94	1031	285	80	TA	0.02	0.014
FDSE0094	X_1^{evac}	FDSF0004	94	1031	264	135	TA	0.01	0.009
FDSE0095	X_1^{evac}	FDSF0000	25	600	115	81	TA	0.00	0.000
FDSE0096	X_{1a}^{evac}	FDSF0001	200	600	133	92	FA	0.70	0.046
FDSE0097	X_{1a}^{evac}	FDSF0002	25	1200	182	62	FA	0.00	0.000
FDSE0098	X_{1a}^{evac}	FDSF0006	151	962	171	155	FA	0.18	0.031

name	ED	name (fire)	HRR_{max} /MW	t_{max} /s	t_{pre} /s	N_{tu}	fa	$\mu(\widetilde{\xi^c})$	$\sigma(\widetilde{\xi^c})$
FDSE0099	X_{1a}^{evac}	FDSF0006	151	962	137	49	FA	0.15	0.043
FDSE0100	X_{1a}^{evac}	FDSF0006	151	962	287	114	FA	0.25	0.045
FDSE0101	X_{1a}^{evac}	FDSF0001	200	600	218	53	FA	0.80	0.056
FDSE0102	X_{1a}^{evac}	FDSF0002	25	1200	267	102	FA	0.00	0.000
FDSE0103	X_{1a}^{evac}	FDSF0003	200	1200	209	125	FA	0.16	0.034
FDSE0104	X_{1a}^{evac}	FDSF0003	200	1200	144	87	FA	0.11	0.035
FDSE0105	X_{1a}^{evac}	FDSF0001	200	600	261	100	FA	0.84	0.041
FDSE0106	X_{1a}^{evac}	FDSF0000	25	600	202	70	FA	0.00	0.000
FDSE0107	X_{1a}^{evac}	FDSF0007	74	836	255	140	FA	0.04	0.016
FDSE0108	X_{1a}^{evac}	FDSF0006	151	962	250	76	FA	0.23	0.045
FDSE0109	X_{1a}^{evac}	FDSF0006	151	962	114	168	FA	0.14	0.029
FDSE0110	X_{1a}^{evac}	FDSF0000	25	600	121	88	FA	0.00	0.000
FDSE0111	X_{1a}^{evac}	FDSF0001	200	600	184	158	FA	0.80	0.031
FDSE0112	X_{1a}^{evac}	FDSF0002	25	1200	213	167	FA	0.00	0.000
FDSE0113	X_{1a}^{evac}	FDSF0003	200	1200	225	57	FA	0.17	0.054
FDSE0114	X_{1a}^{evac}	FDSF0006	151	962	200	107	FA	0.20	0.036
FDSE0115	X_{1a}^{evac}	FDSF0007	74	836	190	149	FA	0.02	0.011
FDSE0116	X_{1a}^{evac}	FDSF0007	74	836	158	172	FA	0.01	0.008
FDSE0117	X_{1a}^{evac}	FDSF0000	25	600	169	135	FA	0.00	0.000
FDSE0118	X_{1a}^{evac}	FDSF0000	25	600	271	114	FA	0.00	0.000
FDSE0119	X_{1a}^{evac}	FDSF0007	74	836	148	122	FA	0.01	0.007
FDSE0120	X_{1a}^{evac}	FDSF0007	74	836	161	71	FA	0.01	0.014
FDSE0121	X_{1a}^{evac}	FDSF0003	200	1200	291	127	FA	0.21	0.040
FDSE0122	X_{1a}^{evac}	FDSF0006	151	962	231	36	FA	0.21	0.063
FDSE0123	X_{1a}^{evac}	FDSF0007	74	836	236	43	FA	0.03	0.026
FDSE0124	X_{1a}^{evac}	FDSF0006	151	962	242	153	FA	0.23	0.034
FDSE0125	X_{1a}^{evac}	FDSF0007	74	836	279	82	FA	0.06	0.026
FDSE0126	X_{1a}^{evac}	FDSF0006	151	962	124	96	FA	0.14	0.035
FDSE0127	X_{1a}^{evac}	FDSF0002	25	1200	108	101	FA	0.00	0.000
FDSE0128	X_{1a}^{evac}	FDSF0001	200	600	133	92	TA	0.37	0.052
FDSE0129	X_{1a}^{evac}	FDSF0002	25	1200	182	62	TA	0.00	0.000
FDSE0130	X_{1a}^{evac}	FDSF0006	151	962	171	155	TA	0.02	0.012
FDSE0131	X_{1a}^{evac}	FDSF0006	151	962	137	49	TA	0.00	0.008
FDSE0132	X_{1a}^{evac}	FDSF0006	151	962	287	114	TA	0.13	0.033
FDSE0133	X_{1a}^{evac}	FDSF0001	200	600	218	53	TA	0.55	0.065
FDSE0134	X_{1a}^{evac}	FDSF0002	25	1200	267	102	TA	0.00	0.000
FDSE0135	X_{1a}^{evac}	FDSF0003	200	1200	209	125	TA	0.05	0.020
FDSE0136	X_{1a}^{evac}	FDSF0003	200	1200	144	87	TA	0.00	0.005
FDSE0137	X_{1a}^{evac}	FDSF0001	200	600	261	100	TA	0.64	0.052
FDSE0138	X_{1a}^{evac}	FDSF0000	25	600	202	70	TA	0.00	0.000
FDSE0139	X_{1a}^{evac}	FDSF0007	74	836	255	140	TA	0.00	0.003
FDSE0140	X_{1a}^{evac}	FDSF0006	151	962	250	76	TA	0.09	0.034
FDSE0141	X_{1a}^{evac}	FDSF0006	151	962	114	168	TA	0.00	0.000
FDSE0142	X_{1a}^{evac}	FDSF0000	25	600	121	88	TA	0.00	0.000
FDSE0143	X_{1a}^{evac}	FDSF0001	200	600	184	158	TA	0.54	0.046
FDSE0144	X_{1a}^{evac}	FDSF0002	25	1200	213	167	TA	0.00	0.000
FDSE0145	X_{1a}^{evac}	FDSF0003	200	1200	225	57	TA	0.06	0.030
FDSE0146	X_{1a}^{evac}	FDSF0006	151	962	200	107	TA	0.05	0.023
FDSE0147	X_{1a}^{evac}	FDSF0007	74	836	190	149	TA	0.00	0.000
FDSE0148	X_{1a}^{evac}	FDSF0007	74	836	158	172	TA	0.00	0.000
FDSE0149	X_{1a}^{evac}	FDSF0000	25	600	169	135	TA	0.00	0.000
FDSE0150	X_{1a}^{evac}	FDSF0000	25	600	271	114	TA	0.00	0.000
FDSE0151	X_{1a}^{evac}	FDSF0007	74	836	148	122	TA	0.00	0.000
FDSE0152	X_{1a}^{evac}	FDSF0007	74	836	161	71	TA	0.00	0.000
FDSE0153	X_{1a}^{evac}	FDSF0003	200	1200	291	127	TA	0.11	0.028
FDSE0154	X_{1a}^{evac}	FDSF0006	151	962	231	36	TA	0.08	0.045
FDSE0155	X_{1a}^{evac}	FDSF0007	74	836	236	43	TA	0.00	0.000
FDSE0156	X_{1a}^{evac}	FDSF0006	151	962	242	153	TA	0.09	0.023
FDSE0157	X_{1a}^{evac}	FDSF0007	74	836	279	82	TA	0.00	0.007
FDSE0158	X_{1a}^{evac}	FDSF0006	151	962	124	96	TA	0.00	0.002
FDSE0159	X_{1a}^{evac}	FDSF0002	25	1200	108	101	TA	0.00	0.000
FDSE0160	X_{2}^{evac}	FDSF0010	79	671	273	126	FA	0.17	0.034
FDSE0161	X_{2}^{evac}	FDSF0009	185	856	270	136	FA	0.50	0.046
FDSE0162	X_{2}^{evac}	FDSF0009	185	856	179	59	FA	0.30	0.063
FDSE0163	X_{2}^{evac}	FDSF0008	41	946	118	35	FA	0.00	0.000
FDSE0164	X_{2}^{evac}	FDSF0011	145	1136	294	147	FA	0.16	0.033
FDSE0165	X_{2}^{evac}	FDSF0011	145	1136	132	160	FA	0.06	0.021

name	ED	name (fire)	HRR_{max} /MW	t_{max} /s	t_{pre} /s	N_{tu}	fa	$\mu(\widetilde{\xi^c})$	$\sigma(\widetilde{\xi^c})$
FDSE0166	X_2^{evac}	FDSF0011	145	1136	236	142	FA	0.13	0.030
FDSE0167	X_2^{evac}	FDSF0001	200	600	257	51	FA	0.83	0.054
FDSE0168	X_2^{evac}	FDSF0009	185	856	138	156	FA	0.28	0.034
FDSE0169	X_2^{evac}	FDSF0009	185	856	104	44	FA	0.25	0.074
FDSE0170	X_2^{evac}	FDSF0008	41	946	297	128	FA	0.00	0.000
FDSE0171	X_2^{evac}	FDSF0009	185	856	115	167	FA	0.26	0.032
FDSE0172	X_2^{evac}	FDSF0003	200	1200	261	52	FA	0.18	0.054
FDSE0173	X_2^{evac}	FDSF0010	79	671	225	63	FA	0.14	0.043
FDSE0174	X_2^{evac}	FDSF0011	145	1136	292	48	FA	0.15	0.055
FDSE0175	X_2^{evac}	FDSF0003	200	1200	106	85	FA	0.08	0.028
FDSE0176	X_2^{evac}	FDSF0004	94	1031	104	159	FA	0.00	0.002
FDSE0177	X_2^{evac}	FDSF0010	79	671	102	31	FA	0.05	0.038
FDSE0178	X_2^{evac}	FDSF0010	79	671	129	89	FA	0.09	0.034
FDSE0179	X_2^{evac}	FDSF0003	200	1200	198	107	FA	0.15	0.035
FDSE0180	X_2^{evac}	FDSF0001	200	600	162	174	FA	0.79	0.029
FDSE0181	X_2^{evac}	FDSF0000	25	600	298	100	FA	0.00	0.000
FDSE0182	X_2^{evac}	FDSF0008	41	946	146	143	FA	0.00	0.000
FDSE0183	X_2^{evac}	FDSF0011	145	1136	128	118	FA	0.05	0.021
FDSE0184	X_2^{evac}	FDSF0002	25	1200	111	150	FA	0.00	0.000
FDSE0185	X_2^{evac}	FDSF0009	185	856	184	134	FA	0.32	0.040
FDSE0186	X_2^{evac}	FDSF0008	41	946	278	168	FA	0.00	0.000
FDSE0187	X_2^{evac}	FDSF0000	25	600	235	152	FA	0.00	0.000
FDSE0188	X_2^{evac}	FDSF0001	200	600	112	73	FA	0.66	0.053
FDSE0189	X_2^{evac}	FDSF0005	131	770	210	93	FA	0.29	0.048
FDSE0190	X_2^{evac}	FDSF0004	94	1031	157	60	FA	0.02	0.016
FDSE0191	X_2^{evac}	FDSF0002	25	1200	152	68	FA	0.00	0.000
FDSE0192	X_2^{evac}	FDSF0008	41	946	167	67	FA	0.00	0.000
FDSE0193	X_2^{evac}	FDSF0011	145	1136	119	36	FA	0.05	0.035
FDSE0194	X_2^{evac}	FDSF0009	185	856	274	77	FA	0.48	0.059
FDSE0195	X_2^{evac}	FDSF0011	145	1136	259	172	FA	0.15	0.030
FDSE0196	X_2^{evac}	FDSF0008	41	946	108	162	FA	0.00	0.000
FDSE0197	X_2^{evac}	FDSF0000	25	600	137	176	FA	0.00	0.000
FDSE0198	X_2^{evac}	FDSF0010	79	671	288	34	FA	0.17	0.062
FDSE0199	X_2^{evac}	FDSF0009	185	856	268	36	FA	0.46	0.083
FDSE0200	X_2^{evac}	FDSF0003	200	1200	252	173	FA	0.20	0.033
FDSE0201	X_2^{evac}	FDSF0010	79	671	213	179	FA	0.14	0.031
FDSE0202	X_2^{evac}	FDSF0000	25	600	246	41	FA	0.00	0.000
FDSE0203	X_2^{evac}	FDSF0010	79	671	123	165	FA	0.08	0.025
FDSE0204	X_2^{evac}	FDSF0009	185	856	291	178	FA	0.54	0.040
FDSE0205	X_2^{evac}	FDSF0010	79	671	282	171	FA	0.18	0.032
FDSE0206	X_2^{evac}	FDSF0008	41	946	285	33	FA	0.00	0.000
FDSE0207	X_2^{evac}	FDSF0005	131	770	295	45	FA	0.40	0.071
FDSE0208	X_2^{evac}	FDSF0010	79	671	273	126	TA	0.05	0.018
FDSE0209	X_2^{evac}	FDSF0009	185	856	270	136	TA	0.32	0.046
FDSE0210	X_2^{evac}	FDSF0009	185	856	179	59	TA	0.10	0.041
FDSE0211	X_2^{evac}	FDSF0008	41	946	118	35	TA	0.00	0.000
FDSE0212	X_2^{evac}	FDSF0011	145	1136	294	147	TA	0.08	0.027
FDSE0213	X_2^{evac}	FDSF0011	145	1136	132	160	TA	0.00	0.000
FDSE0214	X_2^{evac}	FDSF0011	145	1136	236	142	TA	0.04	0.017
FDSE0215	X_2^{evac}	FDSF0001	200	600	257	51	TA	0.61	0.076
FDSE0216	X_2^{evac}	FDSF0009	185	856	138	156	TA	0.04	0.016
FDSE0217	X_2^{evac}	FDSF0009	185	856	104	44	TA	0.01	0.013
FDSE0218	X_2^{evac}	FDSF0008	41	946	297	128	TA	0.00	0.000
FDSE0219	X_2^{evac}	FDSF0009	185	856	115	167	TA	0.02	0.012
FDSE0220	X_2^{evac}	FDSF0003	200	1200	261	52	TA	0.09	0.042
FDSE0221	X_2^{evac}	FDSF0010	79	671	225	63	TA	0.02	0.019
FDSE0222	X_2^{evac}	FDSF0011	145	1136	292	48	TA	0.08	0.041
FDSE0223	X_2^{evac}	FDSF0003	200	1200	106	85	TA	0.00	0.000
FDSE0224	X_2^{evac}	FDSF0004	94	1031	104	159	TA	0.00	0.000
FDSE0225	X_2^{evac}	FDSF0010	79	671	102	31	TA	0.00	0.000
FDSE0226	X_2^{evac}	FDSF0010	79	671	129	89	TA	0.00	0.000
FDSE0227	X_2^{evac}	FDSF0003	200	1200	198	107	TA	0.04	0.017
FDSE0228	X_2^{evac}	FDSF0001	200	600	162	174	TA	0.51	0.037
FDSE0229	X_2^{evac}	FDSF0000	25	600	298	100	TA	0.00	0.000
FDSE0230	X_2^{evac}	FDSF0008	41	946	146	143	TA	0.00	0.000
FDSE0231	X_2^{evac}	FDSF0011	145	1136	128	118	TA	0.00	0.000
FDSE0232	X_2^{evac}	FDSF0002	25	1200	111	150	TA	0.00	0.000

name	ED	name (fire)	HRR_{max} /MW	t_{max} /s	t_{pre} /s	N_{tu}	fa	$\mu(\widetilde{\xi^c})$	$\sigma(\widetilde{\xi^c})$
FDSE0233	X_2^{evac}	FDSF0009	185	856	184	134	TA	0.12	0.029
FDSE0234	X_2^{evac}	FDSF0008	41	946	278	168	TA	0.00	0.000
FDSE0235	X_2^{evac}	FDSF0000	25	600	235	152	TA	0.00	0.000
FDSE0236	X_2^{evac}	FDSF0001	200	600	112	73	TA	0.29	0.056
FDSE0237	X_2^{evac}	FDSF0005	131	770	210	93	TA	0.11	0.034
FDSE0238	X_2^{evac}	FDSF0004	94	1031	157	60	TA	0.00	0.000
FDSE0239	X_2^{evac}	FDSF0002	25	1200	152	68	TA	0.00	0.000
FDSE0240	X_2^{evac}	FDSF0008	41	946	167	67	TA	0.00	0.000
FDSE0241	X_2^{evac}	FDSF0011	145	1136	119	36	TA	0.00	0.000
FDSE0242	X_2^{evac}	FDSF0009	185	856	274	77	TA	0.31	0.057
FDSE0243	X_2^{evac}	FDSF0011	145	1136	259	172	TA	0.06	0.020
FDSE0244	X_2^{evac}	FDSF0008	41	946	108	162	TA	0.00	0.000
FDSE0245	X_2^{evac}	FDSF0000	25	600	137	176	TA	0.00	0.000
FDSE0246	X_2^{evac}	FDSF0010	79	671	288	34	TA	0.05	0.038
FDSE0247	X_2^{evac}	FDSF0009	185	856	268	36	TA	0.29	0.076
FDSE0248	X_2^{evac}	FDSF0003	200	1200	252	173	TA	0.09	0.024
FDSE0249	X_2^{evac}	FDSF0010	79	671	213	179	TA	0.02	0.010
FDSE0250	X_2^{evac}	FDSF0000	25	600	246	41	TA	0.00	0.000
FDSE0251	X_2^{evac}	FDSF0010	79	671	123	165	TA	0.00	0.000
FDSE0252	X_2^{evac}	FDSF0009	185	856	291	178	TA	0.38	0.044
FDSE0253	X_2^{evac}	FDSF0010	79	671	282	171	TA	0.05	0.019
FDSE0254	X_2^{evac}	FDSF0008	41	946	285	33	TA	0.00	0.000
FDSE0255	X_2^{evac}	FDSF0005	131	770	295	45	TA	0.25	0.073
FDSE0256	X_3^{evac}	FDSF0013	35	720	136	62	FA	0.00	0.000
FDSE0257	X_3^{evac}	FDSF0015	59	1162	281	178	FA	0.00	0.000
FDSE0258	X_3^{evac}	FDSF0009	185	856	290	96	FA	0.51	0.057
FDSE0259	X_3^{evac}	FDSF0014	191	1079	287	38	FA	0.25	0.076
FDSE0260	X_3^{evac}	FDSF0015	59	1162	130	57	FA	0.00	0.000
FDSE0261	X_3^{evac}	FDSF0002	25	1200	222	40	FA	0.00	0.000
FDSE0262	X_3^{evac}	FDSF0015	59	1162	127	32	FA	0.00	0.000
FDSE0263	X_3^{evac}	FDSF0015	59	1162	269	139	FA	0.00	0.000
FDSE0264	X_3^{evac}	FDSF0011	145	1136	249	36	FA	0.13	0.056
FDSE0265	X_3^{evac}	FDSF0011	145	1136	155	49	FA	0.07	0.034
FDSE0266	X_3^{evac}	FDSF0005	131	770	297	172	FA	0.46	0.056
FDSE0267	X_3^{evac}	FDSF0008	41	946	102	125	FA	0.00	0.000
FDSE0268	X_3^{evac}	FDSF0012	165	632	297	148	FA	0.80	0.034
FDSE0269	X_3^{evac}	FDSF0000	25	600	272	163	FA	0.00	0.000
FDSE0270	X_3^{evac}	FDSF0014	191	1079	286	149	FA	0.26	0.035
FDSE0271	X_3^{evac}	FDSF0010	79	671	176	171	FA	0.12	0.028
FDSE0272	X_3^{evac}	FDSF0008	41	946	160	169	FA	0.00	0.000
FDSE0273	X_3^{evac}	FDSF0009	185	856	245	174	FA	0.47	0.038
FDSE0274	X_3^{evac}	FDSF0012	165	632	277	177	FA	0.80	0.032
FDSE0275	X_3^{evac}	FDSF0015	59	1162	139	161	FA	0.00	0.000
FDSE0276	X_3^{evac}	FDSF0012	165	632	114	165	FA	0.59	0.036
FDSE0277	X_3^{evac}	FDSF0013	35	720	192	153	FA	0.00	0.000
FDSE0278	X_3^{evac}	FDSF0013	35	720	253	83	FA	0.00	0.000
FDSE0279	X_3^{evac}	FDSF0013	35	720	283	145	FA	0.00	0.000
FDSE0280	X_3^{evac}	FDSF0009	185	856	144	38	FA	0.27	0.075
FDSE0281	X_3^{evac}	FDSF0004	94	1031	120	78	FA	0.00	0.006
FDSE0282	X_3^{evac}	FDSF0014	191	1079	167	55	FA	0.17	0.048
FDSE0283	X_3^{evac}	FDSF0012	165	632	125	66	FA	0.52	0.062
FDSE0284	X_3^{evac}	FDSF0008	41	946	263	131	FA	0.00	0.000
FDSE0285	X_3^{evac}	FDSF0014	191	1079	116	46	FA	0.13	0.049
FDSE0286	X_3^{evac}	FDSF0013	35	720	108	157	FA	0.00	0.000
FDSE0287	X_3^{evac}	FDSF0012	165	632	299	47	FA	0.78	0.064
FDSE0288	X_3^{evac}	FDSF0008	41	946	101	54	FA	0.00	0.000
FDSE0289	X_3^{evac}	FDSF0012	165	632	106	50	FA	0.49	0.076
FDSE0290	X_3^{evac}	FDSF0004	94	1031	118	179	FA	0.00	0.004
FDSE0291	X_3^{evac}	FDSF0004	94	1031	291	42	FA	0.09	0.045
FDSE0292	X_3^{evac}	FDSF0013	35	720	103	33	FA	0.00	0.000
FDSE0293	X_3^{evac}	FDSF0015	59	1162	293	30	FA	0.00	0.000
FDSE0294	X_3^{evac}	FDSF0004	94	1031	107	39	FA	0.00	0.005
FDSE0295	X_3^{evac}	FDSF0011	145	1136	112	173	FA	0.04	0.018
FDSE0296	X_3^{evac}	FDSF0005	131	770	104	176	FA	0.22	0.030
FDSE0297	X_3^{evac}	FDSF0014	191	1079	114	179	FA	0.14	0.029
FDSE0298	X_3^{evac}	FDSF0013	35	720	295	35	FA	0.00	0.000
FDSE0299	X_3^{evac}	FDSF0005	131	770	109	37	FA	0.21	0.064

name	ED	name (fire)	$\mathrm{HRR}_{max}\,/MW$	$t_{max}\,/s$	$t_{pre}\,/s$	N_{tu}	fa	$\mu(\widetilde{\xi^c})$	$\sigma(\widetilde{\xi^c})$
FDSE0300	X_3^{evac}	FDSF0013	35	720	292	166	FA	0.00	0.000
FDSE0301	X_3^{evac}	FDSF0011	145	1136	284	178	FA	0.16	0.032
FDSE0302	X_3^{evac}	FDSF0011	145	1136	296	31	FA	0.16	0.065
FDSE0303	X_3^{evac}	FDSF0015	59	1162	105	179	FA	0.00	0.000
FDSE0304	X_3^{evac}	FDSF0013	35	720	136	62	TA	0.00	0.000
FDSE0305	X_3^{evac}	FDSF0015	59	1162	281	178	TA	0.00	0.000
FDSE0306	X_3^{evac}	FDSF0009	185	856	290	96	TA	0.35	0.050
FDSE0307	X_3^{evac}	FDSF0014	191	1079	287	38	TA	0.13	0.055
FDSE0308	X_3^{evac}	FDSF0015	59	1162	130	57	TA	0.00	0.000
FDSE0309	X_3^{evac}	FDSF0002	25	1200	222	40	TA	0.00	0.000
FDSE0310	X_3^{evac}	FDSF0015	59	1162	127	32	TA	0.00	0.000
FDSE0311	X_3^{evac}	FDSF0015	59	1162	269	139	TA	0.00	0.000
FDSE0312	X_3^{evac}	FDSF0011	145	1136	249	36	TA	0.05	0.037
FDSE0313	X_3^{evac}	FDSF0011	145	1136	155	49	TA	0.00	0.003
FDSE0314	X_3^{evac}	FDSF0005	131	770	297	172	TA	0.29	0.047
FDSE0315	X_3^{evac}	FDSF0008	41	946	102	125	TA	0.00	0.000
FDSE0316	X_3^{evac}	FDSF0012	165	632	297	148	TA	0.62	0.046
FDSE0317	X_3^{evac}	FDSF0000	25	600	272	163	TA	0.00	0.000
FDSE0318	X_3^{evac}	FDSF0014	191	1079	286	149	TA	0.14	0.029
FDSE0319	X_3^{evac}	FDSF0010	79	671	176	171	TA	0.00	0.004
FDSE0320	X_3^{evac}	FDSF0008	41	946	160	169	TA	0.00	0.000
FDSE0321	X_3^{evac}	FDSF0009	185	856	245	174	TA	0.29	0.040
FDSE0322	X_3^{evac}	FDSF0012	165	632	277	177	TA	0.60	0.041
FDSE0323	X_3^{evac}	FDSF0015	59	1162	139	161	TA	0.00	0.000
FDSE0324	X_3^{evac}	FDSF0012	165	632	114	165	TA	0.22	0.036
FDSE0325	X_3^{evac}	FDSF0013	35	720	192	153	TA	0.00	0.000
FDSE0326	X_3^{evac}	FDSF0013	35	720	253	83	TA	0.00	0.000
FDSE0327	X_3^{evac}	FDSF0013	35	720	283	145	TA	0.00	0.000
FDSE0328	X_3^{evac}	FDSF0009	185	856	144	38	TA	0.05	0.034
FDSE0329	X_3^{evac}	FDSF0004	94	1031	120	78	TA	0.00	0.000
FDSE0330	X_3^{evac}	FDSF0014	191	1079	167	55	TA	0.03	0.022
FDSE0331	X_3^{evac}	FDSF0012	165	632	125	66	TA	0.21	0.054
FDSE0332	X_3^{evac}	FDSF0008	41	946	263	131	TA	0.00	0.000
FDSE0333	X_3^{evac}	FDSF0014	191	1079	116	46	TA	0.00	0.003
FDSE0334	X_3^{evac}	FDSF0013	35	720	108	157	TA	0.00	0.000
FDSE0335	X_3^{evac}	FDSF0012	165	632	299	47	TA	0.58	0.082
FDSE0336	X_3^{evac}	FDSF0008	41	946	101	54	TA	0.00	0.000
FDSE0337	X_3^{evac}	FDSF0012	165	632	106	50	TA	0.13	0.056
FDSE0338	X_3^{evac}	FDSF0004	94	1031	118	179	TA	0.00	0.000
FDSE0339	X_3^{evac}	FDSF0004	94	1031	291	42	TA	0.02	0.022
FDSE0340	X_3^{evac}	FDSF0013	35	720	103	33	TA	0.00	0.000
FDSE0341	X_3^{evac}	FDSF0015	59	1162	293	30	TA	0.00	0.000
FDSE0342	X_3^{evac}	FDSF0004	94	1031	107	39	TA	0.00	0.000
FDSE0343	X_3^{evac}	FDSF0011	145	1136	112	173	TA	0.00	0.000
FDSE0344	X_3^{evac}	FDSF0005	131	770	104	176	TA	0.00	0.003
FDSE0345	X_3^{evac}	FDSF0014	191	1079	114	179	TA	0.00	0.001
FDSE0346	X_3^{evac}	FDSF0013	35	720	295	35	TA	0.00	0.000
FDSE0347	X_3^{evac}	FDSF0005	131	770	109	37	TA	0.00	0.008
FDSE0348	X_3^{evac}	FDSF0013	35	720	292	166	TA	0.00	0.000
FDSE0349	X_3^{evac}	FDSF0011	145	1136	284	178	TA	0.08	0.024
FDSE0350	X_3^{evac}	FDSF0011	145	1136	296	31	TA	0.08	0.048
FDSE0351	X_3^{evac}	FDSF0015	59	1162	105	179	TA	0.00	0.000
FDSE0352	X_b^{evac}	FDSF0016	115	1121	202	52	FA	0.06	0.035
FDSE0353	X_b^{evac}	FDSF0000	25	600	177	80	FA	0.00	0.000
FDSE0354	X_b^{evac}	FDSF0016	115	1121	289	66	FA	0.11	0.039
FDSE0355	X_b^{evac}	FDSF0003	200	1200	141	98	FA	0.11	0.036
FDSE0356	X_b^{evac}	FDSF0000	25	600	144	92	FA	0.00	0.000
FDSE0357	X_b^{evac}	FDSF0003	200	1200	187	96	FA	0.15	0.036
FDSE0358	X_b^{evac}	FDSF0017	156	764	232	79	FA	0.46	0.056
FDSE0359	X_b^{evac}	FDSF0017	156	764	248	54	FA	0.48	0.069
FDSE0360	X_b^{evac}	FDSF0021	170	992	256	127	FA	0.25	0.041
FDSE0361	X_b^{evac}	FDSF0001	200	600	161	177	FA	0.79	0.028
FDSE0362	X_b^{evac}	FDSF0016	115	1121	156	41	FA	0.03	0.029
FDSE0363	X_b^{evac}	FDSF0002	25	1200	260	74	FA	0.00	0.000
FDSE0364	X_b^{evac}	FDSF0017	156	764	104	148	FA	0.27	0.036
FDSE0365	X_b^{evac}	FDSF0018	47	934	295	92	FA	0.00	0.000
FDSE0366	X_b^{evac}	FDSF0003	200	1200	120	135	FA	0.09	0.028

name	ED	name (fire)	$\mathrm{HRR}_{max}\,/MW$	$t_{max}\,/s$	$t_{pre}\,/s$	N_{tu}	fa	$\mu(\widetilde{\xi^c})$	$\sigma(\widetilde{\xi^c})$
FDSE0367	X_b^{evac}	FDSF0002	25	1200	192	144	FA	0.00	0.000
FDSE0368	X_b^{evac}	FDSF0016	115	1121	109	132	FA	0.01	0.008
FDSE0369	X_b^{evac}	FDSF0018	47	934	226	39	FA	0.00	0.000
FDSE0370	X_b^{evac}	FDSF0018	47	934	238	111	FA	0.00	0.000
FDSE0371	X_b^{evac}	FDSF0020	110	890	280	166	FA	0.20	0.033
FDSE0372	X_b^{evac}	FDSF0002	25	1200	167	124	FA	0.00	0.000
FDSE0373	X_b^{evac}	FDSF0020	110	890	240	114	FA	0.17	0.042
FDSE0374	X_b^{evac}	FDSF0003	200	1200	222	108	FA	0.17	0.035
FDSE0375	X_b^{evac}	FDSF0003	200	1200	269	123	FA	0.20	0.036
FDSE0376	X_b^{evac}	FDSF0017	156	764	129	115	FA	0.29	0.041
FDSE0377	X_b^{evac}	FDSF0017	156	764	263	175	FA	0.55	0.042
FDSE0378	X_b^{evac}	FDSF0001	200	600	197	120	FA	0.80	0.037
FDSE0379	X_b^{evac}	FDSF0017	156	764	176	90	FA	0.34	0.054
FDSE0380	X_b^{evac}	FDSF0021	170	992	172	35	FA	0.19	0.065
FDSE0381	X_b^{evac}	FDSF0020	110	890	210	71	FA	0.15	0.046
FDSE0382	X_b^{evac}	FDSF0017	156	764	179	137	FA	0.38	0.045
FDSE0383	X_b^{evac}	FDSF0020	110	890	292	84	FA	0.19	0.044
FDSE0384	X_b^{evac}	FDSF0017	156	764	164	171	FA	0.37	0.040
FDSE0385	X_b^{evac}	FDSF0018	47	934	282	44	FA	0.00	0.000
FDSE0386	X_b^{evac}	FDSF0002	25	1200	119	126	FA	0.00	0.000
FDSE0387	X_b^{evac}	FDSF0001	200	600	235	49	FA	0.81	0.058
FDSE0388	X_b^{evac}	FDSF0018	47	934	274	149	FA	0.00	0.000
FDSE0389	X_b^{evac}	FDSF0003	200	1200	195	61	FA	0.15	0.048
FDSE0390	X_b^{evac}	FDSF0016	115	1121	297	106	FA	0.11	0.031
FDSE0391	X_b^{evac}	FDSF0017	156	764	278	70	FA	0.53	0.061
FDSE0392	X_b^{evac}	FDSF0018	47	934	230	73	FA	0.00	0.000
FDSE0393	X_b^{evac}	FDSF0018	47	934	199	118	FA	0.00	0.000
FDSE0394	X_b^{evac}	FDSF0002	25	1200	253	116	FA	0.00	0.000
FDSE0395	X_b^{evac}	FDSF0021	170	992	206	64	FA	0.22	0.056
FDSE0396	X_b^{evac}	FDSF0019	91	676	147	141	FA	0.16	0.038
FDSE0397	X_b^{evac}	FDSF0003	200	1200	216	145	FA	0.17	0.035
FDSE0398	X_b^{evac}	FDSF0001	200	600	245	76	FA	0.83	0.044
FDSE0399	X_b^{evac}	FDSF0021	170	992	272	45	FA	0.26	0.066
FDSE0400	X_b^{evac}	FDSF0019	91	676	265	47	FA	0.22	0.060
FDSE0401	X_b^{evac}	FDSF0001	200	600	111	140	FA	0.70	0.039
FDSE0402	X_b^{evac}	FDSF0021	170	992	144	156	FA	0.19	0.032
FDSE0403	X_b^{evac}	FDSF0016	115	1121	132	161	FA	0.02	0.012
FDSE0404	X_b^{evac}	FDSF0001	200	600	163	61	FA	0.74	0.058
FDSE0405	X_b^{evac}	FDSF0018	47	934	156	33	FA	0.00	0.000
FDSE0406	X_b^{evac}	FDSF0021	170	992	190	133	FA	0.21	0.035
FDSE0407	X_b^{evac}	FDSF0019	91	676	181	158	FA	0.18	0.033
FDSE0408	X_b^{evac}	FDSF0000	25	600	183	40	FA	0.00	0.000
FDSE0409	X_b^{evac}	FDSF0000	25	600	169	171	FA	0.00	0.000
FDSE0410	X_b^{evac}	FDSF0019	91	676	214	81	FA	0.19	0.043
FDSE0411	X_b^{evac}	FDSF0019	91	676	152	56	FA	0.15	0.054
FDSE0412	X_b^{evac}	FDSF0018	47	934	151	101	FA	0.00	0.000
FDSE0413	X_b^{evac}	FDSF0002	25	1200	218	87	FA	0.00	0.000
FDSE0414	X_b^{evac}	FDSF0021	170	992	135	36	FA	0.17	0.069
FDSE0415	X_b^{evac}	FDSF0018	47	934	122	129	FA	0.00	0.000
FDSE0416	X_b^{evac}	FDSF0020	110	890	208	164	FA	0.15	0.028
FDSE0417	X_b^{evac}	FDSF0017	156	764	223	110	FA	0.44	0.048
FDSE0418	X_b^{evac}	FDSF0019	91	676	258	165	FA	0.24	0.038
FDSE0419	X_b^{evac}	FDSF0019	91	676	106	102	FA	0.13	0.035
FDSE0420	X_b^{evac}	FDSF0001	200	600	204	142	FA	0.82	0.033
FDSE0421	X_b^{evac}	FDSF0019	91	676	286	104	FA	0.24	0.047
FDSE0422	X_b^{evac}	FDSF0016	115	1121	243	153	FA	0.09	0.025
FDSE0423	X_b^{evac}	FDSF0017	156	764	114	52	FA	0.28	0.060
FDSE0424	X_b^{evac}	FDSF0021	170	992	266	97	FA	0.26	0.045
FDSE0425	X_b^{evac}	FDSF0000	25	600	283	85	FA	0.00	0.000
FDSE0426	X_b^{evac}	FDSF0021	170	992	251	151	FA	0.25	0.035
FDSE0427	X_b^{evac}	FDSF0018	47	934	115	59	FA	0.00	0.000
FDSE0428	X_b^{evac}	FDSF0002	25	1200	125	68	FA	0.00	0.000
FDSE0429	X_b^{evac}	FDSF0000	25	600	227	173	FA	0.00	0.000
FDSE0430	X_b^{evac}	FDSF0018	47	934	133	155	FA	0.00	0.000
FDSE0431	X_b^{evac}	FDSF0019	91	676	139	168	FA	0.16	0.033
FDSE0432	X_b^{evac}	FDSF0016	115	1121	202	52	TA	0.00	0.007
FDSE0433	X_b^{evac}	FDSF0000	25	600	177	80	TA	0.00	0.000

name	ED	name (fire)	HRR_{max} /MW	t_{max} /s	t_{pre} /s	N_{tu}	fa	$\mu(\widetilde{\xi^c})$	$\sigma(\widetilde{\xi^c})$
FDSE0434	X_b^{evac}	FDSF0016	115	1121	289	66	TA	0.04	0.027
FDSE0435	X_b^{evac}	FDSF0003	200	1200	141	98	TA	0.00	0.004
FDSE0436	X_b^{evac}	FDSF0000	25	600	144	92	TA	0.00	0.000
FDSE0437	X_b^{evac}	FDSF0003	200	1200	187	96	TA	0.03	0.017
FDSE0438	X_b^{evac}	FDSF0017	156	764	232	79	TA	0.26	0.051
FDSE0439	X_b^{evac}	FDSF0017	156	764	248	54	TA	0.28	0.065
FDSE0440	X_b^{evac}	FDSF0021	170	992	256	127	TA	0.12	0.029
FDSE0441	X_b^{evac}	FDSF0001	200	600	161	177	TA	0.51	0.037
FDSE0442	X_b^{evac}	FDSF0016	115	1121	156	41	TA	0.00	0.000
FDSE0443	X_b^{evac}	FDSF0002	25	1200	260	74	TA	0.00	0.000
FDSE0444	X_b^{evac}	FDSF0017	156	764	104	148	TA	0.01	0.008
FDSE0445	X_b^{evac}	FDSF0018	47	934	295	92	TA	0.00	0.000
FDSE0446	X_b^{evac}	FDSF0003	200	1200	120	135	TA	0.00	0.000
FDSE0447	X_b^{evac}	FDSF0002	25	1200	192	144	TA	0.00	0.000
FDSE0448	X_b^{evac}	FDSF0016	115	1121	109	132	TA	0.00	0.000
FDSE0449	X_b^{evac}	FDSF0018	47	934	226	39	TA	0.00	0.000
FDSE0450	X_b^{evac}	FDSF0018	47	934	238	111	TA	0.00	0.000
FDSE0451	X_b^{evac}	FDSF0020	110	890	280	166	TA	0.08	0.021
FDSE0452	X_b^{evac}	FDSF0002	25	1200	167	124	TA	0.00	0.000
FDSE0453	X_b^{evac}	FDSF0020	110	890	240	114	TA	0.05	0.021
FDSE0454	X_b^{evac}	FDSF0003	200	1200	222	108	TA	0.06	0.022
FDSE0455	X_b^{evac}	FDSF0003	200	1200	269	123	TA	0.10	0.033
FDSE0456	X_b^{evac}	FDSF0017	156	764	129	115	TA	0.04	0.020
FDSE0457	X_b^{evac}	FDSF0017	156	764	263	175	TA	0.36	0.043
FDSE0458	X_b^{evac}	FDSF0001	200	600	197	120	TA	0.54	0.050
FDSE0459	X_b^{evac}	FDSF0017	156	764	176	90	TA	0.12	0.037
FDSE0460	X_b^{evac}	FDSF0021	170	992	172	35	TA	0.03	0.031
FDSE0461	X_b^{evac}	FDSF0020	110	890	210	71	TA	0.03	0.019
FDSE0462	X_b^{evac}	FDSF0017	156	764	179	137	TA	0.15	0.038
FDSE0463	X_b^{evac}	FDSF0020	110	890	292	84	TA	0.08	0.030
FDSE0464	X_b^{evac}	FDSF0017	156	764	164	171	TA	0.12	0.034
FDSE0465	X_b^{evac}	FDSF0018	47	934	282	44	TA	0.00	0.000
FDSE0466	X_b^{evac}	FDSF0002	25	1200	119	126	TA	0.00	0.000
FDSE0467	X_b^{evac}	FDSF0001	200	600	235	49	TA	0.58	0.078
FDSE0468	X_b^{evac}	FDSF0018	47	934	274	149	TA	0.00	0.000
FDSE0469	X_b^{evac}	FDSF0003	200	1200	195	61	TA	0.03	0.024
FDSE0470	X_b^{evac}	FDSF0016	115	1121	297	106	TA	0.05	0.023
FDSE0471	X_b^{evac}	FDSF0017	156	764	278	70	TA	0.35	0.056
FDSE0472	X_b^{evac}	FDSF0018	47	934	230	73	TA	0.00	0.000
FDSE0473	X_b^{evac}	FDSF0018	47	934	199	118	TA	0.00	0.000
FDSE0474	X_b^{evac}	FDSF0002	25	1200	253	116	TA	0.00	0.000
FDSE0475	X_b^{evac}	FDSF0021	170	992	206	64	TA	0.07	0.032
FDSE0476	X_b^{evac}	FDSF0019	91	676	147	141	TA	0.00	0.005
FDSE0477	X_b^{evac}	FDSF0003	200	1200	216	145	TA	0.05	0.018
FDSE0478	X_b^{evac}	FDSF0001	200	600	245	76	TA	0.60	0.057
FDSE0479	X_b^{evac}	FDSF0021	170	992	272	45	TA	0.12	0.048
FDSE0480	X_b^{evac}	FDSF0019	91	676	265	47	TA	0.07	0.040
FDSE0481	X_b^{evac}	FDSF0001	200	600	111	140	TA	0.33	0.043
FDSE0482	X_b^{evac}	FDSF0021	170	992	144	156	TA	0.01	0.010
FDSE0483	X_b^{evac}	FDSF0016	115	1121	132	161	TA	0.00	0.000
FDSE0484	X_b^{evac}	FDSF0001	200	600	163	61	TA	0.44	0.061
FDSE0485	X_b^{evac}	FDSF0018	47	934	156	33	TA	0.00	0.000
FDSE0486	X_b^{evac}	FDSF0021	170	992	190	133	TA	0.06	0.022
FDSE0487	X_b^{evac}	FDSF0019	91	676	181	158	TA	0.02	0.013
FDSE0488	X_b^{evac}	FDSF0000	25	600	183	40	TA	0.00	0.000
FDSE0489	X_b^{evac}	FDSF0000	25	600	169	171	TA	0.00	0.000
FDSE0490	X_b^{evac}	FDSF0019	91	676	214	81	TA	0.04	0.024
FDSE0491	X_b^{evac}	FDSF0019	91	676	152	56	TA	0.01	0.010
FDSE0492	X_b^{evac}	FDSF0018	47	934	151	101	TA	0.00	0.000
FDSE0493	X_b^{evac}	FDSF0002	25	1200	218	87	TA	0.00	0.000
FDSE0494	X_b^{evac}	FDSF0021	170	992	135	36	TA	0.01	0.013
FDSE0495	X_b^{evac}	FDSF0018	47	934	122	129	TA	0.00	0.000
FDSE0496	X_b^{evac}	FDSF0020	110	890	208	164	TA	0.03	0.014
FDSE0497	X_b^{evac}	FDSF0017	156	764	223	110	TA	0.25	0.047
FDSE0498	X_b^{evac}	FDSF0019	91	676	258	165	TA	0.08	0.026
FDSE0499	X_b^{evac}	FDSF0019	91	676	106	102	TA	0.00	0.000
FDSE0500	X_b^{evac}	FDSF0001	200	600	204	142	TA	0.57	0.044

name	ED	name (fire)	$\mathrm{HRR}_{max}\,/MW$	$t_{max}\,/s$	$t_{pre}\,/s$	N_{tu}	fa	$\mu(\widetilde{\xi^c})$	$\sigma(\widetilde{\xi^c})$
FDSE0501	X_b^{evac}	FDSF0019	91	676	286	104	TA	0.10	0.031
FDSE0502	X_b^{evac}	FDSF0016	115	1121	243	153	TA	0.02	0.011
FDSE0503	X_b^{evac}	FDSF0017	156	764	114	52	TA	0.02	0.020
FDSE0504	X_b^{evac}	FDSF0021	170	992	266	97	TA	0.13	0.036
FDSE0505	X_b^{evac}	FDSF0000	25	600	283	85	TA	0.00	0.000
FDSE0506	X_b^{evac}	FDSF0021	170	992	251	151	TA	0.11	0.028
FDSE0507	X_b^{evac}	FDSF0018	47	934	115	59	TA	0.00	0.000
FDSE0508	X_b^{evac}	FDSF0002	25	1200	125	68	TA	0.00	0.000
FDSE0509	X_b^{evac}	FDSF0000	25	600	227	173	TA	0.00	0.000
FDSE0510	X_b^{evac}	FDSF0018	47	934	133	155	TA	0.00	0.000
FDSE0511	X_b^{evac}	FDSF0019	91	676	139	168	TA	0.00	0.003

G.8 Prerequisites for reproducible results in the methodology for risk analysis

Objective 1 (metamodel) requires the reproducibility for the results of the methodology for risk analysis. As prerequisites, the following subsections first, evaluate the accuracy of the indirect mode over fixed points and second, establish defaults for risk analyses to ensure the convergence of risk measures.

Integration of the RSM into the system model

Subs. 'Integration of MLS models into the system model' (p. 45) describes two modes to integrate the RSMs of MLS into the system model, namely the direct mode and the indirect mode over fixed points. To prove the accuracy of the indirect mode, two system model simulations with $N_{\mathrm{mcs}} = 10^6$ random scenarios are compared, first, with the direct mode $\mathcal{S}^{\mathrm{dir}}$ and second, with the indirect mode over fixed points $\mathcal{S}^{\mathrm{fps}}$. The FF in the system models $\bar{\Xi}^{\mathrm{dir}}$ and $\bar{\Xi}^{\mathrm{fps}}$ consider neither the metamodel uncertainty nor the evacuation uncertainty and are both based on the data base $\bar{\boldsymbol{\xi}}^c_{X_2}$.

Fig. G.6a illustrates the frequency distribution of the results of both metamodels in a quantile plot and Fig. G.6b depicts the societal risk curves. Both figures reveal nearly identical results of the system model simulations which also yields for the individual risk. Furthermore, the indirect mode over fixed points outperformed the run time of the direct mode by a factor of less than 0.01.

To conclude, the indirect mode over fixed points, i.e. an additional RSM, has negligible effects on the results of Monte-Carlo simulations in the system model but reduces the run time considerably. Of course, parallel computing in the implementation of MLS might be another option to reduce the run time. This improvement would at the same time simplify the data flow sketched in Fig. G.1 (p. G-9) and could be realised in further developments of the metamodel. But for now, the indirect mode is considered to be accurate and the notation in this dissertation does not differentiate between the two modes.

Convergence of risk measures during Monte-Carlo simulation

Section B.1 outlines that methodologies for risk analysis commonly use Monte-Carlo simulations to quantify the risk measures. In particular, it is important to consider scenarios with rare events, i.e. fires with maximum HRRs of $\mathrm{HRR}_{max} = 100\,MW$ together with FA. However, scenarios with rare events occur infrequently in Monte-Carlo simulations which demands a large number of random scenarios to achieve convergence of risk measures during Monte-Carlo simulation. To reduce the required number of random scenarios, the risk factors HRR_{max} and fa employ importance sampling detailed in Section B.2 and Section B.3. Thus,

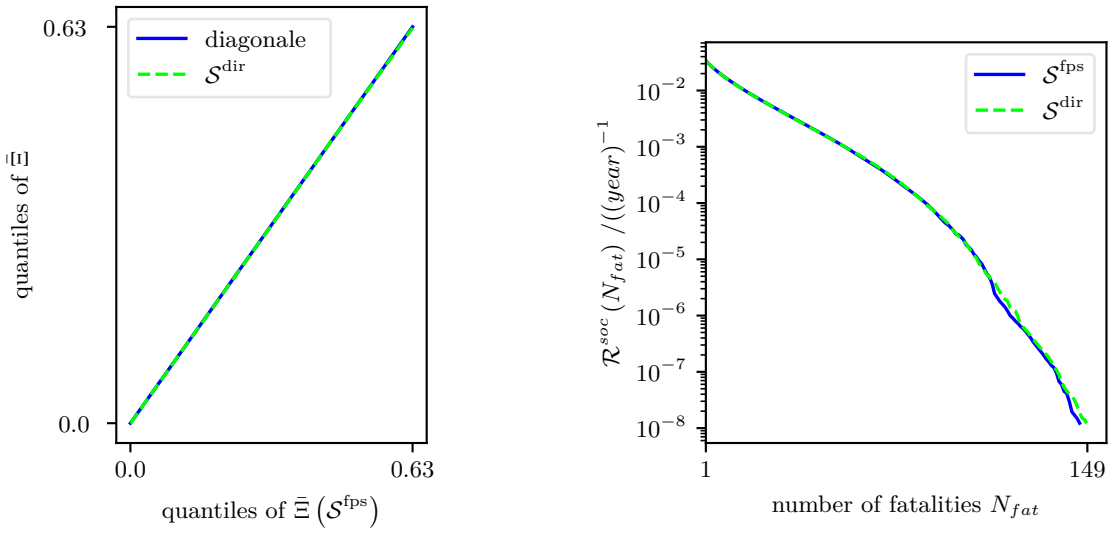

(a) quantile plot of $\bar{\Xi}$ relative to $\bar{\Xi}^{\text{fps}}$ **(b)** societal risk curves

Figure G.6: Effects of the indirect mode over fixed points in the system model simulations $\mathcal{S}^{\text{fps}}$ in comparison to the the direct mode $\mathcal{S}^{\text{dir}}$.

Table G.8: Risk analyses $\mathcal{R}_{\text{HRR}_{max},fa}$ with importance sampling (IS) in risk factors HRR_{max} and fa.

$\mathcal{R}$	IS in HRR_{max}	IS in fa
$\mathcal{R}_{0,0}$	no	no
$\mathcal{R}_{0,1}$	no	yes
$\mathcal{R}_{1,0}$	yes	no
$\mathcal{R}_{1,1}$	yes	yes

it is important for the reproducibility of results of risk analysis to: verify the importance sampling in both risk factors; and to determine the required number of random scenarios. With these aims, this evaluation compares different risk analyses provided in Tab. G.8. The risk analyses apply the default RSM $\bar{\boldsymbol{\xi}}_{X_2}$ without metamodel uncertainty or evacuation uncertainty to emphasise the effects of importance sampling. They produce results in $N_{\text{mcs}} = 10^6$ random scenarios which comprise: first, the number of random scenarios with rare events $\left\|\widetilde{X}_{rare}\right\|$; second, the FF in the system model $\bar{\Xi}$; third, the individual risk $\mathcal{R}^{ind}$; and fourth, the societal risk curve. The convergence of the FF and the individual risk is quantified with the convergence measure υ_{conv} defined with Eq. B.7 (p. 28) in Section B.5. The figures illustrating the convergence as well as the convergence measures are by nature subjected to remarkable aleatory uncertainties. However, the results reflect the common gain of importance sampling.

With regard to the verification of importance sampling, Fig. G.7a and Fig. G.7b illustrate the convergence of the individual risk and of the FFs for all risk analyses using importance sampling towards the risk analysis $\mathcal{R}_{0,0}$ without importance sampling. Also, the numbers of random scenarios with rare events are in accordance to the probabilistic models used for importance sampling shown in Tab. B.3 on p. 19. Hence, importance sampling in the Monte-Carlo simulation generates accurate results.

Fig. G.7c and Fig. G.7d, focussing on the first $N_{\text{mcs}} = 10^5$ random scenarios, give better insight to the convergence of the individual risk and the FF. In general, the risk analyses

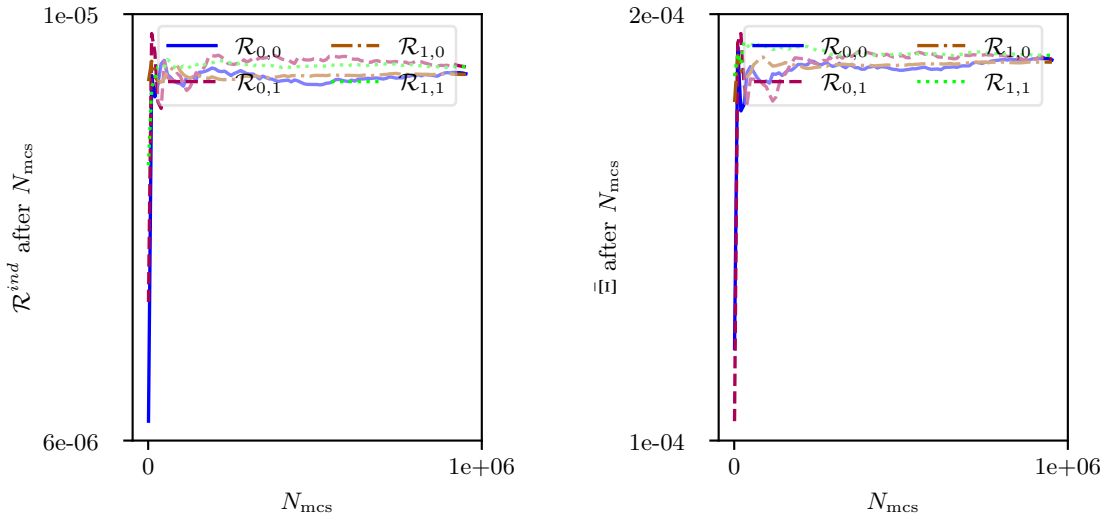

(a) $\mathcal{R}^{ind}\left(N_{\text{mcs}} = 10^6\right)$ **(b)** $\bar{\Xi}\left(N_{\text{mcs}} = 10^6\right)$

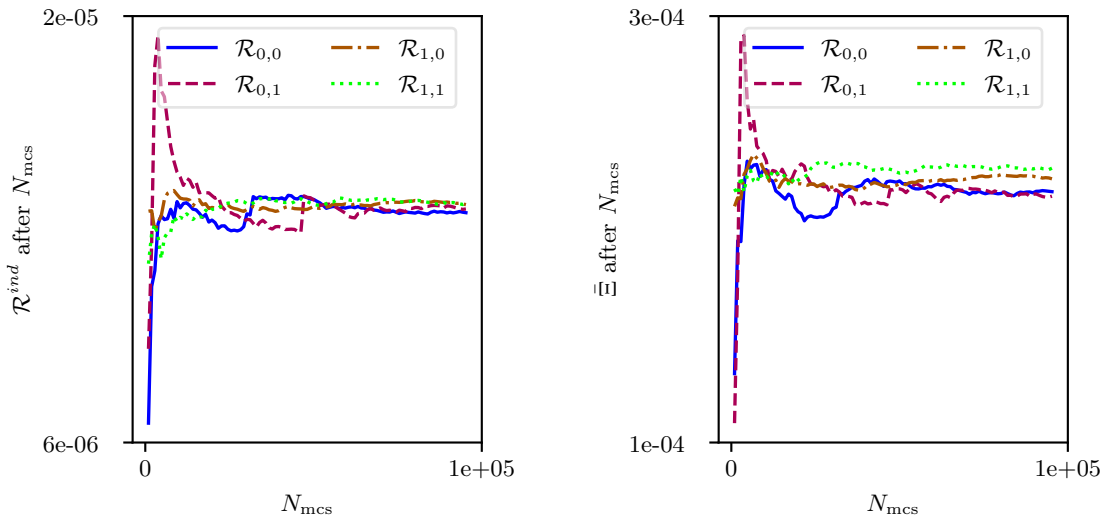

(c) $\mathcal{R}^{ind}\left(N_{\text{mcs}} = 10^5\right)$ **(d)** $\bar{\Xi}\left(N_{\text{mcs}} = 10^5\right)$

Figure G.7: Convergence of the individual risk $\mathcal{R}^{ind}$ and the FF in the system model $\bar{\Xi}$ of risk analyses $\mathcal{R}_{\text{HRR}_{max},fa}$ with importance sampling in the risk factors HRR_{max} and fa for $N_{\text{mcs}} = 10^6$ random scenarios (above) and the focus on the first $N_{\text{mcs}} = 10^5$ random scenarios (below).

Table G.9: Results of risk analyses with importance sampling: frequency of random scenario with rare events and convergence measure v_{conv} for the individual risk $\mathcal{R}^{ind}$ and the FF in the system model $\bar{\Xi}$; $\left\|\widetilde{X}_{rare}\right\|$ is the number of random scenarios with rare events.

	$\frac{\left\|\widetilde{X}_{rare}\right\|}{N_{\text{mcs}}}$	$v_{conv}\left(\mathcal{R}^{ind}\right)$	$v_{conv}\left(\mathcal{R}^{ind}\right)$	$v_{conv}\left(\bar{\Xi}\right)$	$v_{conv}\left(\bar{\Xi}\right)$
$\mathcal{R}$ \ N_{mcs}	10^6	10^5	10^6	10^5	10^6
$\mathcal{R}_{0,0}$	$1 \cdot 10^{-6}$	$2 \cdot 10^{-2}$	$10 \cdot 10^{-4}$	$1 \cdot 10^{-3}$	$4 \cdot 10^{-4}$
$\mathcal{R}_{0,1}$	$50 \cdot 10^{-6}$	$2 \cdot 10^{-2}$	$3 \cdot 10^{-4}$	$15 \cdot 10^{-3}$	$6 \cdot 10^{-4}$
$\mathcal{R}_{1,0}$	$2.9 \cdot 10^{-3}$	$1 \cdot 10^{-2}$	$0.8 \cdot 10^{-4}$	$3 \cdot 10^{-3}$	$8 \cdot 10^{-4}$
$\mathcal{R}_{1,1}$	0.15	$1 \cdot 10^{-2}$	$5 \cdot 10^{-4}$	$15 \cdot 10^{-3}$	$1 \cdot 10^{-4}$

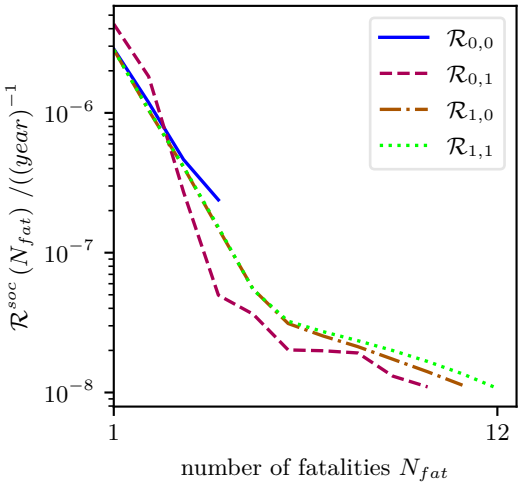

Figure G.8: Effect of importance sampling in risk factors HRR_{max} and fa on the societal risk curves of risk analyses $\mathcal{R}$ with $N_{\text{mcs}} = 10^6$ random scenarios.

$\mathcal{R}_{1,1}$ with importance sampling in both risk factors converged fastest. These results comply with the convergence measures in Tab. G.9. Namely, both risk analyses $\mathcal{R}_{1,1}$ and $\mathcal{R}_{1,0}$ using importance sampling in the risk factor HRR_{max} had the smallest convergence measures. Further, the convergence measures decreased with more than one order of magnitude from $N_{\text{mcs}} = 10^5$ to $N_{\text{mcs}} = 10^6$ random scenarios. At last, Fig. G.8 describes the societal risk curves. The risk analyses $\mathcal{R}_{1,1}$ and $\mathcal{R}_{1,0}$ revealed similar results and the risk analyses $\mathcal{R}_{0,0}$ without importance sampling deviated strikingly. This latter result derives from the small number of random scenario with rare events. In numbers, the risk analysis $\mathcal{R}_{0,0}$ requires about 10^3 times more random scenarios to get a comparable number of random scenarios with rare events as $\mathcal{R}_{1,0}$ and thus a comparable societal risk curve as $\mathcal{R}_{1,1}$.

Briefly, the importance sampling reduces the required number of random scenarios. Since, the convergence measures between $N_{\text{mcs}} = 10^5$ and $N_{\text{mcs}} = 10^6$ random scenarios still deviate, $N_{\text{mcs}} = 10^6$ random scenarios as well as importance sampling in the risk factors HRR_{max} and fa are required for convergence of risk measures in risk analyses. This conclusion serves as default for the following risk analyses.

Table G.10: MLS attributes for RSMs additionally subjected to manual data points for scenarios with TA (above) and FA (below).

RSM	weighting type	polynomial degree	parameter ω
$\bar{\boldsymbol{\xi}}_{X_{2m,0}}$	w_g	2	0.459
$\bar{\boldsymbol{\xi}}_{X_{3m,0}}$	w_p	2	0.987
$\bar{\boldsymbol{\xi}}_{X_{2m,1}}$	w_g	2	0.459
$\bar{\boldsymbol{\xi}}_{X_{3m,1}}$	w_p	2	0.870

G.9 Improvement of the metamodel uncertainty by additional data points

Section E.2.1 reveals the drawback of the prediction interval method. The drawback occurs in regions of the domain where the results of the complex model and of the metamodel are close to zero. In these regions, the metamodel uncertainty is expected to be small but the prediction variance contradicts this expectation as illustrated in Fig. E.13a (p. 71) and Fig. E.14a. Additionally, Section E.2.1 outlines two approaches to cope with this drawback. Now, this section exemplifies the second approach to reduce the metamodel uncertainty locally, namely to extend the data base with manual data points.

For this purpose, 81 manual data points with results of zero $\widetilde{\boldsymbol{\xi}}^c_{manual} = \left[\vec{0}, \ldots, \right]$ extend the data base $\widetilde{\boldsymbol{\xi}}^c_2$ and consequently also $\widetilde{\boldsymbol{\xi}}^c_3$. The manual data points derive from a FFD $X_{manual} = X^{\mathrm{FFD}}$ with three levels highlighted in Fig. G.9a. Their distinct region of $25\,MW \leq \mathrm{HRR}_{max} \leq 75\,MW$ $1000\,s \leq t_{max} \leq 1200\,s$, $100\,s \leq t_{pre} \leq 125\,s$, $30 \leq N_{tu} \leq 150$ derives from previous results, i.e. Fig. E.11a, Fig. E.11b on p. 67 and Fig. E.13b, Fig. E.13a on p. 71. The latter two figures result from scenarios with higher pre-evacuation times of $t_{pre} = 194\,s$ and thus show higher FF as expected in the region of the manual data points. Consequently, the data bases are subjected to the EDs $X_{2m} = \left[{X_2}^T, X^T_{manual}\right]^T$ and $X_{3m} = \left[{X_3}^T, X^T_{manual}\right]^T$ and lead to the RSMs in Tab. G.10.

As a result, the results of the RSM $\bar{\boldsymbol{\xi}}_{X_{2m}}$ are mostly similar to the former RSM $\bar{\boldsymbol{\xi}}_{X_2}$ as shown in Fig. G.9a. The largest differences appear at the transition between the region of the manual data points to the region with high gradients as visible in Fig. G.9b. With regard to the prediction variance, the manual data points cause a global decrease in comparison to the prediction variance of the RSM $\bar{\boldsymbol{\xi}}_{X_2}$ but the prediction interval of the RSM $\bar{\boldsymbol{\xi}}_{X_{2m}}$ is still conservative to results of the RSMs $\bar{\boldsymbol{\xi}}_{X_2}$ and $\bar{\boldsymbol{\xi}}_{X_{3m}}$. And more important, the manual data points reduce the prediction variance locally in comparison the other regions as revealed in Fig. G.9c and Fig. G.9d.

To sum up, this example proves that manual data points can reduce the drawback of the prediction interval method. Thus, the approach would be, plainly spoken, the cherry on the cake within the system model. However, these manual data points of this example could be located more efficiently after a sensitivity analysis, esp. to limit their effects on the shape of the RSM. They also increased the local number of data points in comparison to other regions. Consequently, the weighting function of MLS in Subs. 'Weighting functions' (p. 44) could be improved with a local weighting parameter or a prediction window as in Salemi 2016 [29].

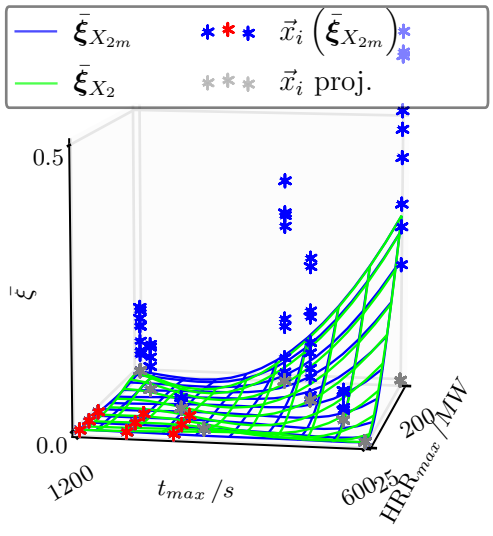

(a) results of the RSM (TA)

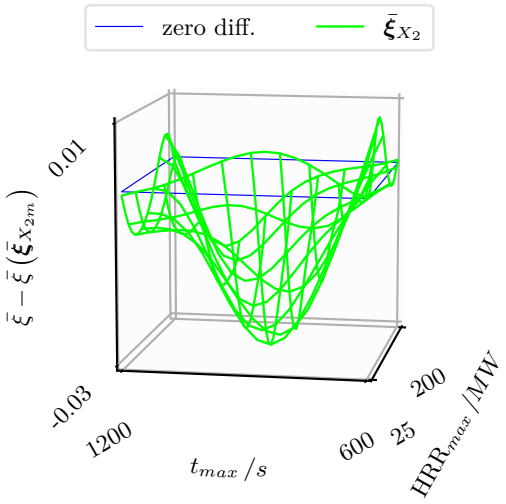

(b) difference to $\bar{\xi}_{X_{2m}}$ (TA)

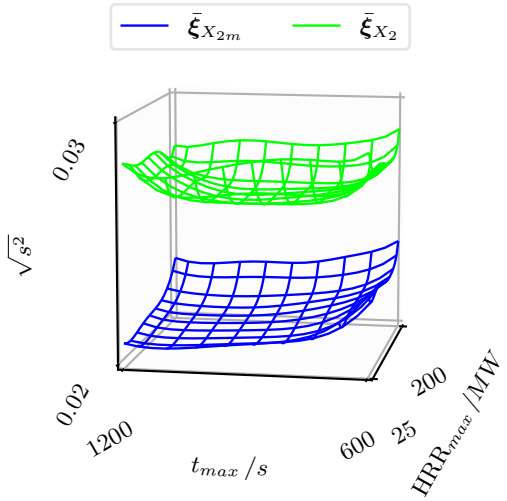

(c) prediction variance $\sqrt{s^2}$ (TA)

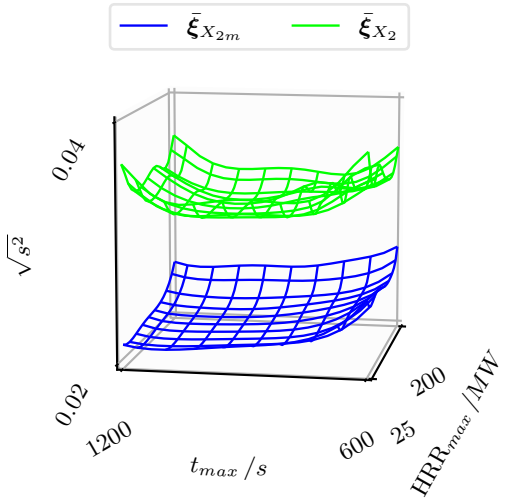

(d) prediction variance $\sqrt{s^2}$ (FA)

Figure G.9: Effects of the manual data points on the RSM and the prediction variance in the region of sc(− MW, − s, 112 s, 92, $fa = -$); the manual data points of the FFD are highlighted red; the scales differ between the figures.

Additional bibliography from [72]

[72] Stanley Kaplan and B. John Garrick. "On The Quantitative Definition of Risk". In: *Risk Analysis* 1.1 (1981), pp. 11–27. ISSN: 0272-4332.

[73] International Organization for Standardization. *Risk management - Principles and guidelines: ISO 31000:2009(E): ICS Notation 03.100.01.* 1.0. Berlin: Beuth Verlag GmbH, 2009.

[74] Deutsches Institut für Normung. *Brandingenieurwesen - Teil 1: Grundsätze und Regeln für die Anwendung: DIN 18009-1: ICS Notation 13.220.01.* 1st ed. Berlin: Beuth Verlag GmbH, 2016.

[75] Peter Burgherr, Petrissa Eckle, and Stefan Hirschberg. "Comparative assessment of severe accident risks in the coal, oil and natural gas chains". In: *Reliability Engineering & System Safety* 105 (2012), pp. 97–103. ISSN: 09518320. DOI: 10.1016/j.ress.2012.03.020.

[76] G. De Sanctis. "Generic risk assessment for fire safety: Performance evaluation and optimisation of design provisions". PhD thesis. Zürich: ETH Zürich, Schweiz, 2015.

[77] Wei-Shing Wu et al. "Risk assessment by integrating interpretive structural modeling and Bayesian network, case of offshore pipeline project". In: *Reliability Engineering & System Safety* 142 (2015), pp. 515–524. ISSN: 09518320. DOI: 10.1016/j.ress.2015.06.013.

[78] International Organization for Standardization. *Fire safety engineering - Procedures and requirements for verification and validation of fire methods - Part 1: General (Draft): ISO 16730-1: ICS Notation 13.220.01.* 1st ed. Geneva: ISO, 2014.

[79] ILF Consulting Engineers. *Auswertung der ASFINAG-Tunnelbrandstatistik 2006-2012: RVS-Arbeitsausschuss 09.03.11 TuRisMo: 14.10.2013.* Linz, 2013.

[80] Ulrich Schneider and Johannes Horvath. *Brandschutz-Praxis in Tunnelbauten: Brandverhalten, Brandschutzmaßnahmen, Sanierung - Mit Projektbeispielen.* 1st ed. Berlin: Bauwerk-Verlag, 2006. ISBN: 3-89932-037-9.

[81] A. R. Nilsen and T. Log. "Results from three models compared to full-scale tunnel fires tests". In: *Fire Safety Journal* 44.1 (2009), pp. 33–49. ISSN: 03797112.

[82] Marc L. Janssens. *Development of a database of full-scale calorimeter tests of motor vehicle burns: Final report: SwRI Project No. 01.06939.01.003.* Charlottesville, VA and USA, 2008.

[83] Haukur Ingason. "Design Fires in Tunnels". In: *Safe & Reliable Tunnels, Innovative European Achievements: Second International Symposium.* Lausanne, 2006, pp. 1–11.

[84] Thomas Wagener. *Berücksichtigung der Belange behinderter Personen bei Ausstattung und Betrieb von Straßentunneln: Bericht zum Forschungsprojekt FE03.405/2005/FRB.* Bremerhaven: Wirtschaftsverlag NW, Verlag für Neue Wissenschaft GmbH, 2009. ISBN: 978-3-86509-947-1.

[85] T. J. Shields. "Human behaviour during tunnel fires". In: *The handbook of tunnel fire safety.* Ed. by Alan Beard and Richard Carvel. London: ICE, 2012, pp. 399–420. ISBN: 978-0-7277-4153-0.

[86] Daniel Nilsson, Maria Johansson, and Håkan Frantzich. "Evacuation experiment in a road tunnel: A study of human behaviour and technical installations". In: *Fire Safety Journal* 44.4 (2009), pp. 458–468. ISSN: 03797112.

[87] Max Kinateder et al. "Human behaviour in severe tunnel accidents: Effects of information and behavioural training". In: *Transportation Research Part F: Traffic Psychology and Behaviour* 17 (2013), pp. 20–32. ISSN: 13698478.

[88] Enrico Ronchi et al. "The evaluation of different evacuation models for assessing road tunnel safety analysis". In: *Tunnelling and Underground Space Technology* 30 (2012), pp. 74–84. ISSN: 08867798.

[89] RiMEA. *Richtlinie für Mikroskopische Entfluchtungsanalysen (RiMEA): Version 2.2.1.* Ed. by RiMEA. Duisburg, 2009.

[90] Anders Norén and Joel Winér. *Modelling Crowd Evacuation from Road and Train Tunnels: Data and design for faster evacuations: Report 5127, Lund 2003.* Ed. by Lund University, Department of Fire Safety Engineering. Lund, 2003.

[91] Bundesanstalt für Straßenwesen (BASt). *Verfahren zur Kategorisierung von Straßentunneln gemäß ADR 2007: Schlussbericht 2009.* Bergisch Gladbach, 2009.

[92] Tor-Olav Nævestad and Sunniva Meyer. "A survey of vehicle fires in Norwegian road tunnels 2008–2011". In: *Tunnelling and Underground Space Technology* 41 (2014), pp. 104–112. ISSN: 08867798.

[93] Ciro Caliendo and De Guglielmo, Maria Luisa. "Accident Rates in Road Tunnels and Social Cost Evaluation". In: *Procedia - Social and Behavioral Sciences* 53 (2012), pp. 166–177. ISSN: 18770428.

[94] Bundesanstalt für Straßenwesen (BASt). *Manuelle Straßenverkehrszählung 2010.* 2011. URL: `http://www.bast.de/DE/Statistik/Verkehrsdaten-Downloads/2010/Manuelle-Zaehlung-2010.html?nn=605200` (visited on 03/26/2014).

[95] Regierungspräsidium Stuttgart - Baureferat Ost - Baubüro Schwäbisch Gmünd. *B29 OU Schwäbisch Gmünd - Gmünder Einhorn Tunnel.* Ed. by Regierungspräsidium Stuttgart - Baureferat Ost - Baubüro Schwäbisch Gmünd. 2013. URL: `http://www.tunnel-gd.de/` (visited on 05/30/2015).

[96] Z. G. Liu et al. "Findings of the International Road Tunnel Fire Detection Research Project". In: *Fire Technology* 46.3 (2010), pp. 697–718. ISSN: 0015-2684.

[97] Haukur Ingason, Ying Zhen Li, and Anders Lönnermark. *Tunnel Fire Dynamics.* New York: Springer Science+Business Media, 2015. ISBN: 978-1-4939-2198-0.

[98] Morgan J. Hurley et al. *SFPE Handbook of Fire Protection Engineering.* New York, NY: Springer New York, 2016. ISBN: 978-1-4939-2564-3.

[99] George W. Mulholland. "Smoke Production and Properties". In: *SFPE Handbook of Fire Protection Engineering.* Ed. by Philip J. DiNenno et al. Quincy Massachusetts, 2003, pp. 2/258–2/268.

This page is intended to be blank.

Der Lebenslauf ist in der Online-Version aus Gründen des Datenschutzes nicht enthalten.